UNIVERSITY OF SOUTHAMPTON

FACULTY OF ENGINEERING AND PHYSICAL SCIENCES

APPLICATION OF TWO- AND THREE-PHASE FLOW IN SUBMERGED FLAT-SHEET ANAEROBIC MEMBRANE BIOREACTORS FOR DAIRY WASTEWATER TREATMENT

by

Pakpong Sriprasert

Thesis for the degree of Doctor of Philosophy

June 2019

Supervisors: Prof Sonia Heaven and Em Prof Charles J Banks

DECLARATION OF AUTHORSHIP

I, Pakpong Sriprasert, declare that this thesis entitled

APPLICATION OF TWO- AND THREE-PHASE FLOW IN SUBMERGED FLAT-SHEET ANAEROBIC MEMBRANE BIOREACTORS FOR DAIRY WASTEWATER TREATMENT

declare that this thesis and the work presented in it are my own and has been generated by me as the result of my own original research. I confirm that:

1. This work was done wholly or mainly while in candidature for a research degree at this University;
2. Where any part of this thesis has previously been submitted for a degree or any other qualification at this University or any other institution, this has been clearly stated;
3. Where I have consulted the published work of others, this is always clearly attributed;
4. Where I have quoted from the work of others, the source is always given. With the exception of such quotations, this thesis is entirely my own work;
5. I have acknowledged all main sources of help;
6. Where the thesis is based on work done by myself jointly with others, I have made clear exactly what was done by others and what I have contributed myself;
7. Parts of this work have been published as:

    - S. Pakpong, S. Heaven and C.J. Banks (2015). Evaluation of bubbles sizes, sizes distribution and crossflow velocities between flat-sheet membranes in membrane bioreactor. The AD Network BBSRC NIBB, Early Career Researcher Conference, Warwick, The UK, 29-30 June 2015. (poster presentation)
    - S. Pakpong, S. Heaven and C.J. Banks (2016). Implementation of non-adsorbed granules in gas-sparged anaerobic membrane bioreactor for fouling mitigation. The AD Network BBSRC NIBB, Early Career Researcher Conference, Birmingham, The UK, 4-5 July 2016. (oral presentation)
    - S. Pakpong, S. Heaven and C.J. Banks (2016). Implementation of non-adsorbed granules in gas-sparged anaerobic membrane bioreactor for fouling mitigation. BiogasScience2016 in Szeged, Hungary, 21-24 August 2016. (oral presentation)

Signed: .....

Date:.....

UNIVERSITY OF SOUTHAMPTON

ABSTRACT

FACULTY OF ENGINEERING AND PHYSICAL SCIENCES

Civil and Environmental Engineering

Thesis for the degree of Doctor of Philosophy

APPLICATION OF TWO- AND THREE-PHASE FLOW IN SUBMERGED FLAT-SHEET ANAEROBIC MEMBRANE BIOREACTORS FOR DAIRY WASTEWATER TREATMENT

Pakpong Sriprasert

The association of anaerobic process with membrane filtration in anaerobic membrane bioreactors (AnMBR) is a recent development in high rate anaerobic systems. This technology offers complete biomass retention regardless of settling properties, and enables the decoupling of hydraulic retention time (HRT) and solids retention time (SRT), with superior effluent qualities and small footprint areas. However, membrane fouling, an unavoidable circumstance, is still a crucial obstacle for AnMBR implementation.

Gas-liquid two-phase air/gas sparging has been applied extensively for both aerobic membrane bioreactors (AeMBR) and AnMBR systems, but sparging for fouling control purposes is always the largest energy demand for MBRs operation. Hence, sophisticated hydrodynamics design is of prime importance to achieve effective exploitation of the energy input.

The first stage of this study aimed to optimise two-phase flow hydrodynamic parameters such as gas flow rate, nozzle size and tank geometry for a gaslift-loop submerged flat-sheet MBR. The results showed that a Ø 3 mm nozzle sparger gave the largest bubble-membrane contact area. Threshold superficial air velocity was observed at 0.033 m s^{-1}, while the increase in liquid upward flow velocity plateaued at a sparging rate of 6 $Lmin^{-1}$.

Adding suspended media is regarded as a promising strategy for membrane cleaning, with active adsorbents utilised most widely in either gas-sparged or fluidized bed MBRs. However, once the sorption capacity is diminished, then membrane scouring dominates. The introduction of non-adsorbent suspended particle has also been proposed. It has been reported that external irreversible fouling, which most of the time represents the major contributor to the total fouling, has been diminished effectively by the particles abrasion.

This approach has successfully been operated with various AeMBR, while information on applying non-adsorbent suspended media in AnMBR, in which fouling phenomena are considered to be more intense when compared to AeMBR, is still very limited.

Therefore, the overall aim of this research was to study the use of non-adsorbent particles coupled with conventional gas sparged AnMBR (GSAnMBR) functioning as a three-phase (solid/gas/liquid) flow for fouling mitigation and flux enhancement purposes, in an attempt to operate as a high-rate moving bed AnMBR (MBAnMBR) for dairy wastewater treatment.

Trials were carried out to evaluate the feasibility and the related operational parameters of using non-adsorbent suspended particles associated with gas sparging in AnMBR. The experiments were carried out under simulated MBAnMBR conditions with low density polyethylene beads (SG 0.86 - 0.96, 2 - 3 mm apparent size) at different filling densities. Critical flux (J_{crit}), supra-critical flux filtrations and resistance-in-series model experiments were carried out. The results demonstrated that J_{crit} for 0, 11.1 and 22.2 % (v/v filling ratio) were 6, 7.5 and 9 L m^{-2} h^{-1} (LMH). Total filtration resistances (R_t) were 14.1 x 10^{12}, 8.38 x10^{12} and 1.61 x 10^{12} m^{-1}, of which cake resistance (R_c) represented the major contributor to R_t of 95.0, 92.3 and 62.1 %, respectively. This indicated that R_t has been decreased effectively by 40.6 - 88.6 % with the assistance of scouring particles.

Long-term continuous operation for more than 300 days of 6.6 L lab-scale GSAnMBR and MBAnMBR was carried out under mesophilic conditions (37 °C) for synthetic dairy wastewater treatment. Systems were installed with a single A4 size flat sheet membrane (Kubota) made of chlorinated polyethylene with a nominal pore size of 0.4 μm and total filtration area of 0.1 m^2. Biogas from the reactor headspace was circulated at a rate of 5 $Lmin^{-1}$ to create gas sparging for both reactors. Polyethylene glycol (PEG) granules, cylindrical in shape with the size and SG of 4 x 4 mm and 1.01 - 1.05 were applied as scouring media in MBAnMBR (10 % by volume fraction). Initial MLVSS was set at 4,500 mgL^{-1} and controlled to below 14,000 mg L^{-1}. Net fluxes were initially set constant at 3.5 - 3.8 LMH resulting in HRT of 17 - 19 h and OLR were increased stepwise from 0.7 to 5.0 g $COD_{removed}$ L^{-1} d^{-1} by influent concentration adjustment for the first 100 days of operation. Thereafter, influent concentration was fixed in the range of 3,600 - 3,900 mgL^{-1} until the end of experiments in which attainable OLRs were determined by achievable fluxes and SRTs were varied. The results illustrated that high total COD removal of 98 - 99 % could be achieved for both reactors under stable conditions corresponding to OLRs in range of 2.2 - 7.0 g $COD_{removed}$ L^{-1} d^{-1} with F/M ratios of 0.25 - 0.65 g $COD_{removed}$ g VSS d^{-1}. Attainable net fluxes for long-term operation without rapid increases in TMP were at 2.8 and 3.7 LMH for GSAnMBR and MBAnMBR. This indicated that under the same given energy input for gas sparging, net flux could be enhanced by at least 24.3 % (even up to 35 %) with the assistance of scouring particles at a lower suction pressure. Additionally, MBAnMBR could be operated continuously for more than 300 days without backflushing or chemical cleaning. The higher VMP range of 0.63 - 2.30 L CH_4 L^{-1} reactor day^{-1} for the MBAnMBR when compared to 0.68 - 1.86 L CH_4 L^{-1} reactor day^{-1} for the GSAnMBR was due to higher OLRs causes by greater producible flux. A methane yield of 0.31- 0.32 L CH_4 g^{-1} $COD_{removed}$ which represents 90 - 92% of theoretical methane conversion was seen from both reactors. Similar observed biomass yields (Y_{obs}) of 0.057 - 0.059 and 0.059 - 0.072 g VSS g^{-1} $COD_{removed}$ were found for the GSAnMBR and MBAnMBR. R_c represents the major contributor to the R_t for both reactors. However, R_c in MBAnMBR is about 12-fold lower than in GSAnMBR with values of 4.8 x 10^{11} m^{-1} and 57.6 x 10^{11} m^{-1}, respectively. Cake/gel forming could be alleviated effectively. Hence, particle addition could minimise the frequency of chemical cleaning, possibly prolonging membrane lifespan as well as reducing operational and maintenance expenses. No significant damage was observed on the membrane surface from using PEG granules as scouring agents under 5 L min^{-1} sparging after 308 days of operation.

Keyword: non-adsorbsent particles, moving bed, AnMBR, scouring media, dairy wastewater

Acknowledgements

Studying PhD abroad is one of my dreams that I would like to pursue. I really glad that I, finally, can make it come true. My PhD journey is filled with several moments of self-doubt and fear. I could not possible to achieve PhD without the support and guidance of many people.

Firstly, I gratefully acknowledge the funding from the Ministry of Science and Technology (MOST), The Royal Thai Government that gives me opportunities for undertaking PhD and having a wonderful experience of living aboard. My sincere thank also goes to the Office of Educational Affairs, the Royal Thai Embassy in London for their care and support to overcome obstacles during the time in the UK. My appreciation and thank you to Mahasarakham University, Thailand for supporting the supply of materials and good advice.

I would like to express my sincere gratitude to my supervisor: Prof Sonia Heaven and Em Prof Charles J Banks, for supervision, time and effort they put over the past few years to make this research finally possible. My genuine thanks are also due to my thesis examiners: Prof Bruce Jefferson and Dr Yongqiang Liu, for their constructive comments which give a better version of my thesis.

Most sincere thanks due to our professional technicians, Pilar Pascual-Hidalgo and Dr Dominic Mann for their technical support and for their huge efforts to make the lab a safe and happy place to work in. I also would like to acknowledge all my colleagues in our group research who have lent their helping hands throughout my PhD.

Many thanks my friends in Thailand for their thoughts and well-wishes sending across miles. A million thanks to all Thai-Soton friends for being by my side and making me feel like we are not just friend, but we are family.

Definitely, without my beloved family, I could not come this far. I would also like to express my special thanks to my parent and my brother for their unconditional love and for believing in me and supporting me to follow my dream.

Finally, my heartfelt thanks to my better half, Mrs Nanthanat Sriprasert who always encouraged and cheered me up when I was disheartened and frustrated during the difficult time of my PhD study. Thanks for her constant motivation, all the support and love. Thank you very much for following our dreams and have had a great time spent together.

Table of Contents

List of tables

List of figures

Definitions and Abbreviations

AD	Anaerobic Digestion
AeMBR	Aerobic Membrane Bioreactors
AF	Anaerobic Filter
AFMBR	Anaerobic Fluidized Membrane Bioreactor
AnMBR	Anaerobic Membrane Bioreactors
BC-N	Bio Contact-N
BPC	Biopolymer Clusters
CFD	Computational Fluid Dynamics
CIA	Cleaning-In-Air
CIP	Cleaning-In-Place
COD	Chemical Oxygen Demand
CSTR	Continuously Stirred Tank Reactor
DAF	Dissolved Air Flotation
DBP	Daily Biogas Production
DC	Direct Current
DI	Deionised
DOTM	Direct Observation Through the Membrane
EGSB	Expanded Granular Sludge Bed
EPS	Extracellular Polymeric Substances
FOG	Fat, Oil and Grease
GAC	Granular Activated Carbon
G-AnMBR	Granular-AnMBR
GSAnMBR	Gas-Sparged AnMBR
HLR	Hydraulic Loading Rate
HMBR	Hybrid Membrane Bioreactor
HRT	Hydraulic Retention Time
LDPE	Low Density Polyethylene
MBR	Membrane Bioreactors
MCP	Mechanical Cleaning Process
MLSS	Mixed Liquor Suspended Solids
MBAnMBR	Moving Bed AnMBR
MF	Microfiltration
NF	Nanofiltration
OHPA	Obligate Hydrogen Producing Acetogens

OLR	Organic Loading Rate
PAC	Powder Activated Carbon
PC	Personal Computer
PE	Polyethylene
PEG	Polyethylene Glycol
PES	Polyethersulfone
PET	Polyethylene Terephthalate
PP	Polypropylene
PSF	Polysulfone
PVC	Polyvinyl Chloride
PVDF	Polyvinylidene Difluoride
rpm	revolutions per minute
SBP	Specific Biogas Production
SEM	Scanning Electron Microscope
SG	Specific Gravity
SMA	Specific Methanogenic Activity
SMP	Specific Methane Production
SMP	Soluble Microbial Products
SOLR	Sludge Organic Loading Rate
SRB	Sulphate Reducing Bacteria
SRT	Solid Retention Time
SS	Suspended Solids
STP	Standard Temperature and Pressure
TOC	Total Organic Carbon
TCOD	Total Chemical Oxygen Demand
TE	Trace Element
TIF	Tagged Interchange File format
TMP	Transmembrane Pressure
TSS	Total Suspended Solids
UASB	Up-flow Anaerobic Sludge Blanket
UF	Ultrafiltration
VBP	Volumetric Biogas Production
VFA	Volatile Fatty Acid
VMP	Volumetric Methane Production
VSS	Volatile Suspended Solids

Chapter 1: **Introduction**

1.1 Background

Food industries are normally considered as the largest source of wastewaters that are characterised by high concentrations of organic pollutants. Among these industries, the dairy production process is one of the major wastewater generators due to the high water consumption and various effluent characteristics (Gutiérrez, Encina and Fdz-Polanco, 1991). Wastewater from this industry is generated from washing of processing equipment and product containers, with the major constituents being lactose, soluble milk proteins, carbohydrate and lipids, mineral salts, and chemicals and detergents (Chatzipaschali and Stamatis, 2012). Organic content in dairy wastewater is typically in the range of 2 - 6 g COD L^{-1} and can reach up to 15 g COD L^{-1} according to the type of processing applied. For certain dairy products, such as cheese and cheese whey wastewater, the effluent strength may exceed 50 - 70 g COD L^{-1} (Omil *et al.*, 2003; Carvalho, Prazeres and Rivas, 2013; Karadag *et al.*, 2015). Dairy effluents have therefore generally been regarded as representing a relatively high organic load with a high biodegradable content, which provides some advantageous characteristics for biological treatment processes.

Typically, the application of anaerobic digestion is more favourable as a forefront or mainstream process for diary wastewater treatment due to its combined advantages of high organic matter removal and energy recovery. In order to utilise this potential, however, a number of challenges need to be addressed. In particular, the high volume and medium to dilute wastewater strength means that the reactor type and volume will generally be determined by the permissible hydraulic loading rate (HLR) rather than by the incoming concentration or organic loading rate (OLR), in order to avoid biomass wash out (Lettinga, Rebac and Zeeman, 2001).

Over the last two decades, based in part on growing experience with aerobic membrane bioreactors (AeMBR) (Santos, Ma and Judd, 2011), the use of membranes coupled with anaerobic processes has attracted increasing attention. Anaerobic membrane bioreactors (AnMBR) can be considered the most recent development in high rate anaerobic treatment. The AnMBR offers complete biomass retention regardless of its settling properties, and thus enables the decoupling of hydraulic retention time (HRT) and solids retention time (SRT) (Liao, Kraemer and Bagley, 2006; Stuckey, 2012). As with aerobic membrane processes, AnMBR offer the superior effluent qualities free of suspended solids, and a small footprint requirement. Therefore, this technology has become an attractive alternative for many industrial wastewater treatment processes.

The central target of this research is to study the application of single-stage AnMBR to treat a low-to-medium strength particulate organic substrate such as diary wastewater, where slow-

growing anaerobic biomass can be completely retained inside reactor operating as a high rate anaerobic system in which the stages from hydrolysis to methanogenesis and gas/liquid/solid separation could occur in one reactor without a pre-treatment unit.

1.2 Justification and aim of the proposed research

Despite the many advantages of membrane bioreactors (MBRs), membrane fouling leading to low flux production and flux decline in long-term filtration with high membrane cleaning and operational costs, remains a crucial limitation that hampers the extensive implementation of MBR. Membrane fouling is an unavoidable circumstance and this phenomenon appears to be more severe in AnMBR than in aerobic systems due to their particular rheology (Liao, Kraemer and Bagley, 2006; Lin *et al.*, 2013). Generally, AnMBRs are operated at high biomass concentrations resulting in high viscosity of mixed liquor suspended solids (MLSS) (Le-Clech *et al.*, 2003), causing low sludge filterability which favours membrane fouling (Spagni *et al.*, 2010). Additionally, complex extracellular polymeric substances (EPS) and soluble microbial products (SMP) combined with small fine microbial particles and biomass composition lead to a more rapid and dense build-up of the cake layer when compared to AeMBR (Chang and Judd, 2002; Jeison and van Lier, 2006; Visvanathan and Abeynayaka, 2012).

Several approaches to understanding fouling mechanisms and mitigations in both AeMBR and AnMBR have been proposed and applied, and are reported in several comprehensive review papers (Le-Clech, Chen and Fane, 2006; Meng *et al.*, 2009; Drews, 2010; Lin *et al.*, 2013; Wang *et al.*, 2014). These are briefly outlined below.

1.2.1 Gas-liquid two-phase flow for MBRs

Air/gas sparging has been demonstrated significantly to enhance performance, and has been applied extensively to various membrane processes since the 1990s (Cui, Chang and Fane, 2003).

Typically, however, energy consumption for fouling mitigation by air/gas scouring always represents the largest proportion of energy required for MBR operations and can reach 70% of the total energy demand (Judd, 2011). This suggests that optimisation of two-phase gas-liquid flow and fluid dynamics in order to minimise energy demand are emerging aspects of prime importance for MBR system.

In the past, extensive research has been carried out on external inside-out tubular membrane systems. In spite of the recent growth in interest in submerged MBR systems due to their energy-saving features, however, research about air/gas sparging in submerged MBRs, particularly for flat sheet configuration is still very limited.

Although gas sparging has been applied widely in MBRs, the flow patterns are still not fully understood for submerged configurations since the dynamic flow fields in the vicinity of the membrane surface are very complex and slug bubbling cannot be completely formed.

Various sparger designs have been introduced by different flat sheet MBR manufacturers. For example, Kubota first used circular nozzles with 10 mm diameter on perforated tubes, and then changed the nozzles design to 4 mm diameter; whilst Microdyn Nadir applied fine porous tubes as bubble diffusers. Under the same sparging rate, porous bubble diffusers may present more favourable mass transfer characteristics than perforated tube spargers due to the high total mass transfer surface and uniformity of bubble generation. Nonetheless, a high pressure drop and resistance of porous diffuser must be taken into account with respect to the energy demand for bubbling. Furthermore, porous spargers such as porous ceramic discs or porous membrane tube diffusers could potentially be easily blocked by biomass particles, biofilm and slime, which then causes maldistribution of bubbles. In comparing perforated tube spargers and porous fine diffusers for AnMBR, where the oxygen transfer aspect is not important, pseudo-confined cap bubbles generated from perforated tube spargers are more favourable for fouling removal due to the higher shear stress arising in the gaps between flat plate membranes.

Increasing sparging rates results in better fouling mitigation, but at the same time this means a higher energy requirement. Moreover, beyond certain sparging rates, a plateau in favourable hydrodynamic parameters (such as bubble size, bubble frequency, crossflow velocity and shear stress etc.) has typically reported, with no further improvement in the extent of fouling control.

Therefore, this research proposed to study and optimise hydrodynamic parameters such as sparging intensities, bubble sizes and size distributions related to nozzle sizes on perforated tube spargers, bubble-membrane contact area, liquid flow velocities under various conditions and gaslift-loop tank geometry. This is with the aim of gaining better insight into the application of two-phase gas-liquid flow for fouling mitigation purposes in order to obtain the most effective exploitation of the energy input for gas sparging in submerged flat sheet AnMBR.

1.2.2 Gas-liquid-solid three-phase flow for MBRs

The integration of a mechanical cleaning process (MCP) by adding suspended scouring agents with MBR is one of the most useful techniques for fouling control (Krause *et al.*, 2010; Rosenberger *et al.*, 2011).

Active adsorbents such as granular activated carbon (GAC) or powder activated carbon (PAC) have been widely applied within MBR due to their effective combination of membrane scouring and pollutant adsorption properties. This strategy has limitations, however, since once the

adsorption capacity is reached the dominant mechanism for fouling control becomes physical scouring. In addition, they may also cause to membrane damage through abrasion, and/or clogging as particles disintegrate in long-term operation. Hence, the use of larger non-adsorbent particles as scouring media has been proposed.

This approach has been successfully operated with various AeMBR, but information about applying non-adsorbent suspended media in AnMBR, in which fouling is considered more intense than in AeMBR, is still very scarce. To our knowledge, the combined application of biogas sparging and non-adsorbent particles in AnMBR has never been examined, particularly in a system fed on low to medium-strength industrial wastewater with mainly particulate COD for long-term operation.

Therefore, the overall aim of this research is to study the application of gas-liquid-solid three-phase flow in submerged flat sheet AnMBR for dairy wastewater treatment in order to gain better insight into system performance as well as fouling control aspects, by conducting experiments to compare these with conventional gas sparged two-phase flow AnMBR.

1.3 Research Objectives

The following objectives were identified as necessary to achieve the above aim.

1. To characterise and optimise the effect of hydrodynamic parameters (such as gas flow rate, nozzle size and tank geometry) on gas-liquid two-phase flow characteristics (such as bubble size, size distribution and liquid flow velocity) in order to determine optimum design and operating conditions for a gaslift-loop submerged flat sheet membrane bioreactor.

2. To evaluate the option of using non-adsorbent suspended particles associated with gas sparging for fouling mitigation purposes, using a model feed and mixed suspension simulating an AnMBR system.

3. To examine and compare the performance of conventional gas-sparged two-phase AnMBR (GSAnMBR) with that of three-phase flow (gas-liquid-solid) in form of a moving bed AnMBR (MBAnMBR) with non-adsorbent particles for dairy wastewater treatment.

Chapter 2: **Literature review**

In this chapter, the fundamental principles of anaerobic digestion, the development of high rate anaerobic digestion for wastewater treatment, dairy wastewater characteristics and the importance of using anaerobic systems for dairy wastewater are presented. The development of MBRs as well as operational and fouling control strategies from related previous literature are introduced, particularly focusing on AnMBR since the system is the central object of this research. Attempts that have been made to optimise hydrodynamic conditions using gas-liquid two-phase flow in MBR are reviewed in order to pinpoint the advantages and limitations from literature studies. The approach of applying multi-phase flow as a flux enhancement strategy and for fouling mitigation purpose is also reviewed in detail.

2.1 Principles of anaerobic digestion

Anaerobic digestion (AD) is the degradation of organic matter by microorganisms such as bacteria, archaea and protozoa in the absence of oxygen. The decomposition involves a series of chemical reactions resulting in production of various gases such as methane, carbon dioxide and hydrogen sulphide, as well as other soluble substances such as ammonia (Gerardi, 2003). AD of organic substances is carried out by means of four reaction steps: hydrolysis, acidogenesis, acetogenesis and methanogenesis, which are dependent on each other for food and energy requirements as can be seen in Figure 2-1. Each step is performed by a specific class of microorganisms. In a balanced digestion system, the various biological conversion processes are sufficiently coupled to avoid the accumulation of any intermediate metabolites in the system.

Stage 1: Hydrolysis

Solid organic substances are broken down by hydrolytic bacteria with the aid of exoenzymes. Proteins, carbohydrates and fats are converted into amino acids, monosaccharides, organic acids including fatty acids and alcohols. Fermentative and hydrolytic bacteria convert monosaccharides into short chain fatty acids, alcohols, CO_2 and hydrogen.

Stage 2: Acidogenesis

Hydrolyzed products are degraded by fermentative bacteria into volatile fatty acids. Glycerol is converted into pyruvate, and fatty acid chains are degraded to acetic acid by β-oxidation reaction process. Certain groups of bacteria degrade amino acids by coupled oxidation-reduction reactions (Stickland reaction).

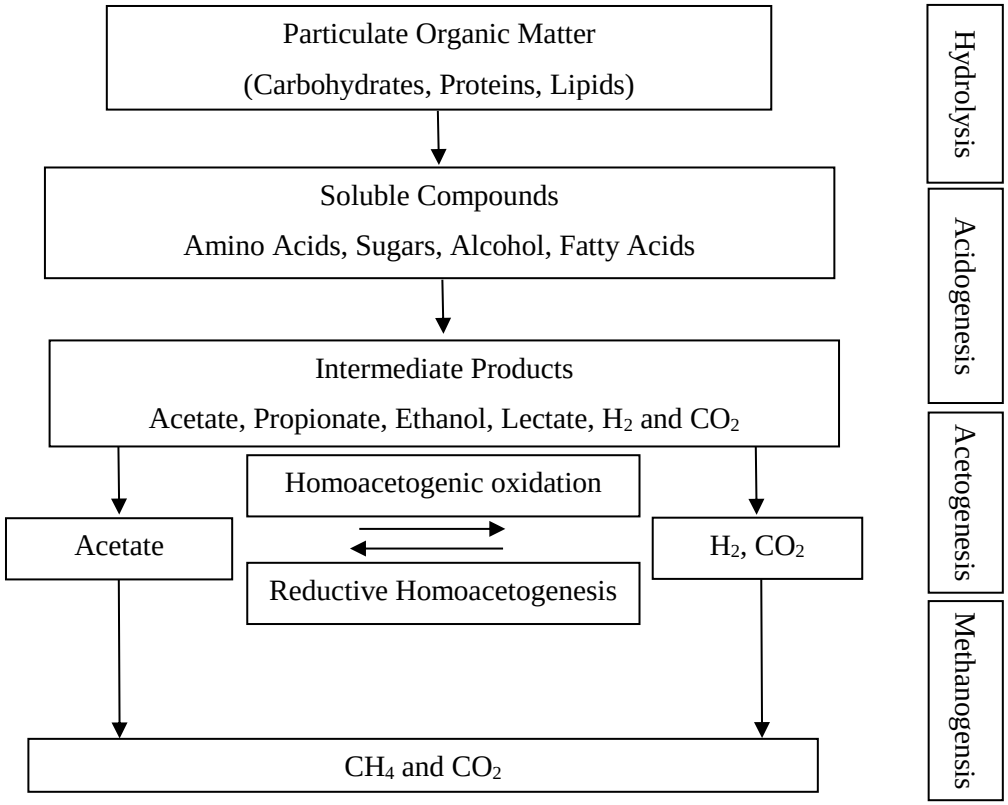

Figure 2-1 Metabolic routes for conversion of organic matter to the methanogenic substrates and finally to CH_4 and CO_2 (modified from Demirel and Scherer (2008))

Stage 3: Acetogenesis

The products of acidogenesis are further oxidised to acetate, hydrogen and carbon dioxide, and mediated by the obligate hydrogen-producing acetogens (OHPA). Acetate and H_2 are primarily derived from the acetogenesis and dehydrogenation of longer chain fatty acids and alcohol. OHPA bacteria are capable of producing acetate, H_2 and CO_2 from longer chain fatty acids, the main substrates for methanogens. For thermodynamic reasons, the conversion of ethanol, propionate, and butyrate into acetate by acetogens is feasible if the hydrogen produced is consumed at the place of origin by methanogenic archaea or sulphate reducing bacteria (SRB). Thus, close association of acetogens and methanogens/SRB is essential (Dhaked, Singh and Singh, 2010).

Stage 4: Methanogenesis

Methanogens are strictly anaerobic archaea that have a narrow substrate spectrum. Methanogens can be sub-divided into two groups: (i) hydrogenophilic or hydrogenotrophic species, which form methane by the reduction of H_2/CO_2 and (ii) acetoclastic or acetotrophic methanogens, which generate methane by acetate decarboxylation. Acetoclastic methanogens are considered the more important methanogenic species, as 70 % of the total methane generated during AD of domestic sewage is via this pathway (Grotenhuis, 1992; Lettinga, 1995).

2.1.1 Temperature ranges for anaerobic digestion

Temperature is one of the most important factors affecting microbial activity within an anaerobic digester, and methane production is strongly temperature dependent (Gerardi, 2003). Microorganisms are classified into 'temperature classes' on the basis of the optimum temperature and the temperature span in which the species is able to grow and metabolize. In fact, there is no clear boundary between these classic groups of psychrophilic, mesophilic and thermophilic microorganisms.

Different sources give slightly different temperature ranges but these can broadly be defined as: 45 - 60 °C, a thermophilic range; 30 - 40 °C, mesophilic; 20 - 30 °C, psychrotrophic and lower than 20 °C, psychrophilic (Safley Jr and Westerman, 1994; Nozhevnikova *et al.*, 2001a; Nozhevnikova *et al.*, 2001b).

Most full-scale anaerobic digesters are operated at mesophilic (24 - 45 °C) or thermophilic (45 - 65 °C) temperature ranges (McHugh, Collins and O'Flaherty, 2006; Ueno *et al.*, 2007). Psychrophilic anaerobic digestion has generally not been considered commercially feasible because of the poor substrate-utilization rates due to exhaustion of cell energy, low biogas production, low microbial activity, leakage of intracellular substances or complete lysis, and increased liquid viscosity and gas solubility under low-temperature conditions (Kettunen and Rintala, 1997; Lettinga *et al.*, 1999). Heating of the wastewater for mesophilic or thermophilic anaerobic digestion increases energy consumption and decreases cost-efficiency, thus resulting in a marginal or negative overall energy yield. Therefore, operation at ambient temperature is essential for economical implementation of anaerobic digesters for biogas production and wastewater treatment.

McKeown *et al.* (2009a), in a long-term study (1,243 days) on anaerobic treatment of acidified wastewater, found increased hydrogenotrophic methanogenic activity at psychrophilic temperatures. They also concluded that, while the temperature of operation certainly impacts on various pathways in anaerobic metabolism, there is no evidence that low temperatures are inhibitory to process performance under the appropriate operational conditions.

In addition, one of the major problems associated with anaerobic treatment and methanogenesis is the presence of sulphate, sulphite or thiosulphate. Sulphate-reducing bacteria (SRB) have the ability to utilise a range of substrates in the presence of sulphate, and therefore competitively interact with other micro-organisms involved in the process, resulting in the formation of H_2S rather than methane (Colleran, Finnegan and Lens, 1995; O'Flaherty *et al.*, 1998; O'Reilly and Colleran, 2005a;b). This competition is favorable to SRB based on thermodynamic considerations, but the actual outcome under operational conditions is not straightforward.

O'Flaherty, Collins and Mahony (2006) outlined the main manifestations of SRB-related problems which include reduction of methane yield, the inhibitory effect of H_2S on many bacterial trophic groups, thus reducing reactor performance as well as malodour and corrosion of piping, pumps, etc., resulting in the necessity for scrubbing of the biogas and effluents to meet discharge standards.

2.1.2 Dairy wastewater characteristics

Dairy industries are of importance worldwide since their products are an essential contribution to human nutrition. Several different products can be produced from raw milk such as pasteurised-, condensed-, skimmed-, and powder-milk, cheese, butter, cheese whey, ice-cream and various types of dessert (Vidal *et al.*, 2000). Dairy effluent volume and characteristics can vary significantly according to the variety of final and by-products, manufacturing processes and cleaning methods (Gutiérrez, Encina and Fdz-Polanco, 1991). Wastewater from this industry is generated from washing of processing equipment and product containers with the major constituents being lactose, soluble milk proteins and carbohydrate, lipid, mineral salts, acidic and alkaline chemicals, high concentrations of suspended solids along with milk solids, detergents, milk wastes, etc. (Chatzipaschali and Stamatis, 2012). Organic content in dairy wastewater is typically in the low to medium strength range for industrial wastewater at about 2 - 6 g COD L^{-1} but can be up to a strength of 15 g COD L^{-1} depending on the different types of processing and pre-treatment systems used. Certain dairy products, such as cheese and cheese whey wastewater, have very high strength effluents in the range of 50 - 70 g COD L^{-1} (Omil *et al.*, 2003; Carvalho, Prazeres and Rivas, 2013; Karadag *et al.*, 2015). Dairy wastewater is also characterised by high biodegradability with a BOD/COD ratio generally above 0.5 (Prazeres, Carvalho and Rivas, 2012). Total suspended solids are typically 0.2 - 5.1 g L^{-1} with more than half of these in volatile form. Furthermore, fat content in the range of 0.1 - 10.6 g L^{-1} and the presence of nutrients (N and P) also cause a high degree of contamination in the waste stream (Carvalho, Prazeres and Rivas, 2013). Most dairy effluents can be regarded as combining relatively high organic loads with ease of biodegradability. This makes them very suited to anaerobic digestion (Demirel, Yenigun and Onay, 2005) due to its capacity to deal with high organic loadings and the potential for energy recovery from the produced biogas.

2.1.3 High-rate anaerobic process for wastewater treatment

Anaerobic treatment of wastewater can be considered a well-established technology with a wide range of applications. In addition, high volumes of medium- to low-strength wastewater also represent a great potential for innovation in biogas production.

However, attempts to treat such diluted wastewater under psychrophilic conditions have not been very successful (Matsushige *et al.*, 1990). As already noted, temperature strongly affects the rate of the anaerobic conversion processes , andthe hydrolysis of retained particulate organic matter is generally considered to be the rate-limiting step in the overall process and requires relatively long retention times (Lettinga, Rebac and Zeeman, 2001; Walker, Banks and Heaven, 2009a; McKeown *et al.*, 2012). Therefore, a long solid retention time (SRT) is essential to maintain the slow growing anaerobic microbial populations in the treatment system and necessitates the elimination of even washout of minor viable biomass; while the required digester volume in the case of treating a high volume of diluted wastewater will generally be determined by the permissible hydraulic loading rate (HLR) rather than by the organic loading rate (OLR). Furthermore, with low temperature, mixed liquor viscosity could be increased which causes difficulty in solid liquid separation facilities. Consequently, more sophisticated reactors are needed.

One of the major successes in the development of anaerobic wastewater technology able to cope with high volume, diluted wastewater conditions was the introduction of high-rate reactors in which biomass and liquid retention are uncoupled (Lettinga, 1995). Micro-organisms may then be efficiently retained in the immobilized/retained biomass, while the enrichment of methanogenic consortia is also promoted by the very low decay rates (Lettinga, Rebac and Zeeman, 2001).

High-rate anaerobic reactors may be classified based on the means of biomass retention: for example, suspended growth systems with membrane separation (e.g. anaerobic membrane reactor (AnMBR)); attached growth systems (e.g. anaerobic filter [AF]); and granular sludge-based systems (e.g. up-flow anaerobic sludge blanket [UASB] and expanded granular sludge bed [EGSB] reactor). Hybrid combinations have also been developed, including sludge bed-fixed bed reactors and granular reactors with an internal/external membrane unit for solid-liquid separation (McKeown *et al.*, 2012).

Granule- and biofilm- based processes represent the traditional methods of biomass augmentation for high rate anaerobic bioreactors in order to achieve high organic loading capacities (Skouteris *et al.*, 2012), due to the poor settling properties of dispersed anaerobic biomass where solid-liquid separation has to rely on gravity sedimentation (Smith *et al.*, 2012). The use of granular sludge in up-flow anaerobic sludge blanket (UASB) reactors is well-established and has been successfully applied to dairy wastewater treatment (Borja and Banks, 1994; Bialek *et al.*, 2011; Buntner, Sánchez and Garrido, 2013), and biofilm process (Borja and Banks, 1995; Hawkes, Donnelly and Anderson, 1995; Karadag *et al.*, 2015). Anaerobic granular sludge is the most commonly used high rate process, in which granule formation and sufficient retention of slow growing biomass

are of prime importance. Certain wastewater characteristics such as high suspended solids (SS), high fat, oil and grease (FOG) content, toxicity, or drastic fluctuations in temperature, organic loading rate (OLR) and hydraulic retention time (HRT) can have negative impacts on sludge granule formation, or even bring about de-granulation (Vidal *et al.*, 2000; Dereli *et al.*, 2012). For instance, the presence of FOG in dairy wastewater may cause sludge flotation and washing out of active microbial biomass in bioreactors (Perle, Kimchie and Shelef, 1995); difficulty in lipids biodegradation has been reported (Petruy and Lettinga, 1997), and these factors may limit overall system performance.

The most recent development in high rate anaerobic treatment is using membranes to separate biomass from the effluent. Anaerobic membrane bioreactors (AnMBRs) offer high quality effluents free of solids and pathogens due to their superior treatment efficiencies, regardless of their settling and/or granulation properties (van Lier *et al.*, 2001) compared to conventional or the other high-rate anaerobic reactors. Additionally, AnMBR can perform as a single (stand-alone) reactor or be integrated with the other high-rate anaerobic reactors as hybrid combinations. Therefore, this technology may present an attractive option for treating of medium to low-strength municipal and/or industrial wastewater (Dereli *et al.*, 2012).

2.2 Membrane bioreactor (MBR)

Over the last two decades, membrane technologies have been successfully used for biological wastewater treatment processing. AnMBR can be simply defined as an anaerobic bioreactor coupled with membrane filtration to provide solid-liquid separation. A complete retention of all microorganisms in the bioreactor can be achieved in membrane bioreactors (MBRs), in which HRT and SRT are decoupled. The AnMBR technology also offers advantages in terms of reduced footprint, low sludge production, capacity for handling wide fluctuations in influent quality and improved effluent quality. Despite these advantages, there are still critical obstacles such as low flux, membrane fouling, high capital and operational costs that limit the extensive use of AnMBRs (Ersu and Ong, 2008; Jeison, van Betuw and van Lier, 2008; Jeong *et al.*, 2010). Recent technical innovations and significant reductions in membrane cost leading to a decrease in capital costs have enabled the acceptance of immersed MBRs for wastewater treatment (Singhania *et al.*, 2012). However, operational costs related to energy requirements for gas/liquid recirculation for membrane fouling control and chemical costs required for membrane cleaning are still heavy burdens on the economic feasibility of AnMBRs (Lin *et al.*, 2013).

2.2.1 Membrane pore size, material and module type

Like commercial aerobic membranes, most anaerobic membrane modules used in AnMBR studies tend to be in the coarse Ultrafiltration (UF) to fine Microfiltration (MF) range (Judd, 2011), with the pore size from 0.03 - 1.0 micrometre as summarised by Lin *et al.* (2013). This pore size range is obviously lower than the size of the most flocs or microorganisms in AnMBR, and therefore can almost completely retain biomass.

Membrane materials can be classified into three major categories: polymeric, metallic and inorganic (ceramic). Ceramic membranes can be backwashed effectively, and provide high resistance to corrosion, abrasion, and fouling as well as increased control of concentration polarization. Metallic membranes have also been used in AnMBR systems, showing better hydraulic performance, better fouling recovery, higher ability to endure impact forces and higher tolerance to oxidation and high temperatures compared to polymeric membranes. However, ceramic or metallic membranes are much more expensive than polymeric membranes leading to a high degree of interest in polymeric membranes. The major preferred polymeric membrane materials are polyvinylidene difluoride (PVDF) and polyethersulfone (PES), while other polymeric materials such as polyethylene (PE), polypropylene (PP) and polysulfone (PSF) are also used on some cases for AnMBR applications (Lin *et al.*, 2013).

Most membrane modules used in AnMBRs are implemented as hollow fibre, flat sheet (plate or frame) or tubular. Due to their high packing density and cost efficiency, hollow fibre membrane modules are most popular for use in submerged MBRs. However, submerged flat sheet membrane modules also retained significant interest for their advantages of good stability, and the ease of cleaning and replacement of defective membranes. A tubular membrane module is made up of several tubular membranes arranged as side-stream configuration. The main advantages include low fouling, relatively easy cleaning, easy handling of suspended solids and viscous fluids and the ability to replace or plug a damaged membrane, while the disadvantages include high capital cost, low packing density, high pumping costs and high dead volume.

In addition, since membranes only serve for solid-liquid separation, and an improved effluent quality might not always be required, there is growing interest in developing low cost filters and using dynamic or secondary membranes in MBRs. The low-cost filters investigated include woven fabric (Ersahin *et al.*, 2014), non-woven (Chang *et al.*, 2006; An *et al.*, 2009a), meshes (Wang *et al.*, 2006; Walker, Banks and Heaven, 2009a;b) and filter cloths (Moghaddam *et al.*, 2006; Ye *et al.*, 2006) as summarized by Meng *et al.* (2009). The sludge cake layer and gel layer that dynamically form on the filtration medium were found effective in enhancing the solid-liquid separation, and the effluent quality could be kept at a stable level with undetectable suspended

solid (SS) concentration (Fan and Huang, 2002; Zhang *et al.*, 2010), suggesting a promising material for separation in AnMBRs.

2.2.2 Anaerobic membrane bioreactor configurations and permeate driven processes

AnMBR can exist in three configurations: pressure-driven external cross-flow, vacuum-driven internal submerged, or vacuum-driven external submerged (Liao, Kraemer and Bagley, 2006).

In a pressure-driven external cross-flow configuration, the membrane unit is separate from the bioreactor and the membranes operate under pressure to produce permeate. Suspended anaerobic biomass maintained in the bioreactor is pumped into the membrane unit, creating a positive pressure that leads to permeate production and generating high cross-flow velocity for fouling mitigation. The rejected biomass or retentate is returned to the bioreactor. Most membrane modules used in this configuration are inside-out flow tubular membranes.

In a vacuum-driven internal submerged membrane configuration, membranes are submerged directly into the suspended biomass in the bioreactor and permeate is produced by exerting a vacuum on the membrane by suction pumps or liquid gravitational head. Because the velocity of the liquid across the membrane cannot be as readily controlled and is much lower compared to the external cross-flow configuration, fouling and cake formation can be disrupted by vigorously bubbling biogas across the membrane surface. Usually flat sheet and hollow fibre modules are applied for the submerged membrane configuration.

Alternatively, membranes may be located in an external chamber separate from the main bioreactor, but still submerged in suspended biomass and operated under vacuum. In an external submerged configuration of this type, suspended biomass from the main bioreactor is pumped to the external chamber, while retentate is returned to the bioreactor. This configuration facilitates membrane cleaning and replacement by allowing isolation of the membrane unit in an external chamber. This separation enables anaerobic conditions to be maintained in the main bioreactor during membrane cleaning or replacement (Smith *et al.*, 2012).

AnMBRs configured with external cross-flow membranes may provide a higher flux and need a lower membrane area in comparison to their submerged counterparts. The energy required for the crossflow pumps would be high, however, due to the high flow needed to provide enough hydraulic shear force (Ozgun *et al.*, 2013). Moreover, high hydraulic shear force may also disrupt anaerobic biomass and generate small particles, which result in significant membrane fouling. The biological activity of anaerobic biomass may also decrease due to the high hydraulic shear force and crossflow velocity (Lin *et al.*, 2010).

2.2.3 Membranes integration with different types of high-rate anaerobic reactors

Membranes can be coupled to various high-rate anaerobic reactors, such as completely stirred tank reactors (CSTR), AF, UASB and EGSB reactors, in different configurations and biomass morphology. In the membrane and CSTR combination, dispersed biomass is maintained in completely suspended condition in the main reactor with either an internal or an external membrane separation unit, which means a secondary clarifier as in conventional CSTRs is not required. In high-rate anaerobic reactors such as sludge bed systems and anaerobic filters, biomass is retained either by the formation of granules and/or thick flocculent digestate or by attachment to a support material. Effluent SS concentration is significantly lower than the overall biomass concentration in the reactor, which makes them feasible for medium to low strength wastewater with high hydraulic loadings. As in these reactors biomass is not directly subjected to membrane filtration, dense cake layer formation and consolidation will be less apparent in comparison with CSTRs when combining these reactors with a membrane module.

2.2.3.1 Completely stirred tank reactors (CSTRs)

To date, CSTR is the most common anaerobic process researched in AnMBR systems (Grundestam and Hellstrom, 2007; Ho, Khanal and Sung, 2007; Hu and Stuckey, 2007; Kocadagistan and Topcu, 2007; Vyrides and Stuckey, 2009; Ho and Sung, 2010; Giménez *et al.*, 2011; Martinez-Sosa *et al.*, 2011) in analogy to the type of bioreactors used in aerobic MBRs. In general, CSTRs are operated at equal HRT and SRT without any internal biomass retention device. In membrane coupled CSTRs, however, the complete retention of solids in the reactor decouples SRT from HRT, which leads to an increase in biomass concentration and thus increase in conversion rates alleviating the rate limiting step, e.g. hydrolysis/solubilisation of solids and/or methanogenesis. Often CSTRs are coupled to external crossflow membranes, resulting in high bioreactor liquid turnover rates, leading to a well-mixed flow regime. Directly submerging the membrane into the bulk digestate results in heavy membrane fouling and low fluxes. Subjecting a high solids concentration to membrane filtration exacerbates cake deposition in CSTR configurations, with either pressure-driven or vacuum-driven membranes. Moreover, sludge recirculation through the membrane feed pump, especially for external cross-flow membranes, results in a substantial decrease in the mean particle size (Martinez-Sosa, Helmreich and Horn, 2012). On the one hand, disruption of particles may positively impact on hydrolysis, but on the other hand it may negatively impact the juxtapositioning of acetogens and methanogens, limiting the required interspecies hydrogen transfer for attaining a high specific methanogenic activity (SMA) (Brockmann and Seyfried, 1997; Padmasiri *et al.*, 2007). Furthermore, it appears that shear itself may inhibit methanogens by increasing cell lysis, and enhance the release of both

extracellular polysaccharide (ECP) and soluble microbial products (SMPs) which causes severe membrane fouling (Ozgun *et al.*, 2013).

Martinez-Sosa *et al.* (2011) studied a pilot-scale AnMBR with a total volume of 350 L for low-strength (average total COD from 398 to 630 mg L^{-1}) municipal wastewater treatment. The system consisted of an external UF flat sheet membrane with a mean pore size of 38 nm and a total membrane surface of 3.5 m^2 coupled to a CSTR. The pilot was operated for 100 days over which the temperature was reduced from 35 to 28 °C on day 69, and then to 20 °C on day 79. Membrane fouling was controlled using biogas sparging, membrane relaxation, and periodic backwashing. The reactor was operated at a sub-critical flux of 7 L m^{-2} hour (LMH) and an HRT of 19.2 hours during the entire operational period. Suspended biomass was only removed from the AnMBR for sampling purposes and therefore the system had an SRT of approximately 680 days. It was found that COD removal efficiencies close to 90 % were achieved at both 35 and 20 °C and the effluent obtained could be used for agricultural irrigation. A stable cake layer formation on the membrane surface may compensate for differences in biological organic matter degradation rates at different temperatures. Although CH_4 recovery at 20 °C is lower, owing to the higher solubility of CH_4 at lower temperatures, the methane content of the biogas was higher at low temperatures due to the difference in gas solubility of CO_2 and CH_4 at 20 °C compared to 35 °C. Lower solubility of methane in comparison to CO_2 at 20 °C resulted in a major proportion of CO_2 in the liquid phase leaving the reactor and an increase in the proportion of methane from 80 to 88 % in the gas phase.

Giménez *et al.* (2011) operated a pilot-scale facility fed with pre-treated diluted wastewater at a 70 day SRT, an HRT ranging from 20 to 6 h, and a temperature of 33 °C. The pilot consisted of an anaerobic CSTR connected to two membrane tanks with 0.05 µm hollow fibre membranes. The total liquid volume of the system was 2500 L. The pilot also included a rotofilter for pre-treatment screening, an equalization tank, and a degasification vessel installed between the membrane tanks and permeate pump. Biogas sparging, relaxation, and back flushing were employed for membrane fouling control. The total and soluble COD concentrations in the influent averaged 445 ± 95 and 73 ± 25 mg L^{-1}, respectively, with particularly high sulphate concentration, averaging 297 ± 54 mg L^{-1}. During the study, COD removal averaged 87 % during stable operation resulting in a permeate COD of 77 mg L^{-1}. The high levels of sulphate in the influent greatly impacted biogas production as methanogens and sulphate reducers compete for substrates. Theoretically, 0.67 mg L^{-1} of COD is consumed per 1 mg L^{-1} of sulphate reduced, therefore, assuming complete sulphate reduction occurred, approximately 45 % of the influent COD would be required for sulphate reduction rather than for methanogenesis. Despite substantial production of sulphides during operation, the methane content in the biogas averaged 55 %. No irreversible fouling was observed during the study, indicating that the combination of relaxation,

backflushing, and biogas sparging was effective at preventing fouling while operating at a sub-critical flux of 10 L m^{-2} $hour^{-1}$(LMH). According to the authors Giménez *et al.* (2012), the pilot was also used to investigate the effect of lower temperature on methane recovery efficiency. They obtained slightly lower values at 20 °C in comparison to 33 °C due to a reduction in the treatment efficiency and an increase in the gas solubility.

2.2.3.2 Upflow anaerobic sludge blanket reactors (UASB)

UASB reactors coupled to membrane separation can be a reasonable option to decrease the SS concentration being sent to the membrane, since the sludge bed would entrap most of the particulate matter by adsorption and biodegradation (Kataoka *et al.*, 1992; An *et al.*, 2009b; Wu *et al.*, 2009; Zhang *et al.*, 2011b). All biological processes take place inside the dense granular and/or thick flocculent digestate bed in the bottom of the reactor. Therefore, UASB reactors can be used as biofilters before membrane treatment, which prevents the membrane from excessive exposure to high SS concentrations. In this context, HRT and upflow velocity in membrane coupled UASB reactors seem to be the critical parameters determining the efficiency and effluent fouling propensity. High SRTs and OLRs can be maintained by applying UASB reactors, without increasing the effluent solids concentration that will be subjected to membrane filtration. Thus, membrane flux may become less dependent on the reactor MLSS concentration, possibly leading to high membrane fluxes.

Despite the expected increase in efficiency from the membrane filtration step, for the treatment of wastewater under sub-mesophilic conditions, hydrolysis of the retained particulates is likely to become the rate-limiting step and particulate matter accumulation in the sludge bed will occur, subsequently resulting in activity loss (Lettinga, Rebac and Zeeman, 2001). Furthermore, a thinner and less porous cake layer on the membrane surface can be expected, possibly leading to more serious pore clogging problems in UASB-coupled AnMBRs, since the membrane would be exposed directly to only fine particles (submicron) instead of a range of particle sizes (Ozgun *et al.*, 2013). In addition, biomass growth on the membrane surface, colloidal solids, soluble microbial products and extracellular polymeric substances (which includes extracellular carbohydrates, proteins, lipids, and nucleic acids) are also important contributors to membrane fouling (Berube, Hall and Sutton, 2006). Therefore, AnMBR designs that limit membrane-biomass contact are not guaranteed to reduce fouling.

Martin Garcia *et al.* (2013) evaluated the low-strength wastewater treatment efficiency of a granular-AnMBR (G-AnMBR) and suspended growth (AnMBR) anaerobic membrane bioreactor under UK weather conditions (8 - 22 °C). The pilot G-AnMBR was comprised of a 95 L granular biomass reactor coupled with an 30 L external submerged membrane tank (hollow fibre PVDF

membrane, pore size of 0.08 µm and surface area of 0.93 m^2). The bed was seeded with 40 L of granular sludge sourced from a sugar processing factory generating a packed sludge bed with a biomass concentration of 70 g VSS L^{-1}. The effluent from the granular biological tank overflowed into the membrane tank through a floating valve, and was then recycled back to maintain an upflow velocity of 0.7 - 1 m $hour^{-1}$. The pilot AnMBR system was a 1,200 L CSTR inoculated with municipal anaerobic digested sludge to making a total concentration of 10 g VSS L^{-1} in the reactor. A submerged 0.04 µm pore size hollow fibre PVDF membrane module with surface area of 12.5 m^2 was installed in a separate chamber. The suspended biomass was cycled between the biological and membrane tanks through external pumps in order to homogenise the reactor contents between both chambers. Nitrogen gas provided by a nitrogen generator was employed for membrane cross flow gas sparging. Gas velocities ranging from 0.02 m s^{-1} to 0.078 m s^{-1} and from 0.02 m s^{-1} to 0.057 m s^{-1} were applied during normal operation in the AnMBR and G-AnMBR. Gas velocities (U_g) were calculated based on the gas flow and the free cross sectional area of the membrane modules (177 cm^2 for AnMBR and 74 cm^2 for G-AnMBR). The permeate was extracted through peristaltic pumps in which the flux was set at 6 LMH equating to a HRT of 16 hours. Biomass was withdrawn from the AnMBR to maintain SRT of 100 days while for the G-AnMBR no biomass was withdraw apart from the 1 - 2 L sampled each week from the membrane tank for analysis. Settled primary wastewater from sewage with average total COD 338 ± 74, soluble COD 183 ± 50 and BOD_5 155 ± 46 mg L^{-1}, respectively, was used as a feed source throughout 250 days of operation. Both systems presented COD and BOD removal efficiencies of 80 - 95 % and > 90 % respectively. However, effluent COD increased from 25 mg L^{-1} to 75 mg L^{-1} as temperature decreased from 25 - 10 °C, indicating the production of non-biodegradable organics at lower temperatures. Recycling of the mixed liquor from the membrane tank to the bioreactor at a low upflow velocity enhanced the interception of solids in the sludge bed of the G-AnMBR, limiting the solid and colloidal load to the membrane as compared to the suspended system. No significant differences were observed between granular and dispersed systems with respect to COD and BOD removal. Although critical flux steps revealed that increasing gas sparging intensities results in enhancement of permeate flux, the results suggested that lower gas sparging intensities were required in the granular system. Therefore, it was demonstrated that the granular AnMBR exhibited greater potential for reducing energy demands especially when backwashing was implemented.

Buntner, Sánchez and Garrido (2013) investigated the feasibility of a combined UASB and AeMBR system for the treatment of semi-synthetic dairy wastewater generated after a dissolved air flotation (DAF) stage (influent COD range 1,000 - 2,000 mg L^{-1}) at ambient temperatures. The system consisted of a 120 L methanogenic UASB stage and a two compartment post-treatment (36 L and 20 L) aerobic MBR stage, with a 0.04 µm pore size and surface area of 0.9 m^2 hollow

fibre membrane UF module. The entire system performed over 292 days in the HRT range of 14 - 20 hours. The system presented a high tolerance to loading changes (up to 4.85 kg COD m^{-3} day^{-1}) and temperature fluctuations (17 - 25 °C). The average total and soluble COD removals were above 95 %, reaching 99 % during stable operating periods. COD removal efficiency in the first methanogenic chamber increased with temperature, causing a diminution of the biodegradable COD supplied to the aerobic stages, which therefore led to a lower MLVSS concentration and a higher fouling rate in the membrane. The observed overall biomass yield was low, from 0.13 to 0.07 g MLVSS g COD^{-1}. Biogas production reached 150 L kg^{-1} of total COD, with an average methane content of 73 %. With respect to membrane performance, permeability values between 140 and 225 L m^{-2} $hour^{-1}$ bar^{-1} were obtained, similar to those reported for aerobic MBR systems. The average flux obtained was 13 L m^{-2} $hour^{-1}$, reaching 19 L m^{-2} $hour^{-1}$during stable operating periods depending on conditions. These values were lower than those observed in AeMBR systems, but much higher than those found in AnMBRs.

2.2.3.3 Expanded granular sludge bed (EGSB)

UASB reactors treating diluted wastewater at low and moderate temperatures are sometimes characterized by a poor mixing regime, which causes a decrease in soluble COD treatment efficiency. To solve this problem, tall reactors (high height : diameter ratio) with a small footprint and external or internal effluent recirculation are being applied, i.e. the so-called EGSB reactors. Bench scale and semi- pilot studies have shown that an EGSB reactor is an attractive alternative, especially for the treatment of low strength wastewaters at ambient temperatures, due to the efficient biomass-substrate contact induced by the applied high upflow velocity (Kato, Field and Lettinga, 1997; Lettinga *et al.*, 1999). Furthermore, it is thought that the high recycle rate may physically strip dissolved metabolic gases from the reactor liquor, and bioenergy yields that are comparable to mesophilic treatments have been demonstrated during low temperature operation trials (Connaughton, Collins and O'Flaherty, 2006). In addition, higher OLRs can be applied in EGSB reactors compared to UASB reactors. Suspended solids removal from the wastewater is limited, however, and biomass wash-out would occur in the system due to the high velocity. The maintenance of 'healthy', well-settling, anaerobic granules under low-temperature conditions, and in the presence of high upflow velocities (with high potential for granule shearing), may be difficult in certain instances, and this may limit the applicability of EGSB systems (Lettinga, Rebac and Zeeman, 2001). Hybrid reactors, incorporating an anaerobic filter section or a membrane unit, which enables slow-growing psychoactive biomass lost from the granular sludge bed to be entrapped as fixed-film growth on a support matrix or completely retained in system can overcome this problem (Wen, Huang and Qian, 1999; Chu, Yang and Zhang, 2005; Collins *et al.*, 2006; McKeown *et al.*, 2009b).

Chu, Yang and Zhang (2005) investigated the performance of an EGSB reactor coupled with hollow fibre membrane filtration for treating synthetic domestic wastewater (total COD in the range of 383 - 849 mg L^{-1}) at moderate to low temperature. The 4.7 L EGSB reactor had an internal diameter of 0.056m and 1.7m height, coupled with a bundle of U-shaped hollow fibre membranes made of polyethylene with a pore size of 0.1 µm and a filtration area of 0.1 m^2, which were submerged in the upper part of the EGSB reactor. The applied high upflow velocity (3 - 8 m $hour^{-1}$) was beneficial in the reduction of membrane fouling due to the increased hydraulic shear stress on the membrane surface. The system was operated under temperatures in the range of 11 - 25 °C for 210 days, at HRT of 3.5 - 5.7 hours and an approximate SRT of 145 days. The results showed that with temperatures above 15 °C, the system was capable of removing 85 - 96 % of total COD and 83 - 94 % of total organic carbon (TOC). At 11 °C, increasing HRT from 3.5 to 5.7 hours increased the total COD removal from 76 to 81 %. Applying a higher upflow velocity contributed to better effluent removal efficiency and higher membrane permeability. Cake layer resistance governed the achievable flux over the hollow fibre membranes, whereas pore blocking was only of minor importance. More EPS tended to accumulate on the membrane surface than in the granules.

According to these results, submerged membrane configurations may be more appropriate than external cross-flow configurations for the use of EGSB reactors in AnMBRs. However, membrane integration eliminates the hydraulic selection pressure required for granulation, by avoiding the wash out of flocculent sludge with poor immobilization characteristics (Ozgun *et al.*, 2013). Therefore, no granulation is expected in EGSB reactors coupled to membrane filtration, which would decrease the settleability of the biomass in long-term operation.

2.2.4 Membrane fouling

Membrane fouling remains the critical obstacle limiting the application of AnMBR. Membrane fouling could decrease permeate flux and system productivity, and hence increases the area of membranes per volume of reactor. It creates a need for frequent cleaning which might reduce the membrane lifespan and result in higher replacement or capital costs, and also increases the energy requirement for sludge recirculation or gas scouring. Fouling is an extremely complex phenomenon which is caused by a combination of components in the reactor (soluble organics, colloidal particles from the feed and cell lysis, and inorganic precipitates). These in turn are influenced by a range of parameters such as the composition of the biological system, membrane type, hydrodynamic conditions, and reactor operating conditions and process performance. Methods to control fouling including manipulating bioreactor conditions, adjusting

hydrodynamics and flux and optimising module design have been applied (Le-Clech, Chen and Fane, 2006).

2.2.4.1 Fouling types and foulants

Although membrane fouling definitions are not consistent in the literature, it can traditionally be classified into reversible fouling which is defined as the fouling that can be remove by physical cleaning; and irreversible fouling which can be removed by chemical cleaning but cannot be remove by the physical methods. Meng *et al.* (2009) further categorised reversible fouling into removable fouling and irremovable fouling. Removable fouling refers to fouling that can be removed by physical means, such as back flushing or relaxation under cross flow conditions; while irremovable fouling refers to fouling that can only be removed by chemical cleaning. The irreversible fouling is a permanent fouling which cannot be eliminated by any cleaning methods.

Potential foulants in AnMBRs are inorganic precipitates such as struvite (Doyle and Parsons, 2002; Salazar-Peláez, Morgan-Sagastume and Noyola, 2011) and other phosphate and calcium salts (Kang, Yoon and Lee, 2002; Trzcinski and Stuckey, 2009), or biological organic material like soluble microbial products (SMP), extracellular polymeric substances (EPS): mainly bound protein-based EPS, biopolymer clusters (BPC) and microbial cells, with biomass composition playing an important role in membrane fouling (An *et al.*, 2009a; Lin *et al.*, 2009; Gao *et al.*, 2010). EPS are generally defined as polymeric materials bound to the cell surface which are extracted using different chemical and physical methods. SMP are defined as microbial products released into the bulk solution as a result of the cell lysis, the hydrolysis of EPS as well as of the interaction of the microorganism with its surroundings. Therefore, while EPS are, by definition, of extracellular origin, SMP originate from cell lysis and decay (Aquino *et al.*, 2006). Finally, BPC are a solute independent of the biomass in the sludge suspension and are much larger than SMP (Wang and Li, 2008).

Membrane fouling can be either internal, due to membrane pore blocking; or external, due to cake formation, with cake layers being defined as porous layers rejected on the membrane surface (Meng *et al.*, 2007b). Internal fouling is usually irreversible, compared to cake formation, which is usually reversible (Jeison *et al.*, 2009). Cake formation has been found to be the main factor governing the applicable membrane permeate fluxes (Jeison and van Lier, 2007a; Gao *et al.*, 2011b). Small flocs, bound-EPS and inorganic materials played an important role in the cake formation process, with the cake layer being found to have a highly heterogeneous structure (Lin *et al.*, 2011c). Especially at lower temperatures of 20 °C, higher concentrations of SMP are present in the mixed-liquor leading to a reduction in the membrane permeate fluxes (Berube, Hall and

Sutton, 2006; Trzcinski and Stuckey, 2010). Once membrane permeate fluxes higher than the critical value are applied, cake formation proceeds rapidly (Jeison and van Lier, 2007b).

2.2.4.2 Measures for membrane fouling mitigation

Though membrane fouling is an unavoidable phenomenon, different measures can be applied to mitigate it. Stuckey (2012) concluded that there are three main ways of managing fouling in an AnMBR: firstly, by operating at high fluxes for short periods of time and then relaxing/back flushing and cleaning the membranes with aggressive acids/bases/oxidants. Secondly, by operating at below critical flux levels (Field *et al.*, 1995; Le Clech *et al.*, 2003) and only relaxing/back flushing and cleaning occasionally. Thirdly, by trying to reduce the degree of fouling by operating the reactor in such a way to minimise SMP/colloid production, using hydrodynamics in the reactor to minimise the fouling layer, or treating the reactor contents to remove the primary foulants (Stuckey, 2012).

2.2.4.2.1 HRT and SRT

HRT and SRT are important operational parameters which affect both treatment performance and membrane fouling. In the context of high volume and low strength wastewater treatment, a low HRT is desirable to reduce reactor size and capital cost, whereas a high SRT may be required to achieve retention of slow growing biomass particularly under lower temperature conditions (O'Flaherty, Collins and Mahony, 2006). However, increasing the SRT, while keeping the HRT constant, increases the suspended biomass concentration potentially leading to decreased permeate flux (Liao, Kraemer and Bagley, 2006; Herrera-Robledo, Morgan-Sagastume and Noyola, 2009). Furthermore, increasing the SRT may stimulate inert decay products (Casu *et al.*, 2012) also resulting in higher SMP and EPS production (Jeison and van Lier, 2006; Huang, Ong and Ng, 2011), and the accumulation of inorganic solids such as Ca, Mg, PO_4 salts and silt (Kang, Yoon and Lee, 2002), which play a significant role in fouling propensity. Therefore, a trade-off could exist between controlling HRT and SRT for membrane fouling mitigation and obtaining the necessary treatment performance (Smith *et al.*, 2012).

Hu and Stuckey (2006) observed a minor decline of approximately 5 % in COD removal when reducing the HRT from 48 hours to 24, 12, 6, and 3 hours during treatment of low-strength synthetic wastewater (influent COD 460 mg L^{-1}) at 35 °C. Even at a HRT of 3 hours, COD removal greater than 90 % was achieved. Comparing HRTs of 3.5, 4.6, and 5.7 hours, Chu, Yang and Zhang (2005) did not observe a correlation between treatment performance and HRT at temperatures greater than 15 °C. In addition, Huang, Ong and Ng (2011) found that treatment performance was independent of HRT when comparing HRTs of 8, 10, and 12 hours in an AnMBR treating a simulated low-

strength wastewater at 25 - 30 °C. Several other studies similarly concluded that HRT had little effect on AnMBR permeate quality (Lew *et al.*, 2009; Baek, Pagilla and Kim, 2010).

However, Salazar-Peláez, Morgan-Sagastume and Noyola (2011) observed an increase in retentate EPS and SMP concentrations at the lowest HRT, which resulted in increased membrane fouling. The authors recommended a lower limit be placed on HRT due to fouling concerns. Furthermore, Huang, Ong and Ng (2011) noted that combining a short HRT with a long SRT leads to increases in suspended biomass concentrations, which positively correlates with membrane fouling rates. Taken together, these studies suggest that adequate AnMBR treatment performance may be obtained at relatively short HRTs even at low temperatures, but that a lower limit on HRT may exist primarily due to concerns with membrane fouling.

The anaerobic microorganisms with their low growth rates could be retained within the systems for operating with a long SRTs in order not only to maintain high MLSS concentration but also to reduce the reactor volume (Ho and Sung, 2010). In principle, the application of long SRT is desirable for high-rate systems since it corresponds to lower excess sludge production and high biomass concentrations to maintain low F/M ratios. However, since SRT is not an independent factor, too long SRT may affect AnMBRs treatment efficiencies and cause fouling issues. For instance, the long SRT causes an increase in TSS concentration, which tends to induce inert solid accumulation inside the reactor as shown by a decrease in VSS/TSS ratio as the TSS in systems increased (Laera *et al.*, 2005; Casu *et al.*, 2012).

In addition, high MLSS concentrations due to long SRT directly affect the filterability of MBRs. Higher MLSS results more retention of sludge particles, fine colloids, macromolecular substances and microbial products which strongly impact on sludge viscosity and mixed suspension rheology (Deng *et al.*, 2016a). Hence, higher MLSS and viscosity could adversely affect membrane performance in terms of higher TMP, more rapid flux decline, reduction of filtration efficiency and greater fouling resistance (Meng *et al.*, 2007a; Kornboonraksa and Lee, 2009; Lay, Liu and Fane, 2010). For example, correlations between MLSS concentrations and fouling have been shown in AeMBRs. Li *et al.* (2012) found that low fouling rates were observed at low MLSS concentrations in the range of 3 - 5 g L^{-1}, while fouling rate almost zero when MLSS rose to 7.9 g L^{-1}. It was believed that MLSS could help to prevent small particles deposition on membrane surface. In contrast Lee and Kim (2013) reported that the fouling rate increased by almost 3 times when MLSS concentrations were > 10 g L^{-1}; thereafter, a 9-fold increase in fouling rate was obtained at a higher MLSS concentration of more than 15 g L^{-1}. They stated that the membrane fouling in high COD loading conditions (2 - 10 g COD L^{-1} day^{-1}) was more sensitive to MLSS concentration than to COD loading.

For AnMBRs, however, the recommended MLSS concentrations are still unclear due to the variety of types, substrates and mixed suspension properties, hydrodynamics, reactor configurations and operational conditions in several studies, altough the fouling caused by high MLSS is believed to be more intense when compared to AeMBR systems.

Baek, Pagilla and Kim (2010) operated a lab-scale AnMBR and reduced the SRT through biomass wasting in five steps from 213 to 40 days. The decrease in SRT did not impact treatment performance or membrane fouling. On the contrary, Huang, Ong and Ng (2011) compared performance during operation at SRTs of 30 and 60 days and for a period without biomass wasting (SRT $\approx \infty$) and observed better treatment performance at longer SRTs but increased membrane fouling resulting from higher suspended biomass concentrations and SMP production. However, a negative correlation between EPS concentrations and SRT was found, which was linked to smaller median particle sizes in the suspended biomass as a function of reduced flocculation in the presence of lower concentrations of EPS. Therefore, EPS may act to reduce membrane fouling by increasing suspended biomass particle size, whereas EPS may directly contribute to membrane fouling when present in excess or when generated directly on the membrane surface by the biofilm or cake layer. These observations suggest that a certain SRT may exist to limit EPS mediated membrane fouling (Smith *et al.*, 2012). However, the role of EPS quantity and characteristics in fouling is a function of SRT as well as other operational constraints which outweigh membrane fouling. Consequently, this strategy only remains a potential method of fouling management (Stuckey, 2012).

2.2.4.2.2 Physical operating modes

Membrane fouling has been mitigated through various physical strategies, which are linked to the membrane modules and configurations. In external crossflow configurations, a high crossflow velocity is applied to limit inorganic and organic foulant formation. Typically, crossflow velocity values of 2 - 3 m s^{-1} are sufficient to prevent the formation of reversible fouling while having no obvious effect on microbial activity (Lin *et al.*, 2011b). In submerged configurations, fouling control is regularly accomplished through gas sparging, back flushing, membrane relaxation and/or even membrane rotating.

Back flushing consists of reversing the flow of permeate (or gas) in order to limit membrane fouling. This method requires a pause in operation and re-use of permeate, however, and remains expensive in time and energy, as well as risky for membrane integrity (Braak *et al.*, 2011) , particularly in flat sheet modules.

The introduction of a relaxation time when the filtration is stopped makes backtransport easier by ending the convective flow. The relaxation mode tends to be more efficient than the continuous

one. Hong *et al.* (2002) managed to improve their MBR performance with intermittent filtration. Ndinisa, Fane and Wiley (2006) reported a slower rate of transmembrane pressure (TMP) increase in intermittent operation (20 min suction and 5 min relaxation) compared to continuous filtration mode. Nonetheless long and frequent relaxation could cause fouling because of the high instantaneous fluxes needed to maintain water production (Metzger *et al.*, 2007).

Gas sparging and/or liquid recirculation is the most common way to provide liquid crossflow velocity and shear conditions in AnMBR. Smith, Skerlos and Raskin (2013) operated low strength domestic wastewater treatment under psychrophilic temperature (15 °C) using flat sheet AnMBR. They concluded that membrane fouling was successfully managed using biogas sparging and permeate backflushing. Comparative fouling experiments suggested that the combination of the two fouling control measures was important: backflushing was necessary to avoid long-term membrane fouling, whereas biogas sparging was a prerequisite to having an operational AnMBR system (Smith, Skerlos and Raskin (2013)).

Fouling control by gas sparging still represents the largest energy demand even for submerged membrane configurations. Martin *et al.* (2011) reported the high variability in biogas sparging intensity (specific gas demands of 0.4 to 3.0 m^3 m^{-2} $hour^{-1}$) and thus energy requirement for fouling control (0.03 to 3.57 kWh m^{-3}) used in submerged AnMBR studies. When comparing aerobic MBR and AnMBR studies, lower permeate fluxes are typically observed in AnMBRs potentially as a result of less flocculation and thus increased concentrations of fine particulates and colloidal solids at the membrane surface (Liao, Kraemer and Bagley, 2006; Martin *et al.*, 2011).

As well as Lin *et al.* (2011a) , they assessed the economic feasibility of a submerged flat sheet AnMBR system for municipal wastewater treatment based on overall costs (assumed capacity of 20,000 m^3 day^{-1} and sustainable flux of 11 LMH). It was reported that membrane costs account for the largest fraction (72 %) followed by the costs of tank construction and screens among capital costs, whereas gas sparging energy represents the most significant operational cost. The operational cost items followed the order: gas scouring energy (46.7 %), chemical consumption (32.5 %), pumping energy (13.7 %) and sludge disposal (7.2 %).

2.2.4.2.3 Modifying mixed liquor properties

Addition of additives or flux enhancers, such as adsorbent agents, coagulants, carriers, suspensible particles and other chemical agents, can modify the properties of the mixed liquor in AnMBRs (Lin *et al.*, 2013). Appropriated additives for fouling mitigation can act through a number of different mechanisms such as adsorption of SMP, coagulation, cross-linking between flocs, and a combination of these (Drews, 2010).

Powdered activated carbon (PAC) or granular activated carbon (GAC) is the most widely used flux enhancer in MBRs. Hu and Stuckey (2007) reported PAC or GAC addition to submerged flat sheet AnMBRs to reduce membrane fouling in conjunction with biogas sparging. Their results suggested that PAC and GAC addition increase membrane flux and enable operation under lower TMP as compared to a control AnMBR in which only biogas sparging was used. In addition, a shift to a relatively higher range in particle size distribution was observed in an AnMBR with activated carbon addition. On the other hand, particle size distribution shifted to a lower size range in the AnMBR without activated carbon addition, which probably led to pore clogging. Moreover, rigid PAC particles may also make the cake layer more porous since they are larger than the biomass flocs. In addition, Vyrides and Stuckey (2009) observed a reduction in gel layer resistance, and thus a TMP reduction after the addition of PAC. Nevertheless, an overdose of PAC could increase membrane fouling because excess PAC itself could be a foulant (Akram and Stuckey, 2008).

Recently, the anaerobic fluidized membrane bioreactor (AFMBR), which combines a membrane system with an anaerobic fluidized bed reactor (AFBR), has been introduced. An AFBR contains particulate media that is suspended in the reactor by the upward velocity of the fluid being treated. Wastewater treatment is effected by a biofilm attached to the media (Kim *et al.*, 2010; McCarty, Bae and Kim, 2011).

Kim *et al.* (2010) and McCarty, Bae and Kim (2011) proposed the use of fluidized GAC through liquid recirculation without biogas sparging for fouling control. Their results showed fouling may be controlled with substantially less energy input than biogas sparging requires.

However, the long-term effects on the membrane material have yet to be established. This is particularly important as many studies used organic membranes, and it has been suggested that aggressive fouling control through the use of PAC, GAC, or other media in contact with the membrane may be better suited for more abrasion resistant inorganic membranes, despite their higher life cycle costs (Ghyoot and Verstraete, 1997). The long-term impact of these aggressive fouling control measures on organic membranes and the operational costs of PAC or GAC adding/wasting should be evaluated.

Since gel/cake layer formation has been found to be a significant contributor for total filtration resistance, particularly for organic membranes, certain studies have introduced suspended biofilm carriers or circulating abrasive particles in order to enhance biocake abrasion.

Yang, Chen and Zhang (2006) first reported the addition of porous and flexible suspended carriers (polyurethane media, density 30 kg m^{-3}, porosity 90 %, average pore size 1.0 - 1.5 mm, size $10\times10\times10$ mm^3, 20 % adding of the total working volume proportion) to enhance the performance

of a hybrid membrane bioreactor (HMBR), in comparison with a flat-shaped hollow-fibre modules (polyethylene with a pore size of 0.1 - 0.2 μm) aerobic MBR. It was found that the addition of suspended carriers in the submerged HMBR improved the membrane permeability and minimized the hydraulic resistance. The critical flux increased by 20 %, the cake resistance decreased by 86 %, and the degree of membrane fouling was far lower compared to that in the MBR. The cake removal induced by the scouring of suspended carriers was considered to be the major contributor to membrane fouling control. The results showed, however, that the suspended carriers in HMBR had appreciable negative effects on the biological characteristics and filterability of the activated sludge suspension (Yang *et al.*, 2009). The mean particle size of biomass in HMBR decreased more sharply than that in MBR during long-term operation (243 days). The shear stress derived from suspended carriers led to breakage of microbial flocs, which thus reduced the floc size and released EPS to bulk suspension.

Jin, Ong and Ng (2013) introduced porous suspended biofilm carriers to aerobic flat sheet submerged ceramic membrane bioreactors (SCMBR) treating domestic wastewater. The suspended carrier used in the study was 12 mm in length, 10 mm in width and 7 mm in height, made of polyethylene with surface area of 500 m^2 m^{-3} and a density of 573.3 kg m^{-3}. The biofilm carriers at a dosage of 5.70 % (v/v) could be circulated throughout the whole reactor, providing a scouring effect on membrane surfaces through aeration (2 L min^{-1}), while the permeate flux was kept constant at 9.13 LMH by adopting an intermittent suction cycle of 8-min on and 2-min off. Their results showed that biofilm carriers addition was effective in mitigating cake formation on the membrane surface which helped to retard membrane fouling. The SCMBR without carriers had 2.7 times higher cake resistance and 1.5 times higher total resistance than the corresponding values observed in the SCMBR with carriers, indicating that the addition of biofilm carriers in SCMBR decreased the cake resistance by 72.7 % over a similar period of operation (60 days). The cake layer, which is composed of volatile suspended solids (VSS), colloidal particles, solutes and inorganic matter was the main contributor to membrane fouling. The higher concentration of both biomass and inorganic matter in the cake layer facilitated a more rapid increase in transmembrane pressure (TMP) in the SCMBR without carriers (Jin, Ong and Ng, 2013).

Ngo, Guo and Xing (2008) added polyester-urethane sponges at a volume fraction of 10 % and besides permeability enhancement also achieved improved effluent quality. Less biomass was suspended which additionally improved filterability (Lee, Kang and Lee, 2006; Leiknes *et al.*, 2006). Even when media were not in contact with the membrane, fouling was decreased by attached growth (Sombatsompop, Visvanathan and Ben Aim, 2006), despite the fact that the attached biomass had a much higher fouling potential than suspended activated sludge (Lee, Ahn and Lee, 2001).

2.2.5 Operational permeate mode and critical flux

Typically, MBR membrane filtration can be operated in two modes (Defrance and Jaffrin, 1999) : constant flux and constant transmembrane pressure. With respect to the application of MBRs for wastewater treatment process, constant flux (with potentially increases in TMP) is more favourable than constant TMP (with the possibility of flux reduction). Most industrial microfiltration and ultrafiltration systems are operated at constant flux which permits a consistent rate of permeate flux production (Miller *et al.*, 2014). The consistent flux production is an important feature for proper system design, whereas other related parameters such as membrane packing density, reactor volume, HRT, OLR, food to microorganism (F/M) ratio, etc., can be designed following constant produced permeate flux rate. Then membrane modules can be cleaned (physical or chemical cleaning) occasionally when the TMP reaches certain undesirable values. This makes the systems more controllable when compared to the constant pressure mode in which unsteady operating condition such as HRT, OLR and system capacity could occur due to the produced flux reduction, particularly in the constant pressure mode driven by gravitational force in which a relatively high suction pressure is required for MBR treating industrial wastewater.

In addition, permeate flux is one of the most important parameters which determine the economics of MBR treatment. A higher permeate flux permits a smaller membrane filtration area for a given hydraulic treatment capacity. However, the so-called critical flux exists for membrane filtration in both constant flux and constant pressure operational mode. Ideally, operating the membrane below the critical flux (sub-critical flux) allows a constant TMP without fouling, while operation above the critical flux (supra-critical flux) causes a rapid increasing in TMP (Cho and Fane, 2002).

One of the key parameter to identify the proper operational conditions in MBR is the so-called "critical flux" (J_{crit}). The original concept of critical flux was first proposed by Field *et al.* (1995) put forward the hypothesis that a critical flux exists below which a decline of flux with time does not occur, and above which fouling is observed.

Two distinct versions of the concept have been defined. In the strong form, the obtained flux during sub-critical flux is equated to the clean water flux obtained under the same condition. This means no fouling is occurring at sub-critical flux in the strong form. Since the mixed suspension properties of most real feeds can cause spontaneously irreversible adsorption, however, which occurs even when there is no convection flow towards the membrane, some degree of fouling will always occur. Consequently, critical in its strong form is unattainable and may never be achieved even at extremely low fluxes in MBR operation (Le-Clech, Chen and Fane, 2006). In the alternative weak form, the sub-critical flux is the flux rapidly established and maintained during the start-up period of the filtration, but does not necessarily equate to the clean water flux, which

means the small amount of fouling occurring at sub-critical flux operation is acceptable (Le Clech *et al.*, 2003; Le-Clech, Chen and Fane, 2006).

Setting out from the original definition, critical flux has become simply a term for a certain flux at which changes in the filtration behaviour can be observed in flux-stepping experiments. Determination of critical flux have been proposed in mainly three categories (Tiranuntakul, Schneider and Jegatheesan, 2011) based on different considerations and analysis method which are based on direct observation through the membrane (DOTM) (Wu, Howell and Field, 1999; Bacchin, Aimar and Field, 2006; Wang *et al.*, 2010), based on particle mass balance (Kwon *et al.*, 2000) and on filtration profile (Le Clech *et al.*, 2003). Drews (2010) also summarised the criteria for the onset of such change in flux-stepping test as being that the so-called critical flux is taken to be the highest flux at which (i) the TMP curve remains horizontal (within experimental accuracy according to the strong form, this cannot happen), (ii) dTMP/dt is lower than an arbitrary value such as 0.1 mbar min^{-1} (Le Clech *et al.*, 2003), (iii) the average TMP plotted against flux remains on a straight line, or (iv) when a reversible deposit is created, e.g., detected by DOTM (Wu, Howell and Field, 1999; Bacchin, Aimar and Field, 2006).

As well as various experimental set-ups and criteria, different experimental protocols have been proposed to evaluate the so-called critical flux. Among these critical flux determination techniques, the most practically popular procedure is filtration profile basis which conducting through flux-stepping method proposed by Le Clech *et al.* (2003). By this method, flux is stepwise increased and impact of TMP transients are recorded and parameters defining the fouling behaviour for each flux-step are calculated according to initial TMP increase (ΔP_0), rate of TMP increase (dTMP/dt), average TMP (P_{ave}) and system permeability (J/P_{ave}) (Le-Clech, Jefferson and Judd, 2003; Le Clech *et al.*, 2003). In attempt to obtain filtration patterns closer to the real plant operation, intermittent filtration with relaxation breaks has also been introduced (Field *et al.*, 1995; van der Marel *et al.*, 2009).

Apart from the measurement protocol (with or without filtration breaks), flux step height, step length and overall duration of experiments all play significant roles in evaluation of the so-called critical flux. For example, in step-flux experiments without filtration breaks, Wu *et al.* (2008b) reported that an increase in step length or step height reduced the critical flux. In principle, many small steps should be applied to enable an accurate critical flux determination. Using many small steps extends the experiment duration, however, so that fouling characteristics might change as a result of continuous pumping, or lack of substrate and of oxygen in the case of AeMBR. In addition, conducting the experiment for a long time at very low fluxes could generate a cake in which small particles are predominant. Moreover, other related factors such as hydrodynamics,

effects of ionic strength and pH on adsorptive or cohesive forces and polymer folding also need to be considered (Bacchin, Aimar and Field, 2006).

Despite the arbitrary aspects of the step-flux method, critical flux determination by this short-term experiment remains an effective approach to assess the fouling propensity of a given filtration system and to compare different operating conditions (Le-Clech, Chen and Fane, 2006). Although definition of critical flux is still controversial and there is no standard method for this parameter measurement, critical flux is often used as a practical guidance for plant design and operation (Guglielmi *et al.*, 2007).

2.2.6 Fluid dynamics for submerged flat sheet MBR fouling mitigation

The high operating costs of MBRs remains the major drawback in comparison to conventional wastewater treatment processes, because up to 70 % of the total energy demand for MBR systems is for fouling mitigation by air/gas sparging (Santos, Ma and Judd, 2011). Gas sparging is the most famous method for fouling control and has been implemented extensively since the 1990s (Cui, Chang and Fane, 2003). The parameters involved in optimising air scour efficiency to generate favourable fluid dynamic conditions are still not fully understood, however, since the transient orthogonal and parallel flows as well as the turbulent eddies created by bubbling generate complex hydrodynamic flow fields in the vicinity of a membrane (Bohm *et al.*, 2012). In addition, gas sparging rate, frequency, bubble shape/size (or sparger ports) and its homogeneity, module and tank geometry (membrane spacing, liquid level, cross-sectional areas of riser and downcomer, etc.) have decisive effects on the achieved crossflow velocity, shear stress and bubble-membrane contact (Drews, 2010).

2.2.6.1 Gas-liquid two-phase flow for membrane efficiency enhancement

Gas-liquid two-phase flow for inside-out tubular membranes, it is widely recognised that slug bubble application is an effective bubble regime for fouling control, since a large bubble or slug could disrupt concentration polarisation; large wake regions create stronger secondary flows which provide shear stress to detach foulants; and falling film areas promote a high crossflow velocity induced by rising bubbles or liquid pumping that enhances back transport flow to remove foulants from the membrane surface.

For flat sheet membranes, however, slug bubbles flow regime cannot be performed completely since the bubbles are not fully restricted in thin channels between membrane spacers, unlike the confined conditions in a tubular configuration, where liquid can flow downward at the unconfined side of rising bubbles. However, shear stresses achieved in two-phase flow were at least three times higher than those obtained by single-phase flow (Bohm *et al.*, 2012).

When two-phase flow occurs in thin channels (which are not as confining as in tubular modules) different flow patterns are observed. According to the respective values of the gas and liquid velocities or the corresponding flow rates, the flow pattern of a gas-liquid two-phase flow can be stated by the gas injection factor defined as:

Equation 2-1

$$\theta = \frac{u_G}{u_G - u_L}$$

where u_G and u_L are the superficial gas and liquid velocities, respectively (Mercier, Fonade and Lafforgue-Delorme, 1997). Certain flow patterns can be seen in rectangular narrow-channel for vertical flow (Wilmarth and Ishii (1994) and Xu (1999)) and horizontal flow (Fouladitajar *et al.* (2014)).

Hwang and Hsu (2009) studied the effect of flow patterns on the performance of air-sparged horizontal crossflow MF of a yeast suspension. A mixed cellulose ester membrane with a mean pore size of 0.1 μm and filtration area of 0.11 m^2 was used. The liquid superficial velocities were set in the range of 0.1 - 0.5 m s^{-1} and gas superficial velocities were in the range of 0.02 - 0.08 m s^{-1}, corresponding to a gas/liquid ratio, θ, of 0.039 - 0.444. The authors observed that the filtration performance was affected by the gas/liquid flow pattern (or wall shear stress) rather than by fluid velocities. A slug flow pattern was found to be more effective for enhancing the flux than a bubbly one.

Wibisono *et al.* (2014) reported the correlation of gas, liquid velocities and gas/liquid ratio with the mean flux enhancement from a collected literature database in their review. They found that the mean flux enhancement is almost independent of the liquid velocity (u_L), and the enhancing effect of the gas velocity (u_g) is much more distinct. In general, at a specific liquid velocity, the higher the θ is, the higher the mean flux enhancement. A peak is indicated at high liquid but low gas velocities, and in that area the mean flux enhancement is significantly higher. The peak is observed at a liquid upward velocity (u_L) of 0.2 m s^{-1} and the gas superficial velocity (u_G) of 0.2 - 0.6 m s^{-1}. This corresponds to θ of 0.5 - 0.75 m s^{-1}. Obviously, this is the range in which slug flow occurs, resulting in higher shear stress and enhanced fouling control (Wibisono *et al.*, 2014).

From many results for gas-liquid two-phase flow, it has been proven that higher u_G (also θ) and slug flow patterns tend to have a significant role in flux enhancement and fouling control rather than increasing only u_L as in a single liquid-phase flow. In some specific module geometries and configurations, however, such as the arrangements of flat-sheet membrane cassettes in pilot or real scale plants, increasing gas flow rates to certain values is expected to lead to plateaus in some useful hydrodynamic parameters (e.g. crossflow velocity, bubble size, bubble frequency, and

shear stress). Stimulating crossflow velocity by intense sparging may also damage the floc structure, reducing their size and releasing EPS as aforementioned. Moreover, over adequate gas supply to induce slug flow condition represents a high energy demand which could affect economic viability. For instance, Gil *et al.* (2010) operated pilot-scale aerobic MBR (10 flat-sheet modules with total area of 16 m^2). It was found that the coarse bubble aeration required the biggest proportion of energy and represented almost 50 % of energy consumption. Similarly, in a full-scale MBR, coarse bubble aeration was the largest consumer at approximately 35 % (Fenu *et al.*, 2010).

2.2.6.2 Bubble characteristics and flows between flat sheet modules

When gas is injected into a stationary liquid, as is the situation in submerged membrane systems, bubbles are formed and move upward driven by buoyancy. The bubble motion also generates a secondary flow behind the bubble as a turbulent wake region. The size of the formed bubbles depends on the way the gas is introduced, the sparger type and gas flow rate. Depending on bubble's size, it tends to take different shapes which determine the strength and extent of the wake region.

The generally observed bubble shapes in narrow channels are spherical, ellipsoidal or hemispherical depending on the bubble size (Cui, Chang and Fane, 2003) and certain bubble shapes and wakes can be seen in Miyahara, Tsuchiya and Fan (1988). Clift, Grace and Weber (2005) investigated and developed a chart to predict the bubble shapes correlating with the Reynolds number and the Eötvös number.

Results from studies on the effect of bubble size, bubble frequency and bubbling regime on fouling control in flat sheet membranes have indicated that slug bubbling was more efficient for flux enhancement than free bubbling, and observed an increase in the mass transfer coefficient (i.e. shear stress) as a function of both bubble size and frequency. However, further increase beyond a critical bubble size and frequency did not increase shear stress significantly (Zhang, Cui and Field, 2009; Zhang *et al.*, 2011a). In addition, slug flow patterns created from one nozzle hole may cause problems of uneven bubble distribution over the entire flat sheet membrane surface, as well requiring a complicated sparger design that is difficult to set up and operate.

Bubble size is an important factor for MBRs. Small bubbles have a good oxygen transfer efficiency (for aerobic MBRs) due to their large surface area to volume ratio. Meanwhile, large bubbles are recognized empirically for fouling mitigation because of their ability to scour the membrane effectively (Gander, Jefferson and Judd, 2000; Le-Clech *et al.*, 2003). Furthermore, the shear stress is related to bubble flow and wall-interactions, which is associated not only with

bubble size, but also membrane clearance and the gas sparging intensity (Yamanoi and Kageyama, 2010).

Ducom, Puech and Cabassud (2002) and Ducom, Puech and Cabassud (2003) studied wall shear stress characteristics between flat-sheet nanofiltration (NF) membranes for clay suspension filtration, and found a higher increase in wall shear stress in two-phase flow. They also observed that the permeate flux increased with averaged shear stress stimulated by air sparging. In a 5 mm membrane clearance, 15.9 mm spherical cap bubbles were found to have a moving velocity range of 18 - 38 cm s^{-1} (Essemiani *et al.*, 2001). This wide range might be caused by the low set-up rectangular-column height (14.7 cm) which did not enable the terminal rise velocity to be reached, but can also be attributed to the fact that velocity magnitudes including sideways movement were reported instead of pure rise velocities.

Zhang, Cui and Field (2009) investigated the influence of bubble size and frequency on shear stress. The results showed that the shear stress on the flat membrane with fixed clearance of 20 mm (1,000 mm height) increased with bubble size up to a value of 60 mL but was insensitive to size beyond that. The use of intermittent slug bubbling through the periodic introduction of large bubbles is an effective strategy to control fouling in MBRs. For a fixed 100 mL bubble, the averaged shear stress reached a maximum value when the gap between the membranes was around 8 mm. With increasing activated sludge viscosity, the averaged shear stress increased only slightly (Wei *et al.*, 2013).

Similar trends were observed by Bohm *et al.* (2012). They reported that the presence of the walls instantaneously changed the bubble shape. Above a certain point at which the bubble diameter equals the membrane spacing, a further increase in bubble size leads to flat cap bubbles. The highest shear could be achieved for narrow gaps (experimental channel range of 3 - 11 mm); however, thin channels may easily become clogged in sludge systems. Due to the increased rigidity of their surfaces, bubbles moved approximately 15 - 20 % slower in activated sludge than in water. Prieske, Drews and Kraume (2008) suggested that the smaller bubble size (1 mm) could induce a slower circulation velocity than large bubbles (2 and 3 mm) due to a higher gas holdup in the downcomer of an airlift-loop reactor, and concluded that larger bubbles seem to be more efficient for air scour of the membrane surface because the resulting drag and lift forces on the membranes are much higher due to higher circulation velocities. An increase of bubble size above a certain diameter did not yield higher shear stress (Prieske *et al.*, 2010).

This is in agreement with Ndinisa, Fane and Wiley (2006) and Ndinisa *et al.* (2006) who investigated the effects of sparger diameter sizes of 0.5 - 2 mm in a 7 mm channel flat-sheet membrane. They reported that most bubbles were found to have sizes between 2 and 5 mm in Milli-Q water and observed that as bubble size increased, so did the cleaning effect. When bubbles

became larger than the channel width, however, a further increase in size only had a minor effect on fouling control. As the membrane clearance was increased from 7 mm to 14 mm, the fouling became worse and the degree of fouling reduction by two phase flow decreased by at least 40 % determined by suction pressure rise (dTMP/dt). In addition, from their computational fluid dynamic (CFD) simulation results, it was found that the flux enhancement by the increasing bubble size was primarily due to an increase in the overall shear stress on the membrane and to more turbulence generated by introduction of the gas phase.

Larger bubbles generated strong turbulences in their wake and following bubbles were accelerated. Providing larger bubbles would enhance the turbulence, and increasing the frequency would improve the effect of bubbles on each other and lead to more homogeneous fouling control. This, however, costs energy (Braak *et al.*, 2011). Also, some favorable characteristics of smaller bubbles over larger ones have been reported in hollow fibre modules. Fane *et al.* (2005) observed that at the same air flow rate, smaller bubbles resulted in slower fouling of submerged hollow fibres, which could be due to increased liquid velocities. In a flat sheet aerobic MBR fed with raw domestic sewage, Sofia, Ng and Ong (2004) controlled fouling better with a 0.5 mm diffuser instead of a 2.0 mm one. Small bubbles were suggested to stimulate higher crossflow velocities and a stronger shearing effect than coarse bubbles (0.69 m s^{-1} against 0.4 m s^{-1}). They were able to operate their MBR for 8 months whereas the maximal TMP value that they set was reached in 4 weeks using coarse bubbles at the same aeration intensity (u_g of 0.017 m^3 m^{-2} s^{-1}). The finer and more uniformly distributed bubbles were thought to make more stable operation possible with lower TMP across the membrane. In contrast, Phattaranawik *et al.* (2007) applied just one fine bubble supply featuring a bubble size transformer (coalescer) to generate coarse bubbles from fine bubbles, after the fine bubbles containing fresh oxygen have been utilised for aeration in the bioreactor, instead of the typical two ports implementation. The coalescer increased bubble diameters from 0.5 - 2 mm to 9 - 18 mm and fouling of a submerged flat sheet module (5 mm gap) was delayed by about 1 week in comparison to a control run during 18 days of operational period. In addition, air requirements reduced by approximately 20 % through increasing bubble sizes.

Yamanoi and Kageyama (2010) evaluated bubble flow properties between 5, 7 and 10 mm spacers of flat-sheet modules in an airlift-loop reactor, with comparison of fine and coarse bubbles generated from 100 - 120 µm glass ball diffusers and Ø 6 mm nozzles. The results showed that u_L increased with u_G (range of 0.01 - 0.15 m s^{-1}). At the same gas superficial velocity, the liquid upward velocity was greater for fine bubbles than for the coarse ones due to their higher void fraction in the riser zone. The average shear stress (measured directly by shear stress meter) was larger for coarse bubbles than for fine bubbles, however, in contrast to the tendency of the liquid upward velocity, perhaps because of the greater friction coefficients and bubble-contact surface

ratio. They concluded that two-dimensional amorphous shape bubbles whose average equivalent diameter (defined as diameter from 50 % of the accumulated volume of total bubbles swarm) was more than twice the membrane clearance could enlarge the friction coefficient and the shear stress effectively. Too large bubbles had a tendency to break up, however, and consequently the bubbles hit each other and they would lose more energy. Most of the maximum local shear stresses in each condition were observed for large bubbles in 7 mm clearance.

2.2.6.3 Reactor design, module geometry and hydrodynamic optimisation

A systematic optimisation of all geometrical and operational parameters which influence submerged flat-sheet MBR hydrodynamics (such as reactor size, liquid level, module height, sparging rate, sparger/bubble size, membrane spacing, riser to downcomer cross-section area ratio, bottom clearance, sparger arrangement and location, from which engineering design rules can be deduced) is one the crucial factors for fouling mitigation.

Since these operational parameters directly affect not only the maintenance of completely-mixed suspended conditions but also crossflow velocity and shear stress, specific energy consumption should be determined at the same time as the optimisation of module geometry through rational design to maximise the flux enhancement. Based on gas bubbling as a major means of hydrodynamic drive and fouling control, certain fluid dynamic improvements have been reported.

Ndinisa, Fane and Wiley (2006) introduced baffles between flat sheet modules for better bubble distribution across one membrane panel. Reduction in fouling rate and approximately 60 % critical flux enhancement at 8 L min^{-1} aeration were observed. The increase in the scoured area and reduction in liquid maldistribution by the use of baffles were the main factors improving filtration performance. Since the authors did not provide a downcomer region outside the module, however, any recirculating flow occurred within the module, whereby the overall flow was slowed down due to the additional resistance caused by the baffles.

The presence of two sections as gaslift-loop configuration in a Kubota MBR plays a significant role in inducing high crossflow velocity for flat sheet modules (Sofia, Ng and Ong, 2004). Gaslift-loop membrane bioreactors are a kind of MBR that contain separating baffles (or membrane cases) in a configuration which divides the bioreactor into a riser and downcomer. The riser is gassed, while the downcomer is ungassed. As a consequence of the density difference between the bubbly mixture in the riser and the liquid in the downcomer, the liquid flow is circulated between these two chambers.

The well-known approach by Chisti, Halard and Moo-Young (1988) to predict the superficial liquid flow velocity in the riser (U_{lr}) depending on superficial gas velocity in the riser (U_{gr}), the height of gas-liquid dispersion (h_D), the relation between the cross section area of the riser (A_r)

and the downcomer (A_d), and the free area for the flow from the downcomer to the riser (A_b) as presented in Equation 2-2 and Equation 2-3.

Equation 2-2

$$U_{lr} = \sqrt{\frac{2gh_D(\varepsilon_r - \varepsilon_d)}{K_B\left(\frac{A_r}{A_d}\right)^2 \frac{1}{(1-\varepsilon_d)^2}}}$$

Equation 2-3

$$\text{With} \quad K_B = 11.402\left(\frac{A_d}{A_b}\right)^{0.789}$$

Where K_B is the frictional loss coefficient for the bottom zone of reactor, g is the gravitational acceleration and the values for the gas holdup in the riser (ε_r) and the downcomer (ε_d) are obtained from Equation 2-4 and Equation 2-5.

Equation 2-4

$$\varepsilon_r = \frac{U_{gr}}{0.24 + 1.35\left(U_{gr} + U_{lr}\right)^{0.93}}$$

Equation 2-5

$$\varepsilon_d = 0.89\varepsilon_r$$

Following the adaptation of a gaslift-loop reactor incorporated with a flat sheet MBR, Liu *et al.* (2000) studied hydraulic characteristics in two pilot-scale submerged MBRs with reactor dimensions of 1.4 m x 0.9 m x 1.9 m (plant A) and 0.9 m x 0.9 m x 2.3 m (plant B) in length x width x height. They observed the highest crossflow velocity of 0.43 m s^{-1} with aeration intensity (u_g) of 0.02 m^3 m^{-2} s^{-1} at the middle of the modules which was 18 - 23 % higher than the values at the sides of the modules in plant A. At the same aeration intensity, plant B achieved higher crossflow velocity than plant A due to a greater A_d/A_r of 1.43 compared to 1.1. With an increase of aeration intensity, the measured average crossflow velocity increased, but the rate of increase gradually fell, and reached a plateau of about 0.43 m s^{-1} at 0.028 m^3 m^{-2} s^{-1} of aeration intensity in plant A. Critical cross flow velocity was found to be approximately 0.3 m s^{-1} at a rate of TMP increase of about 1.5 kPa day^{-1}, which implied that sufficient cross flow velocity should be induced to retard membrane fouling. The authors also suggested that dimensional parameters of MBR are important factors influencing cross flow velocity. For a reactor which has a greater

height, a more compact riser and wider channels in the downcomer and bottom, a higher cross flow velocity could be achieved with the same aeration intensity.

The effect of A_d/A_r ratio on flux stability in flat sheet MBRs has also been reported by Shim, Yoo and Lee (2002). They operated MBR in three reactor geometries as R1, R2 and R3 with total volumes of 21, 21 and 26 L, heights of 39, 160 and 115 cm, A_d/A_r ratios of 4.5, 1.5 and 3.6, and air bubbling by fine, fine and coarse bubble, respectively. According to their results, better filtration stabilities were obtained from R1 and R3 which could be operated under constant TMP for 150 and 80 days, respectively. Meanwhile, rapid increase of TMP in R2 was observed at 25 filtration days. The authors conclude that an A_d/A_r ratio of 1.6 did not generate a sufficient flow for proper cleaning of the membrane surface, and the ratio between 3.6 and 4.5 seemed appropriate for membrane clogging prevention.

Khalili-Garakani *et al.* (2011) carried out CFD simulation to analyze fouling in an airlift-loop flat-sheet MBR. The 22 L activated sludge MBR consisted of two adjustable angled baffles at 90˚, 87.5˚ and 85˚ corresponding to A_d/A_r ratio of 1.0, 1.3 and 2.0, respectively. The results indicated that the main component of fouling is cake resistance at 90˚ and 87.5˚, and adsorption resistance at 85˚. At 85˚, increasing superficial air velocity (u_g) by fine bubbles (flexible membrane diffuser) resulted in decreasing total and cake resistances within a low u_g range of less than 0.0176 m s^{-1}, and which then become constant at high velocities. With the u_g of 0.0352 m s^{-1}, shear stress produced by liquid flow was slightly higher than that generated by air flow. Increasing the A_d/A_r ratio (through decreasing the baffle angle) led to a higher shear stress in which cake resistance and adsorption resistance were reduced while pore blockage resistance slightly increased by increasing the shear stress.

To maximise the superficial liquid flow velocity in the riser (U_{lr}), Prieske *et al.* (2010) attempted to improve the module geometry of the airlift-loop reactor. Based on the fact that bulk liquid velocity is a function of the A_d/A_r ratio, they suggested that frictional loss (K_B) could be minimised by providing a smoother transition between the downcomer and riser sections in the chamber. The position of the bubble diffusers applied for sparging also affects the upward liquid velocity. For example, locating the diffusers at the entrance to the draft tube where they block the available flow cross section causes a slowdown in the internal flow circulation. Therefore, improving the draft tube entrance and relocating the diffusers to the bottom of the tank could enhance the upward liquid velocity in riser sections. Beyond a critical superficial gas velocity, however, the superficial liquid velocity remains relatively constant. This plateauing effect is consistent with the diminishing benefits on fouling control of increasing the air scouring rate beyond a critical value.

2.2.7 Three-phase gas-liquid-solid flow for MBR

The combination of conventional two-phase gas sparging with suspended scouring particles added to enhance the mechanical cleaning process (MCP) in MBR operations is one of the approaches considered for fouling mitigation (Yang, Chen and Zhang, 2006; Krause *et al.*, 2010; Rosenberger *et al.*, 2011). The major mechanism of this process is that suspended media are able to cross the laminar layer to scrub the membrane surface, whereas crossing over this layer to reach the membrane surface cannot be achieved by neither turbulent flow regime nor gas bubbles (Aslam *et al.*, 2017a). Moreover, the turbulence induce by suspended particles movement can enhance backtransport, detaching foulants away from the membrane surface (Huang, Wei and Yu, 2008). As a result, cake/gel layer and external reversible fouling formation can be broken down or alleviated, promoting the reduction in the intensity and frequency of chemical cleaning (Kurita, Kimura and Watanabe, 2014; Rosenberger, Helmus and Drews, 2016).

2.2.7.1 The mechanisms of mechanical cleaning by particle addition

Wang *et al.* (2014) reviewed mechanical cleaning mechanisms using particles and carriers and reported that the major mechanisms are as follows: (i) the membrane surface could be mechanically scoured by the suspended particles/carriers; (ii) the suspended particles/carriers induce turbulent flow that enhance the foulant back-transport away from the membrane surface; (iii) swaying and vibration of hollow fibre (HF) membranes can be enhanced by the movement of suspended particles/carriers; (iv) the suspended particles/carriers can initiate the adsorption of certain polymeric substances and/or fine colloids (Yang, Chen and Zhang, 2006; Huang, Wei and Yu, 2008; Rosenberger *et al.*, 2011).

In general, the first three mechanisms play a dominant role in membrane cleaning. Krause *et al.* (2010) and Rosenberger *et al.* (2011) proposed principles for selection of plastic particles, which might be also applicable to selecting some other particles/carriers. The particle should be regular and without sharp edges (lens or sphere) in order to avoid damage to membranes. The size of the particle should be less than the width or the diameter of the fluid channel of membranes. The density of particles should be close to or a little higher than water density to facilitate their distribution and recirculation in mixed liquor. The material of particles should be inert (biologically resistant), wettable and elastic to some extent. Proper particle elasticity can alleviate membrane damage during long-term operation (Rosenberger *et al.*, 2011). In addition, the recirculation velocity in MBRs is another important factor influencing the suspension of particles/carriers (Rosenberger *et al.*, 2011).

2.2.7.2 Adsorbent agents as scouring media

Active adsorbent such as granular activated carbon (GAC) or powder activated carbon (PAC) has been widely applied with MBR for fouling mitigation proposes due to their effective combination of membrane scouring and foulant adsorption effects. Small amounts of PAC or GAC in the range of 0.5 - 5.0 g L^{-1} have been adopted with conventional air/gas sparged MBR. Aquino *et al.* (2006) operated gas sparged AnMBR with PAC dosing of 1.7 g L^{-1} ; it was found that AnMBR without PAC experienced more intense fouling than AnMBR with PAC addition. Hu and Stuckey (2007) reported that AnMBR with PAC provided better flux than either GAC addition or only gas sparging without PAC/GAC addition, resulting in lower transmembrane pressure (TMP). Akram and Stuckey (2008) reported that 1.67 g L^{-1} of PAC associated with 5 L min^{-1} of gas sparging could significantly improve flux from 2 - 9 L m^{-2} $hour^{-1}$ (LMH) in comparison to controlled AnMBR with gas sparging alone. PAC addition remarkably reduced the deposition of fine particle fractions on the membrane surface, as PAC adsorbed both low and high molecular weight of slowly biodegradable residual COD from the bulk liquid (Park, Choo and Lee, 1999; Akram and Stuckey, 2008; Vyrides and Stuckey, 2009).

Much higher of GAC dosages (over 100 g L^{-1}) have also been tested in the form of fluidized bed AnMBR. Kim *et al.* (2010) developed anaerobic fluidized bed AnMBR by using GAC in conjunction with submerged hollow fibre membrane filtration. GAC particles were fluidized by bulk suspension recirculation under anaerobic conditions without biogas sparging in a so-called anaerobic fluidized membrane bioreactor (AFMBR). GAC with a packing density of approximately 340 g L^{-1} which occupied 60 % of pilot-scaled AFMBR volume (when settled) gave and effective continuous performance for primary-settled domestic wastewater treatment, without chemical cleaning, even under low temperature operation in winter. Consequently, adsorbent scouring media with bulk circulation presented the lowest energy consumption for fouling control in comparison with other typical methods (Shin *et al.*, 2014; Aslam *et al.*, 2017a) such as liquid crossflow velocity or gas sparging. Solid/liquid/gas three-phase flow has also been attempted for fouling alleviation in AnMBR. Chaiprapat *et al.* (2016) demonstrated that substitution of liquid circulation with a small amount of biogas bubbling (0.6 % V/V) to fluidized the GAC (12.8 g L^{-1}) in AnMBR could significantly reduce fouling rates by 55 and 90 % in comparison to GAC fluidizing with liquid circulation and only biogas circulation without GAC media, respectively.

The fresh adsorbents were able to accelerate the combined performance of collision and adsorption on membrane surface. High molecular weight materials such as SMP, EPS and fine colloidal materials could be removed effectively by adsorption mechanisms (Johir *et al.*, 2011; Ng *et al.*, 2013). Additionally, adsorbed GAC/PAC particles are able to attract small biological

flocs helping their aggregation into larger floc (Munz *et al.*, 2007; Remy *et al.*, 2010; Lin *et al.*, 2011d). Therefore, the integration of abrasion and adsorption actions using PAC/GAC could promote the production of large and dense sludge flocs, that minimised foulant release to the bulk liquid. The deposition of small fine particles on the membrane surface could be minimised resulting in formation of a more porous, less compact, cake layer and less membrane pore blockage (Jamal Khan, Visvanathan and Jegatheesan, 2012; Gao *et al.*, 2014; Skouteris *et al.*, 2015).

Despite the advantages of using active adsorbents in MBRs, it can be argued that this application has certain limitations. Aun Ng, Sun and Fane (2006) recommended that adsorption of organic foulants and fine colloids should play an important role for membrane cleaning rather than physical scouring performance by movement of PAC particles in MBRs. Nonetheless, after long-term operation of adsorbents in MBRs, the adsorption capacity will be diminished. Therefore, physical scouring on membrane surface by particles should be a dominant mechanism for fouling control (Aslam *et al.*, 2014; Lee *et al.*, 2016; Aslam *et al.*, 2017a). In addition, fine saturated PAC particles themselves can probably become a foulant. It is inevitable that PAC in the bulk suspension will be deposited on the membrane surface, resulted in acceleration of both membrane pore blockage and cake formation (Ying and Ping, 2006; Iversen *et al.*, 2009; Lee *et al.*, 2009). Once the PAC adsorption capacity reaches equilibrium, the abrasive action of fine PAC media may not be effective because of their very small size (Munz *et al.*, 2007; Ng *et al.*, 2013). In addition, membrane damage caused by abrasion of harsh GAC particles after long-term operation has also been reported (Shin *et al.*, 2016). Based on this context, the removal of inactive adsorbed media may be an unavoidable requirement which could lead to a reduction in sludge concentration as well as active biomass loss (Yang, Spanjers and van Lier, 2012). Furthermore, removal of exhausted adsorbent particles and active adsorbent (also membrane) replacement to avoid the adverse effect of membrane fouling mitigation may have to be taken into account in operational expenditure (OPEX) which could increase the burden for MBR implementations.

2.2.7.3 Non-adsorbent agents as scouring media

The use of non-adsorbent agents as scouring media has also been applied in MBR systems, especially AeMBR. Aeration along the membrane surface for fouling control, which represents the largest proportion of energy requirement for AeMBR operation could be effectively reduced with the assistance of rigid non-porous materials implementation (Kurita, Kimura and Watanabe, 2014).

Yang, Chen and Zhang (2006) applied porous, flexible suspended carriers made of polyurethane at a proportion of 20 % V/V in hollow fibres AeMBR. It was found that critical flux could be increased by 20 %, cake resistance decreased by 86 % and the rate of suction pressure increase

was 30 % of that in AeMBR operated without suspended carriers. It was reported that fouling rate under the mechanical cleaning process produced by introduction of polyethylene glycol granules (5 - 10 % by reactor volume) operated as a moving bed in a flat sheet AeMBR was much lower than that observed in the absence of granules, but the aeration rate was reduced by more than 50 % (Kurita, Kimura and Watanabe, 2014;2015). Additionally, Kurita, Kimura and Watanabe (2015) reported that when a baffle is installed in the membrane reactor and it is operating as airlift-loop configuration, it creates circulation flows which promote vigorous movement of scouring particles and enhance the mechanical cleaning efficiency.

Rigid gear-shape biofilm carriers have also been adopted with ceramic membrane AeMBR. According to Jin, Ong and Ng (2013)'s results, AeMBR without carriers had 2.7 times higher cake resistance and 1.5 times higher total resistance than the corresponding values observed in AeMBR with carriers in which cake resistance could be reduced by 72 % over a similar period of operation.

Another type of non-adsorbent particle that has been used as a scouring agent is sponge media. Lee, Kang and Lee (2006) operated hollow fibre AeMBR coupled with polyurethane sponge cubes coated with activated carbon. They found that AeMBR with sponge cubes had much lower biofouling rates than a conventional AeMBR, as frictional forces exerted by circulating media mitigated the cake layer formation on the membrane surface and thus enhanced the membrane filterability under the same aeration rate. Similar results were obtained by Kurita, Mogi and Kimura (2016) who compared three different biofilm carriers consisting of fixed rope carriers, moving granular carriers and moving sponge carriers in fouling control efficiency for AeMBRs. The results showed that granular polyethylene glycol media and polyethylene sponge with attached biofilm, perfectly removed the cake/gel layer on the membrane surface by scouring actions. Granular media deteriorated the mixed suspension filterability significantly, however, leading to physical irreversible fouling, whereas such deterioration was insignificant with sponge media (Kurita, Mogi and Kimura, 2016).

In fact, using suspended media could affect two different aspects of fouling mitigation. The positive effect of the mechanical cleaning process is to remove the external fouling layer from the membrane surface. The negative effect is due to the microbial floc breaking up, possibly affected by excessive shear force created by scouring media movement in bulk suspension (Yang, Chen and Zhang, 2006; Huang, Wei and Yu, 2008; Yang *et al.*, 2009). Microbial floc disintegration could increase the proportion of small fine colloidal particles, as well as releasing more foulants such as SMP and EPS which can accelerate membrane fouling (Wei *et al.*, 2006; Yang *et al.*, 2009; Shen *et al.*, 2015). Cake formation, however, which is typically regarded as the major contributor to membrane fouling, could be almost entirely alleviated by physical mechanical

cleaning, and the membrane filtration performance is expected to be much more dependent on the mechanical effects of moving media than on the biochemical or physico-chemical effect of mixed liquor suspension (Lee, Kang and Lee, 2006; Chen, Bi and Ng, 2016).

Consequently, applying non-adsorbent media as a scouring agent in MBR is a promising method for energy-efficient membrane fouling reduction in which re-dosing or regeneration and back flushing are not required. This technology could enhance flux production under the same energy input as for bubbling, with a reduction in the frequency and consumption of membrane chemical cleaning, potentially prolonging membrane life span as well as achieving more effective capital and operational expenditure (COPEX).

2.3 Conclusion and hypothesis for justified framework

From the above review, the main conclusions can be summarised as follows:

1. AnMBRs can be considered as sophisticated high-rate reactors for low to medium strength industrial wastewater treatment due to their capacity for complete biomass retention with not only high treatment performance but also the potential for energy recovery from produced biogas.

2. Membrane fouling, an unavoidable circumstance, is the major obstacle for MBR processes. Fouling is an extremely complex phenomenon which is caused by a combination of components in the reactor (soluble organics, fine colloidal particles and mixed suspended solid, inorganic matter etc.) that contribute to both internal pore blockage and external reversible fouling. The latter is widely reported as the major contributor to total fouling resistance. Many approaches for fouling control have been proposed.

3. Two-phase air/gas sparging is the most common practical method that is widely applied for fouling control. Gas sparging is performed to create favourable hydrodynamic condition to disturb concentration polarization, detach foulant from the membrane surface by shear stress and remove foulant away from the membrane vicinity by back transport flow induced from rising bubble and liquid crossflow velocity.

4. Three-phase gas-liquid-solid flow that integrates suspended scouring media with conventional air/gas sparging for fouling minimization has been introduced. The major advantage of this method is that scouring media can cross over the laminar layer to scour and detach foulants from the membrane surface directly, while neither liquid nor bubbles from conventional gas-liquid two phase flow could reach this layer. Adsorbent and non-adsorbent media have been applied as flux enhancers in MBR processes.

Since the major target of this research is to study the application of two- and three-phase flow in submerged flat-sheet AnMBR for dairy wastewater treatment, the hypothesis and justified frameworks are based on these approaches:

- Although two-phase gas/air sparging has been widely recognised as effective method for fouling control, this process always represents the largest proportion of operational energy demand. Therefore, energy minimization for MBR operation is considered of prime importance. In order to achieve maximum effect from the energy input, hydrodynamic conditions for fouling mitigation such as sparging intensity, bubble size and size distribution (related to nozzle size and sparging rate), liquid crossflow velocity and tank geometry should be optimised.

- It is well recognised from inside-out flow tubular membrane studies that slug bubble is an effective bubble regime for fouling control. In the submerged flat sheet configuration, however, slug bubbles cannot be completely performed since the bubbles are not fully confined in the thin channel between membrane spacers. In addition, oxygen transfer aspects are irrelevant in AnMBR. Therefore, pseudo-2D confined cap bubbles generated from perforated tube spargers are more favourable for fouling control because of their higher shear stress contribution between flat plates membrane gap.

- Increasing sparging intensity results in better fouling control, but also requires more energy input. Furthermore, above threshold sparging rates, certain favourable hydrodynamic parameters are limited with no significant further improvements in fouling reduction or even detrimental effects. Hence, a threshold sparging rate should be determined.

- External reversible fouling such as gel/cake layer has always been reported as the major contributor to the total filtration resistance. A mechanical cleaning process by non-adsorbent particles used as scouring media is an attractive method to alleviate this significant fouling component.

- Porous adsorbent and non-adsorbent media have been widely applied as scouring agents in AeMBR systems for flux enhancement purposes and fouling reduction. Fouling phenomena in anaerobic process are widely accepted to be more severe than those in aerobic systems. The application of non-adsorbent particles coupled with conventional gas sparging in a three-phase moving bed AnMBR system, however, has not previously been investigated.

- Therefore, a study applying three-phase gas/liquid/non-adsorbent media moving bed AnMBR in comparison with conventional two-phase gas sparging AnMBR should be conducted. In particular, the experiment should be carried out with real living microorganisms under anaerobic

conditions from the start up period, to gain better insight into the system performance, as well as aspects of fouling control under various conditions in long-term operation.

Chapter 3: **Materials and Methods**

3.1 Laboratory-scale submerged flat sheet filtration resembled to MBR system

3.1.1 Reactor set-up

Experiments were performed on a laboratory-scale unit. The experimental apparatus consisted of a maximum 12.5 L reactor made of acrylic and clear Perspex plastic (open to the atmosphere) with internal dimensions of 7.5 cm (width) x 21.5 cm (length) x 79 cm (height), and slots to fit one submerged flat-sheet membrane panel and separation baffle. In order to enhance flow circulation, the reactor was divided into a riser and downcomer zone by the separation baffle, meaning it could be categorized as a rectangular split-type internal gas-lift loop reactor. The height of the baffle edge from the bottom of reactor was 8.5 cm, representing a transitional flow area (A_b) between the downcomer and riser sections of 182.8 cm^2 (0.215 m x 0.085 m). The liquid depth over the top baffle edge was 3.0 cm, corresponding to an overflow cross-sectional area (A_t) of 64.5 cm^2 (0.215 m x 0.03 m). The liquid depth inside the reactor was kept constant at 68.0 cm giving a maximum working volume of 10.9 L. The width of the reactor was adjustable by inserting up to 3 acrylic sheets (0.9 cm x 21.5 cm x 79 cm) as tank dividers inthe downcomer section, to cut off the rest of the tank. Therefore, the liquid working volume could be varied from 10.9, 9.6, 8.3 to 7.0 L, respectively.

The membrane used in this study was a Kubota flat sheet (A4 size) polymeric micro-filtration membrane, made of chlorinated polyethylene, with a nominal pore size of 0.4 µm and 0.11 m^2 filtration area. The clearances between the membrane to the front wall and to the back separation baffle were fixed at 7 mm. This dimension is important as it defines the width of the flow channel available for bubble flow, which corresponded to the total cross-sectional area of the riser zone minus the area of the membrane panel (thickness 6 mm). According to this arrangement, the effective cross-sectional area of the riser zone (A_r) was equal to 30.1 cm^2 (0.215 m x 0.007 m x 2). By inserting tank dividers, the cross-sectional areas of the downcomer (A_d) could be varied between 111.8, 92.5, 73.1 and 53.8 cm^2, equivalent to the A_d/A_r ratios of 3.7, 3.1, 2.4 and 1.8, respectively. The geometry of the laboratory-scale MBR is presented in Figure 3-1.

Gas sparging was introduced 30 cm beneath the membrane panel through a set of nozzles, made by drilling 4 holes in a dead-end ∅ 6 mm stainless steel tube, for the case of equal hole diameters; and 2 holes (∅ 1.5 mm and ∅ 3 mm) on one open-end tube as a sparger. Small pieces of metal (swarf) inside and outside the tube after drilling were removed by round files and sandpaper in

order to facilitate smooth gas flow inside the sparger tube. Two gas spargers were installed in the riser zone to supply large bubble scouring to the front and the back side of membrane panel equally, with the 8 nozzles located in alternating zigzag positions to avoid bubbles coalescence. The sparger arrangement is presented in Figure 3-2 and Figure 3-3**.** Each sparger was connected to a diaphragm air pump to provide air for bubbling. Air was supplied from the left side to the front sparger, while the back sparger was supplied from the right in an attempt to balance bubble and liquid flow distribution. The total required airflow rates for both spargers were in the range of 2, 4, 6, 8 and 10 L min^{-1}, corresponding to superficial air flow velocities (u_g) of 0.011, 0.022, 0.033, 0.044 and 0.055 m s^{-1}, and were obtained by adjusting a direct current (DC) power supply regulator, monitored by air rotameters located next to the diaphragm air pumps.

Figure 3-1 Geometry of MBR internal set-up

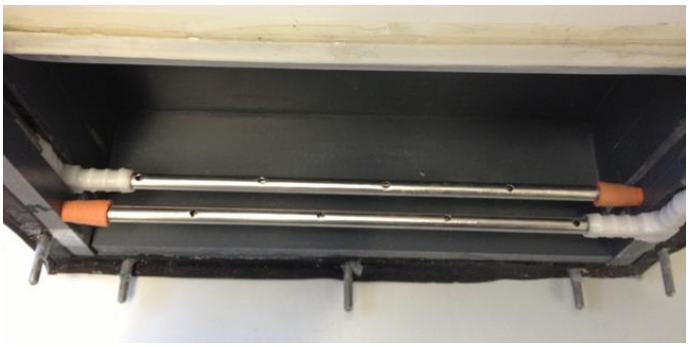

Figure 3-2 Nozzles and spargers arrangement for the case of equal nozzle sizes

Figure 3-3 Nozzles and spargers arrangement for the case of Ø1.5 and 3 mm nozzle sizes

3.1.2 Bubbles analysis method

3.1.2.1 Bubble size determination

The experimental setup utilized in this part of the work resembled that of a bubble flow between narrow channels of flat sheet membranes in the tank geometry of A_d/A_r ratio 3.1 as described above. The main activity involved recording pictures with a digital camera under different conditions. The Kubota flat sheet membrane module was simulated by installing a thin (< 0.5 mm) electro-luminescent panel, with an A4 size brightness area equal to the filtration area of the membrane module, as a background light source, mounted on a 22 cm x 31 cm x 0.6 cm acrylic plate. The tank was filled with tap water and commercial fabric dye (C.I. Reactive Black 5 contained) was added to the liquid at a concentration of 0.05 g L^{-1} in order to enhance the contrast between bubbles and liquid. A piece of graduated tape 20 mm in length was attached to the front of the tank in order to act as a reference scale. A Casio Exilim Pro EX-F1 High Speed Camera, positioned 30 cm away from the tank, was used to take digital snap-shot images of the two-phase flow patterns from one side of the replicated membrane filtration area, with the focal point of the camera set at the centre of the membrane area. The experimental conditions involved the use of spargers with nozzle diameters of 1, 2, 3 and 4 mm under air flow rates of 2, 4, 6, 8 and 10 L min^{-1}. Five pictures of each experimental condition (total 100 pictures) were captured in 1 min at an exposure time of 1/640 s. In order to avoid reflections from external light on the front tank wall, pictures were taken in dark conditions.

After numerous pictures were taken and downloaded to a personal computer (PC), the pictures were then analysed using ImageJ software for particle analysis. For each image processing, the software produced a projected surface area of each bubble occurred in a pseudo two-dimensional (2D) thin rectangular column.

Typically, the images originally captured with true colour (24-bit) had to be converted into 8-bit (grey scale) Tagged Interchange File (TIF) format using ImageJ software. By using this software package, several image processing steps can be automated, which is a necessity when analysing large amount of data. However, the brightness generated from the electro-luminescent panel used in this study was insufficient to distinguish the bubble-covered area from the background area using the automatic software function. Therefore, the bubble perimeter definition was processed manually. In addition, since bubbles did not always appear spherical in shape and bubble shape and size are changeable due to their coalescence and break-up, the perimeters of each single bubble were drawn following the outline (watershed line) of large bubbles from the still images. Samples of original images cropped to the region of interest and analysed bubble perimeter images after processing are shown in Figure 3-4 and Figure 3-5, respectively.

Figure 3-4 Original image of bubble flow in pseudo-2D thin channel (nozzle ∅ 4 mm, 8 L min^{-1} sparging rate)

Figure 3-5 Analysed bubble perimeters (nozzle ∅ 4 mm, 8 L min^{-1} sparging rate)

After the perimeters of each bubble were determined, for each analysed picture, the software then produced the 2D projected area of each bubble, which bubble volume and size were further evaluated by the analysis procedure described below.

Equivalent circle diameters were calculated from the projected areas of the bubbles. Since the clearances of the flow channel were fixed at 7 mm, then a spherical shaped bubble with a diameter of 7 mm represents a projected area of 38.5 mm^2 (calculated from Equation 3-1). Bubble size and volume were then calculated from the assumptions as follows:

Equation 3-1

$$A_p = \frac{\pi D^2}{4}$$

Where:
A_p is bubble projected area (mm^2)
D is equivalent circle diameter (mm)

Case i: without bubble-membrane contact ($A_p \leq 38.5\ mm^2$)

When the observed projected area (A_p) of bubble is smaller than or equal to 38.5 mm^2, bubbles were assumed to be spherical and smaller than the channel width, thus without contact on both sides of the channel, and the flow pattern was assumed to be free bubbly flow. Equivalent diameters were determined by equivalent circular areas from Equation 3-2 and then volumes were calculated from the equivalent circle diameter by Equation 3-3.

Equation 3-2

$$D = \sqrt{\frac{4A_p}{\pi}}$$

Equation 3-3

$$V_b = \frac{\pi D^3}{6}$$

Where:
V_b is bubble volume (mm^3)

Case ii: with bubble-membrane contact ($A_p > 38.5\ mm^2$)

When the observed bubble projected area was greater than 38.5 mm^2, volumes were estimated from the projectedareas (A_p) multiplied by 7 mm depth (Equation 3-4). Because these bubbles were observed to contact both sides of the channel two-dimensionally, the bubble flow pattern

was assumed to be pseudo-2D confined cap bubble flow. Thereafter, equivalent circle diameters were defined by assuming their volumes equaled that of a spherical shape (Equation 3-5).

Equation 3-4

$$V_b = A_p \times 7$$

Where: 7 is channel depth using in this study (mm)

Equation 3-5

$$D = \sqrt[3]{\frac{6V_b}{\pi}}$$

3.1.2.2 Related term definitions

After each single bubble size was determined, related terms for the representative bubble size and size distribution of bubbles in the bubble swarm for both "without contact" and "with contact" cases were defined as follows:

Arithmetic or number mean diameter (D_{10})

The number mean diameter was calculated using Equation 3-6 by adding the mean diameters for all the bubbles from 5 pictures of each condition and dividing by the total number of bubbles

Equation 3-6

$$D_{10} = \frac{\sum_{i=1}^{n} D_i}{n}$$

Where:
D_{10} is number mean diameter (mm)
D_i is equivalent circle diameter (mm)
n is total number of bubble count

Median of volume distribution (D_{v50})

D_{V50} is regarded as the diameter of 50 % of the accumulated volume of the all bubbles in the photographs, with the total accumulated volume for each bubble size was calculated from the observed frequency multiplied by their equivalent circular volume.This indicating to the diameter that 50% of accumulated volume of total bubble swarm is smaller than and 50 % of accumulated volume is larger than this point.

Sauter mean diameter (D_{32})

Sauter mean diameter (D_{32}) is defined as the diameter of a sphere that has the same volume/surface area ratio as a bubble of interest. D_{32} is also known as surface area moment mean, calculated by Equation 3-7 for bubble swarm and the bubbles of both "with contact" and "without contact" cases.

Equation 3-7

$$D_{32} = \frac{\sum_{i=1}^{n} D_i^3}{\sum_{i=1}^{n} D_i^2}$$

Void fraction (α)

The void fraction (α) is defined as the ratio of the bubble volumes in the observed rectangular channel to the total observed channel volume. In this study, the average void ratio was calculated by summing all the bubble volumes divided by 5 pictures per interest volume of A4 area with 7 mm channel depth. α is calculated from Equation 3-8.

Equation 3-8

$$\alpha = \frac{\sum V_b}{5(205\text{mm} \times 290\text{mm} \times 7\text{mm})}$$

Contact surface ratio (ά)

The contact surface ratio (ά) is defined as the average ratio of bubble-membrane contact area from 5 pictures to the whole membrane filtration area (Equation 3-9). For the "without contact" case, the contact surface ratio was considered zero, because bubble equivalent circular diameters are smaller than membrane spacer and there is no contact with the membrane.

Equation 3-9

$$\acute{\alpha} = \frac{\sum(\text{contact surface area})}{5(205\text{mm} \times 290\text{mm})}$$

3.1.3 Flow velocities analysis

The reactor with the real Kubota membrane panel installation, set up in the same geometry as described in section 3.1.1, was used in an experiment to determine the flow velocities in the tank. The reactor was filled with tap water and a small impeller anemometer (NIXON Streamflo Velocity Meter model 423 and 90° angle probe with NIXON 430 Digital Indicator, UK) was mounted at 3 cm over the top edge of the membrane panel (5 cm below the top water level), to measure the two-phase flow velocities of 5 points (left, middle-left, centre, middle-right and right

positions) in the riser zone. Flow velocities of 5 points under a top water level of 35 cm (to minimise the turbulence of bubbles in downward flow) in downcomer zone, were also measured in order to determine the superficial liquid upward flow velocities in the riser (u_{lr}) based on the circulating liquid velocities and the cross-sectional area of the downcomer channel. The velocity measuring positions are presented in Figure 3-6. The actual liquid upward velocities (u_{lr}) were defined as the superficial liquid velocity divided by the liquid fraction (1- α).

The experimental conditions involved the measurement of liquid upward velocities for spargers with nozzles diameters of 1, 2, 3 and 4 mm under air flow rates of 2, 4, 6, 8 and 10 L min^{-1} (equivalent to superficial air flow velocity (u_g) of 0.011, 0.022, 0.033, 0.044 and 0.055 m s^{-1}) related to the A_d/A_r ratios range of 3.7, 3.1, 2.4 and 1.8, respectively.

The flow velocities for each condition were obtained from NIXON 430 Digital Indicator reading signals in Hz with 10 s sampling frequency during a 120 s period and averaged. The signals were converted to flow velocities using the probe calibration chart provided by the manufacturer (Figure 3-7). The experimental set up is shown in Figure 3-8.

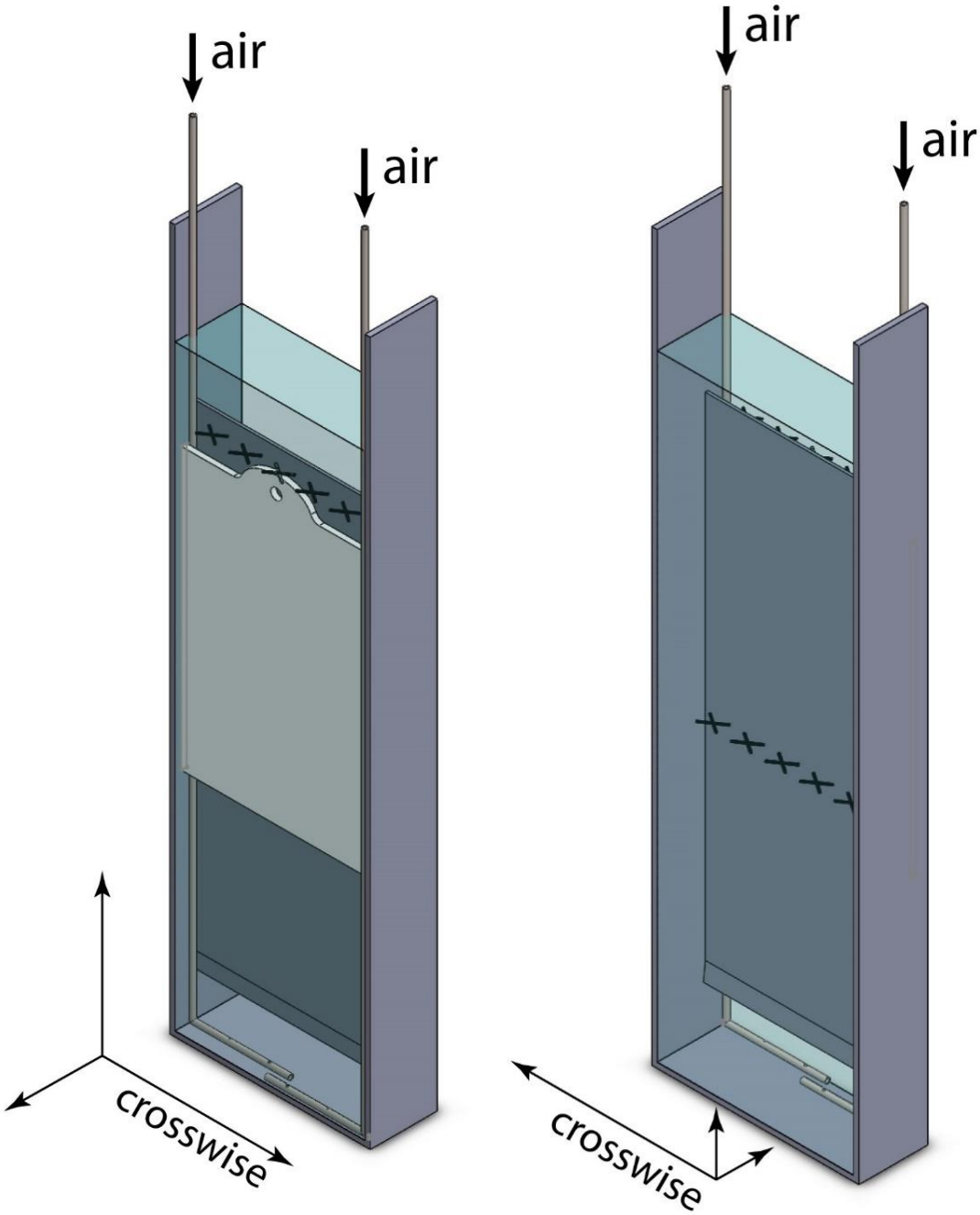

(a) (b)

Figure 3-6 Flow velocity measuring points shown by "X marks" (a) upward flow in riser at the front side and (b) downward flow in downcomer at the backside

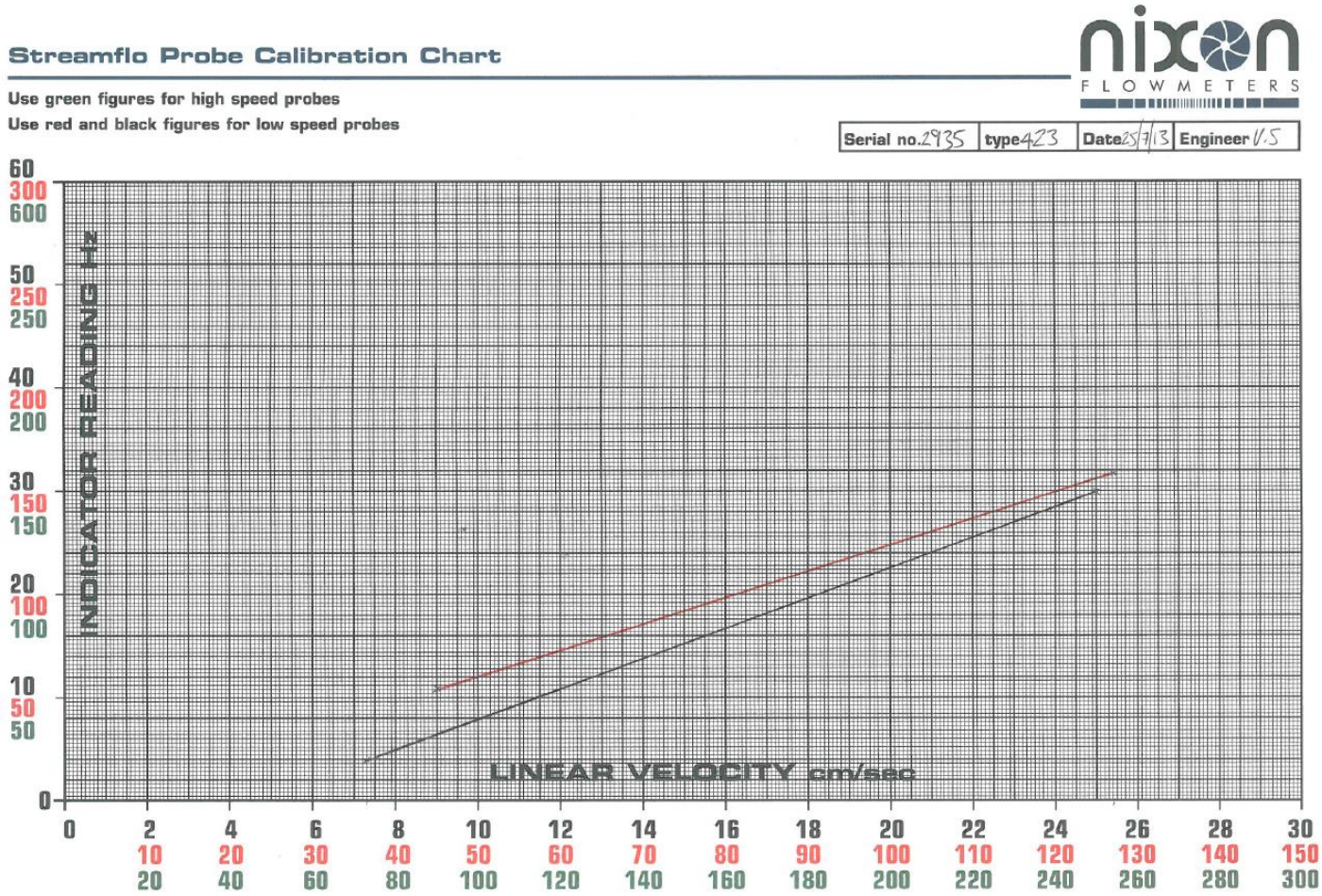

Figure 3-7 Flow velocity calibration chart

Figure 3-8 Flow velocity measurement apparatus set-up

3.1.4 Transmembrane pressure and permeate flux analysis

3.1.4.1 Transmembrane pressure (TMP) and data acquisition system

The TMP was measured via a pressure sensor (Hydrotechnik, PR140 HT-PD) installed on the line between the membrane and the permeate withdrawal pump. The pressure sensor was connected to a 15V DC power supply and transmitted the pressure signal to a data acquisition unit (LabJack, U3-LV) connected to a personal computer (PC) for a data logging purposes.

3.1.4.2 Permeate flux measurement

Permeate flux was withdrawn by variable-speed peristaltic pump (Watson Marlow) and measured by monitoring the rate of change in weight of collected permeate overtime (stopwatch).

3.1.4.3 Liquid level control and influent feeding system

A liquid level control system was set up to avoid deficiency or overflow caused by imbalance between the influent and effluent flows driven by peristaltic, and to maintain a steady liquid level and a stable pressure in the headspace of the reactor (in case of the closed reactor). Influent feeding was by a Cole-Parmer Masterflex L/S pump. The control system was comprised of a control unit (OMRON, 61F-GP-N8) and a sensor with three conductive electrodes (OMRON, PS-31). The sensor with three electrodes was mounted above the reactor in which each electrode represented a reference electro-conductive point (the longest), high-contact point, and low-contact point; the length difference between the high-contact point and low-contact point was set to 4 cm. The level control system was applied to control the influent pump which was supplied from a feeding vessel, by detecting the liquid level positions inside filtration reactor. If the level position was below the low-contact point, the feeding pump would start pumping, whereas the feeding pump would stop if the level reached the high-contact point. The influent feeding vessel was placed on a magnetic stirrer to maintain a homogenous feed concentration.

3.1.5 Scouring media

This part of the study was focused on the application of non-adsorbent particles for fouling mitigation and flux enhancement purposes. Therefore, choosing scouring media is one of the crucial factors to achieve effective performance for mechanical cleaning process. The principles outlined by Rosenberger *et al.* (2011) and summarised in section 2.2.7.1 were therefore applied.

3.1.5.1 Low density polyethylene (LDPE) particles

Round flat-lens shaped rigid LDPE plastic beads with a specific gravity (SG) of 0.86 - 0.96 and ∅ 3 - 4 mm with 1.5 - 2 mm thickness, as shown in Figure 3-9, were applied as scouring media in the work described in Chapter 5.

Figure 3-9 LDPE particles (carriers)

These LDPE plastic beads are cheap and readily available on the commercial market, and were chosen for use as scouring media in some parts of this study. The major drawbacks of these LDPE beads are that they tend to float, making it difficult to re-circulate them in a gaslift-loop reactor; their apparent size of 2-3 mm is relatively small compared to the 7 mm of the membrane panel gap; and the material is in a relatively rigid form.

Although the LDPE beads did not meet all of the criteria for scouring media as recommended by Rosenberger *et al.* (2011), some of their properties were suitable, such as the round shape with no sharp edges, SG of approximately 0.9 which is relatively close to that of water, and the fact that LDPE is an inert material. Therefore, the LDPE beads were applied as scouring agents in experiments with model mixed suspension simulating anaerobic conditions in order to evaluate the feasibility of using non-adsorbent particles in AnMBR systems for the further stage in this work.

3.1.5.2 Polyethylene Glycol (PEG) granules

Engineered PEG plastic granules used in certain parts of this research were manufactured by and supplied from Nisshinbo Chemical Inc., Japan. The plastic granules were originally developed as bio-carriers for wastewater treatment processes since they have a hydrophilic surface that could enhance attached microbial growth in bioreactors. The granules are mainly made of polyethylene glycol and have the commercial name of Bio Contact-N (BC-N) bio-carriers. BC-N carriers were provided and delivered in dried form with an apparent size of 1 - 2 mm (Figure 3-10 (a)). The carriers were soaked in tap water for about 30 minutes to allow granule swelling before filling into the bioreactor (Figure 3-10 (b)).The swelled PEG granules have a cylindrical shape with length and height of 4 mm x 4 mm (maximum dimension of 5.7 mm diagonal), and SG of 1.01 - 1.05, which means they can be easily re-circulated between the 7 mm of membrane clearance. In addition, swelled PEG granules have a soft-flexible hydrogel texture that is believed not to damage the membrane surface even during long-term operation. Hence, swelled PEG granules were chosen for application as scouring agents for long-term moving bed AnMBR operation experiments in Chapter 6.

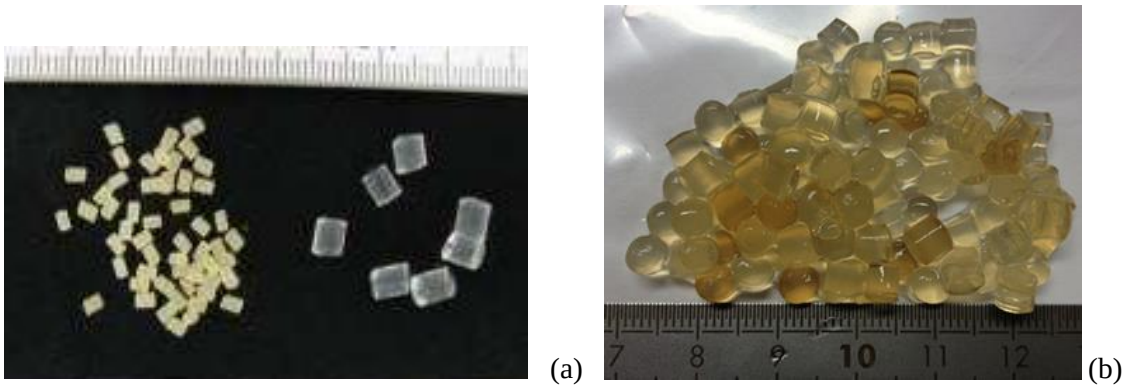

Figure 3-10 Polyethylene glycol granules (a) dried and swelled form and (b) hydrogel texture of swelled PEG granules

3.2 Two-phase gas-sparged AnMBR (GSAnMBR) and three-phase moving bed AnMBR (MBAnMBR) treating dairy wastewater

3.2.1 GSAnMBR and MBAnMBR system

3.2.1.1 Reactors set-up

Single stage laboratory-scale GSAnMBR and MBAnMBR were made of grey and clear polyvinyl chloride (PVC) plastic in the same scale with internal dimensions of 22.6 cm (length) x 6.8 cm (width) x 115 cm (height). Maximum liquid level was kept constant at 65 cm by a conductive level switch controller (OMRON PS-31 probe and OMRON 61F-GP-N8 controller), that controls the feeding pumps to give a liquid working volume of 6.6 L. Single A4 size flat sheet membranes (Kubota) made of chlorinated polyethylene with a nominal pore size of 0.4 μm and total membrane surface of 0.1 m^2 were used in each reactor. Both the GSAnMBR and the MBAnMBR were set up in a split-type gaslift-loop configuration. The reactors were divided into a riser and downcomer zone by a separation baffle, where the membrane panel was installed inside the riser with the membrane clearance between the front wall and the baffle fixed at 7 mm. The cross-sectional area of the riser (minus the membrane shadow) (A_r), downcomer (A_d) and transversal flow at the bottom (A_b) were 30.0, 68.5 and 96.3 cm^2, respectively, which gave A_d/A_r and A_d/A_b ratios of 2.3 and 0.7.

For fouling mitigation and mixing purposes, produced biogas from the reactor headspace was circulated for sparging by vacuum diaphragm pumps (12 V, DC vacuum pump, Airpro). Biogas circulation rates were set at 2.5 L min^{-1} for low flowrate and 5 L min^{-1} for high flowrate, regulated by a DC power supply regulator and determined by inline gas rotameters. The superficial gas velocities in the riser zone (U_g) were calculated as 50 and 100 m $hour^{-1}$. Excess produced biogas

was collected using gas bags installed at the top of the reactors in order to measure biogas production rates and composition. Biogas was introduced via spargers made of ∅ 6 mm stainless tube, with each sparger having two nozzles of ∅ 1.5 and ∅ 3 mm with one open end (Figure 3-3). Permeate was extracted by peristatic pumps (Watson Marlow, 505 series) with an intermittent suction mode of 8 min-on/2 min-off for suction and relaxation. Suction pressures were record by pressure transducers (PR140 HT-PD, Hydrotechnik) connected to a data acquisition unit (LabJack U3-LV).

Both the GSAnMBR and MBAnMBR were operated under mesophilic conditions at temperature of 37 ± 1 °C controlled by a thermocirculator connected to heat loops inside each reactor, while the temperature of the bulk liquid was monitored and logged by thermal sensors.

Swelled BC-N carriers were used as non-adsorbent scouring agents in this study. BC-N granules with the apparent bulk volume of 0.6 L (corresponding to 10 % of reactor volume) were placed in one reactor operated as an MBAnMBR, with the granules completely retained inside the reactor without replenishment throughout the operational period by ∅ 3 mm screen installed at the excess sludge wasting port.

Schematic of the GSAnMBR and MBAnMBR set up, and pictures of the system arrangements are presented in Figure 3-11 - Figure 3-12, respectively.

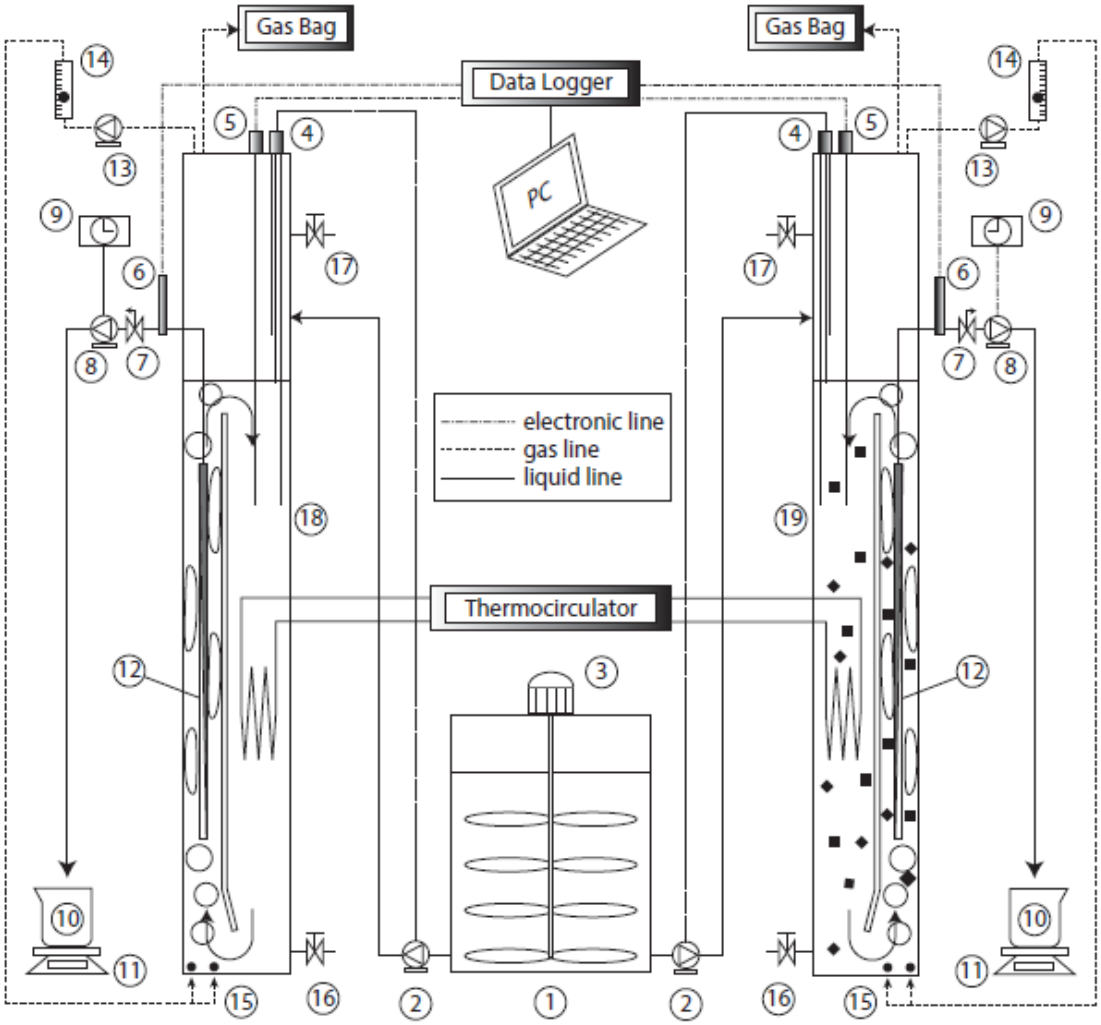

Figure 3-11 Schematic of GSAnMBR and MBAnMBR set-up

Where: 1) feedstock tank, 2) feeding pumps, 3) agitator, 4) level control probes, 5) thermometer probes, 6) pressure transducer, 7) check valves, 8) peristatic pumps, 9) timer switches, 10) permeate collection vessels, 11) digital balances, 12) membrane panels, 13) vacuum diaphragm pumps, 14) rotameters, 15) biogas spargers, 16) wasting/sampling ports, 17) supplementary ports, 18) GSAnMBR and 19) MBAnMBR

Figure 3-12 GSAnMBR and MBAnMBR arrangements

3.2.1.2 Inoculum and synthetic dairy wastewater feeding

Both the GSAnMBR and MBAnMBR were seeded with anaerobic biomass collected from a full-scale mesophilic digester treating municipal wastewater biosolids (Millbrook, Southampton, UK). The inoculum was sieved to eliminate particles larger than 2 mm. This type of inoculum is useful as it contains a consortium of microbes to undertake anaerobic activities from hydrolysis, acidogenesis and acetogenesis to methanogenesis. A strictly anaerobic environment was established by flushing nitrogen gas through the reactors' headspace at the start-up stage.

With the objective of simulating low to medium strength dairy production wastewater in a COD range of 500 - 3,900 mg L^{-1}, the reactors were fed using diluted whole milk powder (Nido instant full cream milk powder, Nestle). Dissolving 0.8 g milk powder L^{-1} of tap water provided an average TSS, TVS and COD of about 275, 268 and 1,000 mg L^{-1} respectively. Synthetic dairy wastewater was prepared daily as a feedstock to design strengths. Feedstock (per 1 L) was supplemented with nutrients and trace elements using the recipe modified from Shelton and Tiedje (1984), which consisted of : 530 mg of NH_4Cl, 75 mg of $CaCl_2 \cdot 2H_2O$, 100 mg of $MgCl \cdot 6H_2O$, 20 mg of $FeCl_2 \cdot 4H_2O$, 0.5 mg of $MnCl_2 \cdot 4H_2O$, 0.05 mg of H_3BO_3, 0.05 mg of $ZnCl_2$, 0.03 mg of $CuCl_2$, 0.01 mg of $NaMO_4 \cdot 2H_2O$, 0.5 mg of $CoCl_2 \cdot 6H_2O$, 0.05 mg of $NiCl_2 \cdot 6H_2O$ and 0.05 mg of Na_2SeO_3, also 250 mg of $NaHCO_3$ was added as a buffer to control the pH at around neutral.

3.2.1.3 Sample collection

Influent, effluent (treated permeate) and mixed liquor were regularly taken from feedstock tank, permeate drawn pumps and sampling ports of both reactors, respectively, for analysis. Net permeate fluxes were determined daily by a weight-time measurement method. Suction pressures were recorded by a data acquisition system. Produced biogas was collected in the gas bags which were replaced daily. The influent COD concentration (COD_{inf}) was determined by averaging values from fresh preparation daily and feedstock left overnight at room temperature. The supernatant samples (S) were obtained by centrifuging the mixed liquor of bioreactors (Eppendorf 5417 C/R, Eppendorf, Hamburg Germany) at 17,900 g (13,000 rpm) for 30 min.

The bioreactor removal efficiency (R_s), representing biological degradation in the reactor and based on centrifuged supernatant liquor, and the total removal efficiency (R_t) including biodegradation and membrane filtration and based on membrane-filtered effluent, were calculated based on Equation 3-10 and Equation 3-11 respectively.

Equation 3-10

$$\mathrm{R_s} = \frac{\mathrm{COD_{inf}} - \mathrm{COD_s}}{\mathrm{COD_{inf}}} \times 100\%$$

Equation 3-11

$$\mathrm{R}_t = \frac{\mathrm{COD_{inf}} - \mathrm{COD}_{eff}}{\mathrm{COD_{inf}}} \times 100\%$$

Where:

COD_{inf}, COD_s and COD_{eff} are the COD of influent, supernatant of centrifuged mixed liquor and effluent (membrane permeate), respectively.

Sample of the initial mixed liquor of inoculum of both reactors (at day 0) and mixed liquor from both reactors on the last day of operation (day 308) were taken to measure particle size distributions analysed by a laser light scattering analysis technique (Saturn DigiSizer II, micromeritics, USA).

At the end of the experimental run, small pieces of membrane surface from both reactors were removed and then dried in a critical point drying apparatus. Thereafter, membrane surface morphologies were examined through Scanning Electron Microscope (SEM) (JCM-6000Plus, JEOL, Japan).

3.2.2 General Analytical Methods

3.2.2.1 Chemical Oxygen Demand (COD)

COD was measured by the closed tube reflux method with titrimetric determination of the end point. If the sample COD was more than 400 mg L^{-1} pre-dilution was carried out. 2 mL of sample (or 2 mL DI water for blanks) was placed into the reflux tubes followed by the addition of 3.8 mL of FICODOX-plus reagent (Fisher Scientific Ltd, UK), the composition of which is shown in Table 3-1. The tube was sealed with a PTFE screw cap and the mixture refluxed at 150 ^{o}C for 2 hours. After cooling, a few drops of ferroin indicator (Table 3-1) were added (Fisher Scientific Ltd, UK) and the mixture titrated with acidified (2% Sulphuric acid) 0.025N ferrous ammonium sulphate solution, the normality of which was calculated using Equation 3-12. The end point was a colour change from blue to red. Dilutions of a standard solution containing 3.8 g L^{-1} of potassium hydrogen phthalate with a COD of 4 g COD L^{-1} were used as a standard to check calculated values of COD. COD values were calculated according to the following Equation 3-13.

Equation 3-12

$$\mathrm{M} = \frac{0.625}{\mathrm{V}}$$

Equation 3-13

$$\mathrm{COD} = \frac{(\mathrm{A} - \mathrm{B}) \times \mathrm{M} \times 4{,}000}{\text{dilution factor}}$$

Where:

M is molarity of FAS

V is volume of FAS titrated in molarity measurement (mL)

COD is Chemical oxygen demand of sample (mg O_2 L^{-1})

A is average volume of FAS used for blank (mL)

B is volume of FAS used for sample (mL)

Table 3-1 FICODOX-plus composition

Chemical	Concentration
Potassium di-chromate	1.7 g L^{-1}
Silver sulphate	8.1 g L^{-1}
Sulphuric acid	81.1%

Modified COD reagent, contains (g L^{-1}):

- Potassium dichromate 1.62 g
- Silver sulphate 7.94 g
- Sulphuric acid 794 mL

3.2.2.2 Total and Volatile Suspended Solids

Total suspended solids (TSS) content was measured by passing a sample of known volume through a 0.4 μm pore size glass fibre filter paper (GF/C, Whatman, UK) of known dry weight (± 0.1 mg). After drying at 105 ºC for 24 hours the paper was again weighed and the difference determined according to the following Equation 3-14 and Equation 3-15.

Equation 3-14

$$SS = \frac{(W_2 - W_1) \times 1{,}000}{V_s}$$

Equation 3-15

$$VSS = \frac{(W_2 - W_3) \times 1{,}000}{V_s}$$

Where:

SS is suspended solids (mg L^{-1})
VSS is volatile suspended solids (mg L^{-1})
W_1 is weight of clean filter paper (mg)
W_2 is weight of filter paper + sample (mg)
W_3 is weight of filter paper + sample after heating to 550°C for 2 hours, (g)
V_s is sample volume (mL)

3.2.2.3 Gas Composition by gas chromatography

Biogas composition (CH_4 and CO_2) was measured using a Varian Star CP-3400 CX gas chromatograph (Varian, Oxford, UK) with a gas sampling loop and thermal conductivity detector with argon as the carrier gas at a flow of 50 mL min^{-1} with the run time of 1.5 min per sample. The GC was fitted with a Hayesep C column and a molecular sieve 13 × (80 - 100 mesh) operating at a temperature of 50 ºC. The GC was calibrated using a standard gas containing 35 % CO_2 and 65 % CH_4 (v/v) (BOC, UK). The small amount of air in the sample normally caused by atmospheric entering digester headspace during feeding is corrected by excluding the volume of air from the total sample volume. During analysis, a 5 mL sample was directly taken from the gas bag for semi-continuous experiments and was injected into the gas sampling loop of this instrument.

3.2.2.4 Gas volume

The volume of biogas collected in gas bags was quantified by a water displacement gasometer (Walker *et al.*, 2009). In this device the biogas flowed from the gas bag to a water column under vacuum and the water displaced was introduced into a tank on a balance which allowed weight determination of discharged water. The procedure included the recording of initial height of the water column before the gas collected with the gas bag was introduced into the column from its headspace, and the weight of water displaced after the gas bag was empty. The ambient temperature (T) and pressure (P) were recorded at the same time. The volume of dry biogas was calculated using equation below, and reported as the volume under standard temperature and pressure (STP) of 0, 101.325 kPa. Weight Gasometer Governing Equation (Walker *et al.*, 2009) was shown in Equation 3-16.

Equation 3-16

$$V_{stp} = \frac{T_{stp}A}{T_{atm}P_{stp}}\left[\left((P_{atm} - P_{H_2O(T_{atm})}\right) - \rho_{H_2O}g(H - h_1 - \frac{m_{H_2O}}{A\rho_{H_2O}}))(h_1 + \frac{m_{H_2O}}{A\rho_{H_2O}}) - (P_{atm} - P_{H_2O(T_{atm})} - \rho_{H_2O}g(H - h_1))h_1)\right]$$

Where:

V_{stp} is biogas volume at standard temperature and pressure (m^3)

P_{stp} is standard pressure, 101325 (Pa)

P_{atm} is ambient pressure (Pa)

T_{stp} is standard temperature, 273.15 (K)

T_{atm} is ambient temperature (K)

$P_{H2O(Tatm)}$ is saturated water vapour pressure at temperature T_{atm} (Pa)

H is total height of gasometer (m)

h_1 is distance from the top of gasometer to liquid surface in gasometer (m)

A is cross-sectional area of water column in gasometer (m^2)

m_{H_2O} is mass of water displaced(kg)

ρ_{H_2O} is density of water, kg m^{-3}

g is gravitational acceleration (m s^{-2})

Chapter 4: **Hydrodynamic parameters in gas-liquid two-phase flow for submerged flat-sheet airlift-loop MBR**

Two-phase air/gas sparging has been applied extensively in membrane bioreactors (MBRs) for three major roles: to mitigate fouling, to provide oxygen in aerobic MBRs (AeMBRs) and to maintain the biomass in suspension. In most cases, sparging for fouling control purposes is the largest energy demand for MBR operation. Hence, improved hydrodynamic designs are of prime importance to obtain the most effective exploitation of the energy input.

Therefore, the objectives of this chapter were to characterise the effect of hydrodynamic operating parameters (such as gas flow rate, nozzle size and tank geometry) on two-phase flow characteristics (such as bubble size and size distribution, liquid flow velocity) and on membrane filtration performance (in term of flux production) in order to determine the optimum two-phase flow operating conditions for a gaslift-loop submerged flat-sheet membrane bioreactor.

4.1 Bubbling characterisation

Based on the results of the literature review (section 2.3), a range of factors including sparging intensity, diffuser port size and sparger arrangement were identified as having a strong effect on bubble size, size distribution and bubble distribution and thus on the shear stress and cross flow velocity. Therefore, bubble sizes and size distributions created from varied nozzle sizes of ∅ 1, 2, 3 and 4 mm on perforated tube spargers under gas sparging intensities of 2, 4, 6, 8 and 10 L min^{-1} are evaluated in this section.

4.1.1 Effect of nozzle parameters on bubble sizes and size distribution

4.1.1.1 Visual observations

The reactor set-up described in section 3.1.1 with A_d/A_r ratio of 3.7 and A_d/A_b of 0.65 and ∅ 6 mm sparger tubes with varied nozzle sizes diameters of 1, 2, 3 and 4 mm was used in these experiments. Still photographs for bubble flow in 7 mm channel depth of each nozzle diameter under sparging rates of 2, 4, 6, 8 and 10 L min^{-1} were taken in order to evaluate bubble sizes and size distributions of each condition, as described in section 3.1.2.

From visual observations during the experiments, bubbles detached from nozzles and rose three-dimensionally for 30 cm before hitting the bottom edge of the simulated flat sheet membrane

module. Subsequently, two-phase flow occurred in 7 mm depth pseudo-2D thin channels for both the front and back sides of the simulated module. Some photographs of analysed bubbles pictures from images processing taken from each nozzle size at different air flow rates are shown in Figure 4-1.


(a)

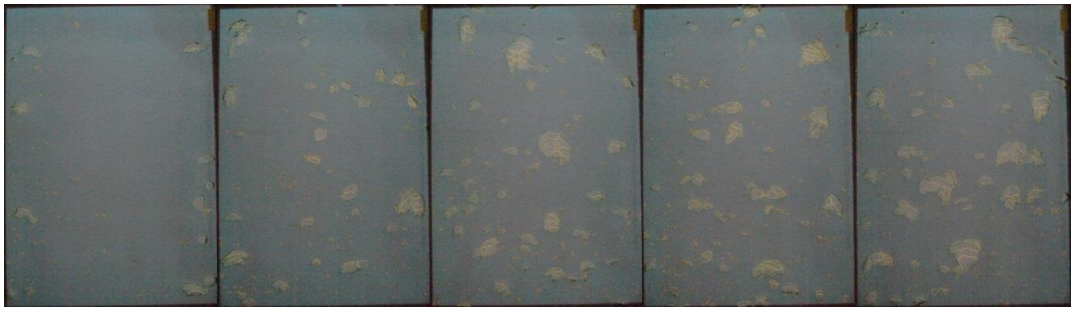
(b)


(c)

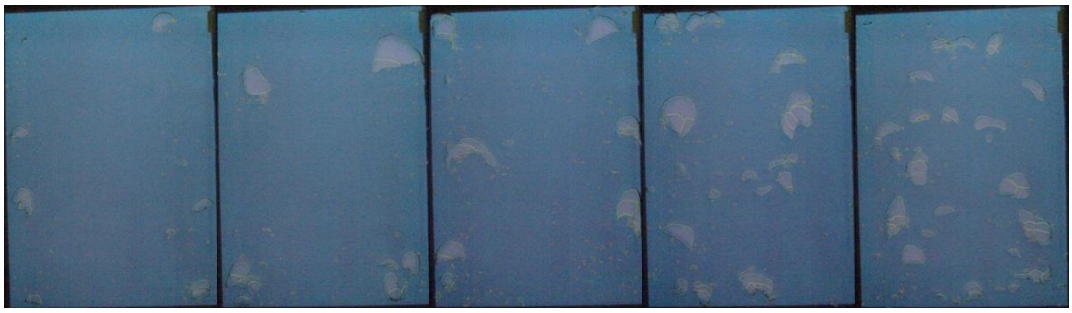
(d)

Figure 4-1 Analysed bubble characteristics by images processing software for nozzles diameters of (a) 1 mm, (b) 2 mm, (c) 3 mm and (d) 4 mm, at air flow rates of 2, 4, 6, 8 and 10 L min^{-1} (from left to right)

The pictures show an increasing bubble population density as the sparging rate increased. Closer visual observation of the pictures shows that bubbles with sizes greater than the 7 mm of membrane clearance exhibited amorphous, two-dimensional confined shapes in the channel, while bubbles smaller than the clearance had circular and ellipsoidal shapes. In addition, from visual observations during experimental period, it was found that bubbles sizes and shapes are changeable due to their clashing, coalesce and break-up. In real wastewater with mixed suspensions such as activated sludge or anaerobic digestate which are non-Newtonian fluids with higher viscosity than tap water, increased rigidity of bubble surfaces is expected that will result in reduction of bubble deformation (Bohm *et al.*, 2012; Sato, Hayashi and Tomiyama, 2015).

The still pictures show that bubbles are well distributed over the simulated membrane surface for small nozzle sizes of 1 mm and 2 mm cases. For the bigger nozzle sizes, nonetheless, more bubbles were observed appearing from nozzles close to the air inlet direction, particularly at the low air flow rates of 2 - 4 L min^{-1}. For ∅ 3 mm nozzles, when the sparging rate was increased to above 6 L min^{-1}, uniform bubbles flow over the membrane surface was observed.

However, unequal bubble detachment from each nozzle was still clearly observed in the case of the ∅ 4 mm nozzle: even when sparging rates were increased up to 6 L min^{-1}, large bubbles were generated from only one nozzle hole closest to the air inlet direction (Figure 4-1 (d)). This result is in agreement with Kira *et al.* (2012) who compared the effect of diffuser hole sizes of ∅ 2, 5 and 8 mm on ∅ 20 mm perforated pipe diffuser, on generated flow rates from each diffuser hole (considered as bubble frequencies and bubble volumes) for total supplied sparging intensity of 30 L min^{-1} from one pipe end. Their results showed that, under the same sparging rate of 30 L min^{-1}, small diffuser holes of ∅ 2 mm presented almost equal air flow distribution from all diffuser holes (5 holes) along the sparger range. Whilst, for the large nozzle hole of 8 mm, most of the air was released from 1 to 2 holes close to the air entering direction. The results indicated that the generated flow rate from each nozzle hole is strongly depended on hole size and orifice coefficient (Kira *et al.*, 2012).

The unequal gas discharge from each nozzle is a major problem for perforated tube spargers. This is due to the fact that in order to obtain uniform gas distribution along the perforated duct, the pressure drop in the gas flow direction due to internal surface wall friction in the tube and the kinetic energy of gas inlet have to be balanced properly. Typically, with the same nozzle size under different given sparging intensity, if the friction is dominant, the holes close to the gas inlet direction discharge almost all of the gas. Conversely, if the input kinetic pressure is strong enough to prevail over friction, the holes at the rear end discharge more gas than the entrance holes (Nguyen Cong Duc *et al.*, 2008). For a perforated tube with the same internal wall friction under the same given gas inlet rate, a bigger nozzle size as ∅ 4 mm in this study has lower sparging

resistance than the smaller ones. Hence, gas discharge and bubble detachment were observed from only one or two nozzle holes close to the gas inlet direction.

An uneven bubble distribution and asymmetric sparger arrangement could create unfavourable flow conditions inside the reactor. Nguyen Cong Duc *et al.* (2008) investigated the local hydrodynamics of aeration in a submerged hollow fibre membrane cassette using perforated tubes with holes of 6 and 8 mm as spargers supplied at an air flow rate of 90 m^3 h^{-1} from one end. According to their findings, the fact that the spargers were not situated centrally in the reactor accompanied by non-uniform bubble distribution along the sparger tubes, led to the creation of a liquid phase circulation loop leading in turn to a lateral motion of the bubble swarm, and thus to a stagnant flow zone. Similar results for uneven bubble distribution were reported by Ndinisa, Fane and Wiley (2006) and Ndinisa *et al.* (2006) who tested a perforated tube sparger with nozzle diameters of 0.5, 1, 1.5 and 2 mm with air flow rates of 2, 4, 6 and 8 L min^{-1} supplied from one end of sparger duct for a flat-sheet membrane. They observed that bubbles towards the centre of the column were flowing up while those near the edges were flowing down or held almost stationary due to the recirculation of fluid flow in that region, which then caused spatial deposition of foulants in this zone. The problem of a liquid stagnant zone also affects the shear stress. The maximum shear stress calculated by Ndinisa, Fane and Wiley (2006) at the highest sparging rate was significantly lower than that observed by Prieske *et al.* (2010) (in comparison between 0.7 and 4.0 Pa). This is mainly due to the fact that the system setup by Ndinisa, Fane and Wiley (2006) did not provide a continuous crossflow (annular recirculation flow) with an upflow section within the membrane module and a downflow zone at the sides or the back of the module (i.e. riser and downcomer). Thus liquid flow recirculation and a flow stagnant zone inevitably occurred within the channel under examination, whereby the overall flow was slowed down.

As a result, in attempt to reduce the problem of uneven bubble distribution along a perforated sparger tube, two sparger pipes with gas supplied from one end (one from the left side and another one from the right side) were installed beneath the membrane module in order to balance bubble flow over the entire membrane surface. Furthermore, in order to minimise the liquid stagnant zone caused by bubble maldistribution, the reactor used in this study was set up as a gaslift-loop configuration in which annular crossflow velocity can be continually enhanced.

4.1.1.2 Number mean diameter (D_{10}) of bubble swarm and bubble size distribution involved occurrence aspect

A large amount of information was obtained from analysis of the photographs with particle imaging software. For each experimental condition, all bubbles from 5 pictures based on both "with bubble-membrane contact" and "without bubble-membrane contact" cases were analysed, and the results were combined in order to obtain an average. In this section, the total number of

bubbles and the average number of bubbles per picture, the mean diameter (D_{10}) number (calculated by adding the diameters for all the bubbles and dividing by the total number of bubbles), and the bubble size distribution were evaluated.

The total number of bubbles produced in each picture and the average total number per picture are shown in Table 4-1 and Figure 4-2, respectively. From Table 4-1 and Figure 4-2, the results show that an increase in the amount of gas injected resulted in an increase in the number of bubbles for the same nozzle size. The maximum bubble population density was found for the 1 mm nozzle, in the range of 147 - 282 average bubbles per picture at the air flow rate of 2 - 10 L min^{-1}. By comparing the results for different nozzle sizes under a fixed air flow rate, it was found that the number of bubbles decreased with an increase in nozzle size from 1 to 3 mm. This is probably due to the size of the bubbles generated from different nozzle diameters, and the frequency of bubble appearance. However, from nozzle size 3 to 4 mm, average bubble counts were observed to increase. This may be due to the break-up of larger bubbles generated from the ∅ 4 mm nozzle itself, or clashing with the bottom edge of the simulated membrane, and consequently producing a larger numbers of small bubbles.

Table 4-1 Total number of bubbles, average bubble numbers per picture and mean diameter (D_{10}) number

nozzle size	gas flow rate	number of bubbles in picture					total number of bubbles	average number of bubbles per picture ± SD	D_{10}
(mm)	(L min^{-1})	1	2	3	4	5			(mm)
1	2	105	184	120	174	151	734	147 ± 34	3.4
	4	134	291	272	230	290	1,217	243 ± 66	3.2
	6	151	243	249	295	196	1,134	227 ± 55	3.6
	8	166	248	281	316	247	1,258	252 ± 56	3.8
	10	185	266	256	336	367	1,410	282 ± 72	3.5
2	2	37	46	120	117	64	384	77 ± 39	3.7
	4	59	188	195	196	126	764	153 ± 60	3.6
	6	156	131	194	212	199	892	178 ± 34	4.0
	8	168	186	301	236	192	1,083	217 ± 53	3.8
	10	190	218	261	187	235	1,091	218 ± 31	4.1
3	2	55	41	38	14	33	181	36 ± 15	11.1
	4	80	87	73	75	54	369	74 ± 12	5.6
	6	105	91	95	86	88	465	93 ± 8	6.0
	8	106	115	125	111	113	570	114 ± 7	5.5
	10	101	100	131	115	106	553	111 ± 13	6.1
4	2	87	78	53	83	92	393	79 ± 15	3.0
	4	116	102	74	128	129	549	110 ± 23	3.5
	6	115	164	195	115	167	756	151 ± 35	3.3
	8	151	153	178	212	151	845	169 ± 27	3.7
	10	126	145	207	301	181	960	192 ± 69	3.6

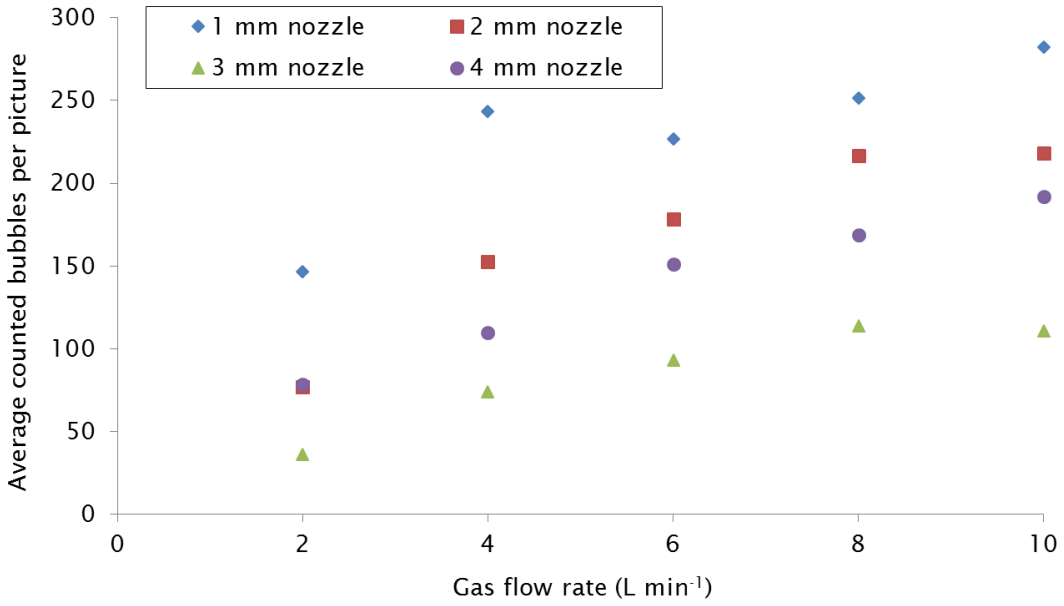

Figure 4-2 Average number of bubbles occurrence per picture of each experimental condition

As mentioned earlier, bubbles were observed to be produced from only one or two nozzle holes close to the air inlet direction in the case of large nozzle diameters such as ∅ 4 mm, with lower frequency but larger bubble sizes when compared to smaller nozzle diameters. From visual observation, a larger plume of bubbles was initially detached in a pulse from the ∅ 4 mm nozzle, which then broke up into a few big bubbles and several small bubbles which then rose to the membrane channel. This caused the number of bubbles in the photograph for the 4 mm nozzle to increase. Consequently, the total numbers of detected bubbles affected the calculated mean bubble diameters as shown in Figure 4-3.

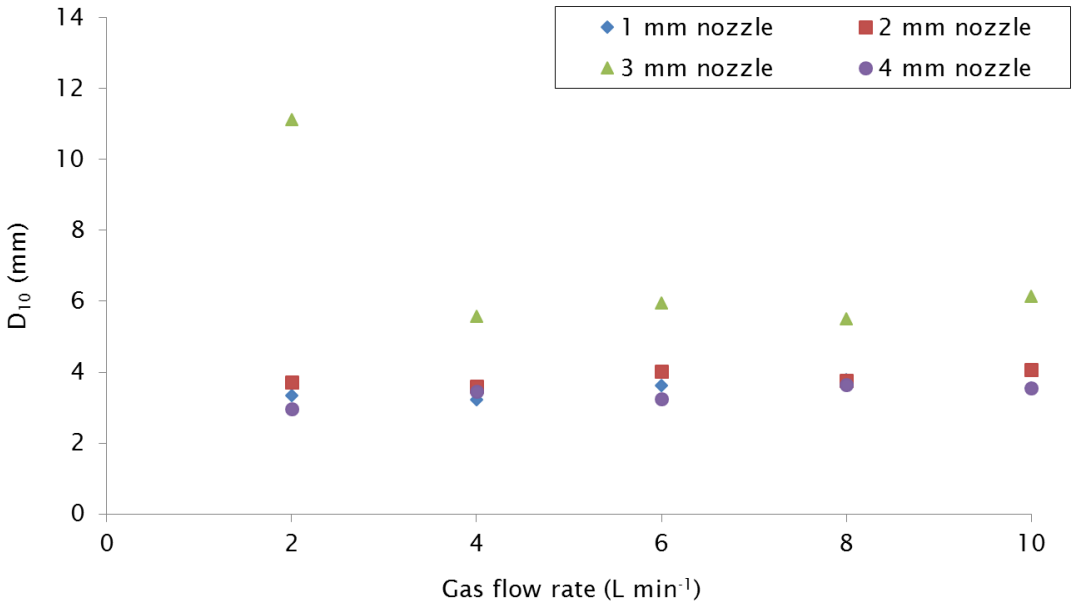

Figure 4-3 Average mean bubble diameters per picture for each set of conditions

From Figure 4-3 and Table 4-1, with the same nozzle size, D_{10} does not seem to be a strong function of gas sparging rate. D_{10} values are almost constant even where the gas flow rate has been increased to 10 L min^{-1} for a given nozzle size. When considering the effect of the nozzle on D_{10} under a fixed given gas flow rate, it can be seen that D_{10} slightly increased for an increase in nozzle size from ∅ 1 to 3 mm due to the larger number of big bubbles observed; while the D_{10} value from the 3 mm nozzle seems to be larger compared to other nozzle sizes at the same air flow rate, especially at 2 L min^{-1}. The highest values of D_{10} were observed as a result of relatively large bubble sizes and a lower population of small bubbles. D_{10} values became smaller again for ∅ 4 mm nozzle, however, due to the breaking-up of large bubble plumes and the increase in the small bubble fraction mentioned earlier.

As the number of bubble occurrences and the individual size of each bubble have a strong effect on representative equivalent bubble size D_{10} for bubble swarms, bubble size distributions for the number of bubbles detected from all 5 pictures are plotted and presented in Figure 4-4.

.

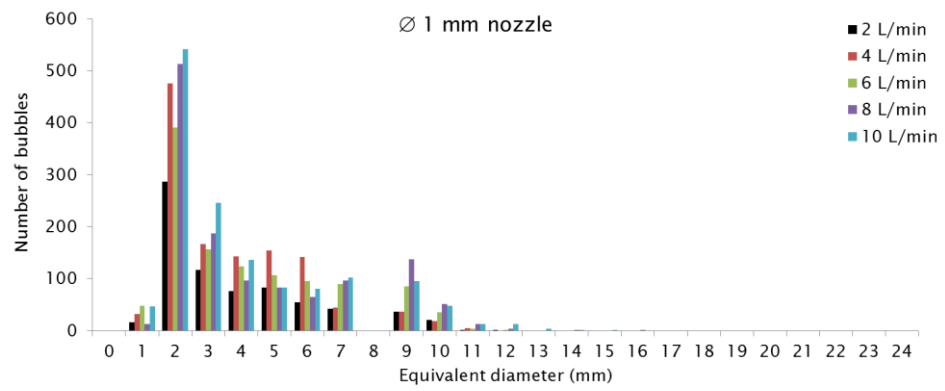

(a)

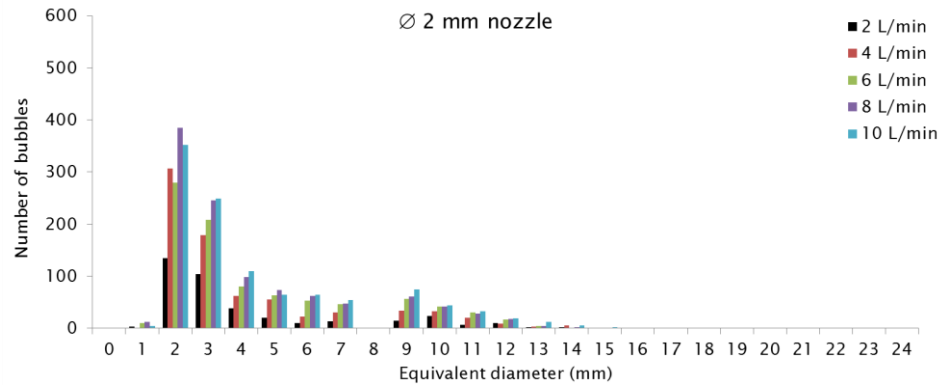

(b)

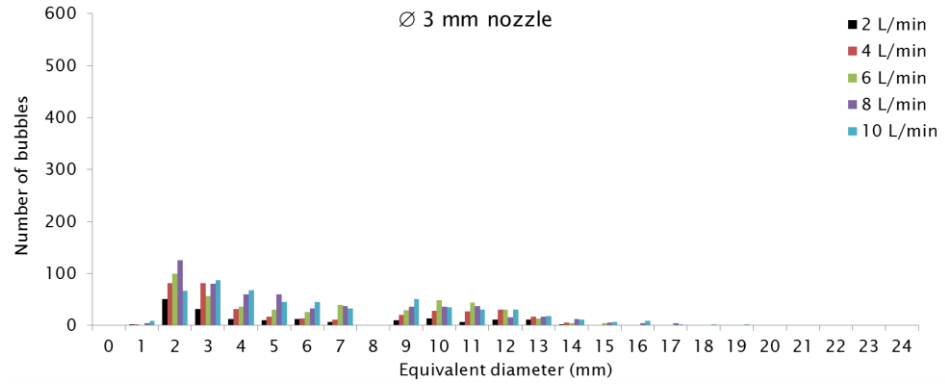

(c)

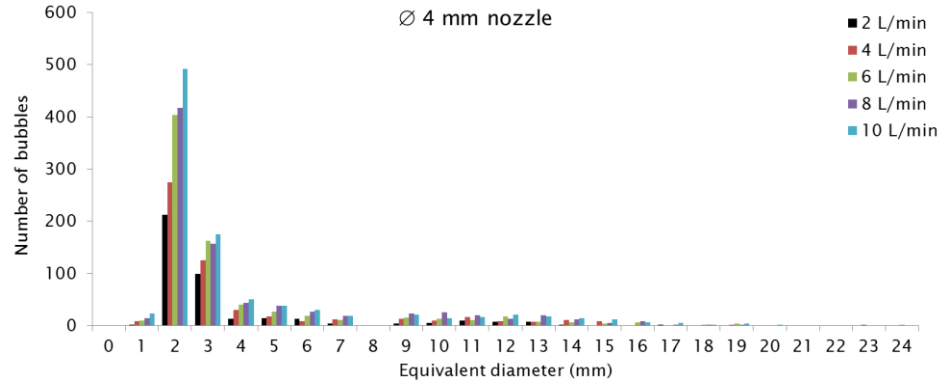

(d)

Figure 4-4 Bubble size distributions related from 5 pictures at 2, 4, 6, 8 and 10 L min^{-1} air flow rate for nozzle size of (a) 1 mm, (b) 2 mm, (c) 3 mm and (d) 4 mm

In general from Figure 4-4, it can be seen that the higher the air flow rate, the greater the number of bubbles for all nozzle sizes. Bubble size 2 mm occurs most frequently for all nozzle sizes at a fixed given air flow rate, except the ∅ 3 mm nozzle at 10 L mim^{-1} sparging rate for which the 3 mm bubble has the highest observed frequency.

For the smallest nozzle size of ∅ 1 mm, most of the bubble population is found scattered in the fraction of small bubble sizes, which are smaller than the membrane gap (∅ bubbles 1 - 7 mm). With an increase in nozzle size to ∅ 2 mm, the proportion of bubbles smaller than 7 mm tends to decrease, while the bubbles bigger than 7 mm slightly increase and expand to larger diameters. The biggest bubbles produced from the ∅ 1 and 2 mm nozzle are 16 and 17 mm in diameter, with one occurrence during the experiment at the same 8 L min^{-1} sparging rate. This trend is more clearly seen in the case of the ∅ 3 mm nozzle, where the fraction of bubbles smaller than 7 mm decreased while the fraction bigger than 7 mm increased as did the bubble diameter. The largest observed bubble diameter is 23 mm with one occurrence at 10 L min^{-1} bubbling rate. For the nozzle size of 4 mm, the number of small bubbles of 2 - 3 mm rose again due to the breakage of large bubble plumes as described before. The observed bubble frequency still included bigger bubbles, however, with the largest produced bubble being 24 mm diameter with once occurrence at 6 L min^{-1} sparging intensity.

Noticeably no bubble with a diameter of 8 mm was reported in the results. This is possibly a result of the image processing analysis procedure. The bubble diameter calculation method in this study is based on the assumption of 2D bubble projected areas which are larger or smaller than the 7 mm channel depth. Observed projection areas which are only slightly greater than 38.5 mm^2, would be multiplied by 7mm giving a volume over 269.5 mm^3. At the volume of 269.5 mm^3, the calculated equivalent circular diameter is 8 mm. By this measurement technique, the projective surface areas between 31.6 and 45.9 mm^2, which give equivalent circular diameters of 7.5 - 8.5 mm, had not been detected during the experiments. Consequently, no bubbles with 8 mm diameter size were observed.

The results in this section showed that most of the mean diameters from all experimental conditions are smaller than the 7 mm membrane gap (Table 4-1 and Figure 4-3). The D_{10} and size distribution related to apparent frequency may not clearly reflect the bubble swarm size distribution, however, since the gas volume from one large bubble might be equivalent to the volume generated from numerous small bubbles. Therefore, therefore the bubble size distribution related to number of bubble occurrences and the generated volume of each bubble size are considered together in the next section.

4.1.1.3 Median of volume distribution (D_{V50}), Sauter mean diameter (D_{32}) and bubble size distribution involved accumulated bubble volume aspect

Bubble size distributions related to accumulated gas volume as shown in Figure 4-5, were calculated by the products of equivalent circular volumes for each equivalent diameter sizes multiplied by their observed frequencies from five pictures.

Overall from Figure 4-5, it can be seen that bubble size distribution related to accumulated volume patterns for every nozzle size tends to exhibit a more bell-shaped normal distribution characteristic when compared to the distribution pattern related to bubble apparent number in Figure 4-4. This is because both the equivalent circular volumes of each bubble size and their observed frequencies are taken into account.

For the smallest nozzle size of 1 mm (Figure 4-5(a)), accumulated gas volumes produced from bubbles smaller than 7 mm still represent considerable proportion of the total accumulated volume; while accumulated gas volumes for bigger bubbles such as those with ∅ > 12 mm, are only observed at a high sparging rate of 8 - 10 L min^{-1}. For the nozzle diameter of 2 mm, the accumulated volume fraction shifts to bubble sizes larger than 7 mm, mostly generated from the increase in bubble sizes 9 - 13 mm with higher gas sparging rates. With the larger nozzle sizes of ∅ 3 and 4 mm, the accumulated volume fractions are clearly observed to extend further into the zone of bubble sizes larger than 7 mm. Although the volume fraction from bubbles smaller than 7 mm rose again slightly due to the breaking-up of large bubbles plumes in case of ∅ 4 mm nozzle, the volume proportion from bubbles larger than 7 mm still dominated.

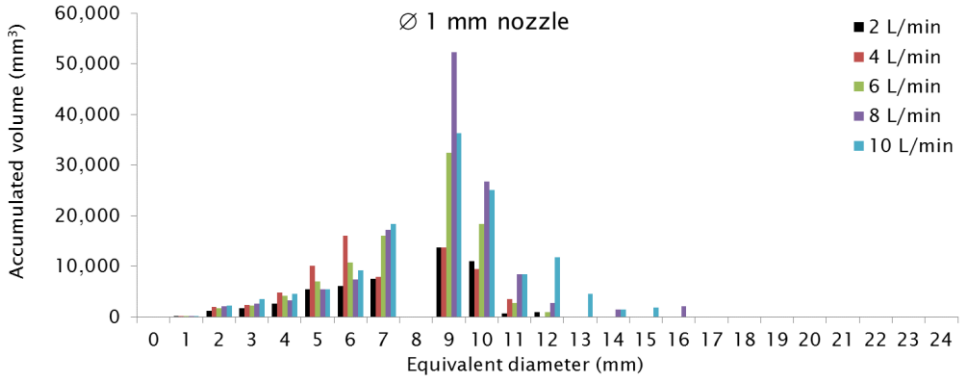

(a)

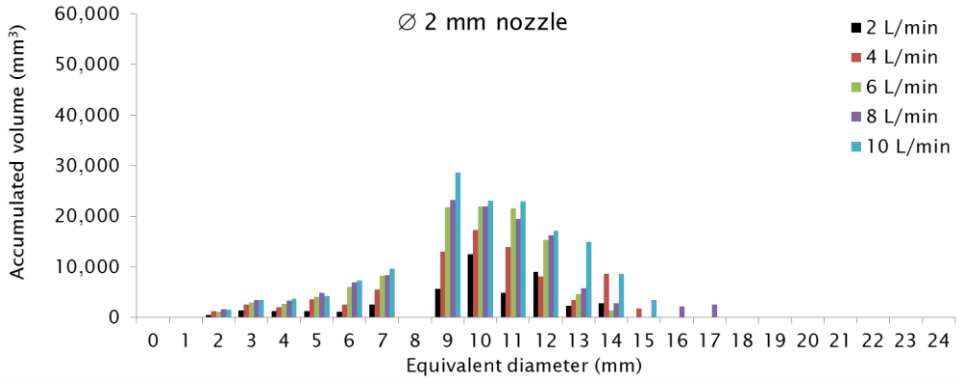

(b)

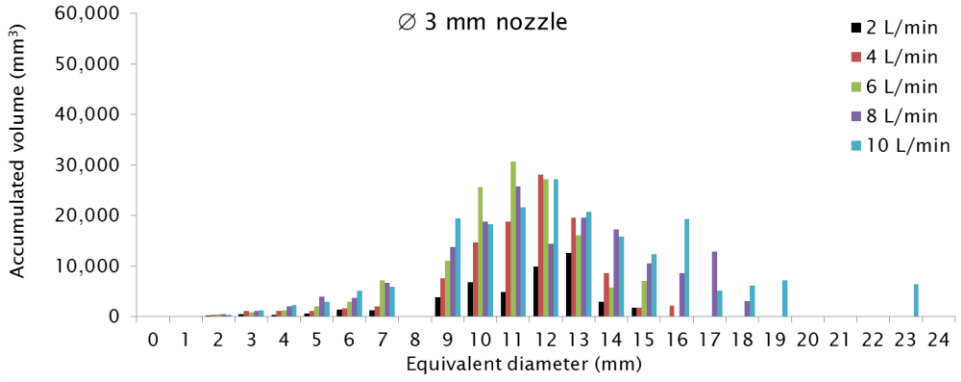

(c)

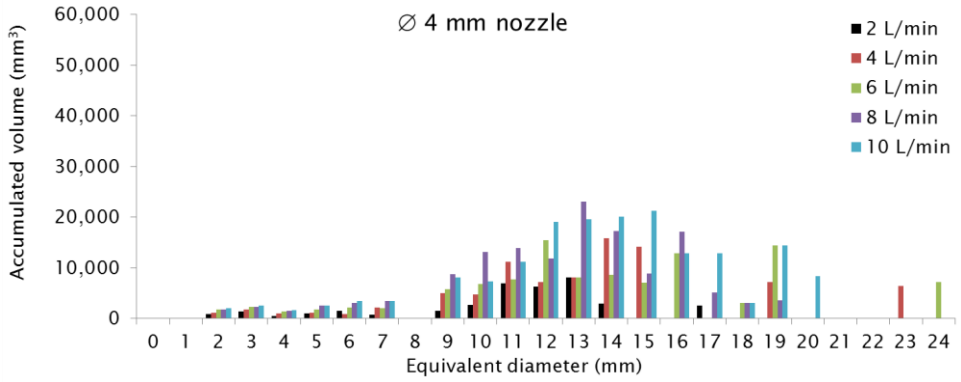

(d)

Figure 4-5 Bubble size distributions related to accumulated volume at air flow rates of 2, 4, 6, 8 and 10 L min^{-1} for nozzle sizes of a) 1 mm, b) 2 mm, c) 3 mm and d) 4 mm

Values of D_{V50} and D_{32} were calculated as described in section 3.1.2.2 above from all bubbles appearing in 5 photographs for each set of experimental conditions, and are presented in Figure 4-6, Figure 4-7 and Table 4-2, respectively.

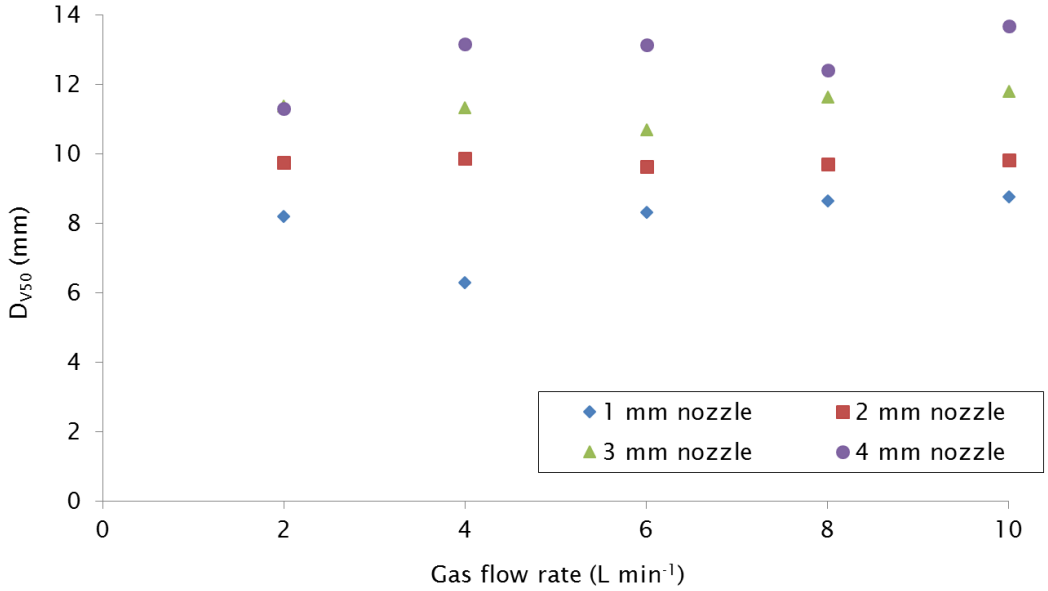

Figure 4-6 D_{V50} of each experimental condition

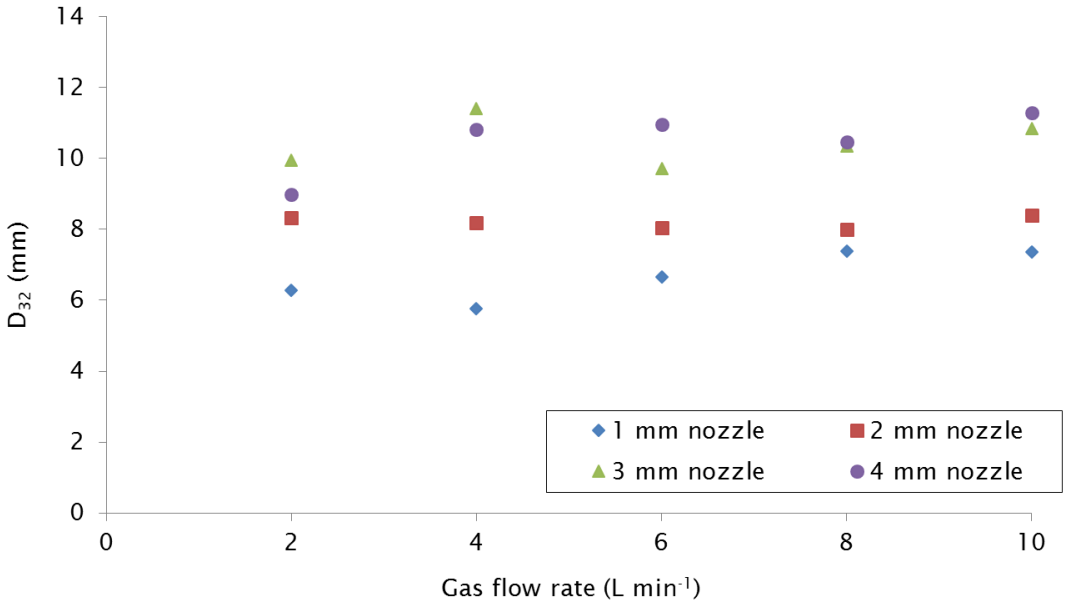

Figure 4-7 D_{32} of each experimental condition

Table 4-2 D_{10}, D_{32} and D_{V50} for each experimental condition

nozzle size (mm)	**gas flow rate** (L min^{-1})	**D_{10}** (mm)	**D_{32}** (mm)	**D_{V50}** (mm)
1	2	3.4	6.28	8.20
	4	3.2	5.76	6.30
	6	3.6	6.65	8.30
	8	3.8	7.38	8.63
	10	3.5	7.36	8.75
2	2	3.7	8.34	9.74
	4	3.6	8.18	9.87
	6	4.0	8.03	9.64
	8	3.8	7.99	9.71
	10	4.1	8.40	9.83
3	2	11.1	9.96	11.36
	4	5.6	11.41	11.32
	6	6.0	9.72	10.69
	8	5.5	10.34	11.64
	10	6.1	10.85	11.78
4	2	3.0	8.98	11.30
	4	3.5	10.83	13.15
	6	3.3	10.95	13.12
	8	3.7	10.46	12.40
	10	3.6	11.29	13.67

It can be seen from Figure 4-6 that increasing the sparging rate did not significantly influence D_{V50}: at a given nozzle size, D_{V50} values are similar even when sparging intensities have been increased up to 10 L min^{-1}. This is because the increased sparging rate only results in a higher accumulated gas volume produced from each bubble size. D_{V50} tends to be a function of nozzle size, however, with higher D_{V50} values corresponding to larger nozzle sizes. D_{32} shows similar behavior, with values found slightly smaller than those for D_{V50} in the same experimental conditions (Figure 4-7and Table 4-2). This indicated that representative bubble diameters related to accumulated volume as D_{V50} and volume/projected area aspect (surface area moment mean) as D_{32} are functions of nozzle hole size (∅ 1 - 4 mm), in contrast to the trend exhibited by representative bubble diameter related to apparent frequency i.e. D_{10}, since D_{10} values did not notably vary according to larger nozzle sizes as shown in Figure 4-3 and Table 4-2.

It is well recognized that bubble size and membrane gap strongly influence the shear stress. Zhang, Cui and Field (2009) reported the critical single bubble volume of 60 mL (equivalent to a spherical bubble diameter of 48 mm) flowed in 20 mm gap (bubble diameter/gap width = 2.4) contributed the highest mass transfer (i.e. shear stress); beyond this bubble size, shear stress

enhancement was negligible. For the bubble swarm, D_{V50} was used as representative bubble diameter in the study of Yamanoi and Kageyama (2010) who evaluated shear stress contributed from bubble flows in thin channels between flat-sheet membranes. The experiment compared bubble swarms generated from fine porous diffusers and ∅ 6 mm nozzle air injectors with membrane gaps of 5, 7 and 10 mm. Their results concerning the effect of bubble flow on the friction coefficient revealed that, to enhance shear stress, the best D_{V50} to membrane gap ratio (D_{V50}/L) was at 2, which means a D_{V50} of more than twice the membrane clearance contributed the highest shear stress. This condition was obtained from big bubbles generated by a ∅ 6 mm nozzle; however, too large bubbles made the shear stress smaller due to bubbles breakage and loss of energy (Yamanoi and Kageyama, 2010).

When considering the D_{V50} values achieved in this section, although the generated D_{V50} from nozzle sizes of 1 - 4 mm under sparging rates of 2 - 4 L min^{-1} could not reach a value of 2-fold larger than the 7 mm of membrane clearance, most of D_{V50} values observed were at least bigger than 7 mm. This means that pseudo-2D confined cap bubbles could be formed in this range of sparging rates and nozzle sizes. Particularly, with the nozzle size of ∅ 3 and 4 mm at the same fixed given gas flow rate, D_{V50} values were achieved in the range of 11 - 13 mm with D_{32} of 9 - 11 mm. This implies that a larger nozzle size of 3 - 4 mm could contribute higher shear stress in comparison to the smaller nozzles of 1 - 2 mm when considering the representative bubble diameters D_{V50} and D_{32}.

4.1.2 Effect of nozzle parameters on area and volume fraction

The previous section showed that bigger nozzle sizes of ∅ 3 and 4 mm tended to contribute higher shear stress than smaller nozzle sizes of ∅ 1 and 2 mm, based on the representative bubble diameters D_{V50} and D_{32} which gave sizes larger than the 7 mm membrane spacing. Therefore, the area and volume fraction in the membrane channel produced by different nozzle sizes were examined in this section. This is based on the hypothesis that bubbles with diameters larger than the membrane channel will act as pseudo-confined cap bubbles with higher benefit to shear stress when compared to bubble sizes smaller than the channel width with a free bubbling flow pattern in membrane spacer.

The summations of total bubble projected areas over one side of the simulated A4 size membrane surface area from 5 pictures were averaged. This total bubble projected area is regarded as the membrane covered area which was calculated from both “with bubble-membrane contact” and “without bubble-membrane contact” cases; whilst the membrane touching areas were calculated from averaged summation areas larger than 38.5 mm^2, which represents bubble sizes larger than 7 mm, only for the case of “with bubble-membrane contact”.

Average bubble covered area and touching area of the bubble swarm over one side of the membrane surface and the ratios of touching area to covered area for each experimental condition are presented in Figure 4-8 and Figure 4-9, respectively.

Figure 4-8 shows that increasing the sparging rate resulted in a higher bubble covered area over the entire membrane surface for every nozzle size, due to an increase in gas hold-up. Touching area refers to effective membrane-bubble scouring by bubbles which have equivalent diameters larger than 7 mm clearance, whilst the different fractions between covered area and touching area imply the area of free bubble flow regime where the membrane surface has not been scoured by pseudo-2D confined cap bubbles. From Figure 4-8, it can be seen that although the covered area for all nozzle sizes shows similar ranges under a fixed given gas flow rate, the ratios between covered area and touching area for small nozzle sizes ∅ 1 and 2 mm seem wider than in the case of larger nozzle size of ∅ 3 and 4 mm. This indicated that small nozzle sizes contribute a lower bubble-scouring effect when compared to larger nozzle sizes, perhaps due to the higher proportion of small bubble sizes (< ∅ 7 mm) as shown in the bubble size distribution pattern related to accumulated volume (Figure 4-5).

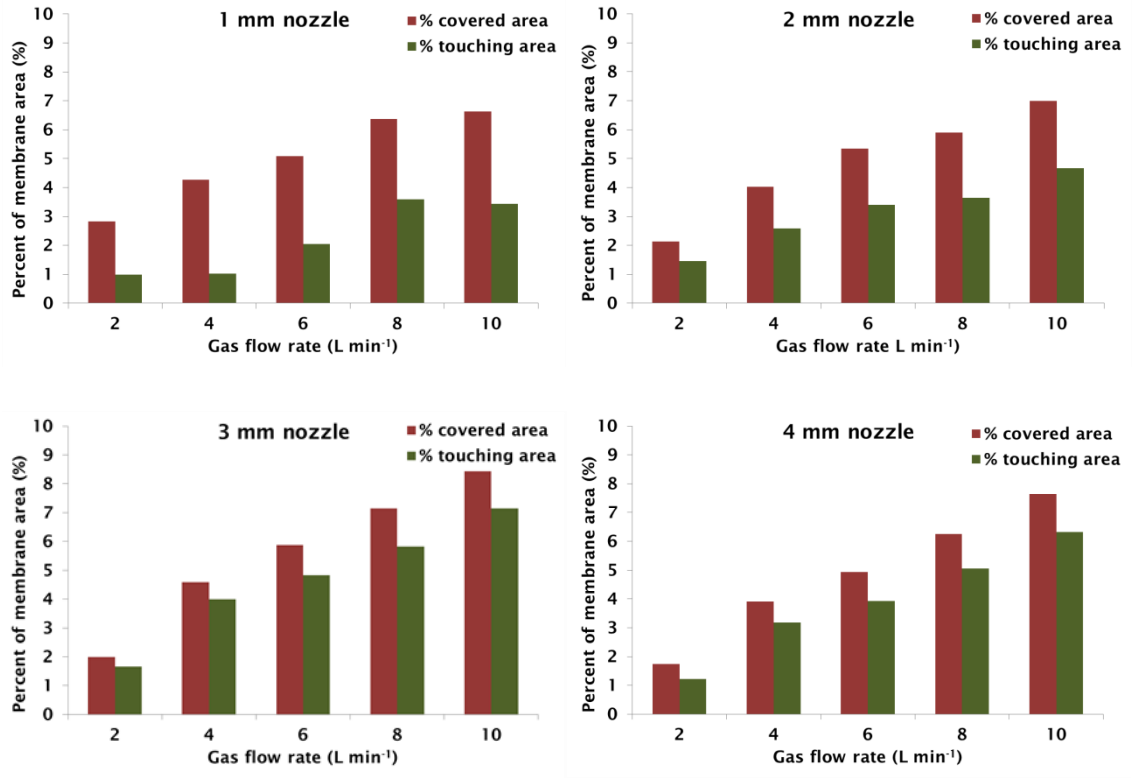

Figure 4-8 Average covered area and average touching area of bubble swarms over membrane surface area

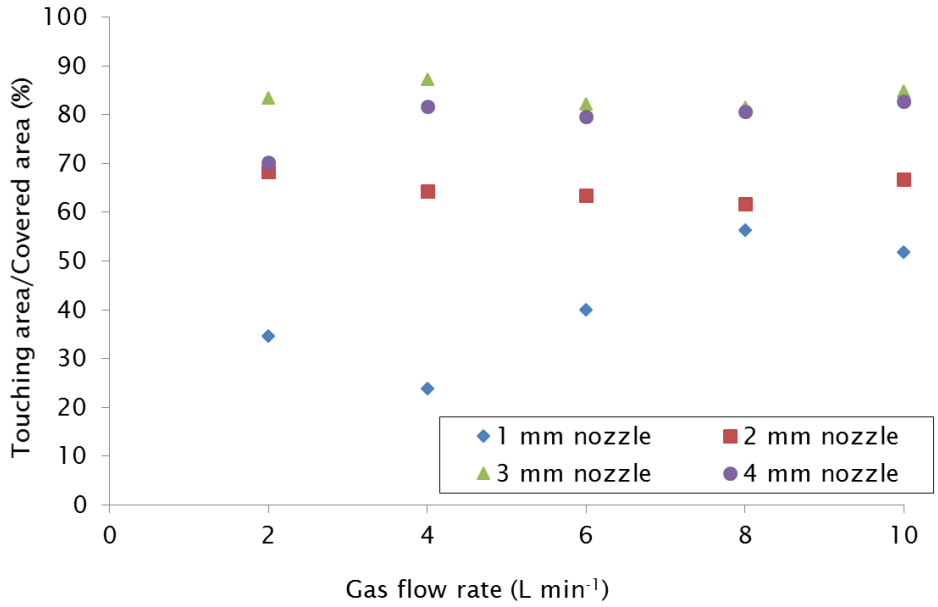

Figure 4-9 Average bubble-membrane touching area/covered area

This trend can be seen more clearly in Figure 4-9. For the ∅ 1 mm nozzle, even though the touching area/covered area ratios increase from about 30 to 50 % following an increase in gas flow rate from 2 - 8 L min^{-1}, further increasing the gas flow rate up to 10 L min^{-1} did not give a significant improvement in the bubble-scouring ratio; whilst the touching/covered area ratios from the ∅ 2 mm nozzle present almost constant values at about 65 % with increasing gas flow rates. Similarly trends are exhibited in the case of the larger nozzle sizes ∅ 3 to 4 mm, in which almost stable values of touching/covered area ratios appear at around 80 - 85 % even with higher sparging rates from 4 - 10 L min^{-1}. This illustrated that, for the nozzle size of 2 - 4 mm, the higher gasing rate does not strongly affect the touching/covered area ratios, potentially due to the fact that touching areas increase proportionally with higher covered area for higher bubbling rates. The results indicated that fractions of bubble sizes with diameter larger than 7 mm increase consistently with higher sparging intensity and total covered area. This was also confirmed by the demonstrated bubble size distribution in Figure 4-5 which shows that the fractions of bubble size distribution related to accumulated volume shifted towards the larger bubble diameter zone with increasing sparging rate. When considering the relation between varied nozzle sizes under fixed given gas flow rates shown in Figure 4-9, with the nozzle size from ∅ 1 to 2 mm, touching/covered area ratios extend to about 2-fold with an increase in gas flow rate of 2 - 6 L min^{-1}; while at the high bubbling rate of 8 - 10 L min^{-1} these ratios for ∅ 1 to 2 mm present the similar value ranges. This means that fractions of bubble size larger than 7 mm for the ∅ 1 mm nozzle increased with higher gas flow rates from 2 - 8 L min^{-1}, then appeared relatively constant with higher bubbling rates up to 10 L min^{-1}. This is in agreement with the accumulated volume size distribution pattern in Figure 4-5 (a) which showed that the large bubble size fractions (such

as ∅ > 12 mm) are present only at the high gasing rate of 8 - 10 L min^{-1}, as was also seen in visual observation in Figure 4-1 (a) and (b).

The nozzle size from ∅ 2 to 3 mm shows improving touching/covered area ratios of approximately 15 - 20 %, while increasing the nozzle size from ∅ 3 to 4 mm does not show any further enhancement of touching/covered area ratio: both of these ratios for the ∅ 3 and 4 mm nozzles are in the range of 82 - 87 %. These results indicated that touching/covered area ratios are a function of nozzle size. In certain cases, however, at the same fixed gasing rate an increase in nozzle diameter such as from ∅ 3 to 4 mm does not enhance this ratio. This may be due to the creation of large bubble fractions, and also to the achievable maximum bubble sizes, so that the total created bubble size fractions in the bubble swarm are reaching their maximum value under the experimental conditions setting-up in this study.

For the "touching area case" from Figure 4-8, where surface areas have been scoured by pseudo-2D confined cap bubbles, average contact area fraction (α′) were plotted in Figure 4-10 to compare the effect of nozzle size on contact area fraction (α′). The data used were taken from 5 photographs under sparging rates of 2, 4, 6, 8 and 10 L min^{-1}, which correspond to gas superficial velocity (U_g) in 7 mm channel width of 0.011, 0.022, 0.033, 0.044 and 0.055 m s^{-1} between two sides of membrane clearance in riser zone. With the same experimental set-up for α′, total accumulated bubble volumes from 5 pictures (from Figure 4-5) for both "with bubble-membrane contact" and "without bubble-membrane contact" cases were averaged to per one picture. Total bubble volume inside the membrane channel (considered as the A4 area with channel depth of 7 mm) presented as gas void fraction (α) is shown in Figure 4-11.

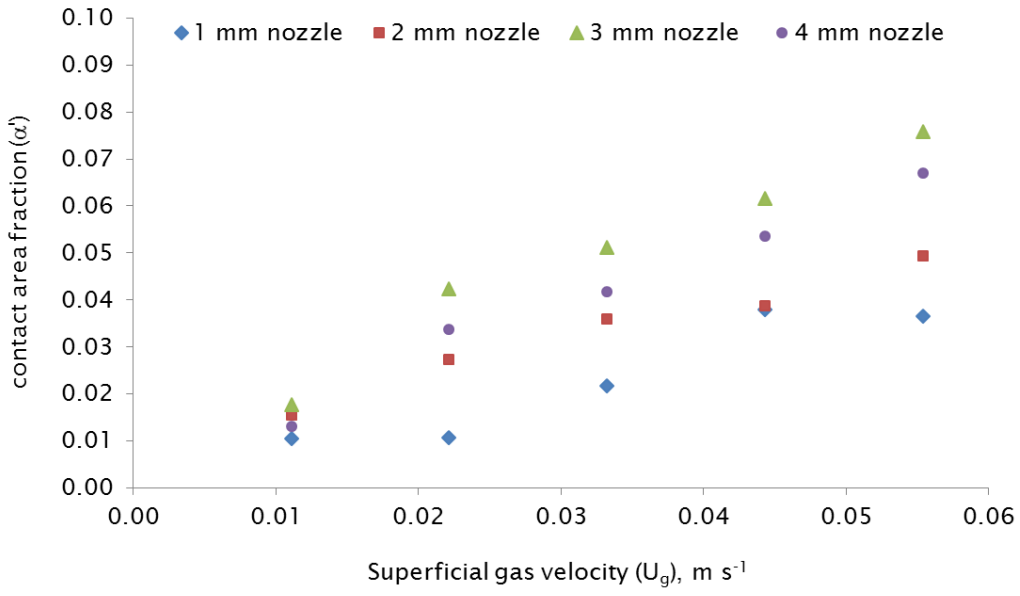

Figure 4-10 Relation between gas superficial velocity (U_g) and contact area fraction

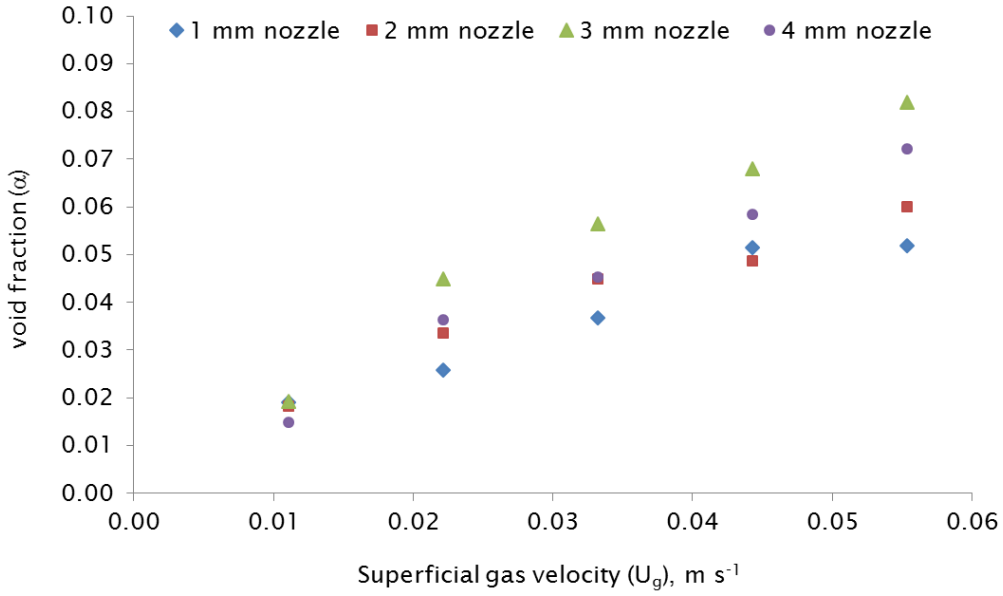

Figure 4-11 Relation between gas superficial velocity (U_g) and void fraction

From Figure 4-10, it can be seen that higher gas superficial velocities induce a higher bubble-membrane contact area fraction for every nozzle size. When comparing different nozzle sizes at a fixed U_g, the larger nozzle sizes of ∅ 3 and 4 mm present larger α′ than the smaller nozzle sizes ∅ 1 and 2 mm, which is mainly caused by the reduction in touching/covered area ratios due to the larger proportions of small bubbles (∅ < 7 mm) as mentioned above. The highest contact area fraction is seen from a nozzle size of ∅ 3 mm, which is slightly higher than the ∅ 4 mm nozzle case. This may be because very large bubbles generated from the ∅ 4 mm nozzle were broken-up while the bubbles were rising to reach their terminal velocities before flowing into membrane channel, resulting in an increase of small bubble fractions.

In conclusion, when considering the largest generated α′ and bubble touching area/covered area, taking into the account the high representative bubble diameters D_{V50} and D_{32}, as well as bubble size distribution patterns, under the fixed given gas sparging intensity in comparison with other nozzle sizes in this study, it could be inferred that generated bubble swarms from the ∅ 3 mm nozzle size contribute the highest two-phase shear stress on the membrane surface. This is mainly because the membrane surface has been scoured efficiently by the fractions of bubble size with equivalent diameters larger than the membrane clearance. These large bubbles act as pseudo-2D confined bubbles in the thin channel of the membrane spacer, which means a higher shear stress induced by secondary turbulent flow following the bubble rising can be achieved when compared to bubbles with equivalent diameters smaller than membrane gap which present a free-bubbling flow pattern between the channel.

Overall from Figure 4-11, it can be seen that an increase in gas superficial velocities at every nozzle size led to a higher void fraction in the narrow channel column due to the greater gas hold-up from the applied bubbling. At a low U_g of 0.011 m s^{-1}, the value of α is in a similar range for every nozzle size. At higher U_g differences in α (as well as α′) were observed which increased with nozzle size. For example, the value of α at U_g of 0.55 m s^{-1} for a ∅ 3 mm nozzle is 0.082 while for a ∅ 1 mm nozzle it is 0.052. Theoretically, α for every nozzle size should fall into a similar range of values for every U_g due to the same fixed given sparging intensity. The wider distribution of α at higher U_g may be affected by the equivalent sphere volume determination assumption used in this study, in which the volumes of large bubbles with projected areas bigger than an equivalent sphere diameter of 7 mm would be multiplied by the 7 mm depth. As a result, the calculated volume of big bubble fractions generated from large nozzle sizes of 3 - 4 mm resulted in higher α when compared to the smaller nozzle sizes of 1 and 2 mm. Although these α distributions might appear wide, however, the actual liquid upward velocity (U_{lr}) determination methods used in the next experiments are based on parameters (1-α): for example $U_{lr} = U_{two\text{-}phase}/(1-\alpha)$ or $U_{lr} = (A_d/A_r)\, U_{ld}\, (1-\alpha)$. From this standpoint, these distributed ranges could be regarded as small. In addition, wider ranges were found more clearly in α′. This can be attributed to the results that, at the same gas injection rate, the bigger nozzle sizes of ∅ 3 and 4 mm tend to have more bubble-scouring efficiency than the small nozzle sizes of ∅ 1 and 2 mm.

Apart from bubble characteristics which mainly affect the achievable shear stress as demonstrated in this section, another essential parameter to enhance fouling mitigation is the fluid dynamics driven by two-phase gas-liquid flow inside the reactor. Hence, the effects of tank geometry designs on crossflow velocities were examined in the next section.

4.2 Fluid dynamic and crossflow velocity in gaslift-loop membrane reactor

Gas sparging has a major role not only in fouling mitigation by bubble scouring and liquid crossflow but also to maintain completely-mixed suspended conditions inside reactors. In order to gain the advantages of fouling control and mixing approaches, gaslift-loop configurations for submerged flat sheet MBR have been considered more energy efficient when compared to the cases where the whole bottom of the reactor is gassed (i.e. gas-mixed without annular loop flow) (Prieske, Drews and Kraume, 2008). In the gaslift-loop reactor, the reactor volume is developed into a downcomer and a gassed riser zone. The different hydrostatic pressure caused by different gas hold-up between both sections induces a recirculating liquid flow velocity. Higher crossflow velocity stimulated by gas-liquid recirculation is advantageous in limiting deposition on the

membrane surface due to the increased shear rates and back transport flow in the rising bubbles regions.

According to the well-known expression for predicted liquid upward flow velocity in a riser section (recirculating liquid flow velocity or liquid crossflow velocity, U_{lr}) by Chisti, Halard and Moo-Young (1988) as shown in Equation 2-2 to Equation 2-5, the recirculating liquid flow velocity depends on bubbling rate, gas hold-up in riser and downcomer (ε_r and ε_d), the cross section area ratio between downcomer and riser (A_d/A_r) and the free area for the transversal flow from downcomer to riser (A_b).

The experimental set up in this section aimed to examine the two-phase upward and liquid downward flow velocity, in order to evaluate the influence of tank geometry and gas sparging rate on crossflow velocity. The effects of A_d/A_r ratios, nozzle sizes and A_d/A_b at various typical gas sparging rate applied in MBRs on crossflow velocity were assessed in an attempt to optimise the tank design for the gas-sparged two-phase flow.

4.2.1 Effect of downcomer to riser cross-sectional area ratio (A_d/A_r) on liquid upward flow velocity

Experiments were carried out to measure five points (left, middle-left, centre, middle-right and right positions) of two-phase upward flow in riser zone (5 cm below water level) and liquid downward flow velocities in downcomer (35 cm below water level) in order to calculate liquid cross flow velocities (positions of flow velocity measurement presented in Figure 3-6). Tap water was used as the medium with a total depth of 68 cm. A single Kubota A4 membrane panel was mounted in the riser zone in which the clearance between membrane and tank wall and baffle were kept constant at 7 mm, giving a fixed riser cross-sectional area of 30.1 cm^2 (minus the membrane panel thickness). Tank dividers were inserted which allowed the cross-sectional areas of downcomer to be adjusted to 111.8, 92.5, 73.1 and 53.8 cm^2, resulting in the A_d/A_r ratios of 1.8, 2.4, 3.1 and 3.7, respectively. The height of the bottom baffle edge was adapted following the downcomer width in order to keep a constant downcomer to transversal area ratio (A_d/A_b) of 0.5 at the bottom of reactor. Air was supplied from two spargers with Ø 3 mm nozzles located 30 cm below the membrane, in the range of 2 - 10 L min^{-1} to produce two-phase crossflow. Measured two-phase upward flow and liquid downward flow velocities from 5 points in various A_d/A_r ratios with different supplied gasing rates are presented in Figure 4-12.

.

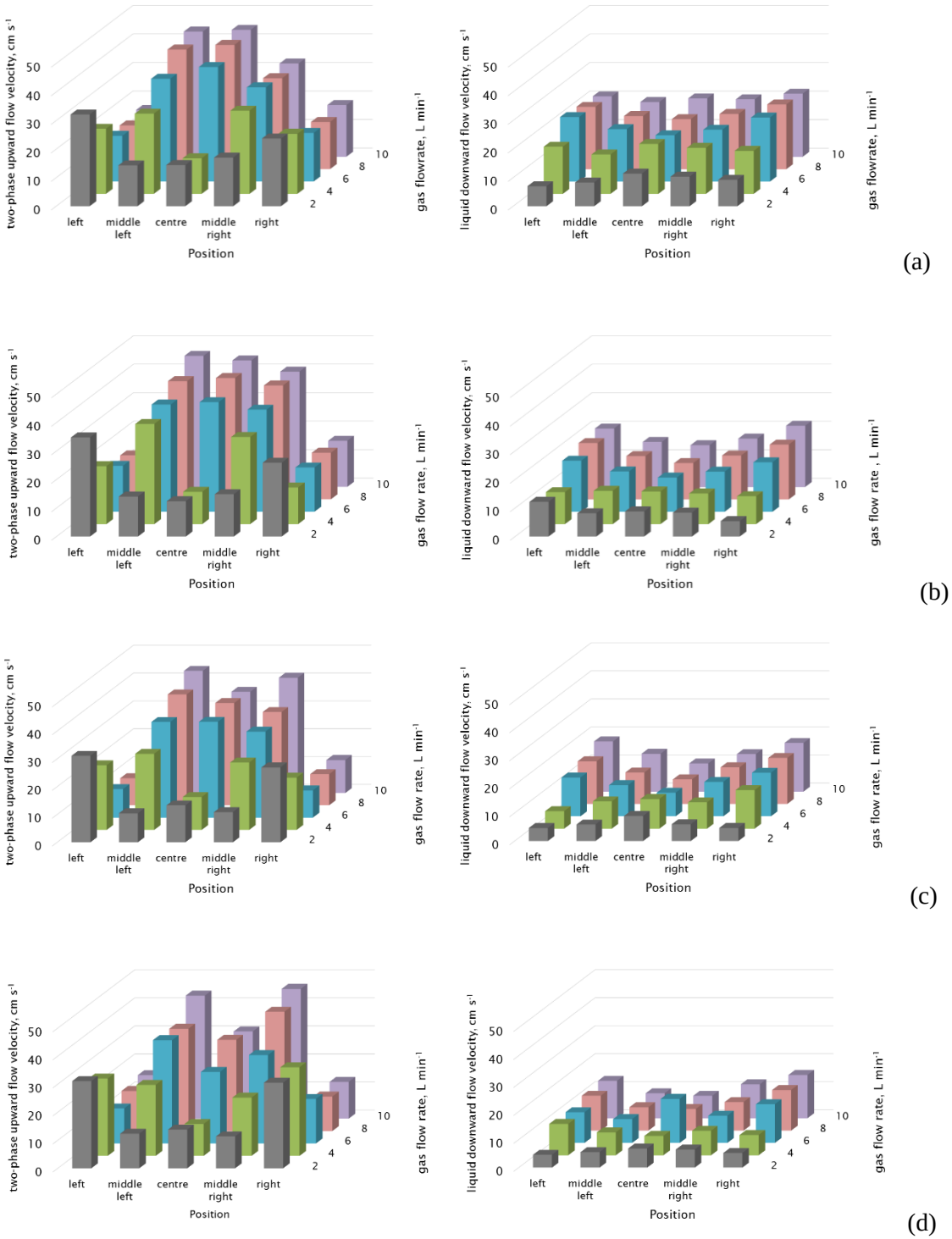

Figure 4-12 Measured two-phase flow velocities (left) and liquid downward flow velocities (right) with varied A_d/A_r ratios of (a) 1.78 (b) 2.43 (c) 3.07 and (d) 3.71

Considering the two-phase upward flow velocitiy profiles in the riser zone presented in Figure 4-12, it can be seen that for every A_d/A_r ratios, the upward flow velocities show characteristics at

the same supplied air flow rate. At a low air supply of 2 L min^{-1}, high upward flow velocities occur at the left and right edge of the membrane panel. Increasing air supply to 4 L min^{-1}, high cross flow velocities are seen at the left, middle-left, middle-right and right regions, while the lowest ones occur at the centre of the membrane panel. When air was supplied at the higher rate of 6 - 10 L min^{-1}, flow velocity profiles exhibit similar patterns. High cross flow velocities are mostly found in the middle and centre zones, and lower at the left and right ends. The variable flow velocity patterns at sparging rates of 2, 4 and 6 - 10 L min^{-1} may be influenced by uneven bubble distribution. Since every nozzle size in this experiment was fixed at ∅ 3 mm, and air was introduced from one end (left or right) of each sparger, therefore, at lower sparging rates of 2 - 4 L min^{-1}, bubbles were observed appearing from nozzles close to the air inlet direction (only 1 - 2 holes) which caused higher two-phase flow velocities at the membrane panel's left and right sides. When sparging at the higher rates of 6 - 10 L min^{-1}, the air input pressure could overcome the resistance inside the sparger tubes resulting in other nozzles (2 - 4 holes) ejecting more bubbles and leading to greater upward flow velocities in the centre and middle zones compared to the left and right regions. These flow velocity profiles are in agreement with visual observation of flow patterns for ∅ 3 mm nozzle shown in Figure 4-1 (c).

Although liquid downward flow velocity profiles of 5 points at the middle width of downcomer were not affected directly by the nozzle arrangement and bubbling rates, certain downward velocity profiles in Figure 4-12 present similar properties to the riser. For all A_d/A_r ratios, downward flow velocities for 5 positions at a low air intensity of 2 L min^{-1} are almost equal and remain so even when the sparging rate has been increased to 4 L min^{-1}. Noticeably, at the higher rates from 6 - 10 L min^{-1}, downward velocities exhibit similar characteristics in which left and right edge flow velocities are higher in comparison to the centre and middle zone for all A_d/A_r ratios. From Figure 4-12, with the same nozzle sizes of ∅ 3 mm at low sparging rates of 2 - 4 L min^{-1}, it seems the two-phase upward flows move rapidly at the left and right side of membrane panel in riser section and liquid downward flows are mostly uniform in velocities in downcomer zone. However, with greater sparging intensities of 6 - 10 L min^{-1}, high two-phase upward velocities occurred at the centre and middle regions of membrane surface, and then liquid downward flows were faster at the outer edges than the centre region of the downcomer.

In order to obtain a clearer view about two-phase upward and liquid downward velocities, average velocities from 5 points of each condition related to A_d/A_r ratios and sparging rates were plotted in Figure 4-13.

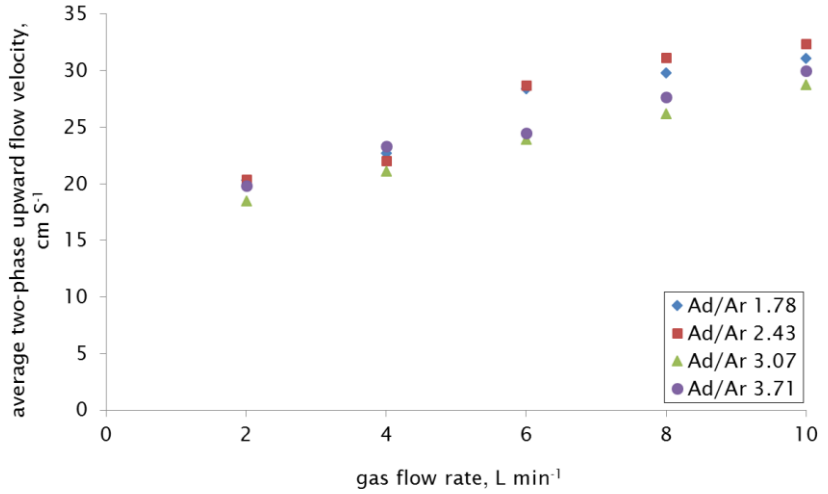

(a)

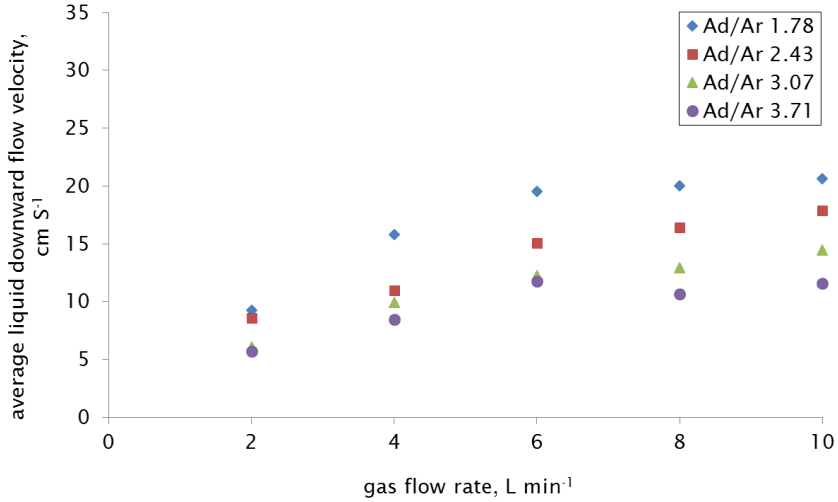

(b)

Figure 4-13 Average flow velocities related to varied A_d/A_r ratios (a) two-phase upward flow velocities (b) liquid downward flow velocities

As can be seen from Figure 4-13(a), the higher the air flowrate, the higher the average measured two-phase flow velocities. This is in agreement with Equation 2-2 and Equation 2-4 that increasing sparging rates increases gas hold-up in the riser (ε_r), leading to higher liquid upward velocities due to the greater difference in hydrostatic pressure between riser and downcomer zone. An increase in A_d/A_r ratios from 1.78 - 3.71 did not seem to affect the two-phase upward velocities significantly, however. Possible reasons why the two-phase upward flow velocities were not improved in accordance with Equation 2-2 are: firstly, the reactor was set with A_r smaller than A_d (opposite of typical air-lift reactors applied in chemical and biological approaches), meaning liquid downward flow velocities (Figure 4-13 (b)) are not strong enough to drag bubbles into the downcomer which is advantageous to enhance continuous recirculation flow inside reactor. Secondly, due to the resistance of the membrane module located in the riser, the liquid recirculation velocities could be reduced. However, flow energy lost due to the module resistance

is related to flow friction that could enhance shear stress and backtransport flow on the membrane surface. Finally, large bubbles generated by ∅ 3 mm nozzle with higher lift force and velocities compared to small bubbles generated by normal porous diffusers are easily released from the riser to the atmosphere above the liquid level instead of plunging back into the downcomer; the presence of small bubbles in the downcomer (term ε_d in Equation 2-2) is the major cause of retarding circulation flow velocities. These experimental results are in agreement with Prieske, Drews and Kraume (2008), who performed numerical simulations to determine the relationship between fixed single bubble sizes of 1, 2 and 3 mm and gas hold-up in riser and downcomer. Their findings indicated that smaller bubbles resulted in lower differences between riser and downcomer gas hold-up corresponding to the term (ε_r - ε_d) in Equation 2-2 that caused crossflow retarding in the riser zone. In comparison with representative bubble diameters D_{10}, D_{V50} and D_{32} for bubble swarms produced by ∅ 3 mm nozzle under 2 - 10 L min^{-1} sparging rates in this study, these representative diameters are larger than 3 mm (3.6-9.9 mm, Table 4-2) and could be considered as big bubbles. As a result, no bubbles were observed being dragged into the downcomer during the experimental trial. It is thought that gas hold-up in downcomer to riser ratios ($\varepsilon_d/\varepsilon_r$) are lesser than 0.89 (Equation 2-3, suggested by Bello, Robinson and Moo-Young (1985)). Consequently, the higher A_d/A_r ratios from 1.78 - 3.71 in this experimental setup given a small difference in two-phase upward velocities.

On the other hand, the higher A_d/A_r ratios result in lower measured liquid downward velocities due to the cross sectional areas extension in the downcomer, as can be seen in Figure 4-13 (b). Although liquid downward flow in the downcomer does not directly affect shear stress over the membrane surface in the riser, with larger A_d/A_r ratio (mostly ≥ 2 in flat-sheet MBR), it could induce recirculation flow which enhances crossflow velocities due to the continual flow recirculation. This also help to maintain completely mixed conditions inside the reactor, because too low recirculation flow velocities in the downcomer section due to very high A_d/A_r ratios may diminish the completely suspended conditions and dead zones can potentially be formed.

In order to evaluate the effect of A_d/A_r ratios on membrane crossflow velocity, the actual liquid upward flow velocity (U_{lr}) was calculated. Actual liquid upward flow velocity was defined as superficial liquid upward flow velocity divided by liquid fraction (1-α) from Figure 4-10 (a). The superficial liquid upward flow velocities were derived from liquid cross flow rates between membrane gaps, which were the product of the average measured two-phase upward velocities and the area of upward channel, or average measured liquid downward velocities and the area of downward channel.

In this case, the two-phase upward flow velocity in riser zone ($U_{two\text{-}phase}$) can be related to U_{lr} following Equation 4-1.

Equation 4-1

$$U_{lr} = \frac{U_{two-phase}}{(1-\alpha)}$$

And liquid downward flow velocity in downcomer zone (U_{ld}) can be related to U_{lr} following Equation 4-2.

Equation 4-2

$$U_{lr} = \frac{U_{ld}}{(1-\alpha)}\left(\frac{A_d}{A_r}\right)$$

Calculated actual liquid upward flow velocities between 7 mm clearance of A_d/A_r 1.78 - 3.71 related to bubbling intensities expressed as superficial gas velocities are presented in Figure 4-14.

From Figure 4-14, actual liquid upward flow velocities, U_{lr} derived from both riser and downcomer with U_g values from 0.011 - 0.55 m s^{-1} show similar trends in the range of 16.8 - 50.3 cm s^{-1}, for all A_d/A_r ratios, although calculated liquid upward flow velocities given by the riser seem to be slightly higher. Considering the U_{lr} values calculated by two-phase upward velocity at U_g between 0.011 - 0.022 m s^{-1}, U_{lr} shows almost the same value for all A_d/A_r ratios. At the higher U_g of 0.033 - 0.055 m s^{-1}, small A_d/A_r ratios of 1.78 and 2.43 tend to give slightly greater U_{lr} compared to large A_d/A_r of 3.71. In contrast to U_{lr} derived from liquid downward velocity, the lowest calculated U_{lr} are observed at the smallest A_d/A_r of 1.78 whilst the highest U_{lr} values are from large A_d/A_r ratio of 3.71 for almost every U_g. For example, at U_g of 0.033 m s^{-1}, U_{lr} for A_d/A_r ratio of 3.71 and 1.78 are 46.2 and 36.8 cm s^{-1}, respectively. These differences between U_{lr} values calculated from two-phase flow in riser and liquid downward flow in downcomer may be because the latter is calculated from actual liquid phase flow, in which the expansion of A_d/A_r ratio results in better liquid recirculation, particularly at the transversal flow position from riser to downcomer section. Hence, by the extension of A_d/A_r ratio, U_{lr} calculated from liquid downward velocity can be enhanced following Equation 2-2. From Figure 4-4, although increasing A_d/A_r ratios from 2.43 to 3.71 does not give a significant improvement in U_{lr}, the results suggest that A_d/A_r should be larger than 1.78. These results are in agreement with the findings of Shim, Yoo and Lee (2002) who studied the effect of A_d/A_r ratios of 1.6, 3.6 and 4.5 on fouling control, who reported that while the ratio of 1.6 in an aerated bioreactor did not generate a sufficient flow for proper cleaning on membrane surface, the ratio between 3.6 and 4.5 was suitable for membrane clogging prevention.

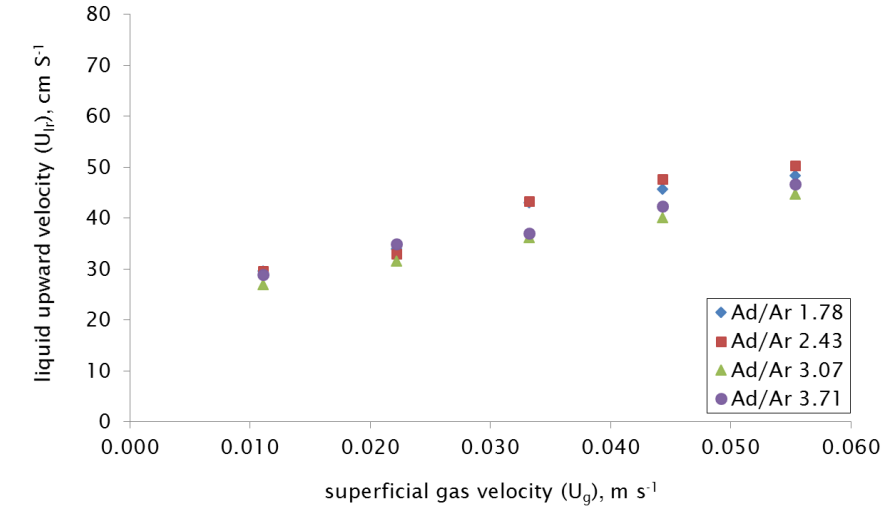

(a)

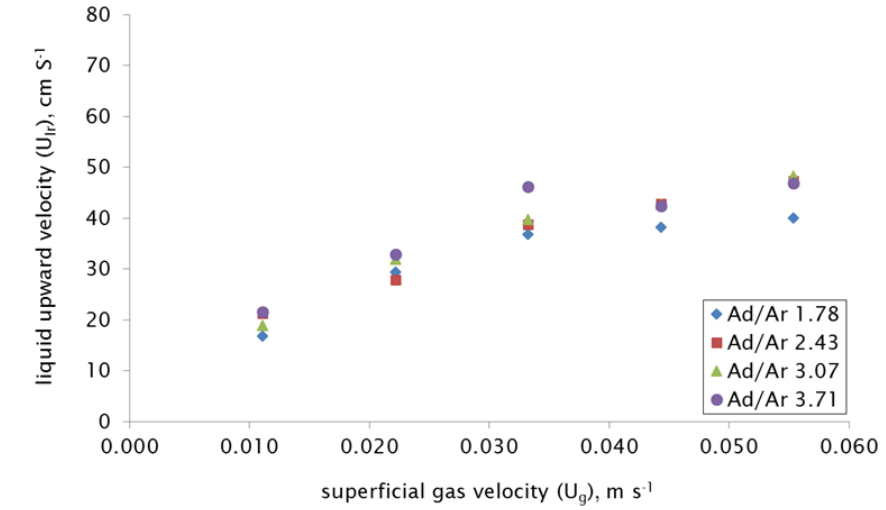

(b)

Figure 4-14 Actual liquid upward flow velocity (U_{lr}) related to superficial gas velocity for different A_d/A_r ratios: (a) calculated from average two-phase upward velocity (b) calculated from average liquid downward velocity

It is noticeable that higher U_g results in higher liquid upward flow velocity. Only a slow increase in crossflow velocities was observed at U_g above 0.033 m s^{-1}, however, which resulted in U_{lr} of 36.8 - 46.2 cm s^{-1} for A_d/A_r ratio between 1.78 - 3.71. It can be clearly seen from Figure 4-13 (b), Figure 4-14 (b) and Figure 4-12 that flow velocity profiles showed a minor transformation after increasing to a 6 - 10 L min^{-1} sparging rate. This effect conforms to the results from some other research groups (Liu *et al.*, 2000; Sofia, Ng and Ong, 2004; Prieske *et al.*, 2010) who found a plateau in liquid upward velocities when bubbling intensities were increased to certain values. This might be due to the fact that U_{lr} does not increase linearly with the higher sparging intensity in the riser zone. When considering the terms U_{lr} and U_{gr} (referred to ε_r) in Equation 2-2 and Equation 2-4, the relation between these two terms is expressed in a quadratic equation which

predicts the potential diminution of improvements in U_{lr} with higher U_{gr}. In addition, the rising velocity of bubble which induced liquid upward velocity is not proportional to gas sparging rate (Braak *et al.*, 2011), hence a plateau in U_{lr} following the increment of sparging intensity is observed in real liquid flow.

According to the demonstrated results, since sparging always represents the largest proportion of energy consumption in typical MBRs operation for fouling mitigation and mixing purposes, then with respect to liquid upward flow velocities, and ignoring any oxygen transfer aspects, it could be deduced that 6 L min^{-1} (U_g = 0.033 m s^{-1}) bubbling rate under the experimental conditions and reactor geometry in this study, is a threshold sparging intensity. Interestingly, this rate falls within similar ranges reported by many researchers. Zhang, Tan and Stuckey (2017) operated an A4 flat-sheet AnMBR and proposed a critical constant sparging rate at 6 L min^{-1} for a flux of 26 LMH. From the same research group, Fox and Stuckey (2015) reported the determined critical sparging rate at 4 L min^{-1} for a flux of 7.2 LMH based on the approach that critical sparging rates existed when reaching them caused a steep rise in TMP. Considering sparging rate in term of U_g, it was found that Ug varies between 0.04 and 0.1 m s^{-1} across a number of modern large pilot and full-scale plants (Verrecht *et al.*, 2008). For hollow fibre membrane, sustainable permeability has been found to increase approximately linearly with aeration rate (Judd, 2008). Le-Clech, Jefferson and Judd (2003) found that increasing U_g always has a positive effect on the critical flux, which increased from 16 to 51 LMH for U_g values of 0.07 and 0.22 m s^{-1}, respectively.

For the flat-sheet configuration, the plateauing effect of U_{lr} has also been reported. Liu *et al.* (2000) reported threshold aeration intensity in terms of U_g at approximately 0.03 m s^{-1} which resulted in a maximum U_{lr} of 0.43 m s^{-1} for their pilot-scale AeMBR treating municipal wastewater. They also suggested a critical crossflow velocity (U_{lr}) of 0.3 m s^{-1}, below which TMP increased sharply. A similar threshold value for U_{lr} was demonstrated by Prieske *et al.* (2010) who reported that a U_g above 0.04 m s^{-1} did not have much additional effect on liquid velocity in flat-sheet modules, where the maximum achievable U_{lr} values at U_g of 0.04 m s^{-1} are in the range of approximately 0.25 - 0.35 m s^{-1}.

From the fluid dynamic viewpoint, identification of the threshold U_g is a crucial step for appropriate reactor design. Below the U_g threshold, filtration performance could be affected by rapid fouling building-up, while exceeding this point may represent excess energy input. As a result, regardless of the need for oxygen transfer and the rheology of mixed suspensions in diverse conditions, it is recommended that optimisation of tank geometry design as well as energy supply should start with threshold U_g determination, whereas other parameters such as membrane spacer, liquid depth, A_d/A_r ratio, nozzle size and sparger arrangement, etc. can be designed following the given threshold U_g.

4.2.2 Effect of nozzle sizes on liquid upward flow velocity

In the previous section it was demonstrated that nozzle size and sparging intensity influence the produced bubble size and size distribution which affect the shear stress over the membrane surface. In this section, the effects of nozzle size and sparging rate on liquid crossflow velocity which affects backtransport flow were examined.

The experiments were set up under similar condition as described in section 4.2.1 with fixed A_d/A_r ratio of 3.07, A_d/A_b of 0.5, and 68 cm tap water depth. Two-phase upward velocities in riser and liquid downward velocities in downcomer were measured with varied nozzle sizes of ∅ 1, 2, 3 and 4 mm under sparging rates between 2 - 10 L min^{-1} (Figure 4-15) in order to assess the effect of nozzle sizes on liquid upward flow velocity between membrane channels.

From Figure 4-15 (a) it can be seen that for ∅ 1 mm nozzle, the two-phase upward velocities from 5 measured positions show similar values even at low sparging rate of 2 L min^{-1}, which indicates the advantageous characteristics of a small nozzle size for uniform bubble distribution, as demonstrated in Figure 4-1 (a). When the sparging rate is increased to 4 L min^{-1} higher upward velocities are seen in the middle-left and middle-right positions, followed by the centre zone of the membrane surface. This upward velocity profile is maintained for sparging rate increments from 4 up to 10 L min^{-1}.

With the larger nozzle sizes of ∅ 2 and 3 mm, the two-phase upward flow profiles in Figure 4-15 (b) and (c) show a similar pattern in which upward velocities are high at the left and the right edge of membrane panel at a sparging rate of 2 L min^{-1}. This is due to the creation of bubbles from the nozzle holes close to the air entrance direction, as discussed in section 4.1.1.1 and shown in Figure 4-1 (b) and (c). Two-phase upward velocities are higher at the middle-left and middle-right zone when the sparging rate has been increased to 4 L min^{-1}. When the sparging rate is increased to 6 L min^{-1}, upward velocities are highest in the middle and centre zone of membrane surface and this two-phase upward velocity profile pattern remains when the sparging rate is further increased to 10 L min^{-1}.

For the ∅ 4 mm nozzle in Figure 4-15 (d), at the low sparging rate of 2 L min^{-1} two-phase upward velocities are highest at the left and right edge of the membrane panel, while the lowest upward velocities occur in the centre zone. This velocity profile pattern continues for sparging rates up to 6 L min^{-1}. With higher sparging rates of 8 - 10 L min^{-1}, the upward velocities present similar patterns in which the high values appear on the middle-left and middle-right sections while the centre zone and the outer edges of the membrane panel still show lower upward velocities. This is mainly because of an uneven distribution of large bubbles along the sparger tube length for nozzle size of ∅ 4 mm as aforementioned.

All two-phase upward flow velocity profiles with varied nozzle size and sparging rates shown in Figure 4-15 are in agreement with the bubble rising distribution pattern visually observed in Figure 4-1.

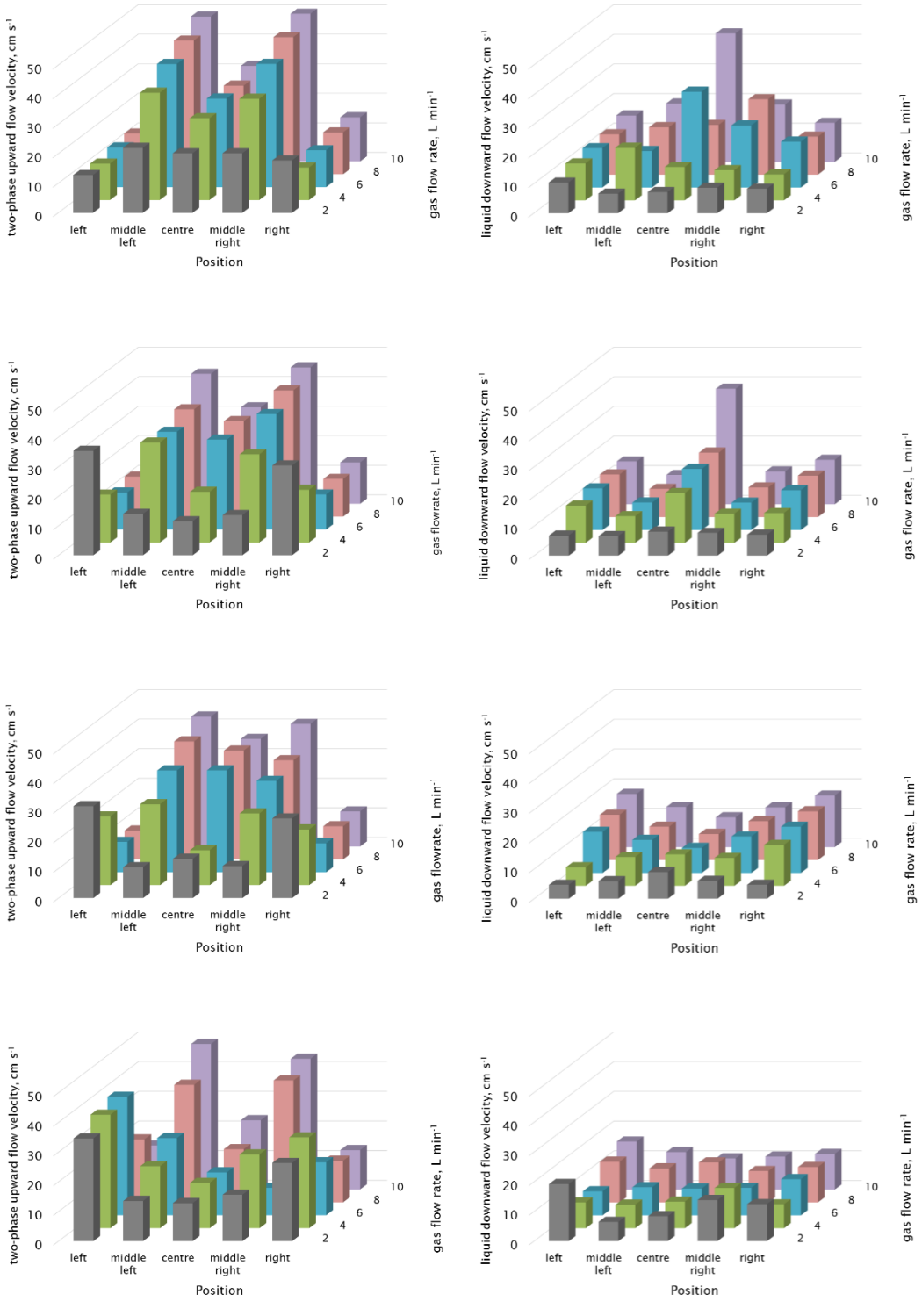

Figure 4-15 Measured two-phase flow velocities (left) and liquid downward flow velocities (right) with varied nozzle sizes of (a) ∅ 1 mm (b) ∅ 2 mm (c) ∅ 3 mm and (d) ∅ 4 mm

Downward liquid two-phase flow profiles for the smaller nozzle sizes of ∅ 1 and 2 mm in Figure 4-15 (a) and (b) exhibit similar characteristics, with the highest values mostly observed at the centre zone for sparging rates of 4 - 10 L min^{-1}. For the larger nozzle sizes of ∅ 3 and 4 mm in Figure 4-15 (c) and (d), liquid downward velocities are slightly higher at the left and right outer edges of the tank for most sparging rates in the range of 2 - 10 L min^{-1}.

For small nozzle sizes of ∅ 1 and 2 mm at 4 - 10 L min^{-1} sparging rates, it appears that two-phase upward flows are faster at the centre and middle-left and -right regions of the membrane surface, and downward flows have high velocities at the centre zone of downcomer section. For a nozzle size of ∅ 3 mm two phase upward flows show high velocity profiles at the middle and centre zone of the riser section at sparging rates of 4 - 10 L min^{-1}. The liquid downward flow shows almost uniform velocities across the cross-section area in the downcomer zone for the larger nozzle sizes of ∅ 3 and 4 mm.

Measured two-phase upward and liquid downward flow velocities from 5 positions of each condition from Figure 4-15 were averaged and shown in Figure 4-16.

Overall from Figure 4-16 (a) it can be seen that the higher sparging rates stimulate higher flow velocities for every nozzle size in both riser and downcomer zones. From Figure 4-16 (a), average two-phase upward velocities tend to decrease at larger nozzle sizes for the same given fixed sparging rate. This trend can be seen more clearly in the liquid downward velocity patterns plotted in Figure 4-16 (b). Since all experimental conditions were conducted under the same tank geometry setup with fixed A_d/A_r of 3.07, A_d/A_b of 0.5 and 68 cm tap water depth, this demonstrated that with a given fixed sparging rate, different nozzle sizes and bubble distributions considerably affected the hydrodynamics inside the tank for both riser and downcomer sections.

The major reason why the flow velocities given by the smaller nozzle sizes of ∅1 and 2 mm are higher than those for the larger nozzles is the more uniform bubble distribution along the sparger tube length. Uniform bubble generation across the membrane cross-section area in the flow channel induces even two-phase (also liquid phase) flows inside the tank that give a high continual crossflow velocity over the entire membrane surface. Another possible reason is that small bubble fractions generated from small nozzle sizes have lower terminal rising velocities in comparison with large pseudo-2D confined cap bubbles. This means small bubbles are retained longer in the flow channel resulting in a higher gas hold-up in riser zone (term ε_r in Equation 2-2), leading to a greater difference in hydrodynamic pressure between riser and downcomer section, and thus stimulating higher upward crossflow velocities.

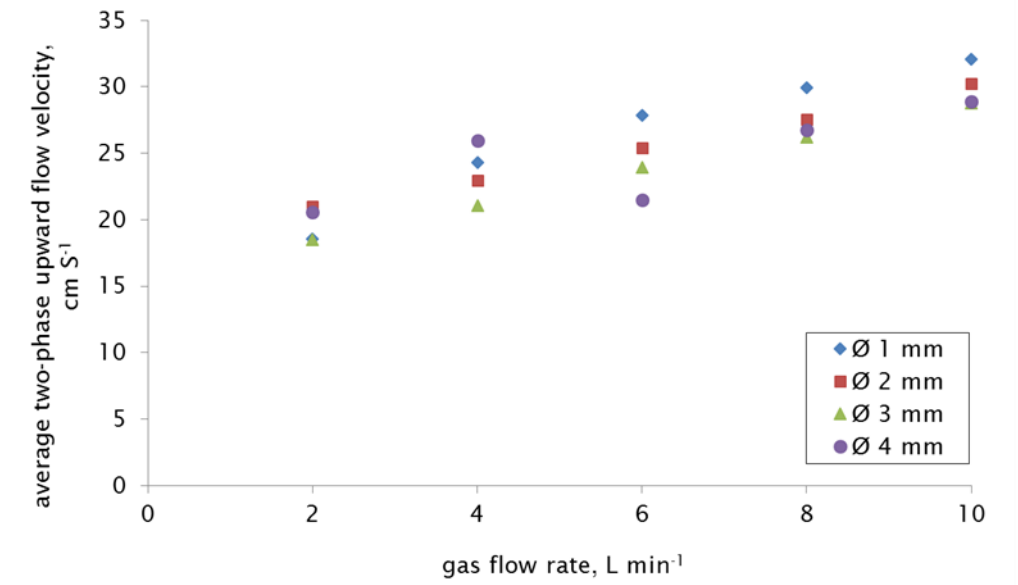

(a)

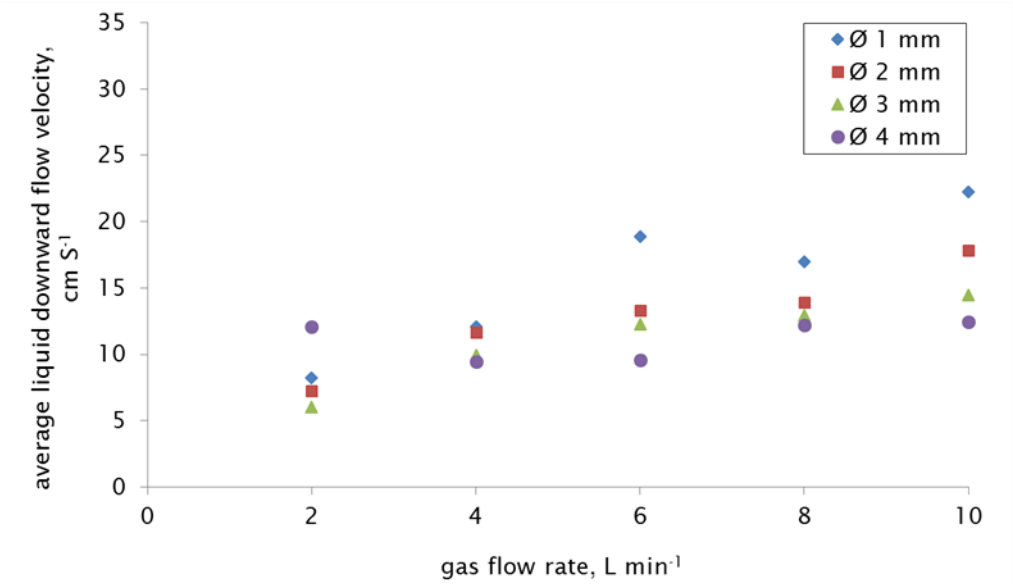

(b)

Figure 4-16 Average flow velocities related to different nozzle sizes (a) two-phase upward flow velocities (b) liquid downward flow velocities

Actual upward velocities (U_{lr}) between membrane channel minus the void fraction for each condition are calculated for both two-phase upward and liquid downward velocity cases. Actual liquid upward flow velocities related to nozzle sizes plotted with U_g are shown in Figure 4-17.

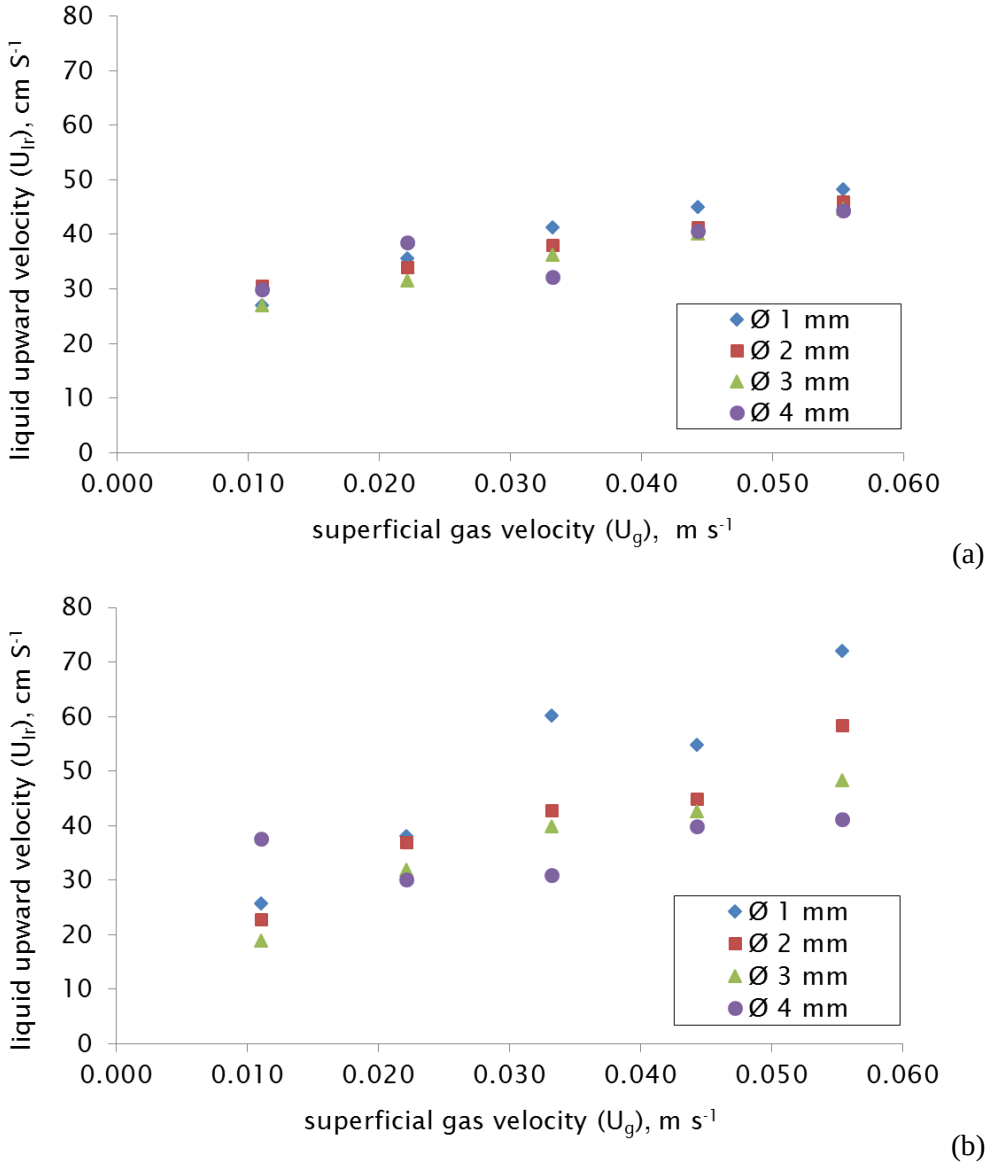

Figure 4-17 Actual liquid upward flow velocity (U_{lr}) related to superficial gas velocity for different nozzle sizes: (a) calculated from average two-phase upward velocity (b) calculated from average liquid downward velocity

In Figure 4-17, it can be seen from both calculated cases that U_{lr} values generated by smaller nozzle sizes of ∅ 1 and 2 mm are higher than those for the larger nozzles of ∅ 3 and 4 mm. Considering U_{lr} values derived from liquid downward flow velocities in Figure 4-17 (b), from sparging rates referring to U_g in the range of 0.022 to 0.055 m s^{-1}, it is clear that the higher U_{lr} occur for smaller nozzle sizes at a fixed given sparging rate. At a threshold U_g of 0.033 m s^{-1}, the highest U_{lr} is 60 m s^{-1} for the ∅ 1 mm nozzle, while the lowest U_{lr} is 31 m s^{-1} with ∅ 4 mm nozzle, with U_{lr} values in the range of 40 - 43 m s^{-1} for ∅ 3 and 2 mm nozzles, respectively. Similar trends for higher U_{lr} from small nozzle sizes compared to large nozzle diameters have been reported elsewhere. Sofia, Ng and Ong (2004) operated a flat sheet MBR for domestic wastewater

treatment and found better fouling control with a ∅ 0.5 mm porous media diffuser instead of ∅ 2 mm nozzles on perforated tube spargers. Small bubbles induced higher crossflow velocities than coarse bubbles. The finer and more uniformly distributed bubbles were thought to make more stable operation possible, with lower fouling across the membrane. They also reported a threshold aeration intensity at U_g of 0.017 m s^{-1} for porous fine diffuser which resulted in U_{lr} of approximately 0.65 m s^{-1} (in tap water), while U_{lr} for coarse bubble diffuser was 0.40 m s^{-1} at this given U_g. Yamanoi and Kageyama (2010) evaluated bubbles flow properties between flat-sheet membranes. They observed that at the fixed given U_g, U_{lr} induced by fine bubbles generated from a glass filter diffuser was greater than for coarse bubbles created by a ∅ 6 mm nozzle. According to their results, however, the average contributed shear stress was larger for large bubbles than for small bubbles.

When comparing U_{lr} from Figure 4-17 (b) with the bubbles-membrane contact surface ratio (which relates to shear stress) in Figure 4-10 (b), at the fixed given U_g, the U_{lr} values produced from small nozzle sizes are greater than the U_{lr} values from large nozzles, in contrast to the trend in the bubble-membrane contact surface ratio. Sparging influences turbulence, liquid velocity and shear stress: the supplied energy from the buoyant force of the bubbles is mainly transferred to the liquid upward velocity and the shear stress on the membrane. Small bubbles may be more effective in stimulating liquid velocity and for their distributed homogeneity; while pseudo-2D confined cap bubbles are more efficient in shear stress contribution due to their stronger secondary wakes (Yamanoi and Kageyama, 2010; Wei *et al.*, 2013). Both shear stress and backtransport velocity play an important role in two-phase gas-liquid flow to remove and transport foulants away from membrane surface. Hence, the balance between shear stress and backtransport velocity contributions and their distributions under given energy supply for gas sparging are of prime importance for proper MBR design.

4.2.3 Effect of downcomer flow area to transitional flow area ratio (A_d/A_b) on liquid upward and transversal flow velocities

Under a specific sparging rate, one possible approach to increase U_{lr} according to Equation 2-2 is to decrease frictional loss coefficient (term K_B in Equation 2-2) for the bottom zone of reactor, which is related to the A_d/A_b ratio in Equation 2-3.

This experiment examined the effect of various A_d/A_b ratios of 0.19, 0.39, 0.78, 1.55, and 3.10 on liquid upward velocities in riser and transversal flow (from downcomer to riser) velocities at the bottom zone of the reactor. The reactor was set up in a fixed A_d/A_r ratio of 2.21 with 7 mm membrane gap and 68 cm tap water depth. Although the threshold sparging obtained from previous results was determined at 6 L min^{-1} (U_g = 0.033 m s^{-1}), this rate is considered to represent

a relatively high energy consumption. Hence, this trial was performed at a constant sparging rate of 2.5 L min^{-1} that represented a U_g of 0.014 m s^{-1}. This rate is typical of the superficial gas velocity range for flat-sheet MBRs of 0.0125 - 0.76 m s^{-1}, resulting in liquid circulation velocities in the riser of approximately 0.1 - 0.3 m s^{-1} (Prieske *et al.*, 2010; Rosenberger, Helmus and Drews, 2016). Additionally, in the attempt to balance bubble distribution under this low sparging rate, a modified nozzles arrangement was introduced. Two modified spargers were used, made of ∅ 6 mm perforated stainless steel tube with open one end, but with only 2 nozzles instead of the previous 4 equal holes in each. The diameters of the nozzles close to the air inlet direction was ∅ 1.5 mm while the further one was 3 mm in diameter. These were installed at the bottom of reactor in riser zone as shown in Figure 3-3.

Results for measured two-phase upward and liquid downward velocities taken from 5 points along the membrane width under a 2.5 L min^{-1} sparging rate with various A_d/A_b ratios between 0.19 - 3.10 are shown in Figure 4-18.

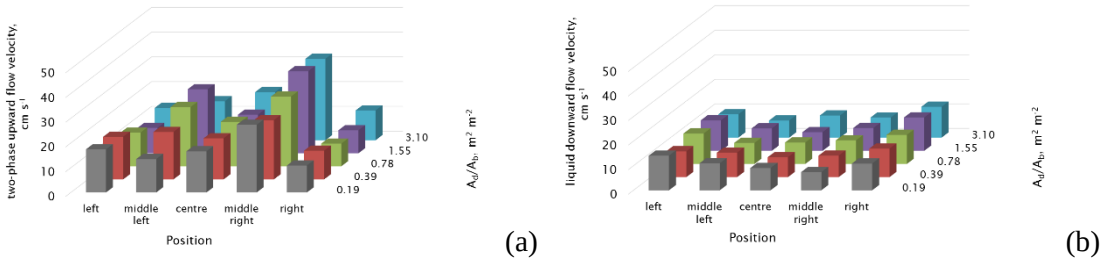

Figure 4-18 Measured flow velocities with varied A_d/A_b ratios of 0.19, 0.39, 0.78, 1.55 and 3.10 of (a) two-phase upward flow velocities and (b) liquid downward flow velocities

From Figure 4-18 it can be seen that two-phase flow velocities in the riser present similar patterns for every A_d/A_b ratios, as well as liquid downward flow. Liquid downward flow velocities Figure 4-18 (b) for every position at each A_d/A_b ratios show similar values of about 10 cm s^{-1}, while the two-phase upward velocities at the middle right position are higher than the others. This was thought the be because one of the sparger tubes that was installed at the back of membrane panel, which at total sparging rate of 2.5 L min^{-1} (1.25 L min^{-1} for each sparger tube) made narrower in upward liquid turning overflow radius. More bubbles were observed appearing at the back side of the membrane panel, resulting in higher upward flow velocities for this region.

Measured two-phase upward velocities in the riser and liquid downward velocities at 5 positions from Figure 4-18 were averaged. Actual liquid upward velocity (U_{lr}) was calculated from both riser and downcomer, as well as actual liquid transversal flow velocities calculated from liquid downward velocities in downcomer. Flow velocities for varied A_d/A_b ratios are presented in Figure 4-19.

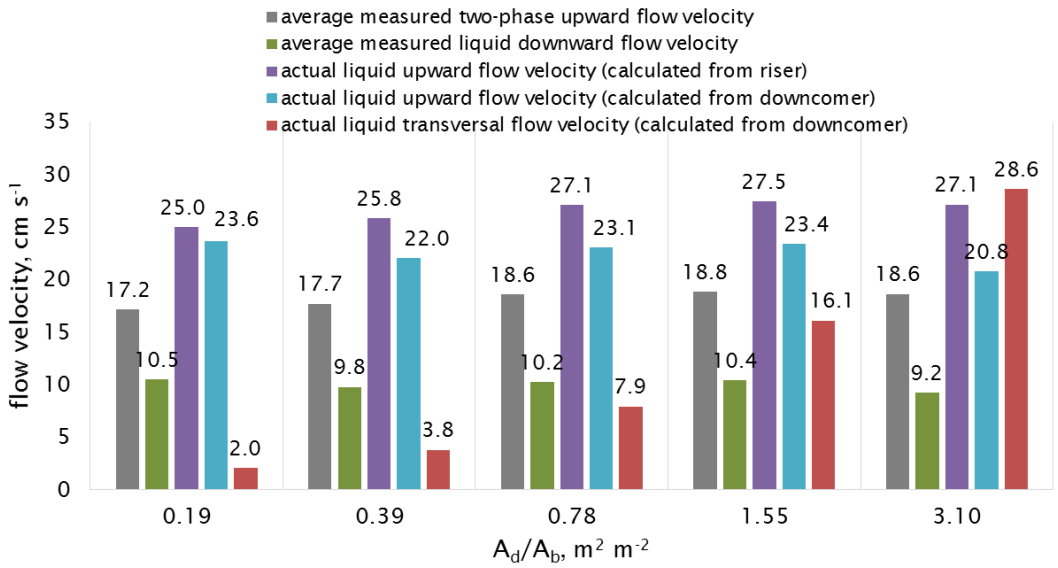

Figure 4-19 Flow velocities related to varied A_d/A_b ratios

Actual liquid upward flow velocities (U_{lr}) in Figure 4-19 show similar values in the range of 25.0 - 27.5 cm s^{-1} (calculated from riser) and 20.8 - 23.6 cm s^{-1} (calculated from downcomer) for A_d/A_b ratios between 0.19 - 3.10. Although the lowest value of 20.8 cm s^{-1} (calculated from downcomer) was observed at the highest A_d/A_b of 3.10 (the narrowest free area for transversal flow between riser and downcomer), it seems A_d/A_b ratios between 0.19 - 3.10 do not affect the actual liquid upward velocities significantly. This might be because term A_d/A_b in Equation 2-3 has only a minor effect on term K_B which is related to U_{lr} in Equation 2-2 in the form of an inverse ratio in the quadratic equation. Hence, A_d/A_b in the range of 0.19 - 3.10 in this trial had only a minor effect on the observed U_{lr}.

Considering other favourable hydrodynamic factors, however, optimisation of the A_d/A_b ratio is still an important aspect, because very high transversal flow velocities at high A_d/A_b ratios such as 1.55 - 3.10 could cause friction head loss between the reactor sections which affect the flow, particularly at the abrupt flow direction change from the downcomer to the riser region. For instance, Prieske *et al.* (2010) investigated favourable hydrodynamic conditions for flat-sheet membrane modules with A_d/A_r of 2 and A_d/A_b of approximately 1. They suggested modifying smooth draft tube edges to achieve lower losses in bends at the transitional flow region, and removing air diffuser tubes from the draft tube entrance to obtain better continual liquid recirculation flow. By this re-design, at the same aeration rate, a 30 - 50 % improvement in liquid circulating velocities was achieved. On the other hand, too low an A_d/A_b ratio would cause very low transversal velocity, as seen in Figure 4-19: at A_d/A_b of 0.19 and 0.39, the achieved transversal velocities are just 2.0 and 3.8 cm s^{-1}. The too low transversal flow velocities could disrupt favourable mixing conditions, potentially leading to settling of the mixed suspension and also formation of dead zones in regions of the tank with extremely small liquid velocity (e.g. reactor

corners and bottom zone). In particular, when attempting to operate gaslift-loop reactors with suspended scouring particles, the required transversal velocities to maintain completely mixed conditions are strongly affected by the specific gravity (SG) of the suspended particles. Rosenberger *et al.* (2011) investigated the use of suspended particles to enhance membrane scouring for airlift-loop flat-sheet membrane modules. They suggested optimum deflection velocities in the reactor bottom zone of 0.4 - 0.5 m s^{-1} for particles with SG of 1.02 - 1.05, while the required deflection velocities to maintain complete dispersion of particles with SG 1.2 - 1.3 were in the range of 0.8 - 1.0 m s^{-1}.

According to the results in Figure 4-19, A_d/A_b in the range of 0.19 - 3.10 caused only minor variations in U_{lr} ; however, for continuity of transverse flow from downcomer to riser, when actual liquid downward velocity in the downcomer is mostly in the range of 9.2 - 10.5 cm s^{-1}, transversal flow velocities should be in a similar range. As a result, in order to optimise transversal flow velocities between the riser and downcomer zone with respect to continuous flow condition, it is recommended that the A_d/A_b ratio is set at approximately 1.

4.3 Flux declining observation in constant pressure filtration mode driven by gravitational static head

This set of experiments was conducted with the objective of evaluating fouling propensities and filtration characteristics using a model mixed suspension as a medium, with comparison between varied nozzle sizes under the same fixed sparging rate in constant pressure suction mode.

The reactor was set up with a 10 L liquid working volume and the tank geometry of A_d/A_r 3.71, A_d/A_b 0.65 and 68 cm liquid depth. The reactor was filled with diluted sieved anaerobic sludge made up to an expected initial MLSS concentration of approximately 7,500 mg L^{-1} using tap water (original anaerobic MLSS concentration approximately 40 g L^{-1}). Two perforated tube spargers with nozzle sizes of ∅ 1, 2, 3 and 4 mm (equal nozzle diameter with 4 holes on each sparger tube) supplied with total 5 L min^{-1} sparging intensity (close to threshold sparging rate of 6 L min^{-1}) were applied for each experimental run. Membrane permeate was extracted continuously under constant pressure suction mode driven by gravitational force from the static head difference between the liquid level inside the reactor and the level of the permeate outlet, which was set at 1 m (0.1 bar). Details of the gravitational filtration set up under constant pressure suction mode described in Ueda and Hata (1999) and Meng *et al.* (2008). Permeate flux was measured by a weight-time method (using a digital balance and stopwatch). Filtered permeate was recycled back into the reactor by a recirculation pump in order to maintain constant MLSS concentration and static head throughout the operational period.

Flux declining characteristics and fouled membrane pictures for each condition over 54 hours of operation are presented in Figure 4-20 and Figure 4-21 respectively.

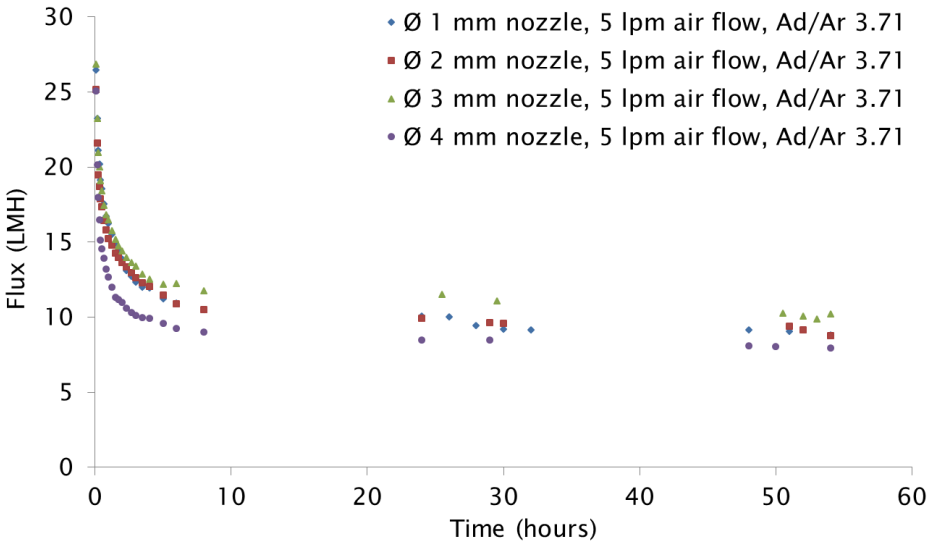

Figure 4-20 Flux declining characteristic under constant filtration pressure mode (gravitational driven) for nozzle size of ∅ 1, 2, 3 and 4 mm

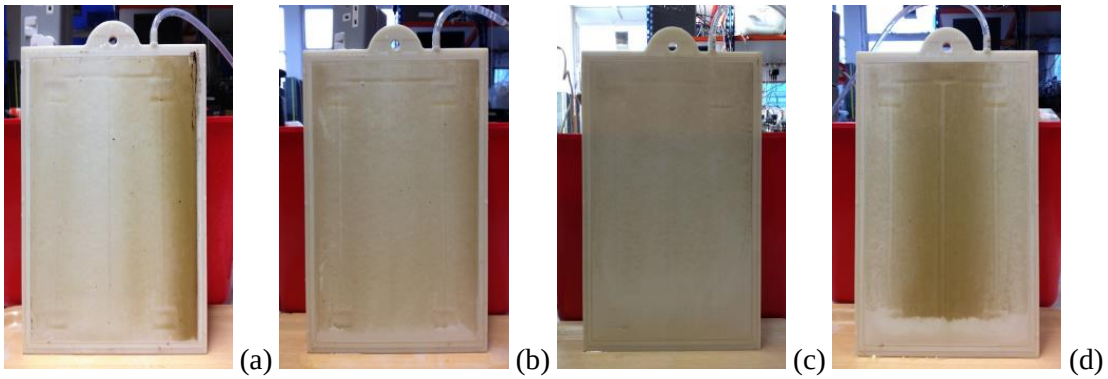

Figure 4-21 Fouled membrane characteristics after 54 hours filtration (a) ∅ 1 mm nozzle, (b) ∅ 2 mm nozzle, (c) ∅ 3 mm nozzle and (d) ∅ 4 mm nozzle

As seen in Figure 4-20, flux declining patterns for every nozzle sizes show similar trends. Initial flux production for the first five minutes of filtration for all nozzle sizes gave similar values of 26.5, 25.2, 26.9 and 25.1 LMH for nozzle sizes of ∅ 1, 2, 3 and 4 mm, respectively. The produced fluxes for all nozzle sizes declined dramatically during the first hour of filtration, following by slower rates of decline for 2-8 hours of filtration. Achieved fluxes at the 8th filtration hour for nozzle sizes of ∅ 1, 2, 3 and 4 mm were 10.5, 10.5, 11.8 and 9.8 LMH, respectively. Thereafter, achieved fluxes slowly reduced to 8.9, 8.8, 10.2 and 8.0 LMH at the 54th hour of filtration for nozzles sizes of ∅ 1, 2, 3 and 4 mm, respectively.

It is not easy to distinguish and difference in fouling propensity for nozzle size ∅ 1 - 4 m in Figure 4-20. This may be due to a number of factors, including small differences in the initial characteristics of the model mixed suspension in each run;, the accuracy of determination of the produced flux by the weight-time measurement method under relatively low constant gravitational driven pressure; and changes in the mixed suspension properties during the experimental period. However, the results from achievable fluxes for each condition at the same filtration period can illustrate the effects of nozzle size on fouling reduction as follows.

Apart from other mixed suspension properties, regarding only the hydrodynamic aspects, the effects of nozzle size on fouling mitigation propensities are considered based on contributed shear stress (which is hypothesised to depend on observed bubble-membrane contact area ratio (α′)), and on backtransport velocity (which depends on liquid upward flow velocity (U_{lr}) derived from liquid downward flow).

Results from previous sections demonstrated that α′ and U_{lr} of each nozzle size under 6 L min^{-1} sparging rates are:

- ∅ 1 mm nozzle, α′ = 3.6 % of total membrane surface and U_{lr} = 60.2 cm s^{-1}
- ∅ 2 mm nozzle, α′ = 4.9 % of total membrane surface and U_{lr} = 42.8 cm s^{-1}
- ∅ 3 mm nozzle, α′ = 7.6 % of total membrane surface and U_{lr} = 39.8 cm s^{-1}
- ∅ 4 mm nozzle, α′ = 6.7 % of total membrane surface and U_{lr} = 30.1 cm s^{-1}.

When comparing the 4 nozzle sizes based on the achieved fluxes at the same filtration period, the nozzle size of ∅ 3 mm presented the best tendency for fouling mitigation. This is thought to be due mainly to its having the highest α′ and relatively high U_{lr} as well as to the even bubble distribution across the entire membrane surface (from visual observation in Figure 4-1 (c) and Figure 4-21 (c)).

The next best for good fouling reduction are the smaller nozzle sizes of ∅ 1 and 2 mm, which showed almost the same behaviour during the filtration period. This is potentially because the smallest nozzle size of ∅ 1 mm contributes the highest U_{lr} with very uniformly distributed bubbles flow between membrane the channel (from visual observation in Figure 4-1 (a)) and U_{lr} in Figure 4-15 (a)) even with its lowest α′. The ∅ 2 mm nozzle had a smaller U_{lr} but this was compensated for by higher α′ and good even bubble generation, giving these nozzles similar patterns of flux decline.

In contrast the ∅ 4 mm nozzle, despite its relatively high α′, presented the poorest fouling mitigation. This result was possibly caused by the lowest achieved U_{lr}. Another major reason is potentially the bubble distribution (shear stress distribution) characteristic compared to other

nozzle sizes. This can be seen in Figure 4-1 (d), and in the flow velocity profile in Figure 4-15 (d) and Figure 4-21 (d), which show that large bubbles always appear at the outer side of membrane edges where other regions on the membrane surface revealed intensive foulant deposition.

As a result, it is difficult to conclude whether shear stress or backtransport velocity dominated the fouling control. Several studies have reported that shear stresses or shear forces contributed from two-phase flow were three to seven times higher than those obtained from single-phase flow and have more effect on fouling than a liquid flow with higher velocity (Chang and Fane, 2001; Bérubé *et al.*, 2006; Bohm *et al.*, 2012). For a gas-sparged two-phase flow applied to a flat-sheet membrane under a fixed given sparging intensity, however, changes in these two important parameters happen at the same time and are strongly related to each other, as demonstrated by the result in this chapter. Moreover, another necessary factor is the homogeneity of shear stress (bubble) and crossflow velocity distribution over the entire membrane surface, which is highly affected by sparger design and tank geometry setup. Therefore, the balance between shear stress, liquid crossflow velocities and their even distribution under a specific sparging intensity via sophisticated sparger and tank design is of prime importance for energy optimisation in two-phase gas-sparged MBR operation.

4.4 Conclusions

In order to achieve effective benefits from energy input for fouling mitigation by two-phase sparging, optimisation of favourable hydrodynamic conditions for MBR tank was carried out in this chapter. The experiments were conducted using perforated sparger tubes with varied nozzle sizes of ∅ 1 - 4 mm, supplied by constant air sparging from one side with sparging intensity in the range of 2 - 10 L min^{-1} (corresponding to U_g of 0.011 - 0.055 m s^{-1} in 7 mm channel depth).

It was found that both gas sparging rate and nozzle sizes have a significant influence on bubble size, bubble size distribution and bubble distribution across the sparger tube length and membrane surface. At the same given sparging rate, small nozzle sizes gave more favourable bubble distribution than large nozzle sizes. For a large nozzle size, such as ∅ 4 mm, the results from still photographs and two-phase upward velocity profiles showed that most bubbles detached from nozzle holes close to the gas inlet direction on the spargers. Unevenly distributed bubbles could cause a stagnant flow zone due to internal liquid circulation loop flow. Increasing the sparging rate can enhance the even bubble distribution across sparger tube but has a higher energy requirement. In order to diminish this problem, spargers were arranged in the position where gas was introduced from both the left and right outer sides of the membrane panel, and the reactor was set in a gaslift-loop configuration in which annular recirculation flow could be promoted.

Although increasing the gas sparging rate resulted in a larger number of bubbles, D_{10} did not appear to be a strong function of either sparging intensity or nozzle size. Relating the bubble size distribution and the occurrence showed that bubbles with sizes smaller than the membrane gap are dominant for every nozzle size case. When considering the representative bubble diameter related to accumulated volume and volume to projected area ratio, as indicated by D_{V50} and D_{32}, the gas injection rate did not significantly influence these representative bubble diameters at fixed nozzle size, since increased sparging rate resulted only in a higher volume of accumulated gas being produced from each bubble size. However, D_{V50} and D_{32} showed dependence on nozzle size at a fixed sparging rate. D_{V50}, D_{32} and the proportions of larger generated bubble sizes increased with nozzle size. Bubble size distribution related to accumulated volume as well as D_{V50} and D_{32} revealed that the fraction of bubbles with sizes larger than the membrane gap increased at a larger nozzle size.

Bubble-membrane covered area and touching area increased with increasing sparging rate due to the higher gas hold-up in the flow channel. Bubble-membrane contact/covered area ratios presented a consistent trend with increasing nozzle size. Increasing the nozzle size from ∅ 1 to 3 mm resulted in higher bubble touching/covered area ratios, whilst a further increase in nozzle sizes from ∅ 3 to 4 mm did not show any significant improvement in contact/covered area ratios. This indicated that nozzle size has a strong effect on produced bubble sizes for bubble swarms flowing in the channel. After the nozzle size and gas flow rate reach certain values, generated bubble sizes are reach a limit. This is potentially caused by the achievable bubble sizes created from each given nozzle size and bubble breakage during rising and flowing between membrane channel. Regarding the bubble-contact area fraction and contact/covered area ratio, nozzle sizes of ∅ 3 and 4 mm showed higher values for these parameters compared to smaller nozzle sizes of ∅ 1 to 2 mm. This is attributed to the fact that nozzle sizes ∅ 3 and 4 mm give higher fractions of bubble sizes larger than the membrane clearance, in which shear stress can be enhanced due to the stronger secondary turbulent flow field created by pseudo-2D confined cap bubble flow regime, in comparison with the free bubble flow pattern induced by bubble sizes smaller than the membrane gap flowing in the channel.

From the viewpoint of geometry optimisation, regarding the gaslift-loop configuration, the results showed that under superficial gas velocities (U_g) of 0.011 - 0.055 m s^{-1}, with fixed nozzle size of ∅ 3 mm, increasing the cross-sectional area of riser to downcomer ratio (A_d/A_r) in the range of 1.78 - 3.71 did not improve actual liquid upward flow velocity (U_{lr}) significantly. However, the highest U_{lr} values (derived from liquid downward flow) were found at large A_d/A_r of 3.71, while the lowest U_{lr} were found at small A_d/A_r of 1.78. Hence, in order to enhance flow continuity, it is recommended that A_d/A_r should be larger than 1.78. A similar tendency was found for bottom

transversal flow, in which a reduction in the cross-sectional area of downcomer to bottom transversal position (A_d/A_b) from 3.10 to 0.19 did not notably promote U_{lr}. Nonetheless, the lowest U_{lr} and the highest transversal flow was shown at high A_d/A_b of 3.10, which indicated higher friction losses due to the very high deflection flow velocity. Regarding annular flow recirculation, therefore, an A_d/A_b ratio close to 1 is suggested.

Under the conditions in this study, threshold U_g was found to be 0.033 m s^{-1} (6 L min^{-1} sparing rate). Further increments of sparging intensity beyond this value only resulted in minor improvements in the achieved U_{lr}. As a result, determination of U_g (from U_{lr}) is an important factor for practical MBR tank geometry design as well as from the aspect of a reasonable energy consumption. Regarding the optimisation of practical tank design, other favourable hydrodynamic parameters such as membrane spacers, liquid depth, A_d/A_r, A_d/A_b, nozzle sizes, sparger arrangement and sparging rates, should be carefully selected following the threshold U_g values in order to obtain effective exploitation from energy inputs.

In contrast to the trend in contributed shear stress from varied nozzle sizes, small nozzle sizes of ∅ 1 to 2 mm gave higher U_{lr} than larger nozzle sizes of ∅ 3 to 4 mm at the same fixed sparging rates. This is due to the homogeneity of the small bubbles distribution along the sparger length, which stimulated high U_{lr} in the flow channel. Hence, it could be seen that evenly distributed small bubbles created from small nozzle sizes induce higher backtransport velocity than big bubbles generated from larger nozzle sizes under the same fixed given U_g.

The results from the MLSS filtration experiment showed that under a near threshold sparging intensity of 5 L min^{-1} (U_g = 0.028 m s^{-1}), nozzle size ∅ 3 mm with the highest shear stress, good U_{lr} and bubbles distribution gave the best filtration performance; followed by nozzle sizes of ∅ 1 and 2 mm with fair shear stress, very good U_{lr} and even bubble distributions. Nozzle size ∅ 4 mm with very high shear stress but poor given U_{lr} and uniformly bubble distribution characteristics show the lowest filtration performance. These results indicated that, under fixed given intensity, the balance between shear stress, liquid upward flow velocity (backtransport velocity) and homogeneity of bubble distribution (i.e. shear stress and U_{lr} distribution) across the entire membrane surface via sophisticated sparging system design is of prime important to achieve productive efficiency from energy supply.

Chapter 5: **Integration of non-adsorbent particles with gas sparging operated as three-phase flow for flat-sheet submerged MBR**

Two-phase gas sparging is the most conventional method that has been widely adopted to minimise fouling. However, when backtransport velocity (generated by liquid cross flow) and shear stress (induced by bubble flow regime) are inadequate compared to the convection flow through membrane surface (driven by permeate suction), a gel layer with solid deposition could lead to severe cake formation. Besides, cake resistance which cannot be removed effectively by either gas bubbling nor liquid crossflow velocity from the two-phase flow, has been reported to be a major contributor to membrane fouling in several MBRs studies (Jeison and van Lier, 2007a; Huang, Wei and Yu, 2008; Xie *et al.*, 2010).

The rationale for introducing suspended scouring particles is discussed in section 2.2.7 of the literature review. The aim of this chapter was therefore to assess the potential of using non-adsorbent suspended particles associated with two-phase gas sparging operated as three-phase moving bed MBR for fouling alleviation purpose.

Non-adsorbent suspended particles (carriers) made of low density polyethylene (LDPE) appear in rigid round flat-lens shape (∅ 3 - 4 mm and 1.5 - 2 mm thickness) with SG of 0.86 - 0.89 (details of LDPE particles shown in section 3.1.5.1) were proposed to be a scouring agent in this chapter. The experiments were carried out with the objective to evaluate the utilisation of suspended carriers as produced flux enhancer under specific given sparging intensities or as an alternative method to reduce energy consumed by sparging at similar achievable fluxes. Experimental setups were related to simulated MBR operational conditions such as the effect of filtration modes and carriers filling ratios on filtration performance, reactor configurations, critical flux etc. The obtained results were expected to provide a guideline for practical three-phase flow designs for AnMBRs in the next chapter.

5.1 The effect of carrier addition on filtration performance under constant pressure filtration mode driven by gravitational static head

The experiments were mainly designed to observe the effect of varied carrier filling rates, sparging intensities and nozzle size design on filtration performance assessed as flux declining propensities under constant filtration mode driven by gravitational static head.

Most of the trials were conducted in similar conditions in which the initial model MLSS concentration was set at approximately 7,500 mg L^{-1}, 68 cm liquid depth, with a gas-lift loop reactor configuration at A_d/A_b of 0.7. Permeates were drawn with constant suction mode driven by gravitational force due to the difference between the liquid level inside the reactor and the permeate outlet level of 1 m (0.1 bar). Permeate flux was measured by weight-time method (using digital balance and stopwatch). Filtered permeate was recycled back into the reactor by recirculation pump in order to maintain a constant MLSS concentration and static head during the operational period.

The experiments were separated into two groups which the first group used a 10 L liquid working volume at A_d/A_r of 3.71 with carrier filling ratio of 0 and 10 % by weight (approximately 0 and 11.1 % by reactor volume). A gas sparging rate of 5 L min^{-1} was supplied via spargers with equal nozzle sizes of ∅ 3 mm. The second group used a 7 L liquid working volume at A_d/A_r of 2.21 with carrier filling ratio of 0, 5 and 10 % by weight (approximately 0, 5.6 and 11.1 % by reactor volume). Gas sparging rates of 2.5 and 5 L min^{-1} were supplied via spargers with unequal nozzle sizes of ∅ 1.5 and 3 mm.

Flux declining trends for the first group with foulants load from 10 L MLSS and A_d/A_r of 3.71 are shown in Figure 5-1 and pictures of fouled membranes after 54 hours of filtration are presented in Figure 5-2.

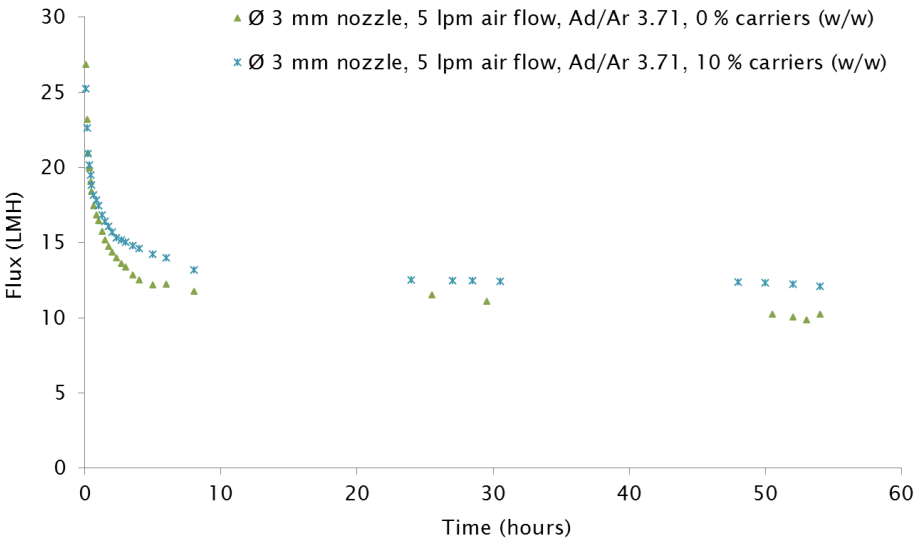

Figure 5-1 Flux declining trends under constant pressure suction mode driven by static gravitational head with foulants load from 10 L of MLSS

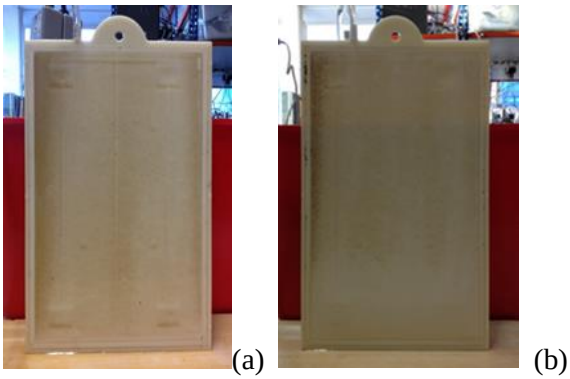

(a) (b)

Figure 5-2 Fouled membrane characteristics from 10 L MLSS foulants load using ∅ 3 mm nozzle, 5 L min^{-1} (lpm) air flow, A_d/A_r 3.71 after 54 hours of filtration (a) 0 and (b) 10 % carriers (w/w)

From Figure 5-1, initial flux productions in the first 5 minutes of filtration for 0 and 10 % (w/w) carriers show similar values of 26.9 and 25.3 LMH. Then, the produced fluxes for both cases declined sharply during the first hour of filtration, followed by a slower decline in the 2^{nd} - 8^{th} hours of operation. Thereafter, achievable fluxes slowly decreased to 10.2 and 12.1 LMH, for 0 and 10 % carriers, respectively, at the 54^{th} hour of the filtration period. Regardless of certain sensitive factors during the conducted experiments as mentioned in section 4.3, the results illustrated that, under the same experimental conditions and fixed energy input for gas sparging in this group, the produced flux could be enhanced up to 18.6 % by the assistance of scouring particles at 10 % (w/w).

For the group of 7 L MLSS with A_d/A_r of 2.21, flux declining trends and pictures of fouled membrane characteristics after 54 hours of filtration period for each condition are presented in Figure 5-3 and Figure 5-4, respectively.

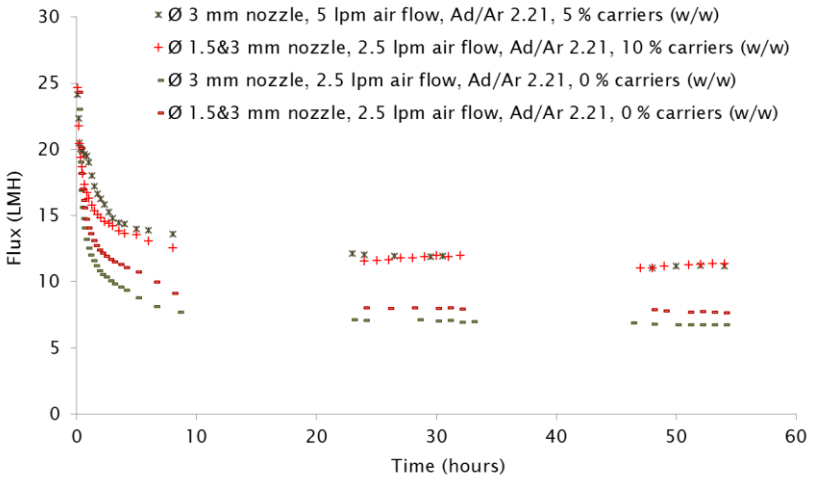

Figure 5-3 Flux declining trends under constant pressure suction mode driven by static gravitational head with foulants load from 7 L of MLSS

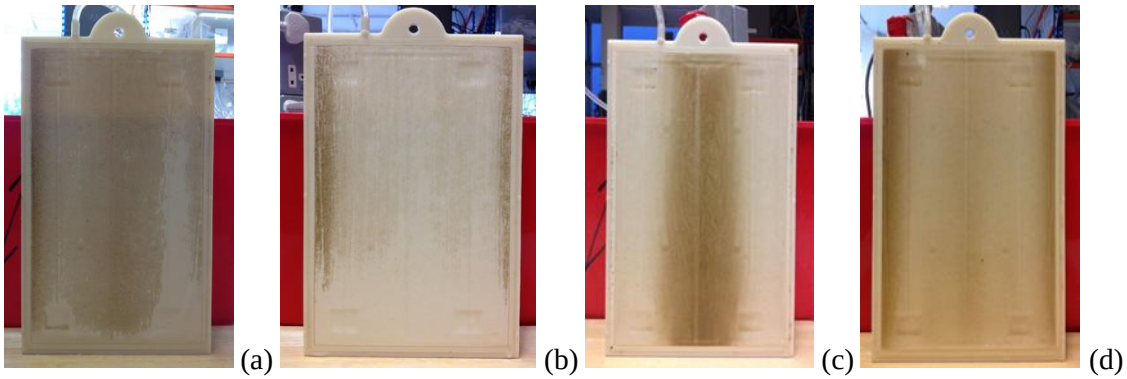

Figure 5-4 Fouled membrane characteristics from 7 L MLSSfoulants load after 54 hours of filtration

(a) ∅ 3 mm nozzle, 5 L min^{-1} air flow, A_d/A_r 2.21, 5 % carriers (w/w)

(b) ∅ 1.5 and 3 mm nozzle, 2.5 L min^{-1} air flow, A_d/A_r 2.21, 10 % carriers (w/w)

(c) ∅ 3 mm nozzle, 2.5 L min^{-1} air flow, A_d/A_r 2.21, 0 % carriers (w/w)

(d) ∅ 1.5 and 3 mm nozzle, 2.5 L min^{-1} air flow, A_d/A_r 2.21, 0 % carriers (w/w)

As can be seen from Figure 5-3, the decline in flux in each set of conditions showed similar patterns to the first group. At 2.5 L min^{-1} air flow with 0 % carriers the produced fluxes at 54^{th} filtration hour were 6.8 and 7.7 LMH for the ∅ 3 mm and the ∅ 1.5 and 3 mm nozzles, respectively, corresponding to a difference of 13.2 %. The main reason is due to the uneven bubbles distribution over the membrane surface (Figure 5-4 (c) and (d)). Although the results from the previous chapter showed that equal nozzle sizes of ∅ 3 mm gave the highest filtration performance at 5 L min^{-1} sparging rate, at 2.5 L min^{-1} sparging intensities, unequal nozzle sizes of ∅ 1.5 and 3 mm shows better trends of filtration performance. This confirms the approach that sophisticate nozzles and spargers should be designed following specific given sparging intensity in order to optimise and balance between contributed shear stress, liquid crossflow velocity and uniform bubble distribution.

When comparing the ∅ 1.5 and 3 mm case at the same 2.5 L min^{-1} sparging rate with 0 or 10 % carriers, at 54 hours of filtration the produced flux could be improved from 7.7 to 11.4 LMH or by up to 48 % (Figure 5-4 (b) and (d)). This achieved flux is almost comparable to the flux produced from ∅ 3 mm nozzles, as a 5 L min^{-1} sparging rate with 5 % carriers, which was 11.2 LMH (Figure 5-4 (a)), while the energy input for sparging can be reduced by half.

According to these results, it is indicated that using non-adsorbent particle as scouring agents with conventional two-phase gas sparging is an effective alternative method for fouling mitigation. Produced flux can be enhanced considerably under the same fixed sparging intensity or a comparable flux could be retained while the energy supply for gas sparging can be significantly reduced.

5.2 Transmembrane pressure (TMP) rising and flux change

The experimental filtrations in this section were operated as nearly as possible in constant flux mode. Permeate fluxes were extracted via peristatic suction pump instead of gravitational driven. Changes in TMP (absolute values) and flux were observed during the experiment.

In order to compare the efficiencies of membrane filtration under varied conditions for the further stages in this chapter, the so-called critical flux mainly based on fouling rates (dTMP/dt) approach were applied (see literature review section 2.2.5). The obtained results were expected to be a useful guideline for reasonable AnMBR designs in the next chapter.

5.2.1 The effect of initial flux value on TMP

Experiments were conducted to observe the effect of initial flux setting on TMP and flux change. These experiments were operated at fixed initial suction pump speed with no further adjustment after starting for either TMP or produced flux during 120 to 180 minutes of observed filtration period.

The MBR was operated at a 7 L liquid working volume with 68 cm liquid depth, A_d/A_r 2.21 and A_d/A_b 0.78, under a 2.5 L min^{-1} sparging rate supplied by ∅ 1.5 and ∅ 3 mm nozzles. The reactor was filled at an initial MLSS concentration of 7,500 g L^{-1}. Permeate drawing was controlled by peristaltic pump speed adjustments at 5, 10 and 20 rpm, corresponding to expected initial fluxes of 6.0, 12.0 and 24.0 LMH at peristaltic pump speeds of 5, 10 and 20 rpm, respectively. Flux productions were observed by weight-time measurement method via digital balance and stop watch throughout the 2 - 3 hour experimental period. Permeate effluent was recirculated back into the reactor to maintain a more or less constant MLSS and liquid level inside the reactor. The relationship between initial constraint fluxes, produced fluxes and TMP variations is plotted in Figure 5-5.

It can be seen from Figure 5-5 that at the initial flux setting of 6 LMH (5 rpm pump speed), TMP rapidly increased to about 0.04 bar in the first 5 minutes and remained relatively constant at this value thereafter until the end of a 180-minute filtration period with stable produced flux of 6 LMH.

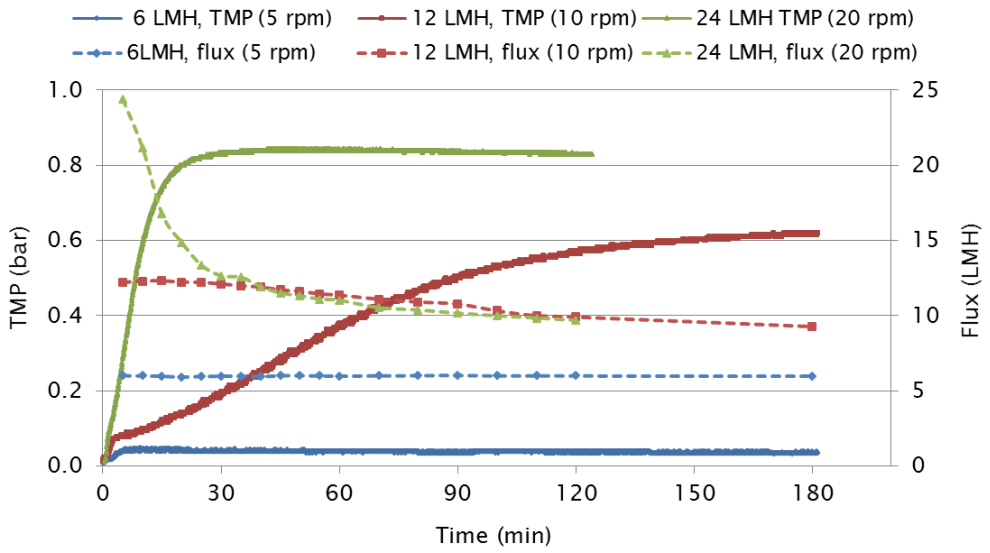

Figure 5-5 Variation in produced fluxes and TMP for different initial flux values

With the initial flux setting at 12 LMH, TMP rapidly increased to 0.07 bar in the first 5 minutes of filtration. Then TMP rose sharply to 0.50 bar at the 90th minute while the produced flux dropped to 10.8 LMH. Thereafter, TMP slowly increased up to 0.62 bar with 9.3 LMH achieved flux at the end of the 180-minute filtration period. The early TMP rises in the first few minutes for both initial fluxes of 6 and 12 LMH were likely due to a combination of concentration polarisation and a short period of rapid fouling (Ghosh, 2002). Thereafter, the TMP increase at the start of fouling for the initial flux of 12 LMH, in which the TMP pattern was concave downwards, indicated the development of concentration polarisation and some rapid initial fouling. The slow TMP rise after rapid initial fouling period until the end of experimental period may correspond to membrane pore blockage caused by adsorption of solutes or colloid and deposition of sludge particles within/onto the membrane surface (Lee, Ahn and Lee, 2001; Ho and Zydney, 2002). Ho and Zydney (2002) reported that pore blockage was the major fouling contributor during the initially slow steady increase in resistance during constant flux operations for protein microfiltration. After the pores were completely blocked, a cake layer began to form which rapidly stimulated filtration resistance. Similar results were found by Ognier, Wisniewski and Grasmick (2004) who studied constant flux mode for bioreactor effluent microfiltration. Their results indicated that the fouling appears to be a self-accelerating phenomenon. When pores gradually become blocked under constant flux filtration, an increase in the local flux for neighbouring pores has to take place in order to maintain the same produced flux over the entire filtration areas. Once many pores are blocked and the local flux is adequately high, cake depositions are formed causing a dramatic increase in filtration resistance.

In addition, at relatively high TMP such as above 0.3 bar, as TMP increased, flux dropped, and degassing and gas bubbles was observed in the permeate suction line. This was caused by the

permeate pump head loss and the so-called pump slippage which then caused cavitation problems in the suction line resulting in the flux dropping to 10.8 LMH at the end of operation for the 12 LMH onset flux case.

For the initial flux onset of 24 LMH, TMP increased dramatically and continuously to 0.8 bar in the first 20 minutes of filtration, along with a rapid reduction in produced flux from 24 to 14.9 LMH. After that TMP gradually increased up to approximately 0.84 bar and remained relatively constant at this value until the end of 120 minutes filtration, while produced flux continually decreased to 9.7 LMH in the same period. In order to prevent an excessive fouling build up within membrane, this experimental run was terminated at 120 minutes of filtration. The rapid fouling seen in this case could imply that the high onset flux of 24 LMH (also 12 LMH) is far higher than the critical flux. Above the so-called critical flux, foulants were conducted to the membrane surface more rapidly than they could be removed by hydraulic shear stress, liquid crossflow or turbulent diffusion. The sharply increased TMP profile likely corresponded to the onset of cake formation (Ho and Zydney, 2002). Accompanied by the low produced flux under high TMP condition as well as cavitation, these factors result in a steep increase in the resistance to permeate transport through the membrane (Ognier, Wisniewski and Grasmick, 2004).

Considering the cases of 6 and 12 LMH initial fluxes, these exhibited lower rates of TMP rise and of produced fluxes decrease, which could be attributed to lower filtration resistances when compared with the onset flux of 24 LMH. As a result, it could be predicted that the so-called critical flux according to the weak form, in which little fouling occurring at sub-critical flux operation is acceptable, might exist in the range of 6 - 12 LMH under the conditions set up in these experiments.

5.2.2 Critical flux determination

As demonstrated in the previous section, the so-called critical flux was predicted to be in the range of 6 - 12 LMH. In this experiment, the critical flux (in its weak form) was evaluated according to the flux-step method proposed by Le Clech *et al.* (2003), in which the critical flux value was determined by the criteria of fouling rate (dTMP/dt), considering the maximum operational flux with dTMP/dt < 0.1 mbar min^{-1} (see literature review section 2.2.5). The obtained result is expected to be a guideline for two-phase gas sparged AnMBR design and control parameters.

The MBR was set up with a 7 L liquid working volume with the same tank geometry as described in section 5.2.1 (68 cm liquid depth, A_d/A_r 2.21, and A_b/A_d 0.78). The experiment was performed under 2.5 L min^{-1} sparging rate supplied by ∅ 1.5 and ∅ 3 mm nozzles. The initial MLSS concentration was 7,500 g L^{-1}. Permeate effluent was recirculated back into the reactor to maintain

more or less constant MLSS and liquid level inside the reactor. The variations of produced flux and TMP (observed via suction pressure) with permeate flux step changes controlled by peristaltic pump speed adjustment were recorded, starting with pump speed 2 rpm for 25 minutes which was equivalent to a permeate flux of 2.3 - 2.5 LMH (where operationally possible). The flux was then increased in step of 2 rpm pump speed every 15 minutes continuously until a flux at pump speed of 16 rpm was reached. Thereafter, flux was then decreased in the same fashion until the pump speed was adjusted back to 2 rpm for 25 minutes in the last step of the operational period.

The relationship between produced flux and TMP for the flux-stepping filtration experiment with step height of 2.3 - 2.5 LMH and step duration of 15 minutes without intermittent relaxation is presented in Figure 5-6, and more detail of ascending filtration period shown in Figure 5-7, respectively.

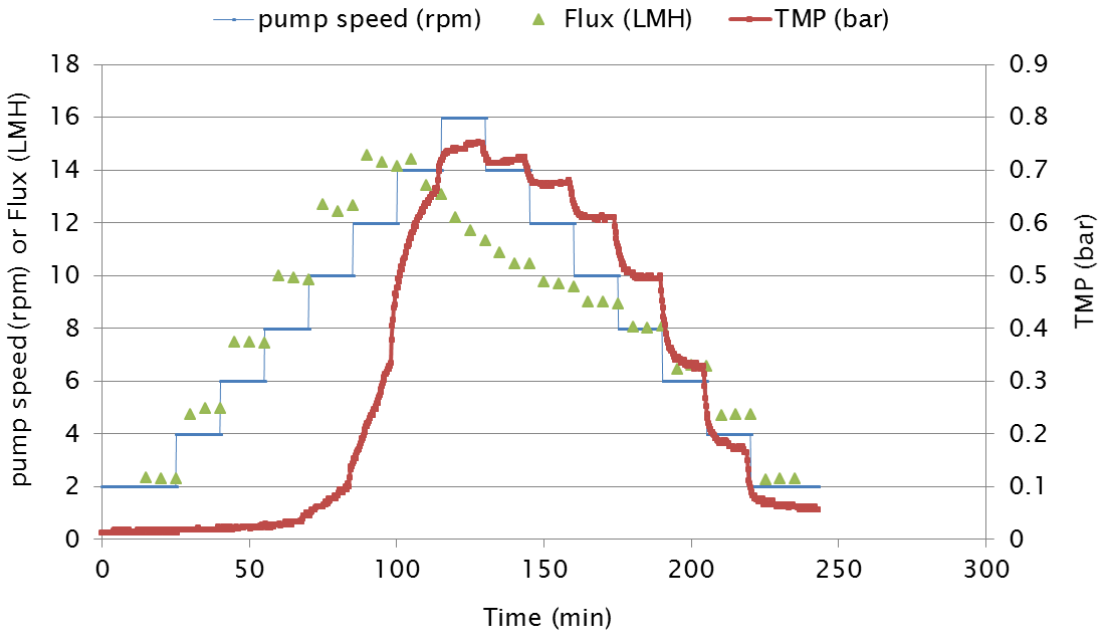

Figure 5-6 Relationship between produced fluxes and TMP during flux-stepping filtration

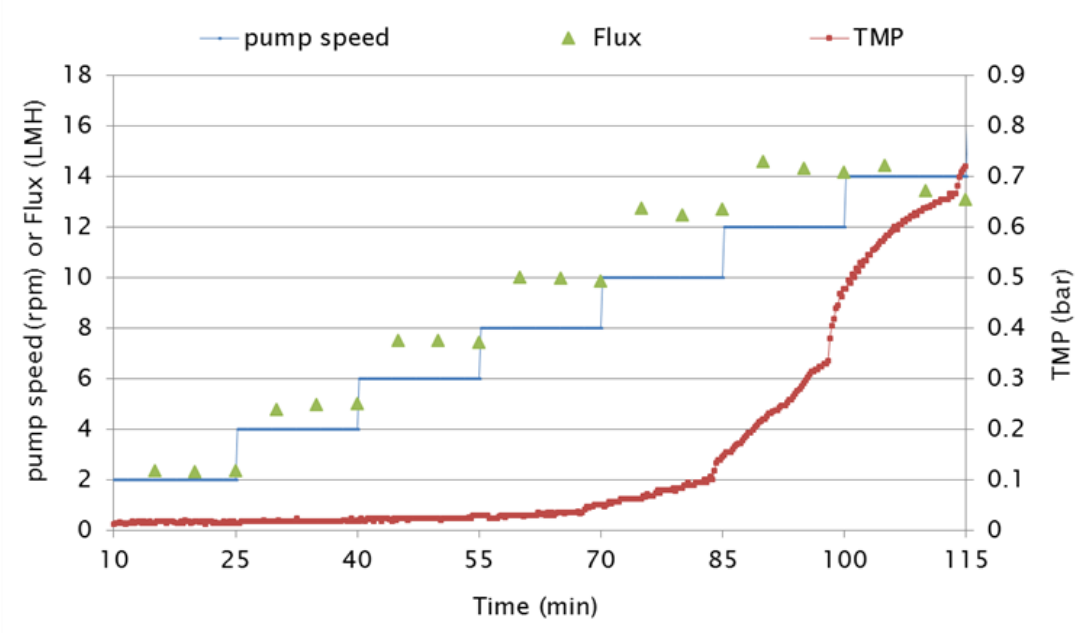

Figure 5-7 Details of produced fluxes and TMP changes for the ascending period in flux-stepping experiment

From Figure 5-6, it can be seen that there is no visible increase in TMP below pump speeds of 2 - 4 rpm which are equivalent to produced fluxes of 2.3 - 5.0 LMH. This indicates that there was little or marginal fouling occurring on the membrane surface during these filtration periods. Although it seems that fouling rates at these produced fluxes appear stable, due to certain experimental errors such as the accuracy of flux measurement method and the sensitivity of pressure transducer for low flux operations, dTMP/dt is not exactly constant and non-zero. Detailed observation of ascending filtration in Figure 5-7 shows that at initial flux-steps of 2.3 and 5.0 LMH, TMPs increase from 12.6 to 13.1 mbar and 17.7 to 18.1 mbar, respectively, over the 15-minute flux-step period. When pump speed was changed from 4 to 6 rpm resulting in an increase in produced flux from 5.0 to 7.5 LMH, a gradual increase in TMP from 18.1 to 23.2 mbar was observed. Similar behaviour of a TMP increase from 23.2 to 34.1 mbar was seen when the pump was adjusted from 6 to 8 rpm (from flux of 7.5 to 9.9 LMH) and this is indicative of gradually incipient fouling build-up.

With an increment in produced flux from 9.9 up to 12.5 LMH, a rapid rise in TMP from 39.6 to 100.3 mbar is noticed, demonstrating that rapid fouling and foulant layer formation were taking place at this point. Thereafter, when expected fluxes were further stepwise increased to 15 and 17.5 LMH, sharp rises in TMP to 334.7 and 665.1 mbar were seen, while the actual produced flux achieved was only 14.3 and 13.4 LMH, respectively, at these TMP values. This is in agreement with the results demonstrated in section 5.2.1, that once the TMP has passed certain values in range about 0.3 - 0.4 bar, the flux could no longer remain constant and the relationship between

pump speed to flux stepping up is straightforward. This is mainly due to the problems of degassing and cavitation occurring in the permeate suction line. A similar phenomenon in which the step flux variation at high TMP was caused by stress on permeate drawn by the peristatic pump was also reported by Hu and Stuckey (2006). The so-called pump slippage effect occurred when peristatic pump was operated beyond its suction capacity, and the required constant flux step increment could not be maintained.

It is also noticeable from Figure 5-6 that reduction of the permeate pump speed did not restore the TMP to its original value. TMP values obtained during the descending stage are higher than the corresponding values during the ascending period. For example, at the incipient flux-step of 2.3 LMH, average TMP is 12.6 and 67.3 mbar for the ascending and descending stages, respectively. This effect agrees with many other research results (Chen *et al.*, 1997; Le Clech *et al.*, 2003; Hu and Stuckey, 2006). This observation indicates that there was formation of an irreversible fouling layer on the membrane surface during the operational period, that cannot be removed by gas-liquid two-phase flow under this sparging intensity or hydrodynamic conditions set up in this experiment.

Results for fouling rate (dTMP/dt) as a function of produced flux from Figure 5-7, for the ascending stage only where produced flux was maintained relatively constant for each flux-step, are plotted in Figure 5-8.

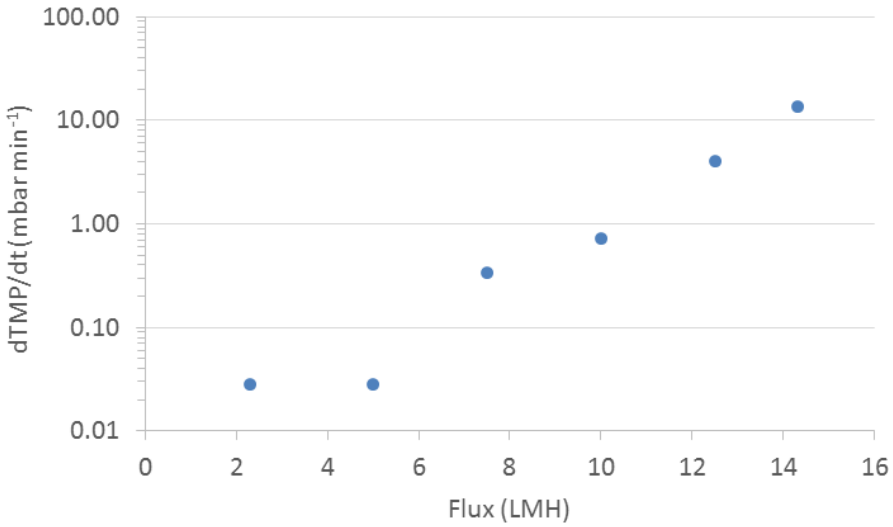

Figure 5-8 Fouling rate as a function of produced flux

As mentioned above, the stepwise flux increase from 2.3 to 7.5 LMH gave only a marginal rise in TMP rise when observed from Figure 5-7. However, considering the fouling rates in Figure 5-8, dTMP/dt actually rose rapidly from 0.028 to 0.337 mbar min^{-1} when the flux was stepped from 5.0 up to 7.5 LMH, and then further increases to 13.43 mbar min^{-1} corresponding to the

stepwise flux increase to 14.3 LMH, respectively. Therefore, regarding dTMP/dt < 0.1 mbar min^{-1} as an indicator of critical fouling rate, the critical flux in its weak form under the conditions of this experiment was determined as 5.0 LMH.

5.3 Effects of particle addition on critical flux and fouling tendency under different reactor configurations

As mentioned earlier, the definition of critical flux is still controversial and there is no standard method for this parameter determination while the absolute measured fouling rates from short-term fouling experiments (step-flux) do not appear to be applicable for real long-term operation (Pollice *et al.*, 2005). However, critical flux is often applied as a useful practical guideline for MBR systems design and operation (Guglielmi *et al.*, 2007). Additionally, a short-term experiment such as the flux-stepping method remains an effective approach to assess the fouling propensity of a given filtration system and to compare different operating conditions (Le-Clech, Chen and Fane, 2006).

Therefore, the experiments in this section were proposed to evaluate the effects of adding particles at varied filling ratios in conventional gas-sparged two-phase MBR on filtration efficiency and fouling tendency via achievable critical fluxes. The experiments were also conducted to assess filtration performance under different tank geometries, mainly in comparisons between the gaslift-loop configuration and a gas-mixed reactor without annular loop for both two- and three-phase flow applications.

The critical flux determination method in this section was still defined according to the criteria of dTMP/dt < 0.1 mbar min^{-1} from flux-stepping experiment. In order to obtain a more accurate critical flux determination and to shorten the duration of experiment, however, the small flux-step height of 1.5 LMH was only used for the flux ascending stage. In an attempt to obtain filtration characteristics closer to real MBR operation, permeate suction relaxation breaks with continuous gas sparging were also applied in the flux-stepping experiments.

In this section, flux-stepping filtration started with a flux-step height of 1.5 LMH and step duration of 15 minutes followed by 5 minutes of permeate suction pause under continuously gas sparging (i.e. membrane relaxation or intermittent suction mode). Thereafter, the flux was stepwise increased with this pattern of step height, step length and pausing period until the flux reached 12 LMH. Subsequently, for the two final flux-steps, flux was further increased to 14 LMH with 5 minutes pausing and then immediately stepped to expected flux of 20 LMH for the last flux-step (2 and 6 LMH flux height for last two flux-steps). Achievable fluxes and TMPs were recorded.

The trials in every experimental run were performed under 2.5 L min^{-1} sparging rates by ∅ 1.5 and 3 mm nozzles from two spargers (corresponding to a specific gas demand per unit membrane area (SGD_m) of 1.5 m^3 m^{-2} $hour^{-1}$) located 30 cm beneath the membrane panel's bottom edge under a liquid depth of 68 cm.

The model mixed suspension was set to be approximately 10,000 mg L^{-1} MLSS (7,500 mg L^{-1} of sieved anaerobic sludge + 2,500 mg L^{-1} whole milk powder made up to the required volume by tap water). Permeate effluent was recirculated back into the reactor in attempt to maintain more or less constant MLSS concentration and liquid depth inside the reactor for every trial conditions.

5.3.1 Effect of carrier addition on critical fluxes in a gaslift-loop reactor

In this section the MBR was operated as a 7 L liquid working volume configured as split type gaslift-loop reactor with 68 cm liquid depth, 7 mm membrane clearance, A_d/A_r 2.21 and A_d/A_b 0.78. LDPE granules (carriers) at filling ratios of 0, 10 and 20 % by weight fraction (corresponding to 0, 11.1 and 22.2 %, v/v) were introduced into the reactor which performed as a moving bed internal annular flow.

Achievable fluxes and TMP increasing characteristics during flux-stepping experiments and fouling rates of each flux- step for gaslift-loop flow pattern are presented in Figure 5-9 and Figure 5-10, respectively.

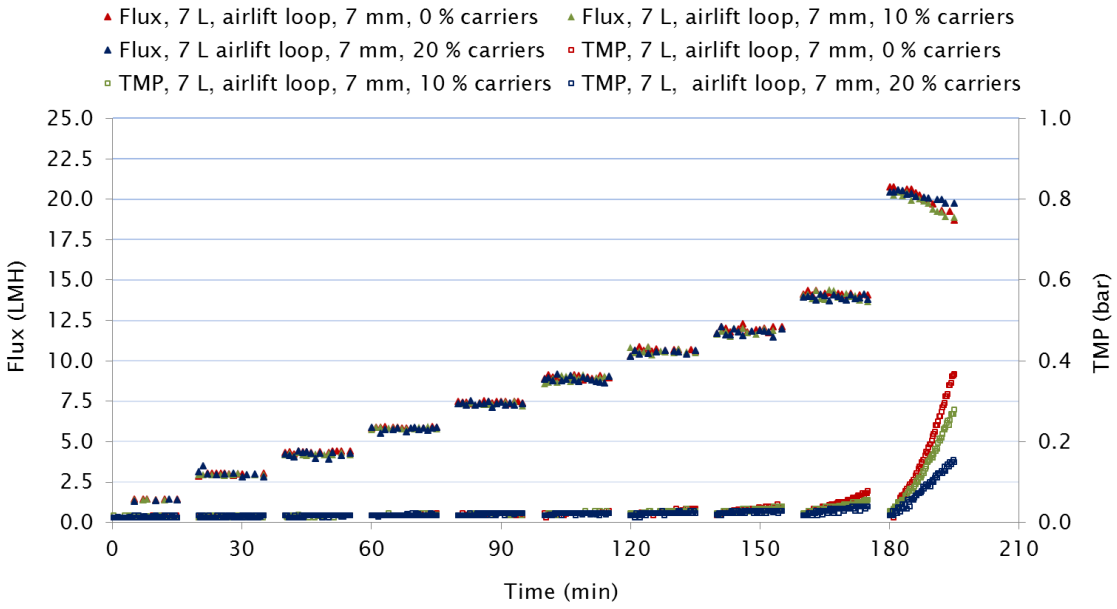

Figure 5-9 Effect of carrier addition on achieved flux and TMP during flux-stepping experiment in an gaslift-loop reactor

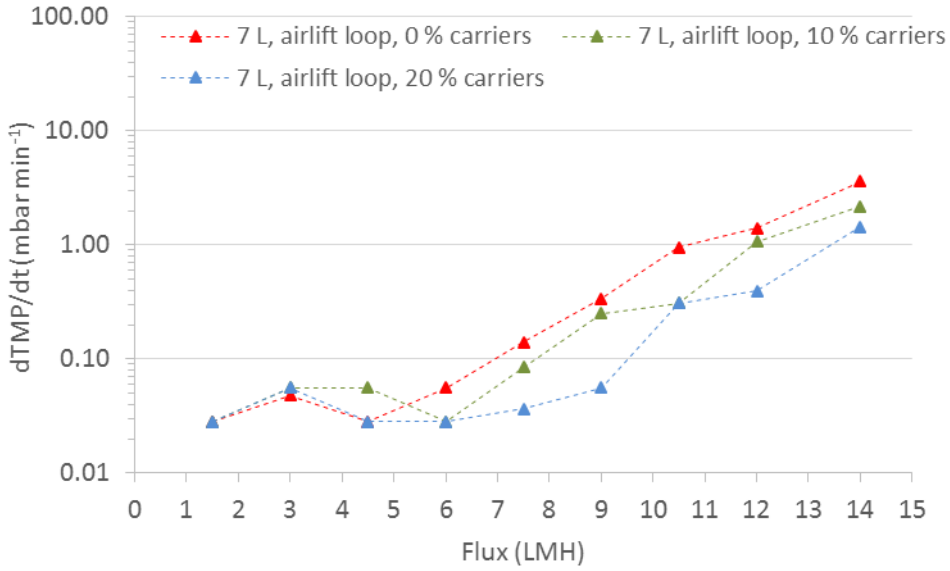

Figure 5-10 Effect of carrier addition on fouling rates during flux-stepping experiments in an gaslift-loop reactor

In Figure 5-9, although there are no clear differences in fouling tendencies for each condition at flux-step of 1.5 to 12 LMH, at higher fluxes of 14 and 20 LMH, the rate of TMP increase is lower at the higher carrier filling ratios of 10 and 20 % by weight fraction, respectively. This trend is more clearly seen for fouling rates plotted with produced fluxes as shown in Figure 5-10. Considering the criteria of dTMP/dt < 0.1 mbar min^{-1}, from Figure 5-10 it can be determined that the critical fluxes for 0, 10 and 20 % carrier addition are 6, 7.5 and 9 LMH, respectively. The main reason for the improvement in critical flux at higher carrier packing ratios is believed to be that external reversible fouling is diminished due to the mechanical cleaning process.

Since the LDPE particles using in this chapter have apparent sizes smaller than 7 mm membrane gap (lenticular shape with ∅ 3 - 4 and 1 - 2 mm thickness), therefore an increment in particle filling ratio from 10 to 20 % results in a higher probability for scouring media to hit each other and the membrane surface. Consequently, effective particle-membrane collision frequency increases as particle dosages increase. This is in agreement with the results of Lee, Kang and Lee (2006) who operated a hollow fibre membrane coupled with coated activated carbon polyurethane cubes as a moving bed AeMBR with packing ratios of 5, 10 and 20 % by volume fraction under aeration rates of 5, 7 and 9 L min^{-1}. According to their findings, increasing the amount of scouring particles and aeration intensity lowered the fouling rate in the filtration system. The results also demonstrated that not only does the particle density result in filtration efficiency improvements but kinetic energy for moving media which depends on mass, moving velocity, number and collision frequency of the moving bed also significantly affects the fouling reduction propensity.

Similar results showing that larger amounts of scouring media gave better fouling mitigation have been demonstrated in several studies (Lee, Kang and Lee, 2006; Kim *et al.*, 2010; Yang *et al.*, 2012; Gao *et al.*, 2014; Chen, Bi and Ng, 2016). However, further increasing the scouring media dosage beyond a certain value does not offer significant improvement in fouling mitigation. Aslam *et al.* (2014) reported that increasing GAC dosage up to 50 % by volume fraction in fluidised AnMBR allowed better fouling mitigation, whist increasing GAC amount to 70 % (v/v) did not provide further beneficial effects on fouling reduction. Similar results were also observed with other scouring agents. Charfi, Aslam and Kim (2018) reported that when increasing the dosages of 3 mm polyethylene terephthalate (PET) beads and 1.5 mm silica particles from 0 to 50 % (v/v) in a fluidised AnMBR with a model mixed suspension, TMP gradually decreased with time. However, when the amounts of both particles were increased to 70 % v/v, TMP was observed to increase again. The results illustrated that above the optimal particle filling ratio, the higher amount of media would lead to friction between media particles which hinders their movement, resulting reduced in scouring and cleaning efficiency (Charfi, Aslam and Kim, 2018).

In real aerobic activated sludge, particle packing amounts also influence mixed suspension rheology. Hu *et al.* (2012) operated AeMBR with hollow cylindrical shape carriers made of polyethylene with an apparent size of ∅ 10 mm and 10 mm length under packing ratios of 10, 20, 30 and 40 % by volume fraction. They concluded that the biochemical effects of carriers on sludge suspension significantly affected membrane fouling where the protein in bounds EPS is the major fouling contributor, and the optimum media volume fraction dosage was recommended at 30 %.

Apart from particle packing density aspect, there are various factors affecting membrane cleaning processes due to the variety of operational conditions setting up in several studies. As a result, it is difficult to compare and determine the optimum scouring agent filling density. Nonetheless, the results in this section showed that with LDPE particles at a packing amount of 10 and 20 % (w/w), critical flux can be enhanced by 25 and 50 % when compared to conventional two-phase flow airlift-loop MBR under the same sparging intensity.

5.3.2 The effect of carrier addition on critical flux in a gas-mixed reactor without annular-loop

One observed drawback of using LDPE granules as scouring agents in this chapter is that their SG of 0.86 - 0.96 is lower than SG of water which made the particles float in the model mixed suspension. Although this can prevent particles sinking into the bottom zone of the reactor, buoyant particles could retard continuous annular flow inside reactor and a higher liquid downward flow velocity in downcomer section may be required for the gaslift-loop configuration.

Hence, the effect of LDPE carrier additions on critical flux in a gas-mixed configuration without annular loop flow was evaluated in this section.

Flux stepping experiments were still performed with the model mixed suspension at initial MLSS concentration of 10,000 mg L^{-1} under 2.5 L min^{-1} sparging intensity supplied by ∅1.5 and 3 mm nozzles from two spargers (corresponding to SGD_m of 1.5 m^3 m^{-2} $hour^{-1}$) located 30 cm beneath the membrane panel's bottom edge under liquid depth of 68 cm.

In order to obtain the gas-mixed without annular loop flow pattern, the internal geometry of the reactor was modified. Details of four different gas-mixed flow reactors without annular loop flow applied in this section are described below:

Case I: 7 L (2 chambers), 7 mm gap, 0 % (w/w) granules

The reactor with a total 7 L liquid working volume was set up with similar internal geometry to the gaslift- loop configuration used in section 5.3.1. However, some minor adaptations were applied. The height of the separation baffle between the former riser and downcomer zones was adjusted to be 15 cm above liquid level, while stainless steel mesh with pore size 2 mm x 2 mm was installed at the bottom of the baffle in the former transversal flow area (A_b) between riser and downcomer. By this adjustment, the reactor was divided into 2 compartments as sparged zone (former riser) with 2.5 L liquid working volume (minus membrane panel volume) and unsparged zone (former downcomer) with liquid working volume 4.5, respectively. Annular liquid flow between two chambers was cut off due to the height the separation baffle above the liquid level. Membrane clearance between front tank wall and baffle was 7 mm and no particles were added to the reactor.

Case II: 7 L (2 chambers), 7 mm gap, 28 % (w/w) granules

The reactor was set up in the same configuration as applied for the 7 L (2 chambers), 7 mm gap, 0 % (w/w) granules case. 700 g of LDPE granules, corresponding to 10 % by weight fraction (11.1 % by volume fraction) of the total liquid working volume inside the reactor, were added to the sparged zone. By the adjustment of baffle height to above the liquid level and installation of the stainless steel mesh at the bottom of the baffle, 700 g of granules were retained in the sparged zone. This made the weight ratio of granules in the sparged zone 28 % (31.1 % by volume fraction).

Case III: 5 L (1 chamber), 16 mm gap, 0 % (w/w) granules

The reactor was set up as one compartment with 5L liquid working volume in rectangular tank dimension of 3.8 cm width x 21.5 cm length x 68 cm liquid depth. A4 membrane panel was

installed in the middle of the tank width 30 cm above reactor bottom, making the gaps between membrane surface and tank walls equivalent to 16 mm and no particles were added to the reactor.

Case IV: 2.5 L (1 chamber), 7 mm gap, 10 % (w/w) granules

The reactor was set up as one compartment with 2.5 L liquid working volume in rectangular tank dimension of 2.0 cm width x 21.5 cm length x 68 cm liquid depth. An A4 membrane panel was installed in the middle of the tank width 30 cm above the reactor bottom, making the gaps between membrane surface and tank walls equal to 7 mm. 250 g of LDPE granules was added to the reactor corresponding to 10% addition by weight fraction (11.1 % by volume fraction).

Achievable fluxes and TMP characteristics during flux-stepping experiments and fouling rates of each flux- step for the gas-mixed without annular loop flow pattern are presented in Figure 5-11 and Figure 5-12, respectively. Achieved critical fluxes for both gaslift-loop and gas-mixed without annular loop flow patterns are also illustrated in Table 5-1.

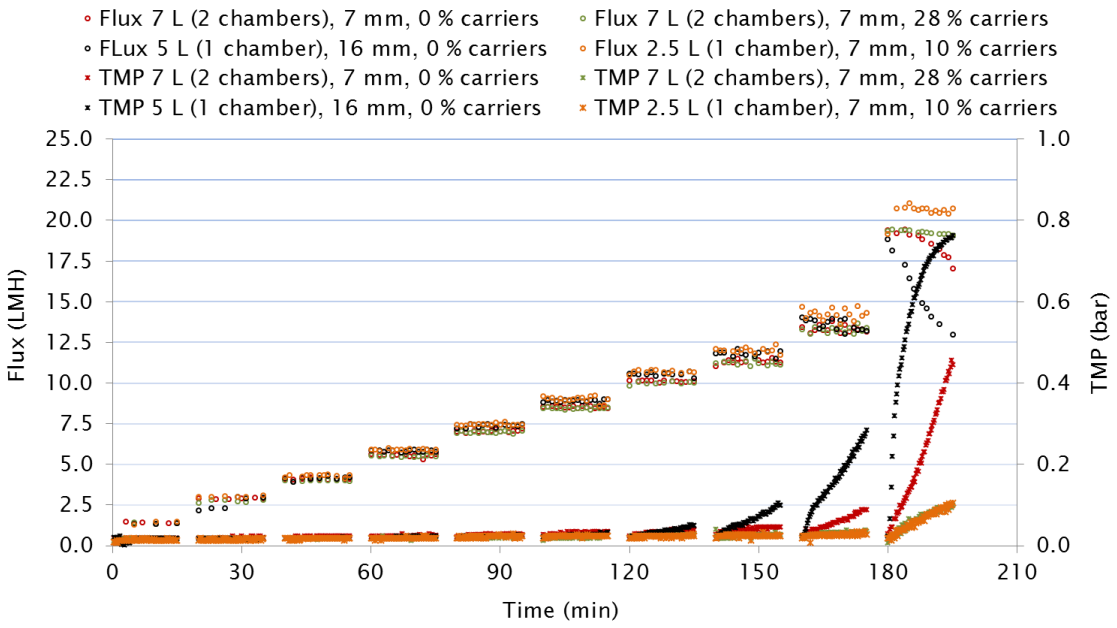

Figure 5-11 Effect of carrier addition on achieved flux and TMP during flux-stepping experiments in a gas-mixed reactor without annular loop

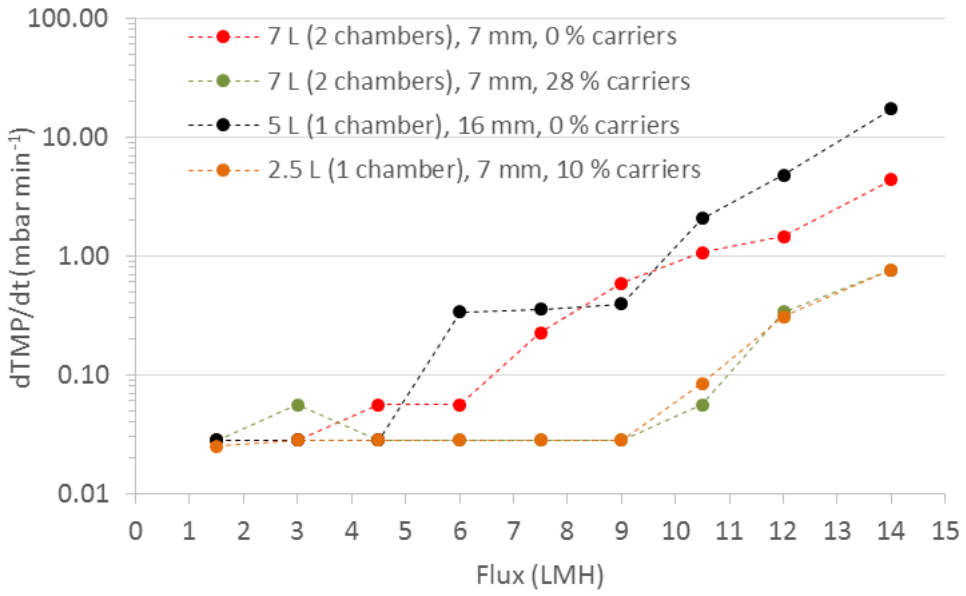

Figure 5-12 Effect of carrier addition on fouling rates during flux-stepping experiment in a gas-mixed reactor without annular loop

Table 5-1 Critical flux for each operational condition in gaslift-loop and gas-mixed without annular loop flow configurations

Reactor	Operational condition	Critical flux
Gaslift-loop flow	7 L (loop flow), 7 mm gap, 0 % (w/w) granules	6.0
	7 L (loop flow), 7 mm gap, 10 % (w/w) granules	7.5
	7 L (loop flow), 7 mm gap, 20 % (w/w) granules	9.0
Gas-mixed without annular loop flow	7 L (2 chambers), 7 mm gap, 0 % (w/w) granules	6.0
	7 L (2 chambers), 7 mm gap, 28% (w/w) granules	10.5
	5 L (1 chamber), 16 mm gap, 0 % (w/w) granules	4.5
	2.5 L (1 chamber), 7 mm gap, 10 % (w/w) granules	10.5

From Figure 5-12 and Table 5-1, for the case I of 7 L (2 chambers), 7 mm gap, 0 % granules, critical flux was determined as 6.0 LMH. When 28 % granules by weight fraction (31.1 %, v/v) were introduced into the reactor for case II, with the same reactor geometry arrangement of 7 L model mixed suspension volume, 7 mm membrane gap and 2.5 L min^{-1} sparging rate, critical flux was increased to 10.5 LMH corresponding to a 75 % improvement. The highest critical flux obtained in this case (Table 5-1) might be due to the relatively high particle filling ratio (28 % w/w in gas sparged component) compared to the other cases. Additionally, the membrane panel that was installed 30 cm above the bottom of the reactor was observed to be scoured vigorously by buoyant particles in the gas sparged chamber for the gas-mixed without annular loop flow configuration. As a result, externally reversible foulants such as gel/cake layer are scrubbed and

removed from the membrane surface, causing lower fouling rates (Figure 5-10 and Figure 5-11) even at supra-critical flux filtration of 14 and 20 LMH during the short-term flux-stepping experiment.

For long-term operation, however, excessive particle scrubbing as applied in this case may possibly result in breaking of microbial flocs in a real MBR system. Microbial floc disintegration could increase the amount of fine colloidal substances released, such as SMP and EPS, resulting in poor mixed suspension filterability and fouling acceleration, including intensive internal membrane pore blockage although reversible fouling is effectively alleviated (Huang, Wei and Yu, 2008; Yang *et al.*, 2009; Jin, Ong and Ng, 2013; Luna *et al.*, 2014).

In addition, another potential problem that could occur in the gas-mixed without loop flow configuration is an uneven mixing condition inside the entire reactor. The reactor geometry for case I and case II in this section was set as 7 L liquid volume, 7 mm membrane gap and 2.5 min^{-1} sparging rate similar to that applied for gaslift-loop conditions in section 5.3.1. Hence, in an attempt to gain a gas-mixed without loop flow regime, the total reactor volume was divided into two components as described above, i.e. by increasing the height of the separation baffle above the liquid level, while a 2 mm x 2 mm mesh was installed in the bottom to retain particles in the filtration zone only. Gas sparging was applied in the filtration zone only where the membrane panel is located. By this design, the continually recirculating annular flow between the two chambers was eliminated. Although the membrane was observed to be scoured vigorously by bubbles (case I) and buoyant particles (case II) in the gased compartment, insufficient mixing conditions and dead zones can potentially be formed in the ungased chamber.

In case III, the reactor was set up with one chamber without a separation baffle. The reactor width was reduced to 3.8 cm which made the total liquid volume 5 L. The membrane panel was installed at the middle of tank width, which made the gap between the tank wall and the membrane 16 mm on each side. A total sparging rate of 2.5 L min^{-1} was applied for fouling mitigation and bulk liquid mixing purposes. From Figure 5-12 and Table 5-1, it can be seen that the achieved critical flux for this case was the lowest at 4.5 LMH in comparison with other conditions. A rapid increase in fouling rate can be clearly observed when step-flux was increased from 10.5 LMH (Figure 5-11). The fast fouling build-up in this case was mainly caused by the lack of particle scouring since there was no particle addition in this trial; the liquid crossflow velocity was also limited as the continuous annular flow was eliminated.

For case IV, the reactor geometry was similar to that in case III. However, in an attempt to obtain a single chamber gas-mixed without loop flow with a 7 mm membrane gap, plastic sheets were inserted into the reactor as tank dividers. As a result of this installation, the total liquid working volume was reduced to 2.5 L. 10 % by weight fraction (11.1 % v/v) of LDPE carriers were added

to the reactor. From Figure 5-12 and Table 5-1, it can be seen that the highest achieved critical flux of 10.5 LMH occurred in this case (2.5 L (1 chamber), 7 mm gap, 10 % (w/w) granules). This critical flux had the same value as that produced from case II (7 L (2 chambers), 7 mm gap, 28 % (w/w) granules) at the same fixed sparging rate and membrane gap but a lower particle filling ratio. The result implied that 10 % by weight fraction of carrier filling can considerably enhance critical flux under a gas-mixed without loop flow configuration. However, the produced critical flux from this case cannot be compared to case II, because the 2.5 L total liquid working volume in this case is lower than the 7 L applied in case II. Since produced permeate was recirculated back into the reactor in order to maintain a more or less constant liquid level and MLSS concentration during the experiments, the total foulant load from 2.5 L mixed suspension in case IV can be considered to be lower than 7 L in case II by 2.8 times. With the same given total membrane filtration area under a relatively low liquid working volume, this design could achieve very high membrane packing density and low hydraulic retention time (HRT). For example, a total 0.1 m^2 of A4 membrane panel installed in 2.5 L liquid working volume results in a membrane area packing density of 40 m^2 m^{-3}. If the system is operated at flux of 10 LMH (lower than the critical flux of 10.5 LMH in this case) without permeate recirculation back to the reactor, this operational condition will result in a liquid flowrate of 1 L $hour^{-1}$ and an HRT of 2.5 h. In a single-stage AnMBR treating low to medium strength wastewater which mainly consists of particulate organic matter, such as dairy production effluent, a HRT of 2.5 hours is considered to be very low and it would be difficult to achieve a useful treatment efficiency in practical operation.

In this section, the effects of addition of buoyant LDPE particles on the critical flux in each run cannot be directly compared because of the different experimental conditions and set-up. However, most of the results demonstrated that, by the assistance of LDPE granules scouring under the same given sparging intensity in the gas-mixed without annular loop flow configuration, fouling rates could be alleviated due to vigorous particle scrubbing on the surface of the membrane installed in the upper part of the reactor.

5.3.3 Comparing fouling tendencies during flux-stepping experiments for gas-sparged two-phase flow

The results of gas-sparged two-phase flow from section 5.3.1 and 5.3.2 during flux-stepping experiments are plotted in Figure 5-13 and Figure 5-14. These experiments were performed with the objective of evaluating and comparing the effect of reactor configuration (gaslift-loop and gas-mixed without annular loop flow patterns) on fouling mitigation for the two-phase gas-liquid regime.

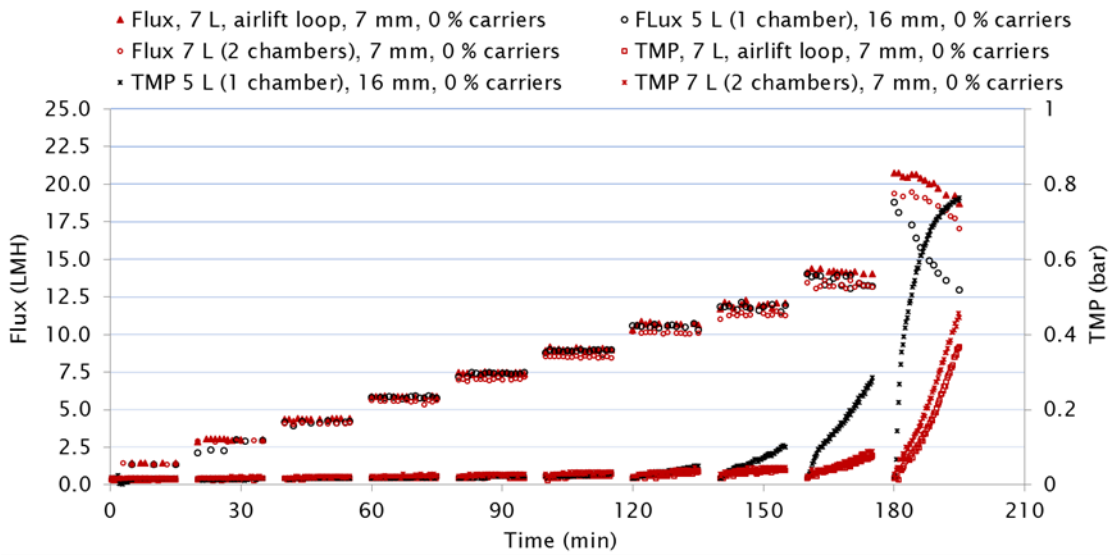

Figure 5-13 Trends in TMP rising during flux-stepping experiments for gas-sparged two-phase flow

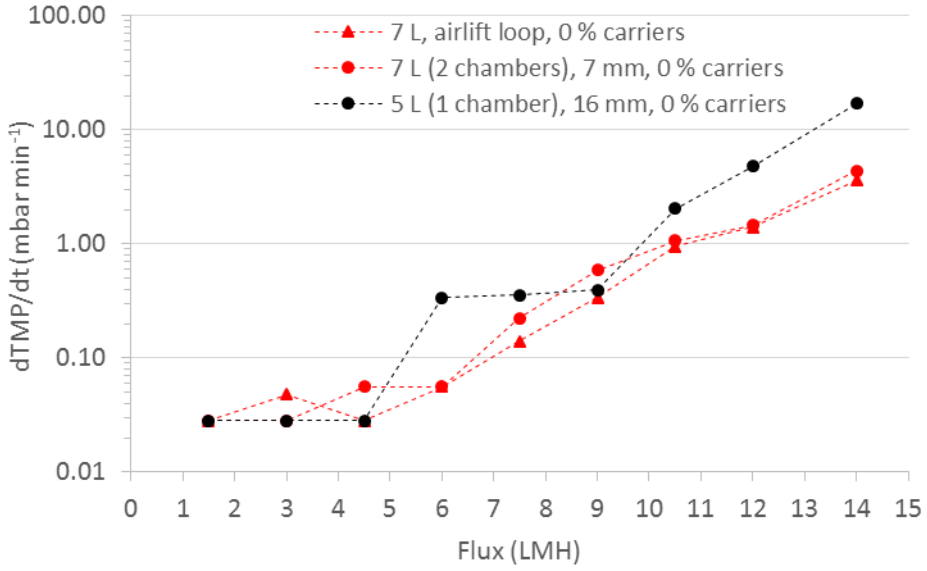

Figure 5-14 Trends in fouling rate during flux-stepping experiments for gas-sparged two-phase flow

Since every experimental case was operated with the same sparging rate of 2.5 L min^{-1} under fixed total filtration area of 0.1 m^2 (single A4 membrane panel), the SGD_m is equal to 1.5 m^3 m^{-2} $hour^{-1}$ for every run.

From Figure 5-13 and Figure 5-14, however, it can be seen that rapid fouling and the lowest achieved critical flux of 4.5 LMH is observed in the case of 5 L (1 chamber), 16 mm membrane gap, 0 % carriers with gas-mixed without loop flow configuration. The poor fouling mitigation in this case is believed potentially to be due to the following reasons. First, since the membrane gaps

of 16 mm in this case are larger than the 7 mm applied in the other cases, with the same fixed sparger nozzle sizes and sparging intensity, achieved bubble sizes tended to be smaller than the membrane channel. Consequently, bubble-membrane contact area ratio and strong liquid turbulent wakes induced by pseudo-2D confined large cap bubble flow regime are diminished, limiting the contributed shear stress in the membrane vicinity. Secondly, under the same given SGD_m, expansion of the membrane gap from 7 to 16 mm results in a reduction of U_g from 0.014 to 0.006 m s^{-1} which reduces gas-liquid two-phase and backtransport flow in the channel. Finally, because this experimental configuration was not designed to promote annular recirculating flow, liquid upward crossflow enhancement due to continuity occurred within the membrane clearance, whereby the overall flow was slowed down. Furthermore, with this design, lateral motion of the bubble swarm and liquid phase circulating loop in flow channel were observed during the experiments. Consequently, with this flow characteristic, liquid flow recirculation and flow stagnant zones inevitably occurred which then caused intensive foulant deposition in this stationary flow region. A similar problem has also been reported by Ndinisa *et al.* (2006), Ndinisa *et al.* (2006) and Nguyen Cong Duc *et al.* (2008).

From Figure 5-14 and Table 5-1 it can be seen that in similar conditions of 7 L model mixed suspension volume, 7 mm membrane gap and 2.5 L min^{-1} sparging rate, the two cases with and without annular loop flow regime showed the same achieved critical flux of 6.0 LMH. However, when considering the trends in fouling build-up in Figure 5-13, it was found that the TMP rising profile in the case of gas-mixed without annular loop flow is slightly higher than that for the gaslift-loop case when both configuration were operated at high supra-critical fluxes of 14 and 20 LMH. This could imply that gaslift-loop flow pattern offers more favourable hydrodynamic condition to enhance backtransport flow velocity and shear stress. The results are in agreement with Prieske *et al.* (2010) who reported that shear stress could be promoted significantly when continuous upward crossflow is exerted in an airlift-loop membrane filtration compared to the shear stress obtained from a single aerated thin bubble column (without annular loop flow). Liu *et al.* (2016) also proposed that an inclusion baffles around membrane modules operated as an airlift-loop reactor could enhance shear stress at the upper part of the flat-sheet membrane module by approximately 30 %.

Besides, since 7 L (2 chambers), 7 mm, gas-mixed without loop flow case was designed as two separate compartments where annular circulation between these two chambers was cut off, it can be predicted that incomplete mixing and formation of dead zones could easily occur in the unsparged chamber. In order to prevent this, good mixing conditions need to be provided in this compartment which means additional energy for mixing purpose must be taken into account in the total energy demand.

Therefore, the results in this section indicated that under the same given energy input for two-phase liquid-gas sparging, the gaslift-loop configuration can offer more effective energy consumption than the gas-mixed without annular loop flow pattern for both fouling mitigation and mixing purposes.

5.3.4 Comparing fouling tendencies during flux stepping experiments for gas-liquid-solid three-phase flow

The results of gas-liquid-solid three-phase flow from section 5.3.1 and 5.3.2 during flux-stepping experiments are plotted in Figure 5-15 and Figure 5-16. These experiments were performed with the aim of evaluating and comparing the effect of reactor configuration (gaslift-loop and gas-mixed without annular loop flow patterns) on fouling mitigation for the three-phase flow regime.

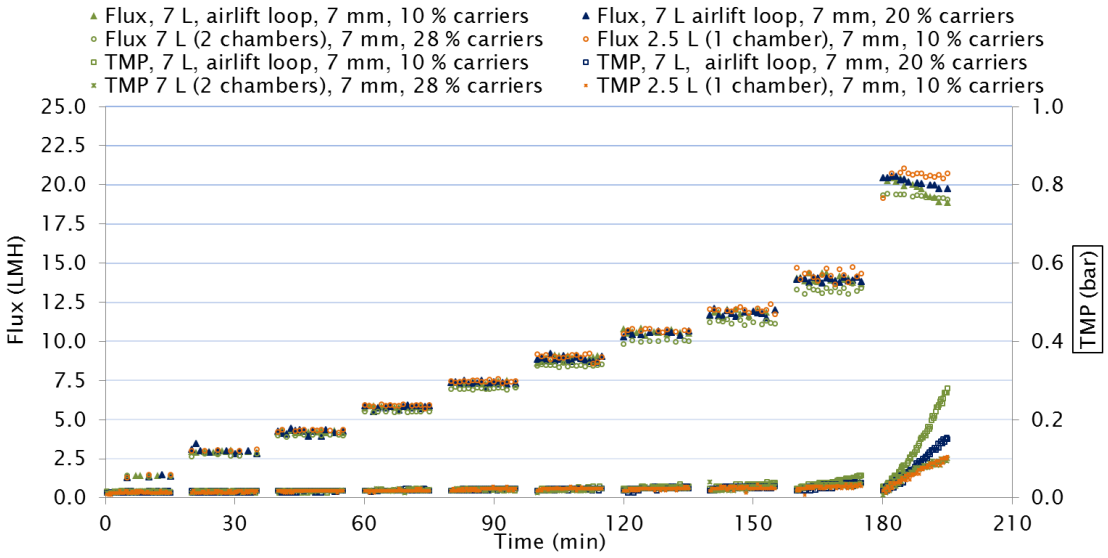

Figure 5-15 Trends in TMP during flux-stepping experiment for three-phase flow

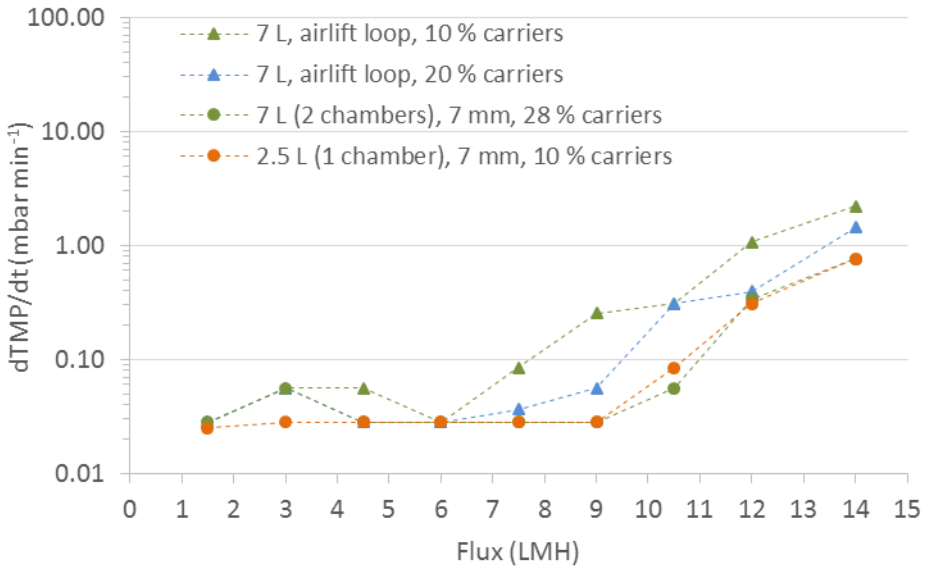

Figure 5-16 Trends in fouling rate during flux-stepping experiment for three-phase flow

From Figure 5-16 and Table 5-1, when comparing the case of the 7 L, gaslift-loop, 7 mm membrane gap, 10 % carriers with the 2.5 (1 chamber), 7 mm, 10 % carriers with gas-mixed without loop flow pattern, it was found that the latter has a higher achievable critical flux of 10.5 LMH. This is equivalent to a 40 % critical flux improvement from 7.5 LMH for the first case. From Figure 5-15 and Figure 5-16, it can also be seen that the fouling rate of the gas-mixed without loop flow case is lower than for the gaslift-loop flow when operated at supra-critical fluxes of 14 and 20 LMH. Although the results from these two cases are not directly comparable due to the different foulant loadings of the 7 L and 2.5 L model mixed suspension, the gas-mixed without annular loop flow pattern tended to give better fouling reduction than the gaslift-loop flow. This might be because, for the flow pattern, all particles are retained in the thin flow channel between the membrane gap and are not recirculated to the compartment where there is no membrane module (e.g. downcomer zone). This means that the probability and frequency particles colliding with the membrane surface is potentially higher than that in the case of gaslift-loop flow under the same fixed sparging rate, membrane gap, U_g and LDPE particle filling ratio of 10 % by weight fraction.

A similar result was found when particle filling densities were increased to 20 - 28 % w/w. With the same foulant amount of 7 L model mixed suspension, when comparing 20 % (w/w) particles with gaslift-loop flow and 28 % (w/w) particles without annular loop flow, the latter case showed a higher critical flux of 10.5 LMH, equal to a 16.7 % improvement in critical flux from 9.0 LMH for the first case. It is notable that, despite the greater increase in carrier filling ratio from 10 to 20 - 28 % (w/w), a smaller critical flux improvement from 40 to 16.7 % was seen. The possible reason for this effect is that, an increment in the amount of particles results in a higher probability

of particles hitting each other and the membrane surface, particularly for the case of gas-mixed without loop flow in which the membrane panel installed in the upper part of reactor was observed to be highly scoured by buoyant LDPE granules.

With the intensive three-phase scrubbing pattern, , another potential problem in addition to microbial floc disintegration is the integrity of membrane material, particularly when rigid materials are applied as scouring agents for long-term operation. For example, Rosenberger, Helmus and Drews (2016) studied the effect of particle filling on flux recovery for fouled membranes in real municipal wastewater treatment plants (flat-sheet AeMBR with 8 mm membrane gap). The compared using TPU beads of 2.5 mm diameter (1.1 SG) and PP beads of 2 mm (1.02 SG) as scouring particles under the same fixed addition of 4 kg m^{-3}. Their results showed that the PP beads gave a better flux recovery than the TPU beads although the loading rate and thus the total momentum was the same. Possible reasons are that: the number of 2 mm PP beads was 2.1-fold higher than the number of 2.5 mm TPU beads; the PP beads have higher shore hardness which results in stronger impact on the fouling layer; and some PP beads had sharp edges which might give a beneficial cutting effect on the fouling layer (Rosenberger, Helmus and Drews, 2016). Nonetheless, Siembida *et al.* (2010) reported that after long-term operation for more than 600 days of flat-sheet AeMBR coupled with PP beads (2.5 mm diameter, 1.05 kg L^{-1} density and 4.0 kg m^{-3}_{tank} filling rate), brush marks were observed on the polyethersulfone polymeric membrane, although the membrane function was not affected. Shin *et al.* (2016) also reported that severe PVDF polymeric membrane damage was detected at the middle and the bottom sections of hollow fibre bundles from an anaerobic fluidised bed membrane bioreactor. The membrane damage was due to intensive abrasion by 0.8 - 4 mm GAC after 765 days of operation.

The results in this section illustrate that increasing the particle packing density resulted in a higher achieved critical flux for both gaslift-loop and gas-mixed without annular loop flow reactors. Results from short-term flux-stepping experiments showed that, under similar conditions, the three-phase flow with gas-mixed without loop flow pattern tended to give better fouling reduction than the gaslift-loop configuration due to the higher probability and frequency of particle-membrane collisions. In this flow driven pattern, a membrane module located in the upper part of the reactor is intensively scrubbed by buoyant LDPE beads (SG < 1). However, certain potential problems such as biological floc crushing and membrane surface damage caused by excessive rigid particle abrasion should be evaluated over long-term operation in further future work.

5.4 Mixed suspension filtration resistance under initial supra-critical flux operation

After short-term flux-stepping experiments from section 5.3 had been carried out and the critical flux of each set of conditions had been determined, it was found that TMP rapidly increased while constant flux could not be maintained and but decreased when fluxes higher than critical value (supra-critical flux) were applied. In this section, therefore, a longer filtration period under initial supra-critical flux was examined. The experiments were performed in an attempt to accelerate fouling formation and to evaluate model mixed suspension filtration resistances during supra-critical flux filtration under varied particle filling densities in comparison between gaslift-loop flow and gas-mixed without annular loop flow configurations.

After about 3 hours of flux-stepping experiments for each condition in section 5.3, the permeate suction pump was stopped but gas sparging continued for one hour at the rate of 2.5 L min^{-1} to reduce fouling. Thereafter, a supra-critical flux constraint of 18 LMH was applied and permeate was continuously drawn with this pump speed for 21 hours. A gas sparging rate of 2.5 L min^{-1} was continuously applied and permeate effluent was recirculated back into the reactor to maintain a more or less constant liquid level and MLSS concentration. Flux declining and TMP decreasing trends were monitored in order to further calculate the model mixed suspension filtration resistance using Equation 5-1.

Equation 5-1

$$R_T = \frac{\Delta P}{\mu J}$$

Where R_T is total filtration resistance (m^{-1}), ΔP is transmembrane pressure (Pa), μ is permeate viscosity taken as being equal to viscosity of water for each operational permeate temperature (Pa.s), and J is permeate flux (m s^{-1}).

5.4.1 Effect of carrier addition on mixed suspension filtration resistance for gaslift - loop configuration

The work in this section used a 7 L liquid working volume MBR configured as split type gaslift-loop reactor with 68 cm liquid depth, 7 mm membrane clearance, A_d/A_r 2.21 and A_d/A_b 0.78, and a model mixed suspension with MLSS concentration of 10,000 mg L^{-1} under a sparging rate of 2.5 mg L^{-1}. LDPE granules (carriers) with filling ratios of 0, 10 and 20 % by weight fraction (corresponding to 0, 11.1 and 22.2 %, v/v) were introduced into the reactor which was operated as a moving bed internal annular flow.

The variations in TMP, produced flux and mixed liquor filtration resistances at different particle filling ratios during initial supra-critical flux constraint are presented in Figure 5-17 and Figure 5-18. Fouled membrane characteristics after 21 hours of experimental period are shown in Figure 5-19.

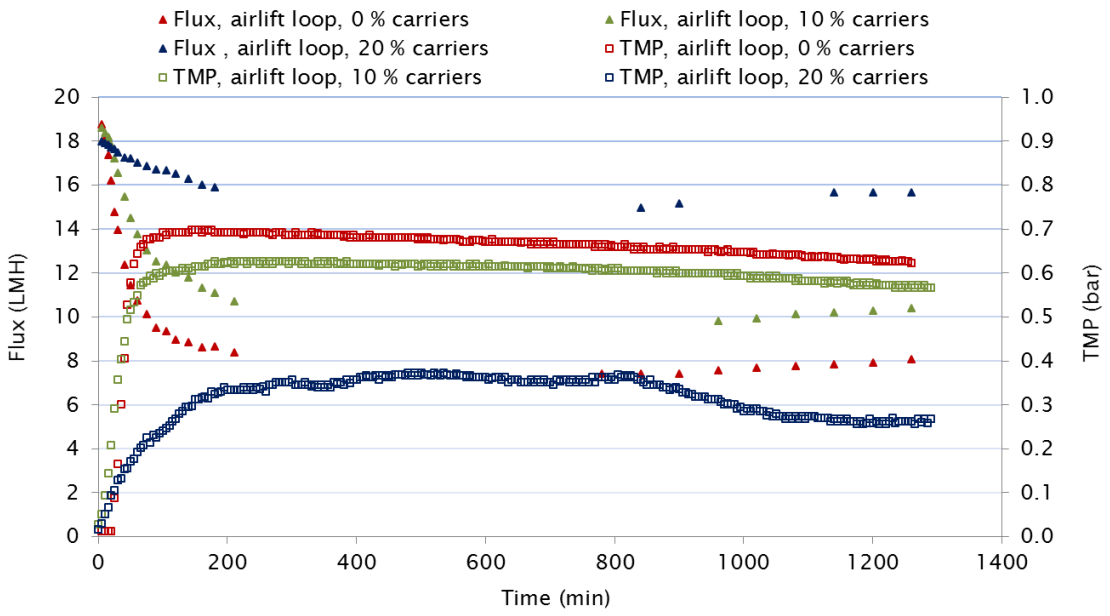

Figure 5-17 Flux and TMP characteristics during supra-critical flux filtration for gaslift-loop configuration

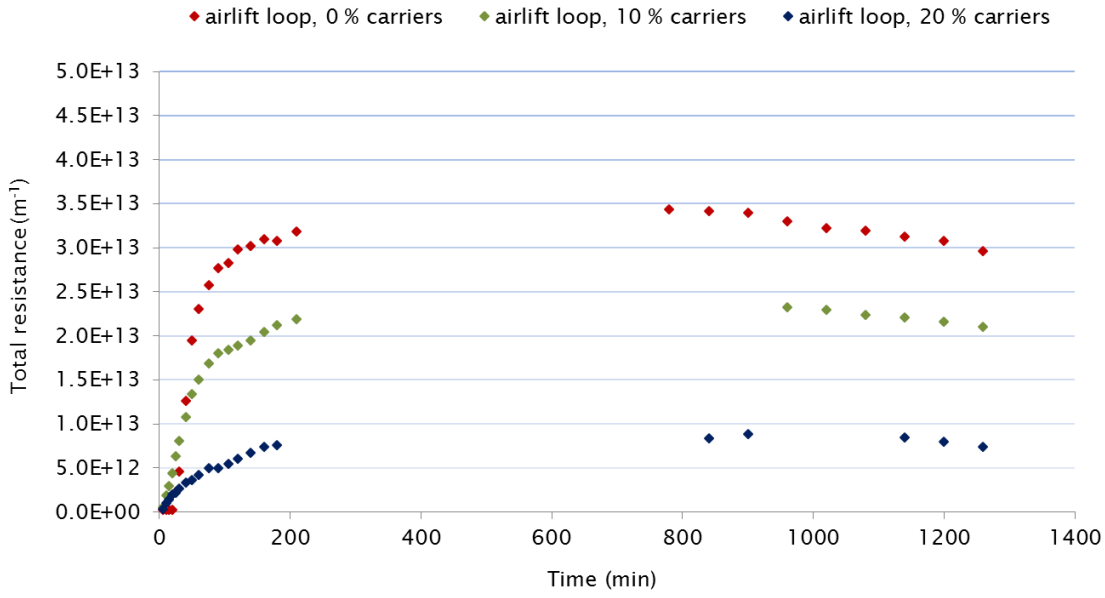

Figure 5-18 Resistance characteristics during supra-critical flux filtration for gaslift-loop configuration

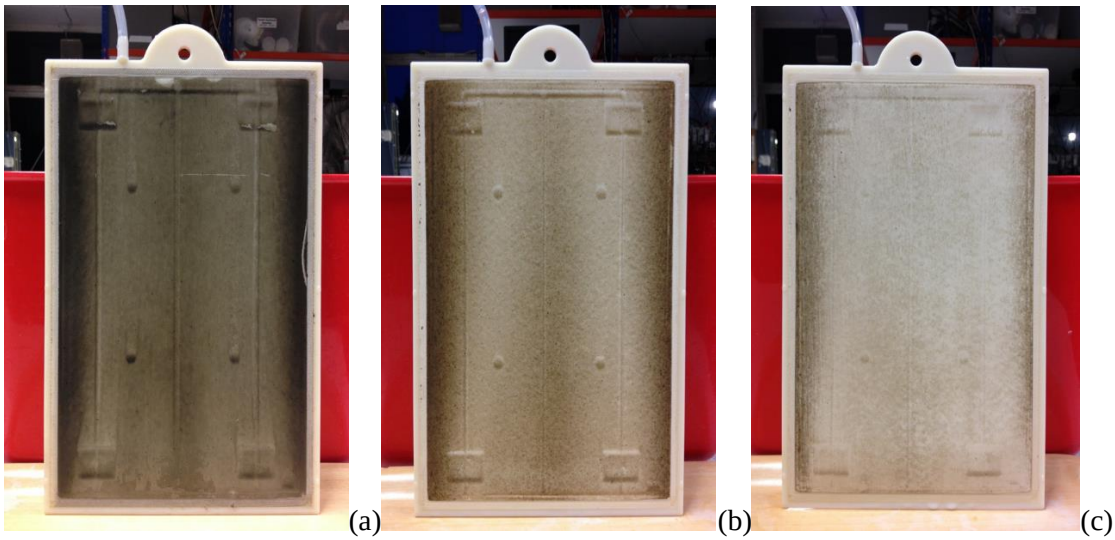

Figure 5-19 Fouled membrane characteristics after 21 hours of supra-critical flux filtration for gaslift-loop configuration: (a) 0 (b) 10 and (c) 20% carriers by weight fraction, respectively.

Since critical fluxes for the cases of 0, 10 and 20 % (w/w) carriers were determined in section 5.3 as 6, 7.5 and 9 LMH, respectively, the initial supra-critical flux setting of 18 LMH caused a rapid TMP increase along with a decline in flux in the first few hours of filtration (Figure 5-17) for every case. Conditions then remained relatively constant until the end of the 21-hour filtration period.

When considering the trend in total filtration resistance (R_T) in Figure 5-18, it can be seen that R_T decreases with increasing particle filling ratios at the same filtration period through the experiments. This is in agreement with the trends in achieved critical flux from the short-term flux-stepping trials. Model mixed suspension filtration resistances at 21 hours of filtration were calculated as 2.97×10^{13}, 2.11×10^{13} and 0.74×10^{13} m^{-1} for 0, 10 and 20 % (w/w) carrier addition, corresponding to filtration resistance reductions of 0, 29 and 75 %, respectively. Filtration resistances can be reduced significantly by the increase in particle filling ratios from 10 to 20 % because of the higher probability and frequency of particle-membrane collisions as already mentioned, particularly under supra-critical flux filtration in which external reversible fouling is accelerated. It can be seen from Figure 5-19 that the cake/gel layer could be removed effectively when LDPE carriers were applied at 10 and 20 % (w/w) in a conventional gas-sparged reactor under a gaslift-loop flow pattern.

5.4.2 Effect of carrier addition on mixed suspension filtration resistance for gas-mixed configuration without annular loop flow

In this section of the work, four cases of the gas-mixed reactor without annular loop flow configured with different geometry and set-up conditions as described in detail in section 5.3.2

were operated under an initial supra-critical flux constraint for 21 hours with sparging rate 2.5 L min^{-1}.

The variations in TMP, produced flux and mixed liquor filtration resistances at different particle filling ratios during initial supra-critical flux constraint for each condition are presented in Figure 5-20 and Figure 5-21. Fouled membrane characteristics after 21 hours of experimental period are shown in Figure 5-22. Model mixed suspension filtration resistances at the 21st hour of operation of every trial are presented in Table 5-2.

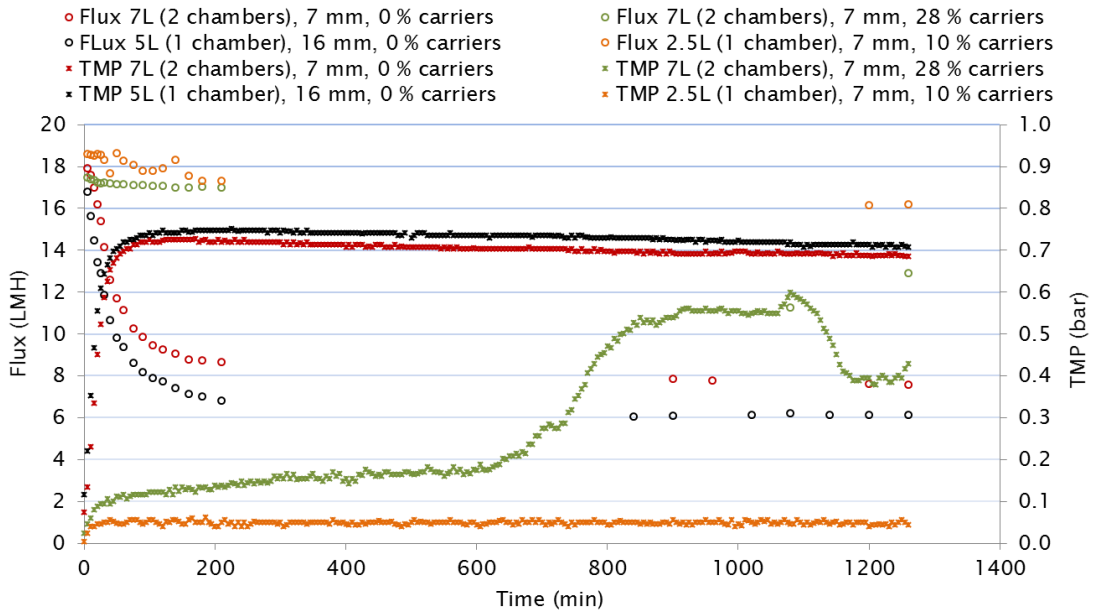

Figure 5-20 Flux and TMP characteristics during supra-critical flux filtration for gas-mixed configuration without annular loop flow

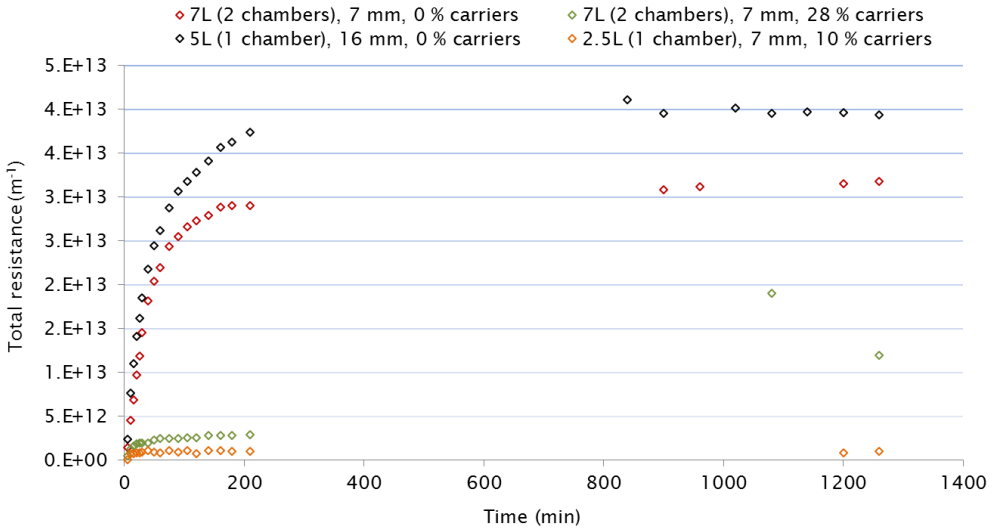

Figure 5-21 Resistance characteristics during supra-critical flux filtration for gas-mixed configuration without annular loop flow

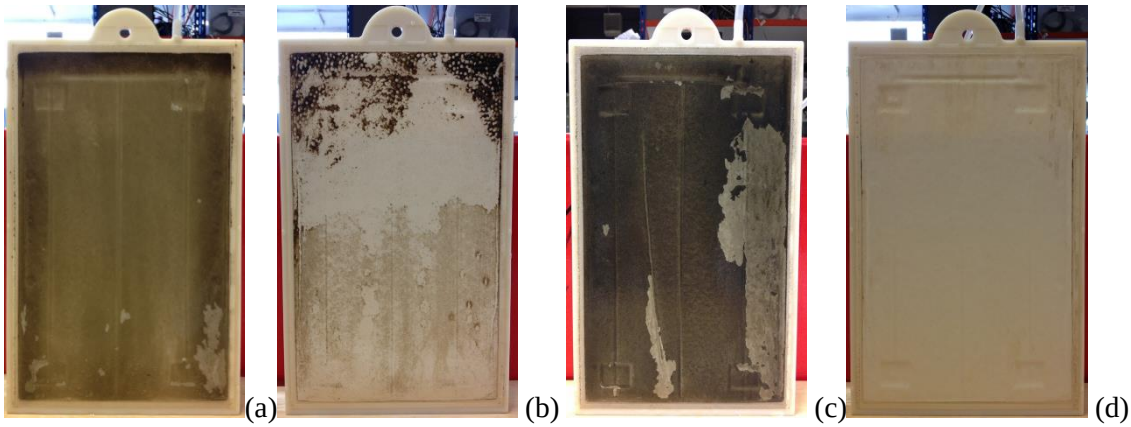

Figure 5-22 Fouled membrane characteristics after 21 hours of supra-critical flux filtration for gas-mixed configuration without annular loop flow

Where: (a) 7L, 7 mm, 0 % (b) 7L, 7 mm, 28 % and (c) 5L, 16 mm, 0 % and (d) 2.5L, 7 mm, 10 % (w/w) carriers addition, respectively

Table 5-2 Critical flux and filtration resistance for each operational condition in gaslift-loop and gas-mixed without annular loop flow configurations

Reactor configuration	Operational condition	Critical flux (LMH)	Filtration resistance ($x10^{13}$ m^{-1})
gaslift-loop flow	7 L (loop flow), 7 mm gap, 0 % (w/w)	6.0	2.97
	7 L (loop flow), 7 mm gap, 10 % (w/w)	7.5	2.11
	7 L (loop flow), 7 mm gap, 20 % (w/w)	9.0	0.74
gas-mixed without annular loop flow	7 L (2 chambers), 7 mm gap, 0 % (w/w)	6.0	3.18
	7 L (2 chambers), 7 mm gap, 28 % (w/w)	10.5	-
	5 L (1 chamber), 16 mm gap, 0 % (w/w)	4.5	3.94
	2.5 L (1 chamber), 7 mm gap, 10 % (w/w)	10.5	0.10

From Figure 5-20 and Figure 5-21 it can be seen that, with the initial supra-critical flux setting, TMP and filtration resistance increased sharply in the first few hours of filtration for the cases of 7 L (2 chambers), 7 mm gap, 0 % (w/w) and 5 L (1 chamber), 16 mm gap, 0 % (w/w) carriers, since there was no particle addition for these cases. A thick cake layer covering the membrane surface can be clearly seen after 21 hours of filtration, as shown in Figure 5-22 (a) and (c). The reversible cake layer formation causes a loss of effective membrane filtration area, resulting in high filtration resistance over the entire surface of 3.18 x 10^{13} and 3.94 x 10^{13} m^{-1} for the cases of 7 L (2 chambers), 7 mm gap, 0 % (w/w) and 5 L (1 chamber), 16 mm gap, 0 % (w/w) carriers, respectively. The results are in agreement with the short-term flux-stepping experiments where low achievable critical fluxes are due to filtration resistance (Table 5-2).

For the 2.5 L (1 chamber), 7 mm gap, 10 % (w/w) carriers case, with the lowest foulant load and 10 % carriers in a gas-mixed configuration without annular loop flow , vigorous scrubbing of the membrane panel by buoyant LDPE particles was observed. As a result, there was no visible sign of severe cake layer formation on the membrane surface after 21 hours of filtration, as shown in Figure 5-22 (d); and the lowest filtration resistance of 0.1 x 10^{13} m^{-1} was achieved.

With higher carrier filling ratios, however, the case of 7 L (2 chambers), 7 mm gap, 28 % (w/w) carriers experienced serious operational problems. Although this case showed the highest achievable critical flux from short-term flux-stepping experiments (Table 5-2), the longer filtration period in this section revealed the problem of particle entrapment in the thin channel between the membrane gap (Figure 5-22 (c) and Figure 5-23) which led to operational failure.

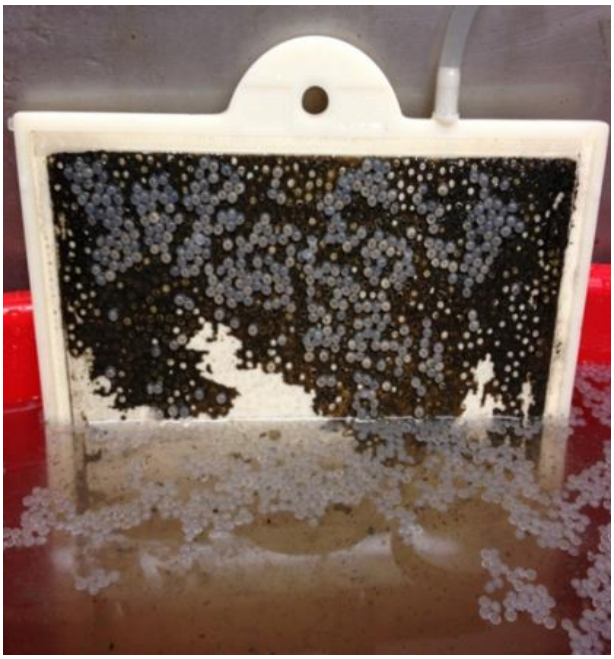

Figure 5-23 LDPE particles trapped between membrane gap during filtration for the case of 7 L (2 chambers), 7 mm gap, 28 % (w/w) carriers

A number of factors may have led to these problems of particle entrapment. Firstly, the LDPE particles used as scouring media in this chapter have an apparent size and shape (flat-lenticular shape with 3 - 4 mm diameter and 1 - 2 mm thickness) smaller than the 7 mm membrane gap. This means a few LDPE beads can become attached together and then trapped between the membrane channel. Secondly, the relatively high filling ratio for LDPE carriers of 28 % by weight fraction (31 % v/v) will increase the likelihood of collisions between particles, hindering their movement in the thin channel causing them to become easily stuck. Finally, when the system was operated under a gas-mixed configuration without annular loop flow with a buoyant scouring agent, internal lateral-loop flows and a stagnant flow regime could enhance foulant deposition and lead to regions of particle entrapment; this stationary trapped zone then resulting in a total

flow slow-down and severe fouling build-up. Similar issues have been identified by Alresheedi and Basu (2014), who compared the effect of using HDPE carriers (hollow cylindrical shape with 20 mm diameter and 20 mm length) with 10, 20 and 30 % v/v filling fraction on fouling rates in a hollow fibre AeMBR system. Their results showed that the lowest media packing gave the highest fouling reduction efficiency, which could be explained by the membrane module design and tank geometry. Based on visual inspection, at 20 and 30 % v/v filling ratios, scouring media were easily entrapped in the hollow fibre bundle and the reactor column, which diminished their scouring efficiency. Whilst with 10 % packing density, scouring media were observed to be smoothly recirculated inside the reactor column, thereby enhancing physical scouring efficiency (Alresheedi and Basu, 2014). As a result, a lower particle packing density and operating with a gaslift-loop configuration could diminish the problems of scouring media entrapment. For example, Kurita, Kimura and Watanabe (2015) operated a flat-sheet AeMBR coupled with 5 % (v/v) PEG granules filling; baffles were installed around the membrane modules and the flow pattern inside the tank could be adapted by adjustment of the liquid level to be above or below the top of baffles. They reported that with liquid level higher than the top of baffles, the airlift-loop flow pattern created circulation flows which induced continual granule movement and enhanced the efficiency of physical scouring process.

In this section, it has been demonstrated that fouling formation and total filtration resistance are stimulated under supra-critical flux filtration. The results are in agreement with the short-term flux-stepping experiments in the previous section, which showed that high critical fluxes could be obtained due to low filtration resistances.

When comparing the gaslift-loop flow and gas-mixed without annular loop flow configurations, the results indicated that the gaslift-loop flow pattern offers better fouling mitigation performance for both the gas-sparged two-phase and the gas-liquid-solid three-phase flow cases. Although the use of buoyant LDPE particles (SG 0.86 - 0.96) could retard liquid flow velocity in the downcomer zone, with smooth annular circulation and a mechanical cleaning process by 10 - 20 % w/w particles filling, fouling could be diminished effectively. For the three-phase flow in a gas-mixed configuration without annular loop flow, the results from the short-term flux-stepping and filtration resistance under supra-critical flux constraint experiments showed that fouling could be minimised significantly. Foulants, particularly the reversible cake layer, were observed to be limited due to vigorous membrane surface scrubbing by buoyant scouring particles under this flow regime. However, certain possible aspects such as incompletely mixed conditions, biological flocs breakage, membrane surface damage due to excessive particle scrubbing and particle entrapment still remain potential problems for the gas-mixed without annular loop flow pattern especially in long-term real flat-sheet MBR operations. Based on this context, with comparable achieved critical flux and fouling control propensities, the gaslift-loop flow pattern appears to be

a more practical design for both two- and three- phase flow operations when compared with the gas-mixed without annular loop flow regime. Therefore, the results and experiments in the next section and the reactor design in next chapter were based only on the gaslift-loop flow configuration.

5.5 Filtration resistance-in-series evaluated by clean water filtration

After acceleration of the fouling process by operating the membrane under an initial supra-flux constraint condition in section 5.4, the fouled membranes from each condition were taken to carry out a clean water flux experiment. The experiments in this section aimed to assess the effect of particle addition on external reversible fouling and internal irreversible fouling on/in the membrane surface.

In this section, the resistance-in-series model was applied to evaluate filtration resistances using Equation 5-1 in which the term R_T is derived in Equation 5-2

Equation 5-2

$$R_T = R_c + R_p + R_m$$

Where R_c is cake resistance formed by gel and cake deposition layer (referring to external reversible fouling that could be removed by a physical cleaning mechanism), R_p is fouling resistance caused by absorption of organic or inorganic into the membrane pores (referring to internal irreversible pore blockage that could be removed by a chemical cleaning process) and R_m is intrinsic membrane resistance.

A 7 L liquid working volume reactor with internal dimensions of 7.5 cm (width) x 21.5 cm (length) x 68 cm (liquid depth) was used for the resistance-in-series experiments.

The fouled membrane from section 5.4 was installed in the middle of the reactor width at 30 cm above the bottom of the reactor to perform clean water (tap water) filtration without any gas sparging or mixing. The permeate suction pump was set at 15 rpm for a 120 minute filtration period, and permeate effluent was recirculated back into the reactor to maintain a more or less constant liquid level inside the reactor. At this stage, the total resistance R_T can be calculated using Equation 5-1. Then, the membrane module was carefully washed with soft-sponge rubbing and running tap water without any air or water backwashing, to remove all visible cake layer from the membrane surface. Thereafter, the membrane with the cake removed was installed back into the reactor for tap water filtration in order to evaluate the term 'R_p+R_m'. Following this, the membrane was taken out of the reactor for chemical cleaning by washing with 4.5 % NaOCl and soft-sponge rubbing to remove visible stains, and then immersed in 0.045 % NaOCl solution for

24 hours. After that, the membrane was washed with tap water and installed back into the reactor for tap water filtration in order to estimate R_m.

In this section, only the cases of gas-lift loop operation are reported. Produced fluxes, TMPs, and filtration resistances of clean water filtration for fouled membrane, membrane with cake layer removed and recovered membrane after chemical cleaning are presented in Figure 5-24. The series of resistances for 0, 10 and 20 % (w/w) particle addition after a 120-minute operating period are shown in Table 5-3.

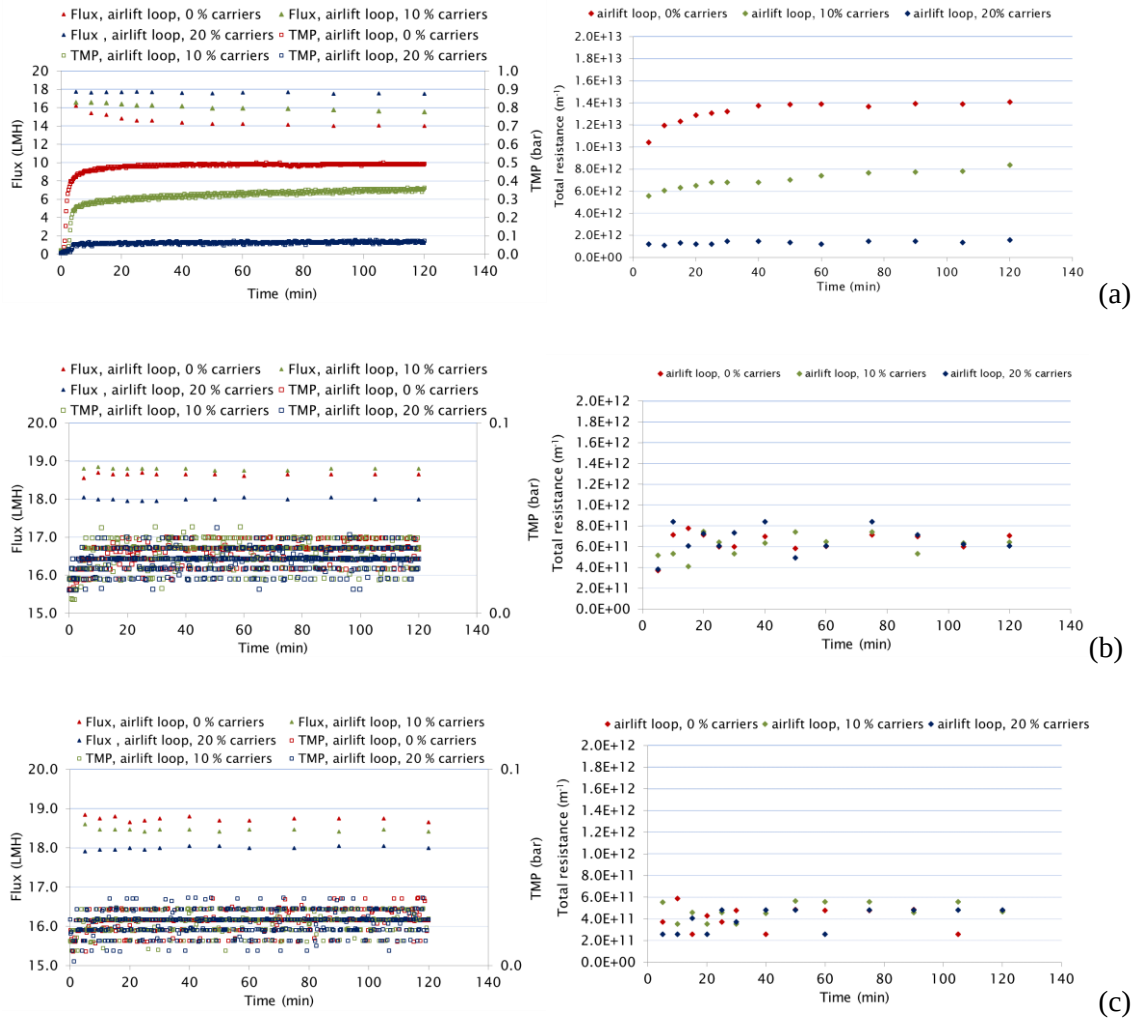

Figure 5-24 Clean water filtration resistance: (a) fouled membrane, (b) membrane with cake removed and (c) recovered membrane after chemical cleaning

Table 5-3 Filtration resistance distribution for 0, 10 and 20 % (w/w) LDPE carriers packing densities and virgin membrane after 120-minute filtration period

Fraction	0 % carriers		10 % carriers		20 % carriers		virgin membrane	
	$x10^{12}$ m^{-1}	(% R_T)	$x10^{12}$ m^{-1}	(% R_T)	$x10^{12}$ m^{-1}	(% R_T)	$x10^{12}$ m^{-1}	(% R_T)
R_c	13.40	(95.0)	7.74	(92.3)	1.00	(62.1)	-	-
R_p	0.23	(1.6)	0.18	(2.1)	0.13	(8.1)	-	-
R_m	0.48	(3.4)	0.47	(5.6)	0.48	(29.8)	0.78	(100)
R_T	14.10	(100)	8.38	(100)	1.61	(100)	0.78	(100)

As seen from Figure 5-24 and Table 5-3, filtration resistances were reduced following the physical and chemical cleaning processes. The results in Table 5-3 demonstrate that cake resistance (R_c) represents the largest proportion of the total filtration resistance (R_T), corresponding to 95, 92.3 and 62.1 % of R_T for the cases of 0, 10 and 20 % (w/w) particles filling, respectively.

Physical and chemical cleaning following the protocol described above could recover membrane filterability to similar values, when considering the intrinsic membrane resistance (R_m) of 0.48 x 10^{12}, 0.47 x 10^{12} and 0.48 x 10^{12} m^{-1} for 0, 10 and 20 % (w/w) particles filling, respectively. These values are lower than 0the .78 x 10^{12} m^{-1} of intrinsic virgin membrane resistance for 38 - 40 %. This might be because the clean water filtration experiment was carried out for the new virgin membrane without any previous physical or chemical cleaning. However, after membrane operations and cleaning according to the above cleaning protocol, the R_m values were still similar. This result could indicate that there was no significant membrane surface damage and or effect on filtration function after membrane operations and cleaning.

Total filtration resistances (R_T) reduced considerably in accordance with increasing particle filling fraction, with R_T values of 14.10 x 10^{12}, 8.38 x 10^{12} and 1.61 x 10^{12} m^{-1} for 0, 10 and 20 % (w/w) carriers, corresponding to an R_T reduction of 40.6 and 88 % for 10 and 20 % (w/w) particles, respectively. This is mainly because R_c which represents the major fouling contributor has been diminished significantly by the particle scouring effect; from Table 5-3, R_c values are 13.4 x 10^{12}, 7.74 x 10^{12} and 1.00 x 10^{12} m^{-1} for 0, 10 and 20 % (w/w) carriers, respectively. In this implementation, when the external gel/cake fouling which acts as a secondary dynamic membrane layer is limited, irreversible internal fouling due to membrane pore adsorption or pore blockage becomes more predominant. Consequently, membrane pore resistances (R_p) proportions increased with particle dosage, with R_p values of 1.6, 2.1 and 8.1 % of R_T for 0, 10 and 20 % (w/w) particle addition, respectively. With the assistance of a scouring agent, however, total

membrane resistance remained far lower than that in the case of two-phase sparging only, R_T and R_c could almost entirely be controlled by the mechanical cleaning of scouring particles.

5.6 Effective fluxes for continuous and intermittent filtration mode

One of the well-recognised physical cleaning methods for MBRs is membrane relaxation. This technique has been widely incorporated in most MBR designs as a standard operating strategy to minimise fouling, even when backflushing is not an option as for certain submerged flat-sheet membranes (Le-Clech, Chen and Fane, 2006), for example the flat-sheet Kubota membrane panel used in this study.

Membrane relaxation or intermittent filtration involves temporary interruption or pausing of the filtration process. TMP is reduced to zero (relaxation period), allowing poorly attached foulants to be removed away from the membrane surface into the mixed liquor by backtransport flow or concentration gradients. These diffusions are mostly further enhanced by gas sparging or liquid crossflow (Wang *et al.*, 2014). Many studies have evaluated the relative efficiency of intermittent suction modes for fouling mitigation (Wu *et al.*, 2008a; Cerón-Vivas, Morgan-Sagastume and Noyola, 2012; Zsirai *et al.*, 2012; Maqbool, Khan and Lee, 2014; Habib *et al.*, 2017). However, relaxation leads to a loss of permeate productivity as filtration is stopped during this period. In order to maintain a certain net permeate production, higher instantaneous fluxes are needed to compensate for the loss of this permeate. Fouling behaviour has been found to be strongly dependent on the applied instantaneous flux, as well as the length and frequency of relaxation period (Metzger *et al.*, 2007; Wu *et al.*, 2008a).

Therefore, experiments in this section were carried out to assess the effective fluxes (net fluxes) achieved from continuous and intermittent filtration modes for both two- and three- phase flow. The results obtained from the experiments were applied as a guideline for AnMBR system designs in next sections.

A 7 L MBR with 70 cm liquid depth, A_d/A_r 2.21 and A_d/A_b 0.71, was operated with a single A4 membrane panel (total filtration area of 0.1 m^2) under 2.5 L min^{-1} continuous gas sparging (corresponding to SGD_m of 1.5 $m^3\ m^{-2}\ hour^{-1}$) in a gaslift-loop flow configuration for both two- and three- phase flow cases. LDPE granules with filling ratio of 20 % (w/w) were introduced into the reactor which operated with internal annular flow for the three-phase flow case. Initial MLSS was set at approximately 10,000 mg L^{-1} (7,500 mg L^{-1} anaerobic digestate + 2,500 mg L^{-1} whole milk powder made up to required volume by tap water).

The feedstock was changed to milk powder basis in this section. This affected some properties of the system performance but it was done in order to simulate a real dairy wastewater. Synthetic

dairy wastewater made of 1.48 g L^{-1} whole milk powder in tap water with an expected COD concentration of 2,000 mg L^{-1} was applied as a feedstock without any permeate effluent recirculation back into the reactor.

Trials were conducted over 72 or 99 hours. Permeate was drawn off with the required rates by peristatic pump continuously in the case of 72-hour trials. For the 99-hour trials, an intermittent suction mode of 8 min suction and 2 min relaxation for every 10 min cycle (8 min on/2 min off) was applied in certain periods. In this intermittent filtration mode, the peristatic pump was programmed using a digital timer switch. The liquid level inside reactor was maintained constant 67 - 70 cm, controlled by a conductive level switch controller. Suction pressures related to achievable fluxes were monitored in order to determine the optimum net flux for each experimental condition.

5.6.1 Effective fluxes for two-phase flow under continuous and intermittent filtration mode

Relationships between achievable fluxes and TMP, and operational conditions for the two-phase flow, are presented in Figure 5-25 and Table 5-4, respectively.

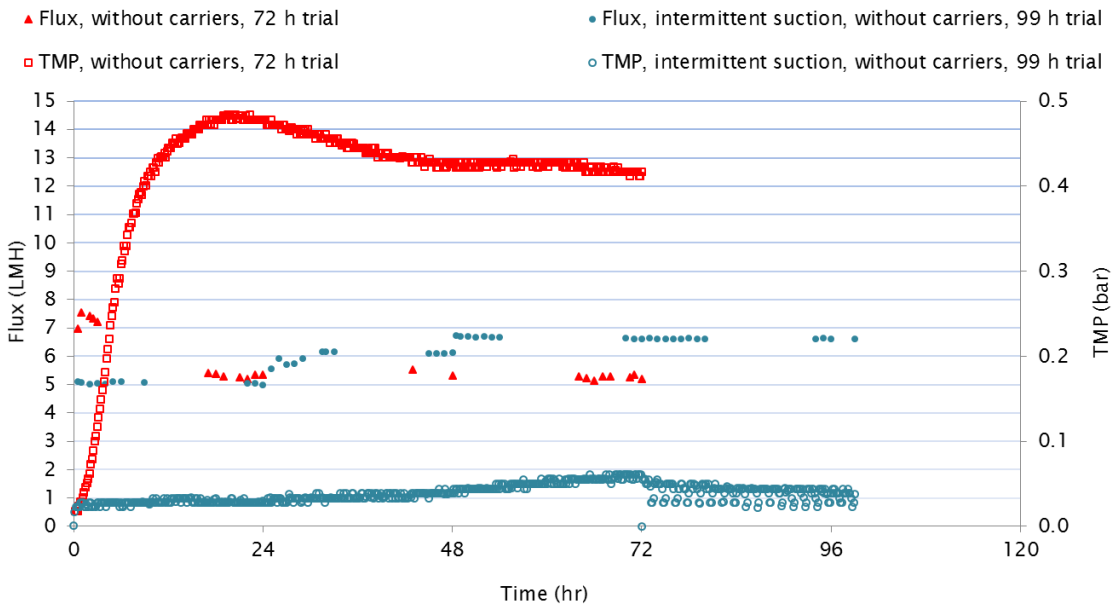

Figure 5-25 Relationship between achievable fluxes and TMP of the two-phase flow for 72 and 99-hour trials

Table 5-4 Operational parameters two-phase flow for 72 and 99-hour trials

Operational parameters	Durations (hours)			
	0-24	24-48	48-72	72-99
Suction mode				
72-hour trial	continuous	continuous	continuous	-
99-hour trial	continuous	continuous	continuous	intermittent
Initial flux constraint (LMH)				
72-hour trial	7.5	7.5	7.5	-
99-hour trial	5.0	6.0	6.5	6.5
Achievable flux or instantaneous flux (LMH)				
72-hour trial	5.4-7.5	5.3	5.3	-
99-hour trial	5.0	6.1	6.6	6.6
Net achievable flux (LMH)				
72-hour trial	5.4	5.3	5.3	-
99-hour trial	5.0	6.1	6.6	5.3

Although the critical flux results from the short-term experiments in section 5.3 are not precisely comparable with the net flux results in this section due to certain error factors and different experimental condition, the critical fluxes determined could be used as a guideline for instantaneous flux setting and achievable fluxes in this section.

For a 72-hour trial with continuous filtration, from Figure 5-25 and Table 5-4, the initial flux was set at 7.5 LMH. Since the instantaneous flux was set at 7.5 LMH, which is higher than the critical flux of 6.0 LMH (from section 5.3), TMP sharply increased to above 0.450 bar with a decrease in flux to 5.4 LMH in the first 24 hours of the filtration period. Thereafter, TMP gradually decreased to about 0.420 - 0.430 bar, while achievable flux remained relatively constant in the range of 5.2 - 5.5 LMH until the end of the 72-hour experimental period.

Hence, for 0 - 24 h with continuous filtration in the 99-hour trial, instantaneous flux was set at 5.0 LMH below critical flux, and it was found that a stable flux could be maintained at this value throughout the 24-h filtration period with TMP below 0.050 bar and a low dTMB/dt of 0.003 mbar min^{-1}. Then, the instantaneous flux was set to 6.0 LMH (equal to the critical flux) with continuous suction in 24 - 48 h of this 99-hour trial. It was found that the achievable flux could be maintained stably at 6.1 LMH with TMB below 0.050 bar and a relatively low fouling rate of 0.08 mbar min^{-1} for 24 h of filtration. In the period between 48 - 72 hours of continuous filtration in this trial, the instantaneous flux was raised to 6.5 LMH, higher than the critical flux. This showed that the achievable flux could remain constant at 6.6 LMH over a 24-h operational period; however, the fouling rate was found to increase to 0.012 mbar min^{-1}. Therefore, an intermittent suction mode (8 min-on/2 min-off) with an instantaneous flux of 6.5 LMH was applied over the

period from 72 - 99 hours. Figure 5-25 shows that the instantaneous flux and actual achievable flux during this period could be maintained constant at 6.6 LMH and the fouling rate is observed to be very low with TMP below 0.050 bar. With this intermittent suction strategy, however, the net achievable flux is 5.3 LMH equivalent to 88 % of the 6.0 LMH critical flux.

The results indicated that filtration coupled with membrane relaxation under the strategy used in this experiments provided better fouling mitigation in continuous filtration mode even when an instantaneous flux higher than the critical flux is applied. This is because when the convective force caused by permeate suction through the membrane surface is stopped, loose particles deposited on the membrane surface could be effectively removed to the bulk mixed suspension by backtransport created from the gas sparged two-phase flow during the relaxation period. Although net producible flux is decreased due to the loss of flux production during relaxation, the intermittent suction mode had a lower fouling rate than the continuous filtration strategy under the same fixed instantaneous flux.

Therefore, a net producible flux of 5.3 LMH for the two-phase flow was chosen as a criterion in order to evaluate other related parameters in the next sections.

5.6.2 Effective fluxes for three-phase flow under continuous and intermittent filtration mode

Relationships between achievable fluxes and TMP, and operational conditions for the three-phase flow (20 % w/w LDPE carriers) are presented in Figure 5-26 and Table 5-5, respectively.

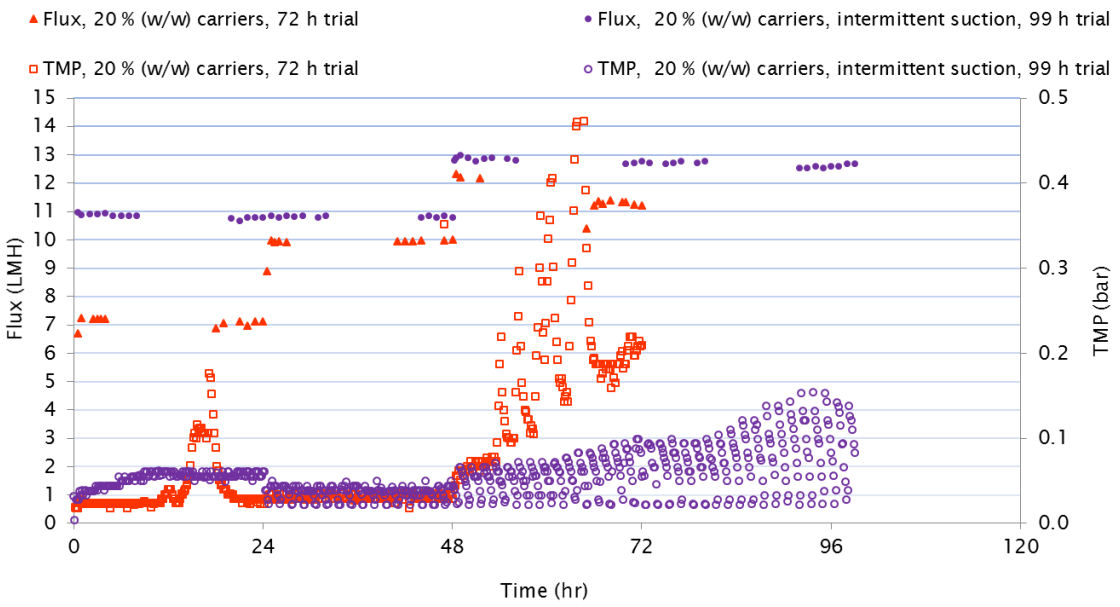

Figure 5-26 Relationship between achievable fluxes and TMP of the three-phase flow for 72 and 99-hour trials

Table 5-5 Operational parameters three-phase flow for 72 and 99-hour trials

Operational parameters	Duration (hours)			
	0 - 24	24 - 48	48 -72	72 - 99
Suction mode				
72-hour trial	continuous	continuous	continuous	-
99-hour trial	continuous	intermittent	intermittent	intermittent
Initial flux constraint (LMH)				
72-hour trial	7.0	10.0	12.0	-
99-hour trial	11.0	11.0	13.0	13.0
Achievable flux or instantaneous flux (LMH)				
72-hour trial	7.1	10.0	11.3-12.0	-
99-hour trial	10.8	10.8	12.6	12.5
Net achievable flux (LMH)				
72-hour trial	7.1	10.0	11.3	-
99-hour trial	10.8	8.4 - 8.6	10.0	10.0

For the 72-hour trial with continuous suction mode (Figure 5-26 and Table 5-5), in the first 24 h of operation, instantaneous flux was initially set at 7.0 LMH (below the critical flux of 9.0 LMH, from section 5.3). It was found that the net achievable flux could be maintained constant at 7.1 LMH over this operational period with an almost constant fouling rate at a TMP below 0.040 bar. It can be seen that unusual TMP fluctuation was seen during the 10^{th} - 20^{th} and the 54^{th} - 65^{th} hours of this experimental period. This was because of a flaw in the DC power generator supply to the pressure transducer which resulted in malfunction of the displayed suction pressure. However, the overall trend in TMP was still predictable. For the period from 24 - 48 hours of continuous filtration, the initial flux was set higher at 10 LMH (above the critical flux of 9.0 LMH), and it was found that an achievable flux of 10.0 LMH could be kept stable over this 24 hours filtration period with dTMP/dt < 0.01 mbar min^{-1} at TMP below 0.040 bar. This implied that, under these experimental conditions, the actual critical flux might be higher than 9 or 10 LMH. Hence, in the period from 48 - 72 hours, the initial flux was increased to 12 LMH. It was found that this value could not be maintained and the flux gradually dropped from 12.0 to 11.3 LMH with a TMP increase to above 0.200 bar (dTMP/dt > 0.10 mbar min^{-1}) by the end of the trial. The results indicated that the achievable flux for medium-term filtration with continuous suction mode under the experimental conditions used in this section was between 10 - 12 LMH.

Therefore, the instantaneous flux was set at 11 LMH with continuous suction mode for the first 0 - 24 hours of the 99-hour trial (Figure 5-26). TMP was found to increase continuously to 0.060 bar in the first 10 hours (dTMP/dt ~ 0.040 mbar min^{-1}) and then remained relatively stable at this value until the end of 24 hours of filtration, while the net achievable flux remained constant at 10.8 LMH during this operational period. For the period from 23 - 48 hours of the 99-hour trial,

an instantaneous flux of 11 LMH was still applied but with 8 min-on/2 min-off intermittent filtration. This showed that a constant achievable flux of 10.8 LMH could be maintained during the suction period, and TMP decreased to below 0.050 bar with a noticeably low fouling rate over the operational duration. However, by this filtration strategy, the net producible flux was equal to 8.6 LMH. From 48 - 99 hours, intermittent filtration was still applied while the instantaneous flux was raised to 13 LMH. It was found that the achievable flux during the suction period decreased slightly from 13 to 12.6 LMH, corresponding to a net achievable flux of 10 LMH until the end of 51 hours of filtration operated according to this strategy. However, a continuous TMP increase with a fouling rate of about 0.025 mbar min^{-1} up to above 0.15 bar was seen at the end of the experiment.

As a result, a net achievable flux of 8.4 - 8.6 LMH in a 24 - 48 hours test duration is considered to be a practical flux for long-term operation due to the low fouling rate demonstrated.

Therefore, the results illustrated that, under simulated AnMBR operation with the experimental condition in this section, the flux that could maintain low fouling rate for this medium-term trial operated in continuous filtration mode is in the range of 9 - 10 LMH. For the 8 min-on/2 min-off intermittent suction mode, a net producible flux of 8.4 - 8.6 LMH with instantaneous flux of 11 LMH is recommended as the optimum operational strategy.

5.7 The approach to scaling-up submerged flat-sheet AnMBR operated with two- and three- phase flow for dairy wastewater treatment

As noted earlier, high operational costs due to the high energy demand of MBR systems compared to other competing wastewater treatment methods remain a major obstacle which hampers the widespread implementation of this technology. Typically, energy demand for fouling control represents the highest proportion of the energy input in MBRs operation. Particularly, energy demand for two-phase air/gas sparging in submerged MBRs could account for up to 70 % of total energy consumption for MBR operation (Fenu *et al.*, 2010; Gil *et al.*, 2010; Santos, Ma and Judd, 2011; Pretel *et al.*, 2014). In contrast to conventional AeMBR, however, one of the main advantages of AnMBR systems is the possibility of recovering energy from methane in biogas, which could potentially compensate for the energy demand for fouling mitigation by the gas sparging method.

Results from simulated AnMBR operations for synthetic dairy wastewater treatment in the previous sections demonstrated that the use of LDPE scouring particles coupled with a conventional two-phase gas sparged system (GSAnMBR) operated as a three-phase moving bed AnMBR (MBAnMBR) is an effective method for fouling mitigation under the same energy input

for gas sparging. Therefore, energy consumption for gas sparging and the opportunities to recover energy from the produced methane were assessed based the obtained results from previous sections. These energy calculations were conducted for both the GSAnMBR and MBAnMBR in lab-scale operations, including energy predictions for the case of scaling-up these systems to pilot-scale with comparable configurations.

5.7.1 Comparing obtained design parameters of GSAnMBR and MBAnMBR to real full-scale submerged flat-sheetKubota AeMBR

Generally, the range of air/gas sparging in submerged flat-sheet MBR is reported as one of the following parameters:

- Actual total gas flow rate, Q_g (m^3 $hour^{-1}$)
- Gas sparging intensity or superficial gas velocity, U_g ($m\ s^{-1}$) :

Equation 5-3

$$U_g = \frac{Q_g}{A_r}$$

Where A_r is the total cross-sectional area of two-phase flow between the flat-sheet membrane gap (m^2)

- Specific gas demand in m^3_{gas} $hour^{-1}$ $m^{-2}_{membrane\ area}$, SGD_m :

Equation 5-4

$$SGD_m = \frac{Q_g}{A_m}$$

Where A_m is total membrane filtration area (m^2)

- Specific gas demand in m^3_{gas} $hour^{-1}$ $m^3_{permeate\ product}$ $hour^{-1}$, SGD_P :

Equation 5-5

$$SGD_P = \frac{Q_g}{JA_m} = \frac{Q_g}{Q_p}$$

Where J is the permeate flux (L m^{-2} $hour^{-1}$, LMH) and Q_p is the produced permeate flow rate (m^3 $hour^{-1}$).

U_g and SGD_m have conventionally been applied for unit design. Considering only these design parameters any result in a flawed solution, however, because the effective scoured-membrane area is strongly dependent on the module arrangement, module types, membrane packing densities and tank geometry (Fox and Stuckey, 2015). For instance, four flat-sheet A4 membrane panels stacked vertically would receive more intense gas scouring than the same membranes situated side-by-side horizontally under the same given gas sparging rate.

SGD_p, which can be related to the similar parameter of specific air demand (SAD_p) for permeate production in AeMBR, is particularly useful for industry. It provides the specific energy demand, E_a, in kWh $m^{-3}_{permeate}$, which is therefore a direct indicator of the MBR and aeration system performances (Judd, 2011). For a given air/gas sparging system at a fixed liquid depth in the reactor, SAD_p relates directly to the specific energy demand for membrane aeration:

Equation 5-6

$$E_a = kSGD_p$$

Where the value of k is as expressed in Equation 5-7, as suggested by Verrecht *et al.* (2008) and Judd (2011)

Equation 5-7

$$k = \frac{pT\lambda}{2.73 \times 10^5 \varsigma(\lambda - 1)}\left[\left(\frac{10{,}000y + p}{p}\right)^{1-(1/\lambda)} - 1\right]$$

where: p is the blower inlet pressure in Pa; T is the air temperature in K; ς is the blower efficiency; λ is the aerator constant ($\sim$1.4) and y is the aerator depth in m.

From Equation 5-5 to Equation 5-7, it can be clearly seen that the effectiveness of energy input is highly dependent on producible flux, sparging intensity and tank geometry (liquid depth).

Since all experiments in this study were performed with a single flat-sheet A4 Kubota microfiltration membrane panel at laboratory scale, therefore, the approach to scale-up of the GSAnMBR and MBAnMBR from results obtained in this chapter was evaluated based on a real full-scale Kubota AeMBR (type 510 ES, single-deck) configuration.

The full-scale Kubota 510 ES AeMBR consists of the type 510 flat-sheet module with a panel height of 1,000 mm (0.8 m^2 of filtration area per panel) installed in a reactor with a liquid depth of at least 2,026 mm (design parameter from manufacturer). Membrane spacing is set at 7 mm and the system is typically operated with a SAD_m of 0.75 m^3 m^{-2} $hour^{-1}$ and U_g of 0.047 m s^{-1} (Prieske *et al.*, 2010).

The lab-scale GSAnMBR and MBAnMBR in this chapter consisted of a flat-sheet A4 module with the panel height 295 mm (0.1 m^2 of filtration area per panel) installed in the reactor with liquid depth of 700 mm. Membrane spacing was set at 7 mm, and systems were operated with a sparging intensity (Q_g) of 2.5 L min^{-1}, corresponding to a SAD_m of 1.5 m^3 m^{-2} $hour^{-1}$ and U_g of 0.014 m s^{-1}.

Liquid in the full-scale Kubota 510 ES AeMBR has to be set at a minimum level of 2,026 mm and single-deck membrane panels with module height of 1,000 mm are installed. This design

means that an A4 membrane panel with a module height of 295 mm could be vertically stacked in 4 decks corresponding to a total module height of 1,180 mm with a similar given liquid depth of 2,000 mm.

Therefore, pilot-scale GSAnMBR and MBAnMBR design parameters were assessed based on the flat-sheet module height of 1,180 mm (0.4 m^2 of total filtration area) installed in the reactor with a liquid depth of 2,000 mm. Membrane spacing was assumed to be set at 7 mm with the system operated at a sparging intensity (Q_g) of 2.5 L min^{-1} corresponding to a SAD_m of 0.375 m^3 m^{-2} $hour^{-1}$ and U_g of 0.014 m s^{-1}. A comparison of the design parameters for lab-scale and pilot-scale AnMBR to a full-scale submerged flat-sheet Kubota 510 ES AeMBR is presented in Table 5-6.

Table 5-6 Comparison of design parameters for lab- and pilot-scale AnMBR to full-scale ES510 Kubota AeMBR

MBR type	membrane spacing, mm	panel length, mm	panel height, mm	liquid depth, mm	filtration area per panel, m^2	SAD_m, m^3m^{-2} $hour^{-1}$	U_g, m s^{-1}
Full-scale AeMBR Kubota 510ES	7	430	1,000	2,026	0.8	0.75	0.047
Lab-scale AnMBR (this study)	7	215	295	700	0.1	1.5	0.014
Pilot-scale AnMBR (this study)	7	215	1,180	2,000	0.4	0.375	0.014

5.7.2 Energy consumption for gas sparging per permeate production

Since gas sparging without backflushing or sludge pumping was applied in this chapter, the energy demand for fouling control in both GSAnMBR and MBAnMBR was calculated only for this method.

The power demand calculation for the gas blower is modified from the power requirement for adiabatic compression in an aeration system (Metcalf & Eddy, 2003) as shown in Equation 5-8.

Equation 5-8

$$P_w = \frac{wRT_1}{29.7ne}\left[\left(\frac{P_2}{P_1}\right)^{0.283} - 1\right]$$

Where

P_w = power requirement of each blower, kW

w = weight of flow of air, kg s^{-1}

R = engineering gas constant for air, 8.314 kJ k mol $^{-1}$ K^{-1}

T_1 = absolute inlet temperature, K

P_1 = absolute inlet pressure, atm

P_2 = absolute outlet pressure, atm

n = (k-1)/k = 0.283 for air

k = 1.395 for air

29.7 = constant for SI unit conversion

e = efficiency (usual range for compressors is 0.70 to 0.90)

Assuming a biogas density of 1.25 kg m^{-3} at STP, at a sparging rate of 2.5 L min^{-1}, the term w in Equation 5-8 is 2.5 x 1.25 / (1,000 x 60) = 5.21 x 10^{-5} kg s^{-1} of biogas flow. For a biogas sparging system operated at a typical mesophilic temperature of 37 °C (310 K), and an assumed blower efficiency of 65% with an inlet pressure of 1 atm, according to Equation 5-8, the power requirement for 2.5 L min^{-1} biogas sparging related to the design liquid depth under these conditions can be derived from Equation 5-9.

Equation 5-9

$$P_w = \frac{(5.21 \times 10^{-5}) \times 8.314 \times 310 \times}{29.7 \times 0.283 \times 0.65}\left[\left(\frac{1 + (0.0968h)}{1}\right)^{0.283} - 1\right]$$

$$P_w = 0.02458\left[\left(\frac{1 + (0.0968h)}{1}\right)^{0.283} - 1\right]$$

Where

h = pressure head or liquid depth, m

0.0968= conversion factor for pressure in m to atm

5.7.2.1 Energy consumption for gas sparging for GSAnMBR

Lab-scale GSAnMBR

According to Equation 5-9, with a liquid depth of 0.7 m (from Table 5-6), the power requirement can be calculated as follow

$$P_w = 0.02458\left[\left(\frac{1+(0.0968\times 0.7)}{1}\right)^{0.283}-1\right]$$

$P_w = 4.60 \times 10^{-4}$ kW

For the net achievable flux of 5.3 LMH (from section 5.6.1, Table 5-4) with 0.1 m^2 total filtration area (from Table 5-6), the produced permeate flow rate is equal to 5.3 x 10^{-4} m^3 $hour^{-1}$. Therefore, energy demand for biogas sparging per permeate (E_{gs}) is

E_{gs} = 4.6 x 10^{-4} kW/ 5.3 x 10^{-4} m^3 $hour^{-1}$

E_{gs} = 0.868 kWh m^{-3} $_{permeate}$

Pilot-scale GSAnMBR

According to Equation 5-9, with liquid depth of 2.0 m (from Table 5-6), then power requirement can be calculated as follow

$$P_w = 0.02458\left[\left(\frac{1+(0.0968\times 2.0)}{1}\right)^{0.283}-1\right]$$

$P_w = 1.26 \times 10^{-3}$ kW

For the net achievable flux of 5.3 LMH (from section 5.6.1, Table 5-4) with 0.4 m^2 total filtration area (from Table 5-6), the produced permeate flow rate is equal to 2.12 x 10^{-3} m^3 $hour^{-1}$. Therefore, the energy demand for biogas sparging per permeate (E_{gs}) is

E_{gs} = 1.26 x 10^{-3} kW/ 2.12x 10^{-3} m^3 $hour^{-1}$

E_{gs} = 0.595 kWh m^{-3} $_{permeate}$

5.7.2.2 Energy consumption for gas sparging for MBAnMBR

Lab-scale MBAnMBR

According to Equation 5-9, with a liquid depth of 0.7 m (from Table 5-6), the power requirement can be calculated as follow

$$P_w = 0.02458\left[\left(\frac{1+(0.0968\times 0.7)}{1}\right)^{0.283}-1\right]$$

$P_w = 4.60 \times 10^{-4}$ kW

For the net achievable flux of 8.4 LMH (from section 5.6.2, Table 5-5) with 0.1 m^2 total filtration area (Table 5-6), the produced permeate flow rate is equal to 8.4 x 10^{-4} m^3 $hour^{-1}$. Therefore, energy demand for biogas sparging per permeate (E_{gs}) is

E_{gs} = 4.6 x 10^{-4} kW/ 8.4 x 10^{-4} m^3 $hour^{-1}$

E_{gs} = 0.548 kWh $m^{-3}_{permeate}$

Pilot-scale MBAnMBR

According to Equation 5-9, with a liquid depth of 2.0 m (from Table 5-6), the power requirement can be calculated as follow

$$P_w = 0.02458\left[\left(\frac{1+(0.0968\times 2.0)}{1}\right)^{0.283}-1\right]$$

$P_w = 1.26 \times 10^{-3}$ kW

For the net achievable flux of 8.4 LMH (from section 5.6.2, Table 5-5) with 0.1 m^2 total filtration area (Table 5-6), the produced permeate flow rate is equal to 8.4 x 10^{-4} m^3 $hour^{-1}$. Therefore, the energy demand for biogas sparging per permeate (E_{gs}) is

E_{gs} = 1.26 x 10^{-3} kW/ 3.36x 10^{-3} m^3 $hour^{-1}$

E_{gs} = 0.375 kWh $m^{-3}_{permeate}$

5.7.3 Obtained electrical energy from produced methane gas in AnMBR treating dairy wastewater

Using the COD concept to estimate methane yield from the equation below

$$CH_4 + 2O_2 \rightarrow CO_2 + H_2O$$

Therefore, 1 kg $COD_{removed}$ is equivalent to 250 g of produced methane, which equals methane gas of 250/16 = 15.6 moles.

At standard temperature and pressure (STP), 1 mole of gas has a volume of 22.4 L. Therefore, at STP 1 kg of $COD_{removed}$ will yield 15.62 x 22.4 / 1000 = 0.35 m^3 of methane gas.

The lower heating value of methane is 36 MJ m^{-3} and 3.6 MJ is equivalent to 1 kWh. Assuming that the methane concentration of the biogas is 70% in real operating conditions.

Hence, 1 kg of $COD_{removed}$ will yield a thermal energy of 0.35 m^3 x 36 MJ m^{-3} x 1 kWh/ 3.6 MJ x 0.7 = 2.45 kWh.

About 33 % of methane energy can be converted into electrical energy, electric motors to drive axial pumps are about 80 % efficient, pump impellers about 85 % efficient and inverters about 95% efficient, giving an overall conversion efficiency of about 21 % (Kim *et al.*, 2010).

Thus, each 1 kg of $COD_{removed}$ could yield electrical energy of 0.21 x 2.45 kWh = 0.5145 kWh or 0.5145 kWh_{elect}/ kg $COD_{removed}$.

5.7.3.1 Electrical energy obtained from produced methane gas for GSAnMBR

With the objective of simulating a low to medium strength dairy effluent typical of that generated after a dissolved air flotation (DAF) process, synthetic dairy wastewater with an initial concentration of 2,000 mg COD L^{-1} was applied as the COD source to allow estimation of the obtained energy from produced methane in the following stages.

For synthetic dairy wastewater with initial COD concentration of 2000 mg L^{-1} (2 kg COD m^{-3}), COD removal efficiency was assumed to be 85 % under 37°C mesophilic conditions in a GSAnMBR.

Therefore, the electrical energy obtained from $COD_{removed}$ can be calculated as 0.5145 kWh_{elect}/ kg $COD_{removed}$ x 0.85 x 2 kg COD $m^{-3}_{permeate}$ = 0.875 kWh_{elect} $m^{-3}_{permeate}$.

5.7.3.2 Electrical energy obtained from produced methane gas for MBAnMBR

For the same synthetic dairy wastewater with initial COD concentration of 2000 mg L^{-1} (2 kg COD m^{-3}), COD removal efficiency is assumed to be 70 % (due to the lack of a secondary self-forming dynamic membrane) under 37 °C mesophilic condition in an MBAnMBR.

Therefore, the electrical energy obtained from $COD_{removed}$ can be calculated as 0.5145 kWh_{elect}/ kg $COD_{removed}$ x 0.70 x 2 kg COD $m^{-3}_{permeate}$ = 0.720 kWh_{elect} $m^{-3}_{permeate}$

5.7.4 Comparisons of simulated design parameters among AnMBRs treating dairy wastewater

Comparisons of simulated design parameters obtained from section 5.6 and 5.7 between lab- and pilot- scale GSAnMBR and MBAnMBR for dairy wastewater treatment are presented in Table 5-7.

Table 5-7 Simulated parameters in AnMBR operations designed for synthetic dairy wastewater treatment with initial COD concentration of 2,000 mg L^{-1}

Design parameters	Unit	AnMBR scale			
		GSAnMBR		MBAnMBR	
		Lab	Pilot	Lab	Pilot
Liquid depth[a]	m	0.7	2.0	0.7	2.0
Total filtration area[a]	m^2	0.1	0.4	0.1	0.4
Biogas sparging rate[a]	L min^{-1}	2.5	2.5	2.5	2.5
U_g[a]	m s^{-1}	0.014	0.014	0.014	0.014
SGD_m[a]	$m^3m^{-2}hour^{-1}$	1.5	0.375	1.5	0.375
Simulated net achievable flux[b]	LMH	5.3	5.3	8.4	8.4
SGD_p	m^3_{gas} $m^{-3}_{permeate}$	283.0	70.8	178.6	44.6
Power requirement for gas blower, P_w[c]	x 10^{-3} kW	0.46	1.26	0.46	1.26
Influent COD concentration[d]	mg L^{-1}	2,000	2,000	2,000	2,000
Expected COD removal efficiency[d]	%	85	85	70	70
Energy requirement for gas sparging, E_{gs}[c]	kWh $m^{-3}_{permeate}$	0.868	0.595	0.548	0.375
Total energy consumption, E_{tc}[e]	kWh $m^{-3}_{permeate}$	1.240	0.850	0.783	0.536
Electrical energy potential from produced methane, E_p[d]	kWh $m^{-3}_{permeate}$	0.875	0.875	0.720	0.720
Energy independency ratio, E_p/E_{tc}		0.71	1.03	0.92	1.34

[a] described in section 5.7.1

[b] obtained results from section 5.6

[c] described in section 5.7.2

[d] described in section 5.7.3

[e] estimated with an assumption that other energy requirement fractions apart from gas sparging are equal to 30 % of total energy consumption (suggested by Lin *et al.* (2011a) and Pretel *et al.* (2014))

From Table 5-7, under the same given sparging rate (Q_g) of 2.5 L min^{-1} and fixed membrane gap of 7 mm, the calculated U_g values are 0.014 m s^{-1} for both lab- and pilot- scale AnMBRs. However,

when the liquid level inside the reactor is simulated to be up to 2.0 m at pilot-scale, the membrane module height could be increased resulting in a larger total filtration area of 0.4 m^2. By this design, with the same fixed Q_g and U_g, SGD_m and SGD_p are reduced proportionally according to the higher total membrane filtration area when the module height is increased in pilot-scale cases, although the power requirement for the gas blower increases from 0.46 x 10^{-3} - 1.26 x10^{-3} kW due to the higher gas sparger depth.

The results from section 5.6 demonstrated that a higher net flux of 8.4 LMH could be achieved in the MBAnMBR case due the assistance of scouring particles, compared to 5.3 LMH for the GSAnMBR. Therefore, under the same given Q_g, U_g and SGD_m, the SGD_p could be minimised for both lab- and pilot- scale MBAnMBR operations. Additionally, with the same given gas sparging intensity in terms of SGD_m, other calculated parameters related to effluent permeate production rates such as the energy requirement for gas sparging (E_{gs}), total energy consumption (E_{tc}) and energy potential from produced methane (E_p) are affected directly by the attainable net flux.

This illustrates that energy consumption for two-phase (also three-phase) AnMBR operation is highly influenced by gas sparging intensity (in term of SGD_m), liquid depth inside reactor (related to membrane filtration area and power requirement for gas blower) and net producible flux.

When considering the energy requirement for fouling control by the two-phase gas sparging method (E_{gs}), in Table 5-7 it can be seen that E_{gs} values are in the range of 0.375 - 0.868 kWh $m^{-3}_{permeate}$ for both lab- and pilot- scale GSAnMBR and MBAnMBR. This is in agreement with the quoted range of 0.25 - 1.0 kWh $m^{-3}_{permeate}$ in AnMBRs that use gas sparging to prevent membrane fouling (Liao, Kraemer and Bagley, 2006). E_{gs} values of 0.868 and 0.548 kWh $m^{-3}_{permeate}$ for lab-scale GSAnMBR and MBAnMBR are similar to the reported range of 0.69 - 5.68 kWh $m^{-3}_{permeate}$ for lab-scale biogas sparging AnMBRs (Martin *et al.*, 2011), while E_{gs} values are improved to 0.595 and 0.375 kWh $m^{-3}_{permeate}$ for pilot-scale GSAnMBR and MBAnMBR, respectively. These values are also similar to the 0.038 - 1.345 kWh $m^{-3}_{permeate}$ (with an average value of 0.41 kWh $m^{-3}_{permeate}$) for estimated energy demands from 7 pilot-scale AnMBRs treating domestic wastewater with biogas sparging for fouling control reported by Shin and Bae (2018). In addition to the energy requirement for biogas sparging, however, energy consumption for the rest of the AnMBR system such as operation of the pre-treatment process and first stage reactor and pumping systems for influent feeding, liquid recirculation between/within reactors and permeate suction systems, etc., also represents a considerable proportion of the total energy demand for AnMBR operations. The diversity of pre-treatment processes and operational methods applied in real full-scale AnMBR for wastewater treatment makes it difficult to evaluate energy requirements for components other than biogas sparging. Thus, the energy demands for other components are assumed to be 30 % (70 % for gas sparging) of the total energy consumption, based on the average value suggested

by two modelling studies on assessment of operating costs for gas-sparged AnMBR treating municipal wastewater (Lin *et al.*, 2011a; Pretel *et al.*, 2014). Therefore, an energy independency ratio which is defined as the ratio of electrical energy potential to the total energy demand (E_p/E_{tc}) could be calculated.

From Table 5-7, although the lab-scale systems have energy independency ratios lower than 1, this value increases to 1.03 and 1.34 at pilot scale for both GSAnMBR and MBAnMBR, suggesting the potential to achieve net positive energy production. This is because permeate production rates can be improved due to the higher total membrane filtration area following the scaling-up of reactor height, which therefore results in a higher energy recovery potential from greater flux production. Particularly, E_p/E_{tc} for pilot-scale MBAnMBR corresponds to a 30 % improvement in energy independency ratio compared to pilot-scale GSAnMBR mainly due to producible flux enhancement because of the beneficial effects of the use of non-adsorbent scouring particles.

The results indicated that the use of non-adsorbent scouring particles coupled with conventional two-phase gas sparging is an alternative effective approach for fouling mitigation in AnMBR operations. Attainable net flux can be improved considerably under the same given energy input for biogas sparging, resulting in the potential to achieve net positive energy production for AnMBR systems treating dairy wastewater in pilot- or real full- scale implementations.

Additionally, one notable aspect is that the calculated design parameters in this section have been obtained from simulated AnMBR operations under 37 °C mesophilic conditions and model dairy wastewater with a concentration of 2,000 mg COD L^{-1}. Therefore, lower flux and methane production can be expected if the systems have to be operated in temperate climates where influent wastewater temperatures could be lower at 8 - 25 °C in ambient conditions (Martin *et al.*, 2011). As a result, energy recovery from methane production, particularly for low to medium strength wastewater could be insufficient to provide enough energy to heat the reactor to 35 - 37 °C mesophilic temperature. Martin *et al.* (2011) reported that the heat required to achieve 35 °C mesophilic conditions in the reactor is only possible with influent wastewater strengths exceeding 4,000 - 5,000 mg COD L^{-1}. Based on this, one of the considerable benefits of applying AnMBR as a mainstream process for dairy wastewater treatment systems is that DAF processes, which typically need to be applied as a pre-treatment unit for other high rate anaerobic systems such as UASB or ABR, could be eliminated. By this approach, raw dairy wastewater effluent from manufacturing with high biodegradable particulate organic matter in the range of 5,000 - 6,000 mg COD L^{-1} could directly be fed to AnMBR as initial influent. Furthermore, the high energy demand for DAF unit operation could be excluded from the total energy consumption for dairy

wastewater treatment. Consequently, implementations of GSAnMBR and MBAnMBR systems are considered to be practical alternative approaches for a dairy wastewater treatment process.

5.8 Conclusions

An integration of non-adsorbent particles with gas sparging operated as a three-phase flow for fouling mitigation purposes in submerged flat-sheet MBR was evaluated. Non-adsorbent particles made of LDPE in rigid round flat-lenticular shape (∅ 3 - 4 mm and 1.5 - 2 mm thickness) with SG of 0.86 - 0.96 were applied as scouring media in this chapter. Experiments were carried out mainly related to simulated AnMBR operational conditions with the aim of applying the obtained results as a guideline for practical MBR designs.

The results from constant pressure filtration mode driven by gravitational static head showed that the use of LDPE scouring particles (10 % w/w filling ratio) coupled with conventional two-phase gas sparging could minimise fouling considerably. Produced flux can be enhanced when compared with the case of without particle filling under the same given gas sparging intensity, or comparable flux could still be remained while gas sparging rate can significantly be reduced.

Results from short-term flux-stepping experiments also demonstrated that, with LDPE particle additions of 10 and 20 % (w/w), critical flux can be improved by up to 25 and 50 % when compared to conventional two-phase flow under the same given gas sparging intensity in a gaslift-loop configuration. As LDPE scouring particles are smaller than the 7 mm membrane spacing, an increment in particle packing amounts from 10 to 20 % (w/w) results in a higher probability and frequency of particles colliding with others and with the membrane surface, therefore enhancing the scouring effect. Results from resistance-in-series tests showed that external reversible gel/cake layer foulants which represent the major contributor to the total filtration resistance were considerably alleviated as the particle filling fraction increased from 10 to 20 % w/w.

In comparisons between the gaslift-loop flow and gas-mixed without annular-loop flow configurations, the former offered better hydrodynamic conditions for fouling mitigation and mixing purposes in both two- and three-phase flow cases. One considerable drawback of applying LDPE particles is that their SG of 0.86 - 0.96 is lower than 1, meaning these buoyant particles could retard the continuous liquid annular flow velocity inside the reactor and a higher liquid downward flow velocity in downcomer zone may be required in the gaslift-loop configuration. With a particles packing density of 10 - 20 % w/w under operating conditions of U_g 0.014 m s^{-1}, A_d/A_r 2.21, A_d/A_b 0.78 and A_d/A_t 1.0, however, it was found that particles could be recirculated smoothly throughout the 99-hour duration of the medium-term experiments. The three-phase flow with particle addition of 28 % w/w (in filtration zone) under a gas-mixed without annular-loop

configuration also showed a critical flux improvement of 75 % in comparison with the same configuration without particles during short-term flux-stepping experiments. Membrane panels installed in the upper part of the reactor were seen to be scrubbed vigorously by buoyant LDPE beads. This case, however, also revealed problems of particle entrapment between the membrane clearance during the medium-term experiments, which then caused severe fouling and system failure. This is due to an internal lateral-loop flow and liquid stagnant flow regime forming on the membrane surface under the gas-mixed without annular-loop configuration, accompanied by the excessive particle filling (28 % w/w) which hindered their movement and caused them to be easily entrapped between the thin membrane spacing. In addition, certain aspects such as biological flocs disintegration, membrane surface damage due to intensive scouring by rigid buoyant particles, as well as incompletely mixed conditions inside the reactor, still remain potential problems for the gas-mixed without annular-loop flow regime in long-term operation. Hence, the gaslift-loop flow regime is considered to be a more practical design for submerged flat-sheet MBR for both two- and three-phase flow cases.

Simulated design parameters obtained from the experimental results have been applied to evaluate the opportunity to scale up GSAnMBR and MBAnMBR systems for dairy wastewater treatment. The energy requirement for biogas sparging per unit of permeate production (E_{gs}) is highly dependent on the gas sparging intensity (in term of SGD_m), liquid depth inside reactor (related to membrane filtration area and power requirement for gas blower) and the net producible flux. According to the model calculation results, the energy independency ratios (E_p/E_{gs}) could be more than 1 when AnMBRs are scaled up, suggesting the potential to achieve net positive energy production. Particularly, a 30 % improvement in E_p/E_{gs} ratio for the MBAnMBR compared to the GSAnMBR was seen due to its higher attainable net flux and methane production.

As a result, an implementation of non-adsorbent scouring particles coupled with conventional two-phase gas sparging AnMBR could be considered an alternative effective approach for fouling mitigation under the same given energy input.

Chapter 6: **Moving bed anaerobic membrane bioreactor for dairy wastewater treatment**

Results from short- and medium- term experiments related to simulated AnMBR operations from Chapter 5 demonstrated that the use of non-adsorbent particles (LDPE beads) coupled with gas-sparged MBR to enhance the in situ membrane mechanical cleaning process is a potentially beneficial approach to apply for dairy wastewater treatment. Hence, the experiments in this chapter were conducted with the objective to study an implementation of non-adsorbent scouring particles (PEG granules) integrated with conventional two-phase gas-sparged AnMBR (GSAnMBR) operating as a three-phase moving bed AnMBR (MBAnMBR) for low- to medium-strength dairy wastewater treatment.

The obtained results relating to optimised reactor configuration design from Chapter 4 and evaluated parameters from Chapter 5 were taken to design and construct lab- scale GSAnMBR and MBAnMBR operating as live AnMBR systems for synthetic dairy wastewater treatment.

The LDPE scouring particles applied in Chapter 4 had certain potential drawbacks for long-term operation as their smaller size could affect scouring performance and the likelihood of particle entrapment, while their SG lower than 1 may influence the efficiency of particle recirculation inside reactor and their rigid texture might cause polymeric membrane surface damage after long-term operation. As a result, soft-flexible plastic granules made of polyethylene glycol (PEG) with SG of 1.01 - 1.05 in 4 mm x 4 mm cylindrical shape (as presented in section 3.1.5) were used as scouring particles in MBAnMBR with a packing ratio of 10 % v/v in this chapter.

The GSAnMBR and MBAnMBR systems were constructed and operated according to the details in section 3.2 for dairy wastewater treatment. Organic treatment, filtration efficiencies and biogas production performance under varied operational conditions for long-term experiments were examined.

6.1 GSAnMBR and MBAnMBR operated with gas sparging rate of 2.5 L min^{-1}

The GSAnMBR and MBAnMBR were seeded with anaerobic digestate collected Millbrook wastewater treatment plant. The initial (day 0) MLSS concentration in both reactors was set at approximately 8,000 mg L^{-1}. Both systems were fed with synthetic dairy wastewater with a total influent COD of about 2,000 mg L^{-1}. Initial permeate fluxes for both reactors were established at 5.5 LMH by the same drawn pump speed with intermittent suction mode of 8 min-on/2 min-off.

Biogas recirculation (biogas sparging rate) for the GSAnMBR and MBAnMBR was 2.5 L min^{-1}. There was no excess sludge wasting for the whole experimental period.

The attainable net permeate flux and suction pressure profiles (TMP) are presented in Figure 6-1.

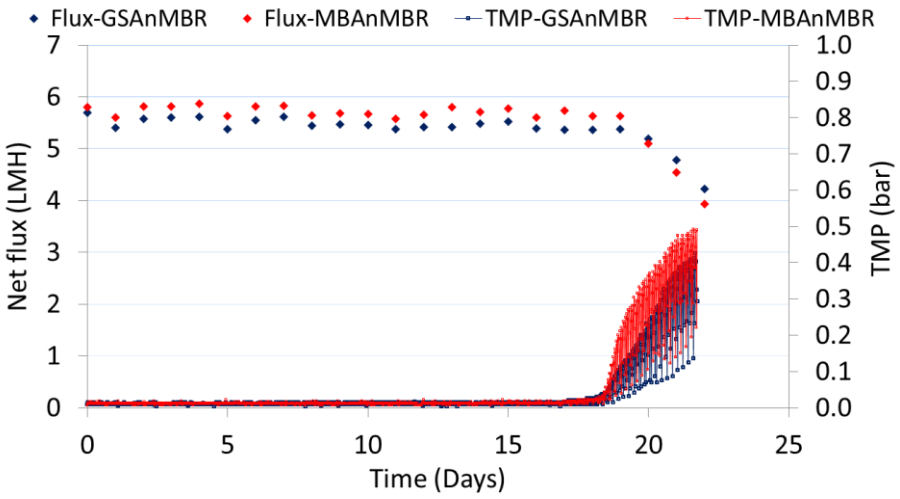

Figure 6-1 Net flux and suction pressure profiles for GSAnMBR and MBAnMBR operating with gas sparging rates of 2.5 L min^{-1}

From Figure 6-1, it can be seen that the GSAnMBR and MBAnMBR produced similar net fluxes of 5.4 - 5.6 and 5.6 - 5.9 LMH, respectively, for 18 days of the filtration period, with suction pressure below 0.02 bar. On the 18th day of operation, however, signs of rising suction pressure were seen in both reactors. Thereafter, suction pressure further increased sharply up to 0.40 and 0.49 bar, while produced net fluxes continuously dropped to 4.2 and 3.9 LMH for the GSAnMBR and MBAnMBR, respectively, until day 22 of the operational period when both reactors were terminated. Fouling characteristics on the membrane surface for the GSAnMBR and MBAnMBR under 2.5 L min^{-1} sparging intensity after termination of this system are presented in Figure 6-2 and Figure 6-3, respectively.

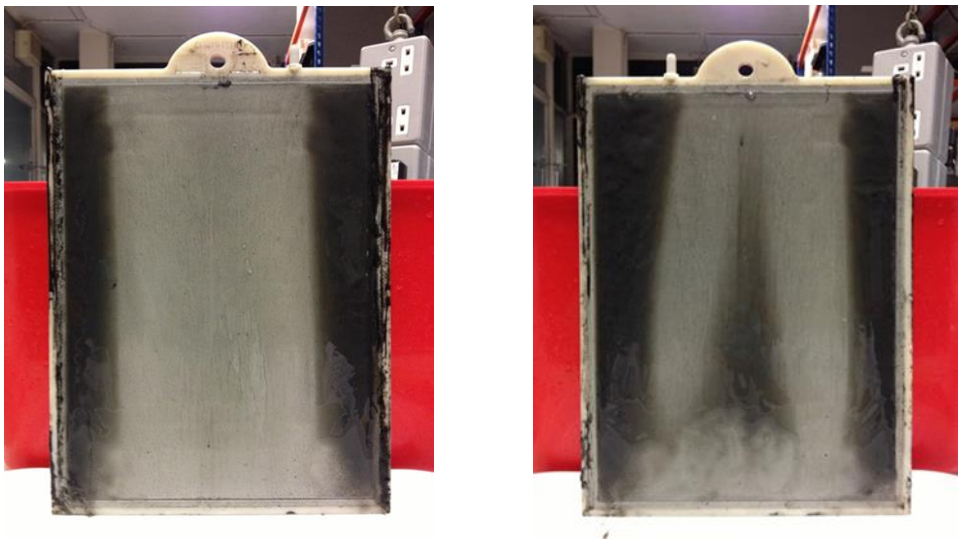

(a) front side (b) back side

Figure 6-2 Fouled membrane characteristics of GSAnMBR under 2.5 L min^{-1} gas sparging rate

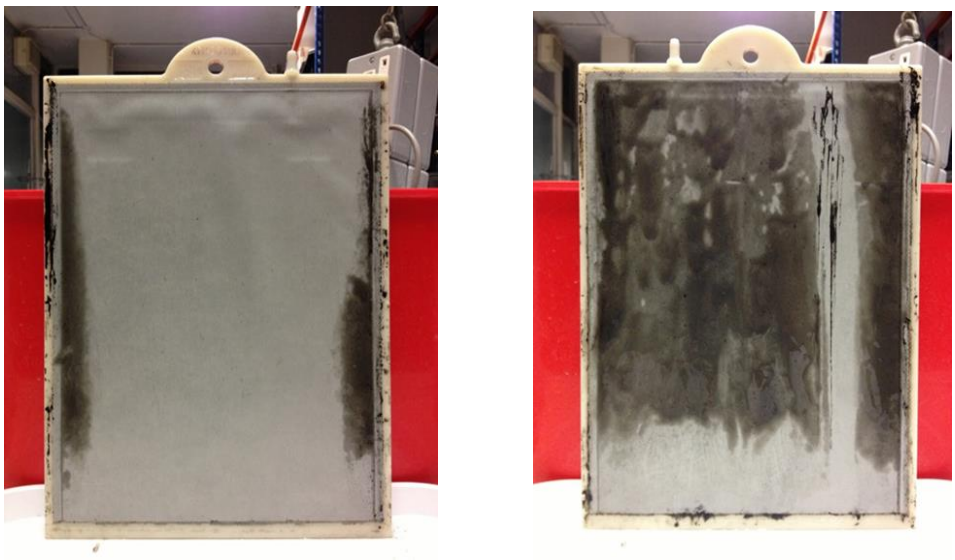

(a) front side (b) back side

Figure 6-3 Fouled membrane characteristics of MBAnMBR under 2.5 L min^{-1} gas sparging rate

The jump in suction pressure occurred approximately 3 weeks after the systems started operating, although they were operated following design criteria obtained from Chapter 5 (e.g. operational flux, initial MLSS concentration, feeding concentration and sparging rate). Operational fluxes for the GSAnMBR and MBAnMBR under 2.5 L min^{-1} of biogas sparging were initially set below both critical flux (6 LMH for the GSAnMBR and 9 LMH for MBAnMBR, from section 5.3) and recommended net fluxes (5.3 LMH for the GSAnMBR and 8.4 LMH for MBAnMBR, from section 5.6). A net produced flux of 5.4 LMH for the GSAnMBR and 5.8 LMH for MBAnMBR could be sustained for 18 days, after which suction pressure jumped in similar periods during day

19 to day 22. This indicated that fouling formation in a live anaerobic system is far more intense than in simulated anaerobic mixed suspension (anaerobic digestate with milk power and tap water) operated under aerobic conditions as conducted in Chapter 5, particularly during the unsteady state period of microbial acclimatisation and adaptation to the new feeding substrate.

The suction pressure jump and fall in flux is caused by the imbalance between convection toward a membrane (permeate extraction) and back transport (induced by gas sparging) (Wu, Howell and Field, 1999). This implies that the biogas sparging rate of 2.5 L min^{-1} is insufficient to remove foulant over the membrane surface in order to maintain attainable net flux of approximately 5.5 LMH for long-term operation. In addition, the uniformity of bubbles scattering over both sides of membrane panels also significantly affects backtransport distribution. From Figure 6-2 and Figure 6-3, the greyish area represents membrane covered by a thin gel layer while the black area is the region enwrapped in a thick cake layer, causing the membrane to lose effective filtration area, which then results in a decline in total permeate production. For the GSAnMBR (Figure 6-2), it can be seen that more bubbles generated by the gas spargers were present at the front side of the membrane panel than at the back. This was potentially caused by the transversal flow (coming from downcomer) at the bottom of the reactor forcing most of the created bubbles to the front side of riser zone, since the reactors were designed in split-type gaslift-loop configuration. This effect is more clearly observed in the case of the MBAnMBR (Figure 6-3), where almost all of the bubbles and granules were confined to the front side of the riser section. Thick cake was formed much more intensively on the back of membrane panel, resulting in a higher suction pressure jump and fall in produced flux for the MBAnMBR when compared to the GSAnMBR during day 19 to day 22 of operation.

As a result, in order to allow the AnMBR systems to be operated for a longer period, a higher gas sparging intensity of 5 L min^{-1} and lower initial net flux constraint of approximately 3.5 LMH was applied in the next experiments.

6.2 GSAnMBR and MBAnMBR operated with gas sparging rate of 5 L min^{-1}

The GSAnMBR and MBAnMBR were seeded with anaerobic digestate in which the initial (day 0) MLSS and MLVSS concentrations for both reactors were set at approximately 5,000 and 4,600 mg L^{-1}, respectively. Biogas sparging for fouling mitigation and mixing purposes in both reactors was applied at the same given rate of 5 L min^{-1} (threshold sparging rate obtained from Chapter 4). Both systems were operated for 10 cycles with varied solid retention times (SRT), flux and volumetric organic loading rates (OLR). Operational strategies for each cycle are presented in Table 6-1. At the end of some cycles (run 4, run 6, run 8 and run 9), a certain amount of digestate

was wasted from both reactors and then tap water with the same volume as the wasted sludge was added to the reactor in order to make up the MLSS concentration to the designed level at around 9,000 - 12,000 mg L^{-1}. Before starting each run, the reactors were left for a few days (1 - 5 days) without feeding and permeate extraction (only gas sparging was applied), to ensure that no volatile fatty acids (VFAs) accumulated in the systems.

Table 6-1 Operational strategies

Run (no.)	day	GSAnMBR				MBAnMBR			
		SRT (day)	Net flux (LMH)	HRT (hour)	OLR (g $COD_{removed}$ L^{-1} day^{-1})	SRT (day)	Net flux (LMH)	HRT (hour)	OLR (g $COD_{removed}L^{-1}$ day^{-1})
1	0-99	>1,200	3.5-3.9	18-19	0.37-4.8	>1,200	3.4-3.8	18-19	0.37-4.57
2	100-119	42	2.6-3.7	18-25	3.49-5.16	32	3.5-3.8	17-19	4.53-5.13
3	120(125)*-153	23	2.3-3.7	18-29	3.17-4.81	20	3.3-3.9	17-20	3.83-5.04
4	154(160)*-188	>1,200	1.7-2.0	33-39	2.26-2.64	240	1.7-2.9	23-39	2.16-3.84
5	189(190)*-202	106	1.8-1.9	35-37	2.32-2.62	80	2.0-2.1	31-33	2.50-2.85
6	203-216	127	2.5-2.7	24-26	3.14-3.71	99	2.8-2.9	23-24	3.81-4.06
7	217(218)*-222	55	4.2-4.5	15-16	5.79-6.13	52	4.6-5.1	13-14	5.67-5.95
8	223(225)*-245	120	2.6-4.1	16-25	3.37-5.76	112	3.5-5.5	12-19	4.62-7.05
9	246(248)*-271	80	2.8-3.0	22-24	3.75-4.11	80	3.5-3.7	18-19	4.80-5.02
10	272(274)*-308	55	2.7-3.6	18-24	4.13-4.84	55	3.5-4.3	15-19	5.10-5.94

Note: *days in brackets are the starting dates for feeding and permeate extraction

6.2.1 COD removal

COD profiles and COD removal efficiencies during the experimental period are presented in Figure 6-4 and Figure 6-5. Average COD removal efficiencies of each operational run are shown in Table 6-2.

Run 1 was an acclimatisation period. The GSAnMBR and MBAnMBR were operated with the same initial net flux setting at around 3.5 LMH (Figure 6-6). OLR in both reactors was increased stepwise by adjusting the total influent COD concentration from approximately 700 to 1,400, 2,100, 3,100, and 3,600 mg L^{-1} on days 0 - 19, 20 - 40, 41 - 60, 61- 81 and 82 - 99 (Figure 6-4), representing expected OLRs in the regions of 0.89, 1.78, 2.67, 3.95 and 4.58 g $COD_{removed}$ L^{-1} day^{-1} respectively. There was no excess sludge wastage from either the GSAnMBR or the MBAnMBR in this run: only small amounts of digestate were taken regularly for analysis based on which the

SRT could be calculated as more than 1,200 days. This was with the objective of allowing microorganism in the inoculum to adapt to the new feed substrate (synthetic dairy wastewater). A low initial OLR, low operational flux and shear rate (sparging rate) as well as long acclimatisation durations have all been recommended, in order to achieve a successful start-up for AnMBR (Trzcinski and Stuckey, 2009).

Total COD removal efficiency started from 50 % on day 1 of operation and then reached up to about 95 % on day 28 (Figure 6-5) for both the GSAnMBR and MBAnMBR, although OLRs were still being increased. Subsequently, both reactors presented the same trends in COD removal efficiencies. Total COD removals of 97 - 98 % were achieved even at the highest OLRs, in the range of 4.10 - 4.80 g $COD_{removed}$ L^{-1} day^{-1} (influent COD ~ 3,600 mg L^{-1}) during day 81 - 99. It was found that total effluent COD (noted as permeate) was generally below 70 - 90 mg L^{-1} in this period (Figure 6-4 and Table 6-2).

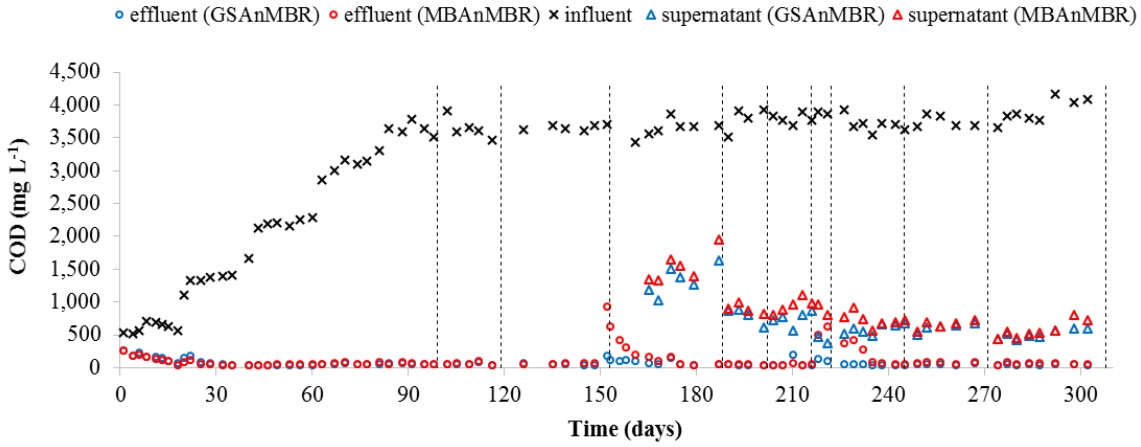

Figure 6-4 COD profiles (vertical dashed lines represent the end of each run)

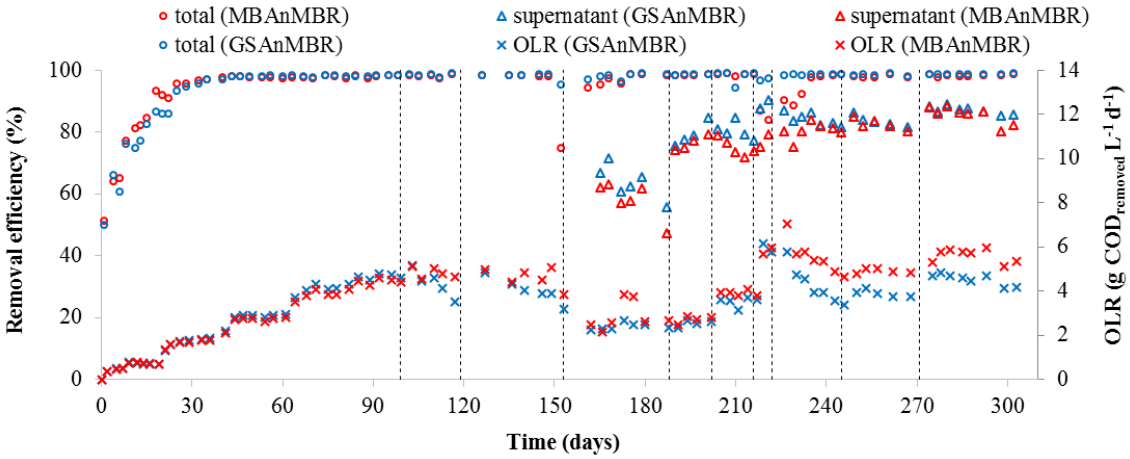

Figure 6-5 COD removal efficiencies (vertical dashed lines represent the end of each run)

Table 6-2 Average COD removal efficiency of each operational run

Run (no.)	SRT (day)		COD_{inf} (mg L^{-1})	COD_{eff} (mg L^{-1})		R_t (%)		COD_s (mg L^{-1})		R_s (%)	
	R1	R2	R1 and R2	R1	R2	R1	R2	R1	R2	R1	R2
1	>1,200	>1,200	2,014 ± 1,127	91 ± 61	84 ± 53	90.4 ± 12.7	91.5 ± 11.8	na	na	na	na
2	42	32	3,646 ± 168	56 ± 18	67 ± 20	98.5 ± 0.5	98.2 ± 0.6	na	na	na	na
3	23	20	3,661 ± 44	82 ± 50	269 ± 360	98.0 ± 1.4	94.3 ± 9.5	na	na	na	na
4	>1,200	240	3,642 ± 129	84 ± 37	169 ± 128	98.0 ± 1.0	96.9 ± 1.8	1,335 ± 220	1,541 ± 236	63.8 ± 5.4	58.1 ± 5.9
5	106	80	3,793 ± 192	47 ± 4	57 ± 7	98.8 ± 0.2	98.5 ± 0.2	789 ± 126	895 ± 73	79.1 ± 3.9	76.4 ± 2.3
6	127	99	3,789 ± 76	74 ± 74	51 ± 11	98.0 ± 2.0	98.7 ± 0.3	748 ± 113	949 ± 110	80.3 ± 2.8	74.9 ± 2.8
7	55	52	3,877 ± 29	116 ± 24	566 ± 83	97.0 ± 0.6	85.4 ± 2.3	427 ± 70	886 ± 121	89.0 ± 1.7	77.2 ± 2.9
8	120	112	3,703 ± 116	49 ± 6	192 ± 161	98.7 ± 0.1	94.9 ± 4.3	588 ± 73	726 ± 106	84.1 ± 2.1	80.4 ± 2.7
9	80	80	3,747 ± 93	56 ± 14	76 ± 16	98.5 ± 0.4	98.0 ± 0.4	616 ± 66	658 ± 71	83.6 ± 1.7	82.4 ± 1.9
10	55	55	3,900 ± 178	48 ± 4	66 ± 14	98.8 ± 0.1	98.3 ± 0.4	510 ± 69	570 ± 129	86.9 ± 1.3	85.5 ± 2.8

Note: 1) R1 is GSAnMBR and R2 is MBAnMBR, 2) na = not applicable and 3) values show in table represent the average ± standard deviation

This confirmed one of the major of advantages of AnMBR operation, in which a short start-up period with superior effluent qualities can be achieved. Although shorter start-up periods of 6 and 12 days for AnMBRs have been reported in the studies of Hu and Stuckey (2006) and Lin *et al.* (2011a), compared to 28 days in this study, this may have been affected by various different operational parameters (e.g., substrate types, operational temperature, initial fluxes and OLRs). The start-up period of AnMBR is considered to be lower than other high-rate anaerobic reactors such as UASB systems, in which this period was in the range of one to several months (Ozgun *et al.*, 2013).

At the end of this run (day 99), signs of a sudden transmembrane pressure increase (TMP jump) were seen in the GSAnMBR, when TSS in the GSAnMBR and MBAnMBR exceeded 13,500 mg L^{-1} (to be discussed in other sections). Therefore, excess sludge wastage was applied in the next run.

According to the general calculation method for SRT in single completely stirred tank reactor (CSTR), SRT could be calculated from total sludge volume in CSTR divided by daily wasting sludge volume from CSTR ($SRT = V/Q_W$). Daily sludge wastage resulting in SRTs of 42 days for the GSAnMBR and 32 days for the MBAnMBR was conducted in run 2. For 20 days (day 100 - 119) of operation in this run, both reactors still achieved high total COD removal efficiencies (97.6 - 98.9 % for GSAnMBR and 97.2 - 98.6 % for MBAnMBR) at OLR of 3.49 - 5.16 g $COD_{removed}$ L^{-1} day^{-1}. However, the achievable OLRs in the GSAnMBR from the middle to the end of this run were reduced due to a continuous fall in produced net flux (Figure 6-6). A TMP jump occurred in the GSAnMBR, although daily sludge wasting was regularly performed. This phenomenon was initially thought to be caused by gel/cake layer formation in the GSAnMBR after long-term filtration. Therefore, the membrane panel from the GSAnMBR was taken out of the reactor for chemical cleaning on day 119, while the digestate was kept inside the reactor at 37 °C without feeding or permeate drawing, as well as in the MBAnMBR which had also been stopped: only gas sparging was performed in both reactors for 6 days.

In run 3, after chemical cleaning, the membrane panel was reinstalled into the GSAnMBR, then both reactors were re-started on day 125, with very short SRT of 23 days and 20 days adopted for the GSAnMBR and MBAnMBR, respectively. Both reactors still achieved stable total COD removal efficiencies (> 98 %) for almost all of the run. A TMP jump occurred in the GSAnMBR again, however, only 6 days of filtration after chemical cleaning of the membrane. Operation of this reactor stopped again for 4 days (day 131 - 134), while the MBAnMBR was still operated continuously (Figure 6-6). Filtration for the GSAnMBR was started again on day 135. Nonetheless, total COD removal efficiencies for both the GSAnMBR and MBAnMBR decreased sharply to 95.2 and 74.6 % with effluent COD of 177 and 932 mg L^{-1}, respectively, along with a

dramatic jump in TMP for both AnMBRs (Figure 6-6). Floating whitish foam was also observed in both reactors, particularly in the MBAnMBR, which appeared to have a more severe foaming problem. When these signs of system failure were seen on day 153, operation of both reactors was stopped for 6 days before starting the new run. The major potential reason for the unstable performance in this run for both reactors was operation under very low SRTs, especially for the MBAnMBR which had been at a shorter SRT under a similar OLR of around 4.5 g $COD_{removed}$ L^{-1} day^{-1} since run 2. In very low SRT applications, excessive loss of biomass from the systems is expected. The point at which the rate of biomass growth is smaller than the biomass discharge rate represents the so-called 'washout' case (Cicek *et al.*, 2001). This washout effect causes the loss of active microorganisms, while incompletely degraded substances and intermediates (e.g. VFAs, SMP and EPS) accumulate inside reactors and permeate, leading to organic overloading which results in the fall in COD removal efficiencies.

In run 4, the recovery run, feeding of systems started on day 160. After the reactors had experienced serious unstable performance in run 3, they were operated at a relatively low initial OLR of about 2.5 g $COD_{removed}$ L^{-1} day^{-1} with long SRTs of >1,200 days for the GSAnMBR and 240 days for the MBAnMBR. Initial OLR was controlled by reduction of net flux production, while influent COD concentration was maintained constant at around 3,600 mg L^{-1}. The supernatants of mixed liquor were taken to measure COD (COD_s), bioreactor removal (R_s) and total removal (R_t) efficiencies, with the difference between R_t and R_s considered to be membrane filtration efficiencies. From Figure 6-5, R_s values for both reactors are relatively low at 55.6 - 71.5 % for the GSAnMBR and 47.1 - 63.0 % for the MBAnMBR. This indicated that certain incompletely degraded COD and intermediates still remained inside the reactors, which the microorganisms were not capable of metabolising even under relatively low OLR operation. R_t was still high, however, in the range of 96.3 - 98.9 % for the GSAnMBR and 94.2 - 98.8 % for the MBAnMBR, indicating that physical and biological treatment by polarisation, gel/cake layer, and pore filtration also played important roles in total COD removal, even for an MBAnMBR in which the secondary dynamic membrane layer is expected to be less than in the GSAnMBR. It is worth noting that, at the middle stage of this run, initial net flux for the MBAnMBR increased to 2.9 LMH (Figure 6-6) from day 172 until day 176 when a malfunction occurred with the programmable peristatic pump for the MBAnMBR. Hence, from day 177 onwards, permeate extractions for both reactors were conducted by one multi-head peristatic pump at the same rotational speed. The R_s values had revealed signs of systems instability, and TSS concentrations for both reactors accumulated to about 13,000 mg L^{-1}; therefore, at the end of this run on day 188, certain amounts of digestate were withdrawn from both reactors. Thereafter, tap water with the same volume as the withdrawn sludge was added to the reactors in order to make up MLSS concentrations to the designed level of approximately 9,500 mg L^{-1}.

Both reactors started operation again on day 190 in run 5. Initial net fluxes were set to 1.8 and 2.0 LMH corresponding to OLRs of 2.3 - 2.6 and 2.7 - 2.8 g $COD_{removed}$ L^{-1} day^{-1}, and SRTs of 106 and 80 days were adopted for the GSAnMBR and MBAnMBR, respectively. R_s for the GSAnMBR and MBAnMBR rose to 75.5 - 84.6 % and 74.3 - 79.2 %, respectively, while R_t for both reactors could sustain superior performances at around 98.5 % throughout the run. From these results, it can be seen that dispersed microorganisms inside bioreactors could be responsible for 70 - 80 % of COD removal. The difference between R_s and R_t of around 10 - 20 % for COD removal implied that a fraction of dissolved COD constituents could be rejected by the membrane. This confirms that membrane separation plays a significant role in maintaining high and stable COD removal efficiencies (Huang, Gui and Qian, 2001) even in comparison with the relatively low R_s of about 50 - 60 % in run 4.

In run 6, initial OLRs were raised to 3.6 and 3.9 g $COD_{removed}$ L^{-1} day^{-1} by adjustment of initial net fluxes and SRTs of 127 and 99 days were implemented for the GSAnMBR and MBAnMBR, respectively. For the 14-day duration of this run (day 203 - day 216) high values for R_s of about 75 - 80 % and for R_t of 98 - 99 % were seen for both reactors, and these excellent efficiencies were characterised as stable organic removal conditions. At the end of this run on day 216, when TSS concentrations inside both reactors exceeded 14,000 mg L^{-1}, excess sludge was withdrawn and tap water substitution was undertaken in order to take the TSS back to about 9,000 mg L^{-1} before starting the next run.

In run 7, initial OLRs in both reactors were raised to about 6 g $COD_{removed}$ L^{-1} day^{-1} by flux increment on day 218. Relatively short SRTs of 55 and 52 days were employed for the GSAnMBR and MBAnMBR, respectively. Slightly better performance of R_s and R_t in the range of 87.8 - 90.2 % and 96.6 - 97.4 % was achieved by the GSAnMBR, compared to 75.1 - 79.2 % and 83.8 - 87.0 % for the MBAnMBR, respectively. However, intensive whitish foam formation was observed inside both reactors, reflecting operation under stress. This sign of system instability was believed to be caused by the organic shock load due to the sudden OLR increment, accompanied by relatively low SRTs. As a result, feeding of the systems was stopped on day 222.

In run 8, high initial OLRs of 5.5 and 7.1 g $COD_{removed}$ L^{-1} day^{-1} were adopted on day 225 for the GSAnMBR and MBAnMBR, respectively. Since the influent COD concentration was kept constant at about 3,600 mg L^{-1}, the difference in achievable OLR between the two reactors was due to the attainable net flux production of each reactor under the same fixed suction pump speed rate. Longer SRTs of 120 days and 112 days were applied for the GSAnMBR and MBAnMBR, respectively. From Figure 6-5, it can be seen that R_s for both reactors decreased initially with the sudden increase in OLR (83.7 % for GSAnMBR and 75.1 % for MBAnMBR on day 229). However, each reactor recovered rapidly from the shock within a few days, and then became

stable again, even the MBAnMBR which received a higher initial OLR of 7.1 g $COD_{removed}$ L^{-1} day^{-1}. The rapid recovery may be because the microorganisms could adapt quickly to the new OLR under the relatively long SRTs, as well as to the gradual diminution of OLRs associated with the reduction of attainable net fluxes (Figure 6-6). High R_s values of 81.6 and 80 % and R_t of 98.8 and 98.6 % with final OLRs of 3.4 and 4.6 g $COD_{removed}$ L^{-1} day^{-1} for the GSAnMBR and MBAnMBR, respectively, could still be achieved at the end of run on day 245 when the TSS concentration in both reactors exceed 12,000 mg L^{-1}. Hence, at this point, MLSS for both reactors was reduced again and made up by tap water addition to the target concentration of about 9,000 mg L^{-1} before starting the next run.

In run 9 the reactors were fed again on day 248, with OLRs of about 4.0 and 5.0 g $COD_{removed}$ L^{-1} day^{-1} for the GSAnMBR and MBAnMBR, respectively. The same SRT of 80 days was applied to both reactors. Throughout this run of about one month, high and stable R_s and R_t values were obtained in both reactors at approximately 80 and 98 % for the GSAnMBR and MBAnMBR, respectively. At the end of this run on day 271, digestate concentrations inside both reactors were adjusted to about 9,000 mg L^{-1} of MLSS prior to starting the new run.

In run 10, both reactors started operating on day 274 with the same SRT of 55 days. The GSAnMBR and MBAnMBR had different OLR of about 4.8 and 5.8 g $COD_{removed}$ L^{-1} day^{-1}, respectively, based on attainable net fluxes. For the duration of this run of more than one month under these operational conditions, before the systems were terminated on day 308, both systems still showed high R_s and R_t of approximately 87 and 99 %, respectively.

6.2.2 Flux, transmembrane pressure and membrane permeability

Attainable net flux, suction pressure (transmembrane pressure, TMP) and average membrane permeability profiles during the experiments are shown in Figure 6-6 and Figure 6-7. Average net flux, TMP and permeability of each operational run is shown in Table 6-3.

In the start-up period in run 1, initial net flux for both reactors was set at around 3.5 LMH with a similar initial digestate inoculum of approximately 5,500 mg TSS L^{-1} and without excess sludge wasting. Both reactors could maintain a net flux of 3.5 LMH with suction pressures below 0.015 bar (reported as absolute value) for almost 30 days when the TSS concentration in both reactors increased to about 6,500 mg L^{-1}. Thereafter, the suction pressure of the GSAnMBR slightly increased to 0.030 bar resulting in a fall in permeability from 412 to 150 L m^{-2} $hour^{-1}$ bar^{-1} (Figure 6-7), while for the MBAnMBR the suction pressure remained below 0.020 bar throughout 99 days of continuous operation in this run. However, from day 95, when the OLRs and TSS of both reactors reached about 4.5 g $COD_{removed}$ L^{-1} day^{-1} and 13,000 mg L^{-1}, respectively, signs of a TMP

jump were seen in which the TMP of the GSAnMBR rose to 0.045 bar. Therefore, in an attempt to control TSS concentration regular daily sludge wastage strategy was applied in the next run.

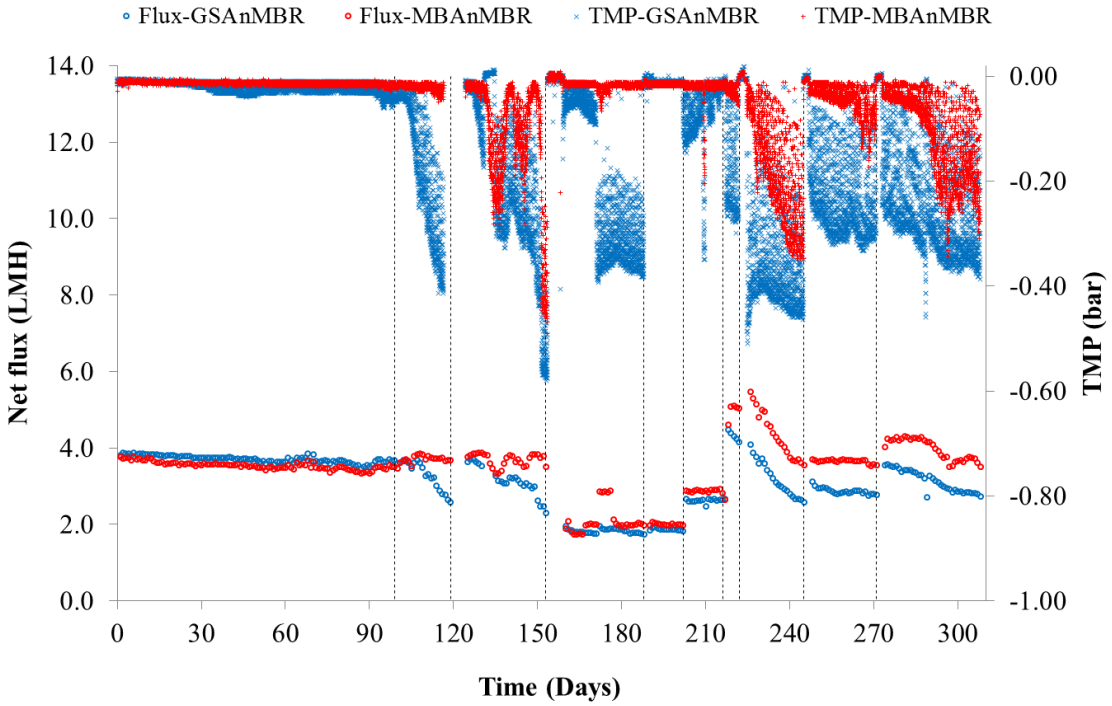

Figure 6-6 Attainable net flux and transmembrane pressure for 5 L min^{-1} sparging rate (vertical dashed lines represent the end of each run)

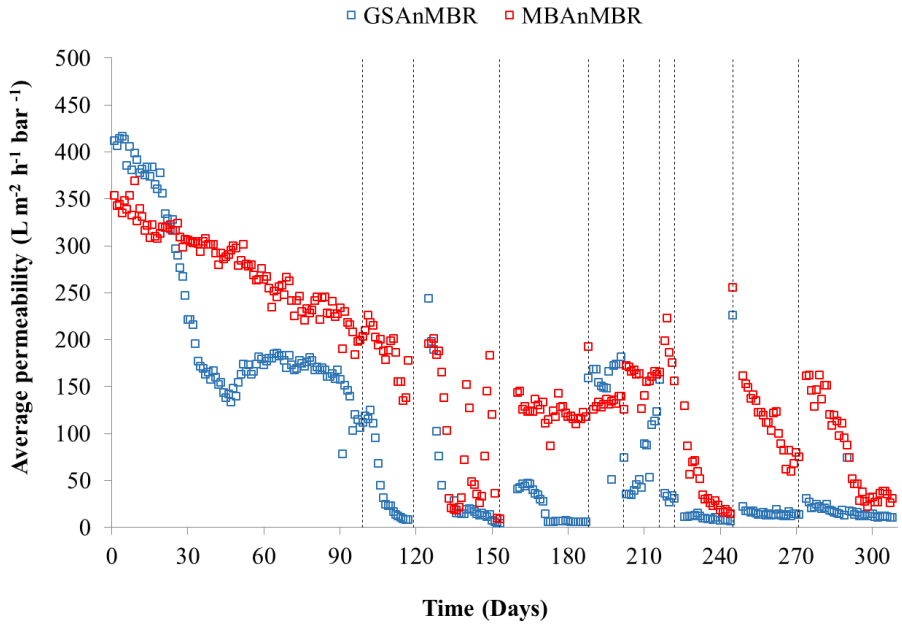

Figure 6-7 Average membrane permeability profiles (vertical dashed lines represent the end of each run)

Table 6-3 Average attainable net flux and membrane permeability of each operational run

Run (no.)	SRT (day)		Net Flux (L m^{-2} $hour^{-1}$)		Permeability (L m^{-2} $hour^{-1}$ bar^{-1})		HRT (hour)	
	R1	R2	R1	R2	R1	R2	R1	R2
1	>1,200	>1,200	3.71 ± 0.09	3.54 ± 0.10	221.4	278.2	17.8 ± 0.4	18.6 ± 0.5
2	42	32	3.29 ± 0.38	3.71 ± 0.10	47.9	187.3	20.4 ± 2.5	17.8 ± 0.5
3	23	20	3.13 ± 0.38	3.69 ± 0.17	45.0	90.9	21.4 ± 2.8	17.9 ± 0.8
4	>1,200	240	1.83 ± 0.06	2.11 ± 0.36	24.5	125.7	36.2 ± 1.2	32.1 ± 4.6
5	106	80	1.87 ± 0.03	2.00 ± 0.03	148.8	132.5	35.3 ± 0.6	33.0 ± 0.4
6	127	99	2.62 ± 0.05	2.88 ± 0.03	72.8	160.0	25.2 ± 0.5	22.9 ± 0.2
7	55	52	4.04 ± 0.68	4.59 ± 0.97	32.4	187.9	16.9 ± 3.9	15.2 ± 4.8
8	120	112	3.18 ± 0.46	4.33 ± 0.62	21.0	53.3	21.2 ± 3.0	15.5 ± 2.1
9	80	80	2.87 ± 0.09	3.65 ± 0.05	15.2	109.4	23.0 ± 0.7	18.1 ± 0.2
10	55	55	3.14 ± 0.29	3.97 ± 0.28	18.2	81.8	21.2 ± 1.9	16.7 ± 1.2

Note: 1) R1 is GSAnMBR and R2 is MBAnMBR, 2) values show in table represent the average ± standard deviation

Daily sludge wastage corresponding to SRT of 42 and 32 days was conducted for the GSAnMBR and MBAnMBR, respectively, from day 100 to day 119 in run 2. Although TSS for both reactors could be controlled to below 13,000 mg L^{-1}, the TMP still increased. This was particularly so for the GSAnMBR, in which TMP jumped dramatically from 0.045 to more than 0.400 bar between day 106 and day 119. This caused a fall in net producible flux from 3.6 to 2.6 LMH, whilst the MBAnMBR could still achieve a net attainable flux of 3.7 LMH under a TMP below 0.05 bar. The sudden rise in TMP in the GSAnMBR was initially thought to be caused by gel/cake layer build up after long-term operation of about 4 months.

Hence, the membrane panel from the GSAnMBR was removed for chemical cleaning on day 120. This result demonstrated that using non-adsorbent granules as a scouring agent is an effective method to control gel/cake layer forming in AnMBR operation.

In run 3, although the GSAnMBR was reset with a similar TSS and initial net flux to the previous run, a sharp increment in TMP to about 0.170 bar was observed with a diminution in flux to 3

LMH. This was despite the fact that the GSAnMBR membrane had just received chemical cleaning, and was operating as short SRT. This result implies that the rapid fouling built-up was not external fouling caused by gel/cake formation. Therefore, the reactor was stopped operation for 4 days, then started again on day 135 with the same conditions as from the beginning run. However, TMP rose suddenly to about 0.310 bar since the first day of filtration. Thereafter, TMP continuously increased to more than 0.580 bar along with a decrease in net flux to 2.3 LMH in association with intense whitish foam formation inside the reactor on day 153. For MBAnMBR, which had been operated continuously from day 125, TMP rose sharply from below 0.030 to 0.300 bar on day 136. Subsequently, TMP continued to increase to almost 0.500 bar, concurrently with the fall in total COD removal and signs of system failure (severe whitish foam forming and low biogas production) observed at the end of the run on day 153. As mentioned above, the major reason for unstable systems performance in this run was believed to be the very low SRTs applications that caused washout of active microorganisms. This indicated that this unstable condition impacted not only on system efficiencies but also on mixed suspension rheology which directly affected the digestate filterability. In the MBAnMBR, however, which had experienced more severe operating conditions (shorter SRT since run 2 with similar OLR and no chemical cleaning application), a net achievable flux of 3.3 - 3.8 LMH and average permeability of 90.9 L m^{-2} $hour^{-1}$ bar^{-1} (Table 6-3) was still achieved. This result is in agreement with Lee, Kang and Lee (2006) who used virgin polyurethane cubes coated with activated carbon (surface area of 35,000 m^2 m^{-3}) as the biofilm carriers for submerged hollow fibre AeMBR. Their findings showed that foulant could be mitigated by creating collisions with membrane surface, and the filtration performance was much more dependent on physical effects of moving media than biochemical effect of mixed liquor. A similar result was obtained by Chen, Bi and Ng (2016) who introduced polypropylene gear-shaped bio-carriers for ceramic AeMBR. Their results showed that bio-carrier scouring on the membrane surface was effective in controlling fouling, and the effect of the bio-carriers depended more on mechanical abrasion than the physio-chemical properties of mixed liquor suspension.

In run 4, the recovery run, feeding of the systems and permeate extraction started on day 160. Both reactors had the same initial net flux of about 2.0 LMH which was lower than applied in the previous run in an effort to reduce OLRs. From day 160 to day 171, the MBAnMBR showed higher permeability in the range of 110 - 144 L m^{-2} $hour^{-1}$ bar^{-1} compared to 15 - 16 L m^{-2} $hour^{-1}$ bar^{-1} for the GSAnMBR. On day 172 net fluxes for the GSAnMBR and MBAnMBR were changed to 2.0 and 2.9 LMH, respectively. On day 176, however, the peristatic pump of the MBAnMBR failed. Hence, from day 177 onwards, permeate extractions for both reactors were performed by one multi-head peristatic pump with the same rotating pump speed. From day 177 - day 188, the MBAnMBR has a higher net flux of about 2.0 LHM with much lower TMP of around 0.018 bar

(116 - 129 L m^{-2} $hour^{-1}$ bar^{-1} permeability), when compared to 1.8 - 1.9 LMH and 0.370 bar (6.0 - 6.4 L m^{-2} $hour^{-1}$ bar^{-1} permeability) for the GSAnMBR. Both reactors still showed the COD removal instabilities, and the TSS reached more than 13,000 mg L^{-1}. Therefore, a certain amount of mixed suspension was extracted to reduce the TSS concentrations in both reactors to about 9,500 mg L^{-1} using tap water, before starting the new run.

Run 5 was started on day 190 and initially the net flux of both reactors was adjusted to about 2.0 LMH. During the 12 days in this run, both reactors could maintain net producible fluxes in a range of about 1.8 - 2.0 LMH with suction pressures below 0.025 bar (average permeability of 133 - 149 L m^{-2} $hour^{-1}$ bar^{-1}). In comparison to run 4, similar net fluxes could be produced. In particular for the GSAnMBR this net flux could be generated under a far lower suction pressure of below 0.025 bar, compared to 0.360 bar. This is potentially due to the lower TSS concentrations, in the range of 9,900 - 11,200 mg L^{-1} compared to 11,000 - 13,500 mg L^{-1} in run 4.

Therefore, in run 6 initial net fluxes for both reactors were increased to 2.5 - 2.9 LMH by pump speed adjustment from day 203 onwards. For around 2 weeks, the MBAnMBR could maintain a net producible flux of 2.9 LMH with a TMP below 0.020 bar (permeability of 166 L m^{-2} $hour^{-1}$ bar^{-1}). At the same time, the GSAnMBR showed a net flux of about 2.8 LMH with an initial TMP of around 0.130 bar (permeability of 35 L m^{-2} $hour^{-1}$ bar^{-1}) at the early stage of this run; after this, TMP gradually reduced to approximately 0.025 bar by the end of the run on day 216. This result showed that high net produced fluxes with low suction pressures could be achieved for both reactors (average permeability of 73 - 160 L m^{-2} $hour^{-1}$ bar^{-1}). On day 210, the sudden TMP jump was caused by thermocirculator failure, which made temperatures inside both reactors drop to about 18 °C. However, the systems were be able to recover within one day. At the end of this run, TSS concentrations in both reactors were again reduced to approximately 9,000 mg L^{-1} using tap water before starting the next run.

In run 7, expected net fluxes were increased to 4.3 and 5.0 LMH with SRTs of 55 and 52 days for the GSAnMBR and MBAnMBR, respectively, from day 218 onwards. Due to the sudden rise in flux, that caused an OLR shock under relatively low SRT, the TMP in the GSAnMBR jumped to around 0.300 bar whilst TMP for the MBAnMBR remained below 0.045 bar (average permeability of 32.4 for GSAnMBR and 188 L m^{-2} $hour^{-1}$ bar^{-1} for MBAnMBR). In addition, signs of system failure were again observed. As a result, the systems were stopped for 4 days before starting the new run.

Run 8 started from day 225 with adjustment of the initial net fluxes to 4.1 and 5.5 LMH and SRTs to 120 and 112 days for the GSAnMBR and MBAnMBR, respectively. For the GSAnMBR, TMP rose sharply to about 0.510 bar from the first day of filtration. Thereafter high suction pressures in the range of 0.420 - 0.450 bar seen, along with a continuous fall in net flux production from 4.1 to

2.6 LMH during the 20 days of operation in this run. The high initial net flux of 5.5 LMH (instantaneous flux of 6.9 LMH) could not be maintained for the MBAnMBR either. Net flux for the MBAnMBR gradually dropped to 3.5 LMH, while TMP rose continuously from 0.088 - 0.035 bar by the end of the run. This result indicated that net fluxes of 4.1 LMH for the GSAnMBR and 5.5 LMH for the MBAnMBR (which were controlled by the same suction pump speed of 6 rpm from the same pump throughout this run) are probably higher than the critical fluxes that could sustain producible net flux without a jump in TMP under these experimental conditions. With the same fixed permeate extraction and biogas sparging intensity under similar operational conditions, however, the MBAnMBR could produce higher net flux by at least 34 - 35 % with lower suction pressure when compared to the conventional GSAnMBR in this run (average permeability of 21 for GSAnMBR and 53 L m^{-2} $hour^{-1}$ bar^{-1} for MBAnMBR). On day 245, when the TSS in both reactors was above 12,000 mg L^{-1}, digestate concentrations for both systems were reduced to about 9,000 - 9,500 mg TSS L^{-1} again by tap water before starting the next run.

In Run 9, feeding and permeate extraction started on day 248 with the same SRT of 80 days adopted for both reactors. The peristatic pump draw speed was adjusted to 4.5 rpm which produced an initial net flux of 3.0 LMH for the GSAnMBR and 3.7 LMH for the MBAnMBR. Throughout about 3 weeks of operation in this run, the attainable net flux for the GSAnMBR fell slightly from 3.0 to 2.8 LMH under suction pressures of 0.250 - 0.320 bar (average permeability of 15.2 L m^{-2} $hour^{-1}$ bar^{-1}). The MBAnMBR flux fell slightly from 3.7 to 3.5 LMH with a lower TMP of 0.033 to 0.173 bar (average permeability of 109.4 L m^{-2} $hour^{-1}$ bar^{-1}). In this run, using non-adsorbent granules as a scouring agent could enhance flux production by 23 - 25 % (resulting in a 7.2-fold improvement in average permeability), while constant flux and relatively low TMP were sustained for about 23 days. At the end of this run on day 271 when the TSS concentration for the GSAnMBR and MBAnMBR reached about 11,000 and 13,000 mg L^{-1}, respectively, TSS concentrations for both reactors were adjusted to about 9,000 mg L^{-1} again before starting the next run.

Run 10 started on day 274. Initial net fluxes were regulated to 3.6 LMH for the GSAnMBR and 4.3 LMH for the MBAnMBR with the same SRT of 55 days applied for both reactors. Net flux of about 4.2 LMH for the MBAnMBR could be achieved for 14 days (day 274 - day 288) with the TMP below 0.090 bar when TSS concentration was below 12,000 mg L^{-1}. Thereafter, from day 289 onwards (when the TSS exceeded 13,000 mg L^{-1}) suction pressure suddenly increased to about 0.250 - 0.340 bar, coinciding with a decline in produced net flux to 3.5 - 3.7 LMH which resulted in a decrease in permeability from about 100 to 30 L m^{-2} $hour^{-1}$ bar^{-1} (Figure 6-7) until the end of the run on day 308. For the GSAnMBR, TMP suddenly rose to around 0.280 bar from the first day of filtration. Subsequently, suction pressure gradually increased to about 0.390 bar in parallel with a slow reduction in net flux to 2.7 LMH leading to average permeabilities in the

range of 20 - 30 L m^{-2} $hour^{-1}$ bar^{-1} until day 308 when both systems were terminated. It should be noted that the sudden TMP jump and fall in net flux for the GSAnMBR on day 289 was caused by a blockage in the feeding line which was caused by slime, fat and grease build-up after long-term operation. Throughout this run, however, the attainable net flux for the MBAnMBR was 17 - 30 % higher in comparison with the GSAnMBR under similar operating conditions.

Based on these results, it can be seen that both reactors could produce an attainable net flux of about 3.5 - 3.8 LMH for almost 4 months with TMP below 0.060 bar (run 1 and 2) under TSS concentration in the range of 5,500 - 14,000 mg L^{-1} with the same given 5 L min^{-1} of biogas sparging intensity. Nevertheless, most of the time, the MBAnMBR showed better net flux production with lower TMP and higher permeability when compared to the GSAnMBR under similar experimental parameters, even with under unhealthy and unstable conditions (run 2 and 3). The recommended sustainable fluxes to maintain net producible flux without severe fouling for long-term operation based on this study are 2.8 and 3.7 LMH for the GSAnMBR and MBAnMBR, respectively (run 6, 9 and 10).

The sustainable fluxes determined in the current study are conservative compared to some literature values due to differences in membrane properties, influent sources, mix suspension characteristics and operational conditions. Saddoud *et al.* (2006) reported successful operation of a staged anaerobic reactor coupled with crossflow tubular ceramic membrane separation treating cheese whey at OLR of up to 19.78 g COD L^{-1} day^{-1} (influent COD of 68.6 g L^{-1}) with a flux of 139.5 LMH under a TMP of 1.75 bar. However, submerged AnMBR used in this study, which it is generally desirable to operate with lower suction pressure compared to crossflow MBR, could sustain net fluxes in the range of 1.8 - 5.3 LMH for long-term operation at far lower TMP. Buntner, Sánchez and Garrido (2013) operated UASB coupled with hollow fibre AeMBR for synthetic dairy wastewater treatment (skimmed milk- basis with influent COD in the range of 1,000 - 1,200 mg L^{-1}) and showed that average fluxes of 13 - 19 LMH could be achieved. Although these values were lower than those observed in AeMBRs, they were much higher than those found in methanogenic AnMBR.

Although the attainable net fluxes found in this study are lower than the general value of 4 - 6 LMH for a submerged flat-sheet AnMBR system treating industrial wastewater reported by Judd (2016), similar membrane fluxes have been seen in high-rate AnMBRs treating other wastewaters. Jensen *et al.* (2015) reported sustainable permeate flux in the range between 3 and 7 LMH for high FOG and particulate COD slaughterhouse wastewater in submerged HF AnMBR with OLRs of 3 - 3.5 g COD L^{-1} day^{-1} and an active biomass inventory of 30,000 - 40,000 mg L^{-1} MLSS. Galib *et al.* (2016) could sustain permeate fluxes of 1.14 - 3.98 LMH with OLRs of 0.4 - 3.2 g COD L^{-1} day^{-1} for an immersed HF AnMBR treating meat-processing wastewater under the

biomass concentration of 1,920 - 2,630 mg L^{-1} TSS for about 38 weeks of operation. Applicable fluxes between 2 and 5 LMH depending on operational conditions were also achieved by Spagni *et al.* (2010) who used flat-sheet AnMBR for synthetic wastewater treatment. OLRs in the range 1.5 - 13 g COD L^{-1} day^{-1} to treat synthetic wastewater (whey and sucrose -basis) and 7 - 13 g COD L^{-1} day^{-1} (entirely sucrose -basis). The recommended sustainable net fluxes of 2.8 and 3.7 LMH in this study are slightly lower than the 2 - 5 LMH reported by Spagni *et al.* (2010). Nevertheless, with a similar membrane configuration and membrane packing density (single A4 Kubota membrane panel), recommended net fluxes in this study could be maintained long-term operation under a lower biogas sparging rate of 5 L min^{-1} when compared to the 20 L min^{-1} applied in Spagni *et al.* (2010) study.

According to the current results, using non-adsorbent particles coupled with biogas sparging as scouring media in AnMBR offers considerable benefits for fouling mitigation. Under stable operating conditions, attainable net fluxes could be improved by up to 17 - 35 % in comparison with a conventional GSAnMBR operated under the same biogas sparging intensity, whilst comparatively high organic treatment efficiencies and superior permeate qualities could still be achieved. This mechanical cleaning process, in which addition of chemical reagents, media regeneration and re-dosing are not required, could be applied successfully in AnMBR as a flux enhancer and for fouling reduction purposes, or this approach could even be used to upgrade the existing conventional GSAnMBR, in order to achieve effective exploitation of the energy input for gas sparging. Additionally, the results also demonstrated that MBAnMBR could operate for more than 300 days without any backflushing or chemical cleaning. This implies that this application may prolong the intervals between chemical cleaning accompanied by a reduction in total operational expenditure per m^3 of permeate production.

6.2.3 Organic loading rate (OLR) and food-to-microorganisms (F/M) ratio

OLR and F/M for the entire study period are shown in Figure 6-8. Average OLRs and F/M ratios for each operational run are shown in Table 6-4.

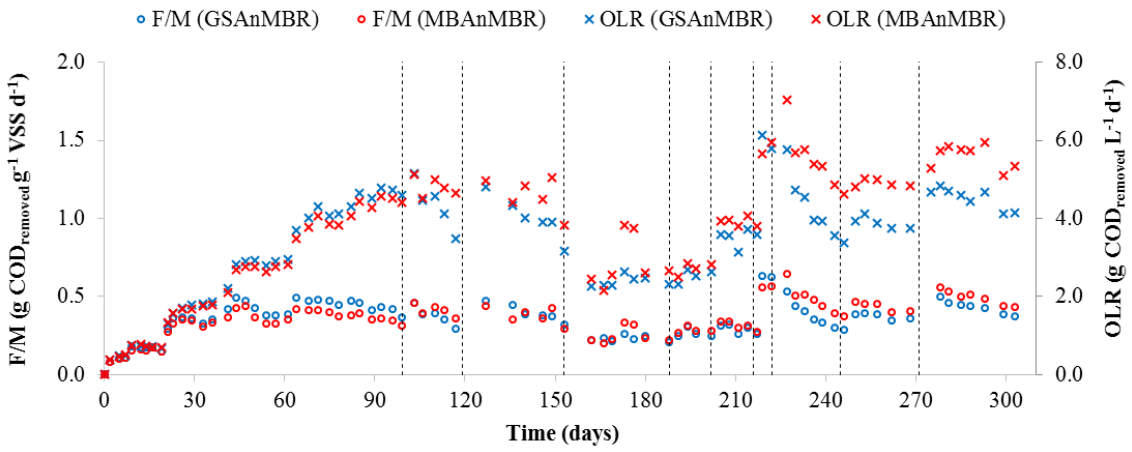

Figure 6-8 OLR and F/M ratio profiles (vertical dashed lines represent the end of each run)

From Figure 6-8, it can be seen that the trends in F/M (i.e. sludge organic loading rate, SOLR) are similar to those in OLR, since both parameters are highly related to each other (F/M = OLR/MLVSS). For the early stage of experiments in run 1, OLR for both reactors rose from about 0.7 to 4.5 g $COD_{removed}$ L^{-1} day^{-1} by incrementing the fed influent strength to the target concentration of 3,600 - 3,900 mg COD L^{-1} while the systems were operated under constant flux mode. In the same period, F/M ratios for both reactors rose from about 0.18 - 0.35 g $COD_{removed}$ g^{-1} VSS day^{-1} from day 15 to day 35. Thereafter, from day 40 to the end of run 1 on day 99 when the R_t values of both reactors reached 97 - 98 %, OLRs increased to about 4.5 g $COD_{removed}$ L^{-1} day^{-1} for both systems. F/M ratios fluctuated in the range of 0.38 - 0.49 g $COD_{removed}$ g^{-1} VSS day^{-1} for the GSAnMBR and 0.33 - 0.42 g $COD_{removed}$ g^{-1} VSS day^{-1} for the MBAnMBR due to the increase in OLR and MLVSS concentrations at the long SRTs of > 1,200 days.

From run 2 to until the end of the experiments, when influent concentrations were fixed in the range of 3,600 - 3,900 mg COD L^{-1}, the OLR and F/M depended directly on the attainable net fluxes, organic treatability and MLVSS concentrations that were controlled by excess sludge wasting rates.

Throughout the experimental duration, F/M for both reactors was between 0.25 to 0.65 g $COD_{removed}$ g^{-1} VSS day^{-1} which falls in the range of typical F/M ratios reported in the literature for AnMBR treating dairy wastewater at 0.2 - 0.6 g $COD_{removed}$ g^{-1} VSS day^{-1} (Arros-Alileche *et al.*, 2008). However, unstable treatment performance and filterabilities were seen in run 2 and 3, even though the reactors were operated with moderate F/M in the range of 0.29 - 0.46 and 0.32 - 0.48 g $COD_{removed}$ g^{-1} VSS day^{-1} for the GSAnMBR and 0.36 - 0.46 and 0.30 - 0.44 g $COD_{removed}$ g^{-1} VSS day^{-1} for the MBAnMBR, respectively. This might be because of the washout of active microorganisms due to very short SRTs as mentioned earlier. In the recovery period in run 4, which was carried out at a relatively low F/M of 0.20 - 0.26 g $COD_{removed}$ g^{-1} VSS day^{-1} (OLR of

2.26 - 2.64 g $COD_{removed}$ L^{-1} day^{-1}) for the GSAnMBR and 0.20 - 0.34 g $COD_{removed}$ g^{-1} VSS day^{-1} (OLR of 2.16 - 3.84 g $COD_{removed}$ L^{-1} day^{-1}) for the MBAnMBR with high SRT of >1,200 and 240 days, respectively, instabilities were still seen in both treatment efficiency and filterability.

Although successful AnMBRs operated with soluble high-strength industrial wastewater and low-strength domestic wastewater have been reported in the literature, there are certain difficulties in operating AnMBRs fed with particulate influent COD by considering only F/M ratios. In particular, for synthetic dairy wastewater (whole milk powder-basis) that contains a high MLVSS/MLSS ratio, using only the MLVSS parameter does not allow any distinction distinguishing between particulate influent and active microorganisms.

Dereli *et al.* (2012) proposed that AnMBR could theoretically be operated at high OLRs and short HRTs. The effect of OLR should be determined together with SRT and biomass activities, however, since the OLR of the system is not an independent parameter. In fact, for a single-stage AnMBR, several parameters are not stand-alone factors. Especially, under a fixed maximum influent concentration and membrane packing density inside the reactor, the attainable flux, HRT, OLR, SRT, F/M, MLVSS concentration and biomass activity are interconnected parameters which strongly affect both treatment capabilities and fouling aspects.

To achieve high performance in treating wastewater at high OLRs, the MLVSS and sludge activity should be high in order to enhance the biodegradation process (Melin *et al.*, 2006), while low F/M ratios still need to be maintained to prevent organic overload. Based on this, it may be necessary to increase the MLVSS concentration by operating with long SRT to prevent high F/M ratios. This tends to promote membrane fouling, however, due to high suspended solids and high sludge viscosity (Jiang *et al.*, 2008).

Huang, Ong and Ng (2011) studied the effect of HRT and SRT on treatment of low-strength synthetic wastewater (glucose basis with influent concentration of 550 mg COD L^{-1}) by submerged AnMBR with SRTs of 30, 60 and infinite days at HRTs of 12, 10 and 8 hours, corresponding to OLRs of 1.1 - 1.65 g COD L^{-1} day^{-1}. They reported that a shorter of HRT associated with longer SRT enhanced SMPs and also the growth of biomass and augmentation of MLSS, resulting in stimulation of fouling built up.

On the other hand, if the F/M ratio is too low this could cause very low biomass growth or even zero generation (Arros-Alileche *et al.*, 2008), leading to microbial starvation and deflocculation of sludge (Lobos *et al.*, 2005). This behaviour, however, may never occur in real high-rate AnMBR operations.

Table 6-4 Average OLRs and F/M ratios of each operational run

Run (no.)	SRT (day)		OLR ($g\ COD_{removed}\ L^{-1}_{reactor}\ day^{-1}$)		VSS ($mg\ L^{-1}$)		F/M ($g\ COD_{removed}\ g^{-1}VSS\ day^{-1}$)	
	R1	R2	R1	R2	R1	R2	R1	R2
1	>1,200	>1,200	2.57 ± 1.53	2.46± 1.43	6,611 ± 2,761	7,219± 3,208	0.35 ± 0.13	0.31± 0.11
2	42	32	4.36 ± 0.61	4.82 ± 0.25	11,552 ± 228	11,758± 665	0.38± 0.06	0.41 ± 0.04
3	23	20	4.02 ± 0.54	4.60 ± 0.45	10,133 ± 296	12,197 ± 599	0.40 ± 0.06	0.38 ± 0.05
4	>1,200	240	2.39 ± 0.14	2.86 ± 0.65	10,332± 500	11,349± 549	0.23± 0.02	0.25 ± 0.05
5	106	80	2.54 ± 0.16	2.72 ± 0.16	9,478 ± 667	9,476 ± 456	0.27 ± 0.03	0.28± 0.02
6	127	99	3.52 ± 0.22	3.91± 0.11	12,130± 951	12,576 ± 1,022	0.29 ± 0.03	0.31 ± 0.03
7	55	52	5.96 ± 0.24	5.81 ± 0.20	9,393± 284	9,897 ± 756	0.63 ± 0.00	0.56 ± 0.01
8	120	112	4.26± 0.82	5.53± 0.79	11,121± 689	11,371± 937	0.38± 0.09	0.48 ± 0.09
9	80	80	3.88 ± 0.15	4.90 ± 0.10	10,281 ± 541	11,169± 1,239	0.38 ± 0.02	0.44 ± 0.03
10	55	55	4.53± 0.26	5.60 ± 0.31	10,108± 752	10,998 ± 1,093	0.43 ± 0.04	0.50± 0.05

Note: 1) R1 is GSAnMBR and R2 is MBAnMBR, 2) values show in table represent the average ± standard deviation

A high F/M ratio provides a high driving force for microbial activity, biomass growth and overall rates for substrate to methane conversion (Lobos *et al.*, 2008), a too high F/M ratio may upset the equilibrium between hydrolysis and methanation processes, disturbing the microbial ecology and resulting in biomass deflocculation and process instability (Liu *et al.*, 2012). High F/M could also stimulate EPS formation due to the high substrate utilisation by microorganisms, which causes poor sludge filterabilities (Meng and Yang, 2007).

Liu *et al.* (2012) operated AnMBRs with HF membranes submerged in UASB reactors without fouling control to treat synthetic low-strength municipal wastewater (glucose-basis). Two AnMBRs were operated under a high F/M ratios of 3.8 g COD g^{-1} VSS day^{-1} (HAnMBR) and a low ratio of 0.1 g COD g^{-1} VSS day^{-1} (LAnMBR). Their results demonstrated that cake resistance represented over 98 % of the total filtration resistance, and fouling in the HAnMBR was more intense than that in the LAnMBR. High SMP and high ratios of tightly-bound to loose-bound EPS were found in the HAnMBR's cake layer, which accounted for higher cake resistance in comparison with LAnMBR. A larger amount of fine particles caused by sludge deflocculation, which in turn accelerated the build-up of serious fouling, was seen in the HAnMBR.

OLR is also a factor that, depending on other set-up conditions, plays an important role in system stability and VFA accumulation in high-rate AnMBR. For example, Saddoud and Sayadi (2007) used an AnMBR as a high-rate system for slaughterhouse wastewater treatment at relatively high OLRs of 4.4 - 13.3 g COD L^{-1} day^{-1}. They reported system failure at an OLR of 16.3 g COD L^{-1} day^{-1} due to the accumulation of VFAs that caused inhibition of methanogenesis in a single stage AnMBR. Similar results for the negative effects of VFA accumulation were also reported by Wijekoon, Visvanathan and Abeynayaka (2011) which showed that when OLR increased, system of performance may deteriorate due to the inhibition of microbial activity caused by VFA accumulation.

Wei *et al.* (2014) operated anaerobic CSTR coupled with side-stream submerged HF anaerobic filtration using sludge recirculation and biogas sparging for fouling control to treat synthetic municipal wastewater (starch, milk powder and yeast -basis) with influent concentrations of 400 - 5,000 mg COD L^{-1} over about 120 days. Based on their results, they proposed the concept of a sustainable OLR and F/M ratio at 6.0 g COD L^{-1} day^{-1} and 0.63 g COD g^{-1} VSS day^{-1} under the attainable flux of 6 LMH to optimise the potential for energy recovery from a typical municipal wastewater through mesophilic AnMBR. When compared to the study by Wei *et al.* (2014), and the F/M ratio below 0.5 reported by Le-Clech, Chen and Fane (2006), the maximum OLR of 7.0 g $COD_{removed}$ L^{-1} day^{-1} and F/M ratio of 0.68 g $COD_{removed}$ g^{-1} VSS day^{-1} in this study (Figure 6-8 and Table 6-4) are in agreement with these recommended ranges.

6.2.4 Biogas production

Biogas production rates, volumetric methane production rates (VMP) and methane yields are presented in Figure 6-9, Figure 6-10 and Figure 6-11, respectively. Average methane production for each experimental run is shown in Table 6-5.

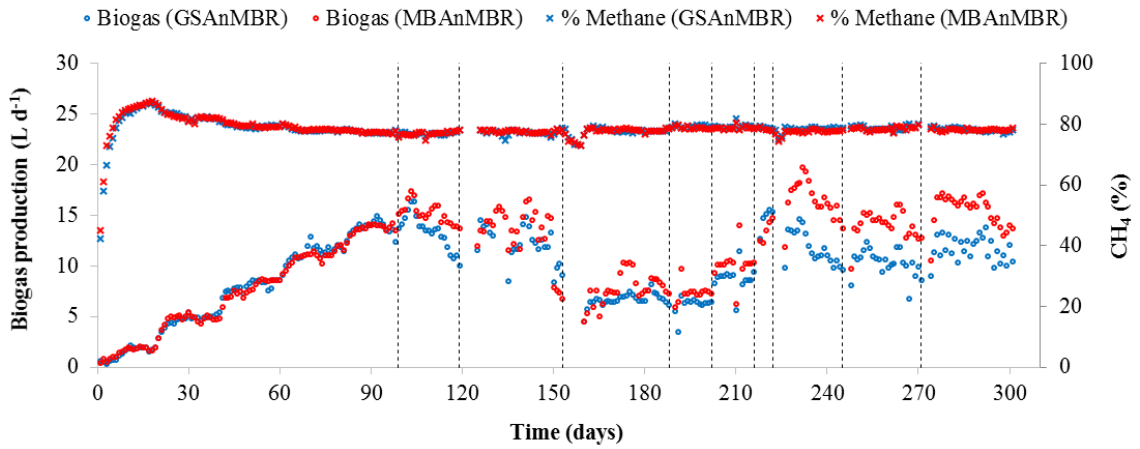

Figure 6-9 Biogas productions (vertical dashed lines represent the end of each run)

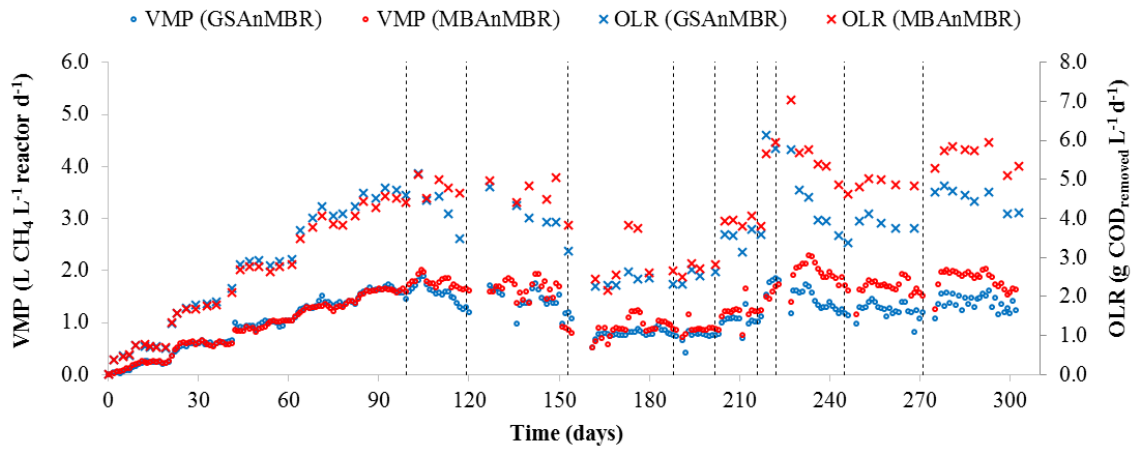

Figure 6-10 Methane productions (vertical dashed lines represent the end of each run)

Figure 6-9 shows the biogas production and methane content in the produced biogas of each reactor. Before starting operation, the reactor headspaces were purged with pure nitrogen gas (N_2). Thereafter, when generation of biogas began, the percentage of N_2, and other mixed gases started decreasing, while CO_2 and CH_4 percentages started increasing. Methane content in the biogas increased from about 40 % from the first day to about 85 % on day 19 in run 1. Thereafter, the methane content dropped slightly to approximately 80 % and then remained constant in the range of 77 - 80 % throughout the whole operating period for both reactors. High average methane contents of 77 - 79 %

for both the GSAnMBR and MBAnMBR, were observed from day 19 until the end of experiments (Table 6-5), even during the period of unstable COD removal performance in run 3 and 4.

Biogas production and VMP rates present the same trend as the OLRs (Figure 6-9 and Figure 6-10). This is similar to the results of Saddoud, Hassaïri and Sayadi (2007) and An *et al.* (2009b) who reported that the biogas yield from AnMBR rose linearly with an increment in OLR. Biogas production of 5.7 - 15.6 L day^{-1} (VMP of 0.68 - 1.86 L CH_4 L^{-1} reactor day^{-1}) and 5.3 - 19.7 L day^{-1} (VMP of 0.63 - 2.30 L CH_4 L^{-1} reactor day^{-1}) under OLRs of 3.2 - 6.1 and 2.2 - 7.0 g $COD_{removed}$ L^{-1} day^{-1} for the GSAnMBR and MBAnMBR, respectively, were found in this study throughout the experimental period.

Under similar operating conditions and in periods of relatively stable organic treatment performance such as in run 8, 9 and 10, the VMPs from the MBAnMBR were higher than those from the GSAnMBR (Figure 6-10 and Table 6-5) due to the higher achieved OLRs caused by higher producible net flux.

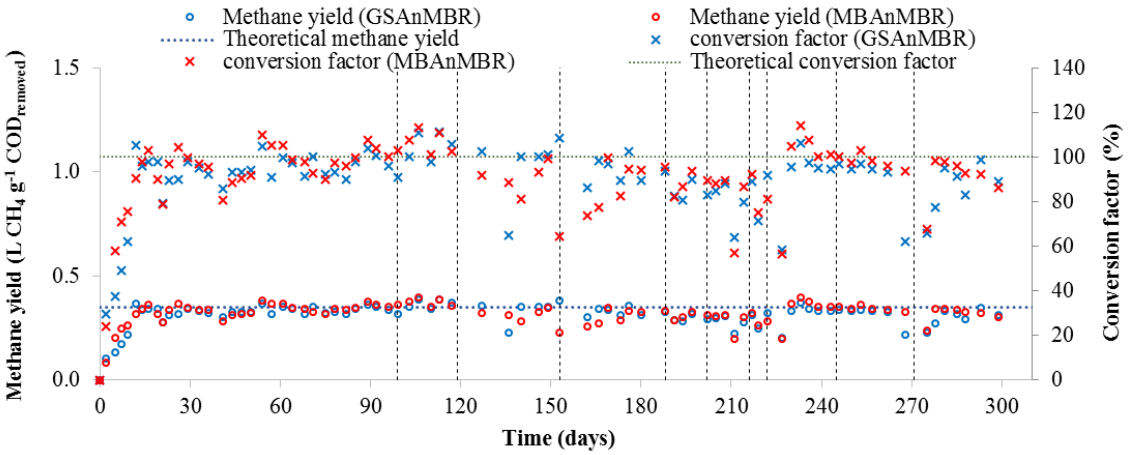

Figure 6-11 Methane yields (vertical dashed lines represent the end of each run)

These VMPs are relatively high when compared to values for methane production from low-strength wastewater treated by AnMBR. For example, Huang, Ong and Ng (2011) reported VMPs of 0.10, 0.14 and 0.20 L CH_4 L^{-1} reactor day^{-1} for treating synthetic domestic wastewater (glucose -basis) at SRTs of 30, 60 and infinite days, with OLRs of 1.10 - 1.65 g COD L^{-1} day^{-1}. They stated that a shorter HRT or longer SRT increased biogas production due to the increment of OLR or enhanced dominancy of methanogens.

Table 6-5 Average methane production of each operational run

Run (no.)	OLR ($g\ COD_{removed}\ L^{-1}_{reactor}\ day^{-1}$)		Methane content (%)		VMP ($m^3CH_4\ m^{-3}_{reactor}\ day^{-1}$)		SMP ($m^3CH_4\ kg^{-1}COD_{removed}$)		Theoretical methane conversion factor (%)	
	R1	R2	R1	R2	R1	R2	R1	R2	R1	R2
1	2.57 ± 1.53	2.46 ± 1.43	79.38 ± 5.43	79.77 ± 5.02	0.93± 0.51	0.92 ± 0.50	0.31 ± 0.06	0.32 ± 0.06	88.61± 18.29	91.95 ± 16.74
2	4.36 ± 0.61	4.82 ± 0.25	76.98± 0.45	76.98 ± 0.73	1.56± 0.20	1.78± 0.11	0.37± 0.02	0.37 ± 0.02	105.21 ± 6.03	107.05 ± 5.39
3	4.02 ± 0.54	4.60 ± 0.45	77.30 ± 0.84	77.60 ± 0.46	1.42± 0.22	1.55± 0.32	0.34 ± 0.05	0.30± 0.04	96.22± 15.64	86.48 ± 12.27
4	2.39 ± 0.14	2.86 ± 0.65	77.44 ± 1.55	77.43± 1.57	0.79 ± 0.08	0.92± 0.18	0.33 ± 0.02	0.31 ± 0.04	93.81± 5.70	88.22 ± 10.14
5	2.54 ± 0.16	2.72 ± 0.16	79.38± 0.42	78.84 ± 0.43	0.74 ± 0.10	0.88 ± 0.10	0.29 ± 0.01	0.31 ± 0.02	84.13 ± 4.05	88.02 ± 5.02
6	3.52 ± 0.22	3.91 ± 0.11	79.34± 0.82	78.80 ± 0.59	1.05 ± 0.13	1.21 ± 0.18	0.28 ± 0.04	0.29 ± 0.05	81.25± 10.22	82.82 ± 14.65
7	5.96 ± 0.24	5.81 ± 0.20	78.98± 0.37	78.42± 0.51	1.76± 0.13	1.59 ± 0.12	0.29 ± 0.05	0.27± 0.01	81.61± 14.47	78.19 ± 4.27
8	4.26 ± 0.82	5.53 ± 0.79	78.32± 0.92	77.45 ± 0.89	1.40± 0.19	1.94 ± 0.22	0.32 ± 0.05	0.34± 0.07	92.02 ± 15.42	97.81± 18.90
9	3.88 ± 0.15	4.90 ± 0.10	78.88± 0.72	78.55± 0.65	1.24± 0.15	1.68 ± 0.16	0.31± 0.05	0.34 ± 0.01	88.31± 14.66	97.70± 3.33
10	4.53 ± 0.26	5.60 ± 0.31	78.24± 0.60	78.20 ± 0.33	1.38± 0.14	1.83± 0.18	0.30± 0.04	0.32± 0.04	85.82± 11.38	90.15 ± 10.75

Note: 1) R1 is GSAnMBR and R2 is MBAnMBR, 2) values show in table represent the average ± standard deviation

As a rule of thumb, AnMBRs operating at long SRTs produce higher specific biogas yield because any reduction in SRT may decrease the extent of reactions needed for digestion stability (Chen *et al.*, 2016). For submerged AnMBRs, however, higher SRT result in a high MLSS concentration which leads to rapid cake formation and compaction that causes a decline in flux (Deng *et al.*, 2016b). Huang, Ong and Ng (2013) studied submerged AnMBR for real domestic wastewater treatment at SRTs of 30, 60 and 90 days. They reported that the maximum biogas production of 0.08 L CH_4 L^{-1} reactor day^{-1} at F/M of 0.13 g COD g^{-1} VSS day^{-1} was found at an SRT of 90 days. A longer SRT benefited biomass accumulation and biogas production: for an increase in SRT from 30 to 90 days, enhancement of hydrolysis from 35 to 56 % was identified as the major reason for more efficient acidification and methanogenesis. According to their results, however, a SRT of 60 days was recommended as giving the best treatment performance and fouling control purposes. When the SRT was increased from 60 to 90 days, the higher MLSS concentration caused more particle deposition on the membrane surface which in turn led to severe fouling.

In this study, the overall average specific methane yield (SMP) for both the GSAnMBR and MBAnMBR was in the range of 0.27 - 0.37 L CH_4 g^{-1} $COD_{removed}$, equivalent to 78 - 107 % of the theoretical methane yield (0.35 L CH_4 g^{-1} COD at STP). Values larger than the theoretical methane yield by 101 - 114 % were sometimes observed (Figure 6-11 and Table 6-5). This is potentially because the influent concentration used were sometimes lower than the actual values, since the concentration of the fed stream was calculated from the average of the freshly prepared and the left-overnight influent. This is particularly the case when the OLRs had been increased by influent concentration adjustment, flux increment or shorter SRT. Under similar operating conditions and in periods of relatively stable organic treatment performance in run 8, 9 and 10, however, the GSAnMBR showed average SMPs in the range of 0.30 - 0.32 m^3 CH_4 kg^{-1} $COD_{removed}$ (theoretical CH_4 conversion of 86 - 92 %) while the MBAnMBR gave 0.32 - 0.34 m^3 CH_4 kg^{-1} $COD_{removed}$ (theoretical CH_4 conversion of 90 - 98 %) (Table 6-5). Attainable methane yields in this study are in agreement with the reported results for high-rate anaerobic systems treating dairy industrial effluent. Saddoud, Hassaïri and Sayadi (2007) achieved SMP of 0.3 m^3 CH_4 $kg^{-1}COD_{removed}$ by applying an external cross-flow AnMBR for cheese whey wastewater treatment under mesophilic condition. Borja and Banks (1995) reported a gas production of 0.33 L g^{-1} $COD_{removed}$ under steady-state conditions from an anaerobic fluidized bed reactor treating ice-cream wastewater with an average influent concentration of 5,200 mg COD L^{-1} (BOD/COD of 0.47) at an operating temperature of 35 °C. Wang *et al.* (2009) also reported a methane yield of 0.341 m^3 CH_4 kg^{-1} $COD_{removed}$ from milk permeate effluent from dairy industry using an anaerobic moving bed biofilm reactor at 35 °C. Methane yields in the range of 0.30 - 0.35 m^3 CH_4 kg^{-1} $COD_{removed}$ which is close to theoretical methane production with methane contents in the range of 63 - 70 % were obtained under mesophilic condition by Rodgers, Zhan and Dolan (2004) who a studied moving

anaerobic biofilm reactor treating whey wastewater. A high methane yield of 0.37 m^3 CH_4 kg^{-1} $COD_{removed}$ was obtained using a high-rate down-flow anaerobic fluidized bed reactor treating dairy wastewater with an influent concentration of 3,200 mg L^{-1} and COD removal efficiency in the range of 85 - 98 % (Haridas *et al.*, 2005). Consequently, these results confirm that effluents from the dairy industry could be regarded as a high organic load waste stream with high biodegradability which provides beneficial characteristics for energy recovery from produced methane.

Other factors that may affect the maximum methane yield are dissolved methane and the fraction produced from endogenous decay. For instance, Wei *et al.* (2014) proposed a maximum theoretical methane yields of 0.382 L CH_4 g^{-1} $COD_{removed}$ for the synthetic municipal wastewater treated by AnMBR. Hu and Stuckey (2006) reported that dissolved methane can reach 15 ml L^{-1} in permeate at 35 °C. In the current study, a relatively high methane conversion of approximately 80 - 90 % (calculated from theoretical methane yields of 0.35 L CH_4 g^{-1} $COD_{removed}$), however, was achieved for both reactors under average OLRs of 2.5 - 6.0 g $COD_{removed}$ L^{-1} day^{-1} (Table 6-5). This confirms that dairy wastewater is viable for anaerobic digestion and the AnMBRs set-up conditions in this study was sufficiently healthy and robust to cope with the applied OLR.

6.2.5 Biomass evolution

MLSS concentrations during the whole operation are shown in Figure 6-12. Average total suspended solid (TSS), VSS/TSS ratios of each operational run are given in Table 6-6.

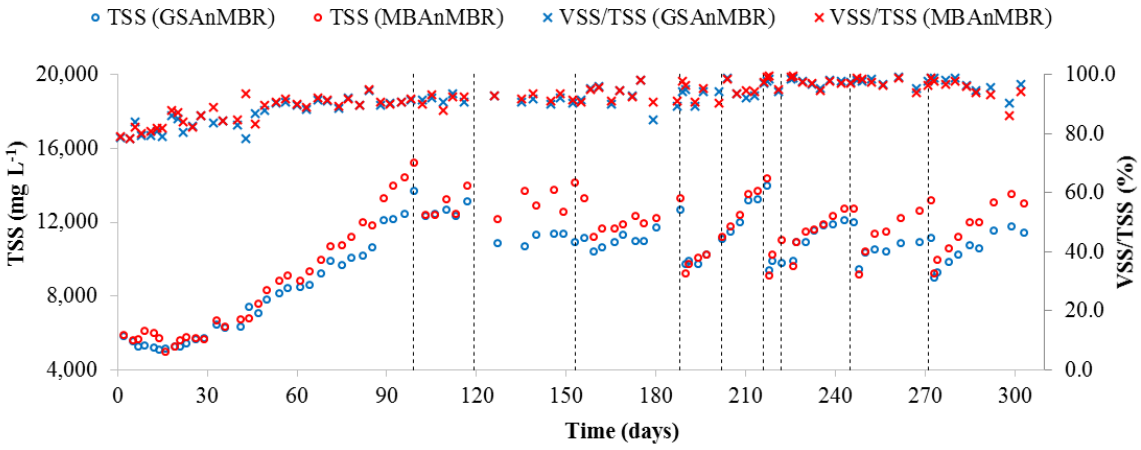

Figure 6-12 Biomass evolutions (vertical dash lines represent the end of each run)

Table 6-6 Average TSS and VSS/TSS ratios of each operational run

Run (no.)	SRT (day)		TSS (mg L^{-1})		VSS/TSS (%)		Observed biomass yield, Y_{obs}* ($gVSS\ g^{-1}\ COD_{removed}$)	
	R1	R2	R1	R2	R1	R2	R1	R2
1	>1,200	>1,200	7,813 ± 2,550	8,431 ± 3,058	86 ± 5	87 ± 5	na	na
2	42	32	12,592 ± 328	12,900 ± 697	92 ± 1	91 ± 2	na	na
3	23	20	11,098 ± 292	13,215 ± 770	91 ± 1	92 ± 1	na	na
4	>1,200	240	11,199 ± 681	12,174 ± 722	92 ± 4	93 ± 3	na	na
5	106	80	10,140 ± 585	10,086 ± 734	93 ± 2	94 ± 3	na	na
6	127	99	12,784 ± 1,024	13,148 ± 1,049	95 ± 3	96 ± 2	na	na
7	55	52	9,707 ± 250	10,120 ± 974	97 ± 2	98 ± 3	na	na
8	120	112	11,391 ± 750	11,676 ± 1,041	98 ± 1	97 ± 2	0.058 ± 0.062	0.059 ± 0.067
9	80	80	10,531 ± 554	11,501 ± 1,379	98 ± 1	97 ± 2	0.059 ± 0.052	0.072 ± 0.054
10	55	55	10,493 ± 984	11,623 ± 1,487	97 ± 3	95 ± 4	0.057 ± 0.023	0.059 ± 0.025

Note: *see Equation 6-1 to Equation 6-3, na = not applicable and values show in table represent the average ± standard deviation

The initial inoculum for both reactors was set at approximately 5,500 mg TSS L^{-1}. During the initial 16 days MLSS concentrations in both reactors were found in range of about 5,300 - 5,500 mg TSS L^{-1}, when reactors were operated at low OLR of about 0.37 - 0.75 g $COD_{removed}$ L^{-1} day^{-1} in this starting period. However, once the inocula were adapted to the new substrate at the very long SRTs of >1,200 days, TSS rose continuously to about 14,000 mg L^{-1} for the GSAnMBR and 15,000 mg L^{-1} for the MBAnMBR in proportion to the increase in OLRs from about 1.80 - 4.5 g $COD_{removed}$ L^{-1} day^{-1} by the end of run 1 at day 99. The rapid increase of TSS and VSS in this run was because there was no regular daily excess sludge removal from either reactor. In a conventional MBR system, new active microorganisms are continuously generated from consumption of the fed organic material while some biomass is removed by endogenous decay processes.

The average VSS/TSS ratios in run 1 were 86 % for the GSAnMBR and 87 % for the MBAnMBR (Table 6-6). Subsequently, average VSS/TSS gradually increased to approximately 90 - 95 % and remained relatively stable in this range until the end of the experiments. This indicated that there was no significant accumulation of inorganic solids fraction within the systems even in runs which were operated with long SRT of >100 days. This could be because there is only a small amount of inorganic solid fraction and non-biodegradable compounds in the synthetic dairy wastewater recipe uses in this study.

From a practical perspective, a sufficient MLSS concentration is essential to ensure stable MBR performance for organics removal with high permeate qualities (Huang, Gui and Qian, 2001). In addition, reactors operated with high biomass concentrations and low microbial activity may be favourable. This is because the risks of an unexpected biomass wash-out or activity loss, which are critical phenomena in the case of low biomass content and high microbial activity, could be diminished (Ho and Sung, 2010). Typically, the application of long SRT is favourable for high-rate systems due to the lower excess sludge generation and high MLSS concentrations to maintain suitable F/M ratios at high OLRs. With respect to filterability, however, high MLSS concentrations related to long SRT directly affect mixed suspension rheology and membrane filterability (see literature review section 2.2.4.2.1).

Overall, it is likely that there is a trade-off between the high fouling propensity of very low SRT (related to very high OLR and F/M ratio) and low membrane permeability caused by very high SRT (related to low F/M ratio, high MLSS and high mixed suspension viscosity) (Le-Clech, Chen and Fane, 2006; Smith *et al.*, 2012; Pacheco-Ruiz, Heaven and Banks, 2017).

When considering the results in the current study, a rapid TMP increase was seen in the GSAnMBR on day 90 in run 1 (Figure 6-6) when the MLSS concentration reached about 14,000 for the GSAnMBR and 15,000 mg L^{-1} for the MBAnMBR (Figure 6-12). Therefore, from run 2 onwards

until the end of the experiments, MLSS concentrations in each run for both reactors were controlled to below 13,000 - 14,000 mg L^{-1} by applying daily excess sludge wastage during each operational run. In addition, at certain periods points such as on days 188, 216, 245 and 271 before starting run 5, 7, 9 and 10, respectively, certain amounts of digestate were extracted and the same volume within the reactors was replaced by tap water in order to reduce MLSS concentrations back to about 9,000 mg L^{-1}. Due to this operating strategy, the systems were considered to be in an unsteady state condition.

Unsteady state due to variations in operating conditions such as unstable influent flow, attainable flux, HRT, F/M and OLR, unintentional mixed suspension wastage and varied SRT can lead to changes in fouling tendencies (Le-Clech, Chen and Fane, 2006). This makes it difficult to predict steady state conditions and to conduct a fair comparison between different operational strategies, while real kinetic parameters cannot be identified from these dynamic restrictions. Moreover, it is widely accepted that in order to evaluate theoretical kinetic parameters such as true microbial growth rate (Y_g) and endogenous decay fraction (K_d), systems need to be operated under steady state conditions for at least 3 SRT to allow real interactions between microbial groups and substrates to be achieved. As a result, real kinetic parameters evaluation could not be carried out under the unsteady operating condition in the current study. However, biomass yields observed from each operational run can be evaluated. Although observed biomass yield is not a true theoretical kinetic parameter, the obtained results can be applied as a guideline for excess sludge wasting strategies.

Huang, Gui and Qian (2001) established a mass balance with respect to fraction of organic matter, suspended solids and liquid phase for single-stage submerged MBR based on the assumption that suspended solids from membrane filtered-effluent (permeate) and active microorganisms from influent are negligible. Thus, two equations were formulated which allowed calculation of the sludge growth rate (R_M) and organic degradation rate ($-R_O$) from MLVSS concentration, influent COD, effluent COD and COD in sludge supernatant. These values could then be used to calculate the observed biomass yield (Y_{obs}) from each operating duration according to Equation 6-1 to Equation 6-3.

Equation 6-1

$$R_M = \left(\frac{X_r}{SRT} + \frac{dX_r}{dt}\right)$$

Equation 6-2

$$-R_O = \left[\frac{C_{inf} - C_{eff}}{HRT} + \frac{C_{inf} - C_s}{SRT} - \frac{dC_s}{dt}\right]$$

Equation 6-3

$$Y_{obs} = R_M / -R_O$$

Where:

R_M is observed sludge growth rate, g VSS L^{-1} day^{-1}

R_O is observed organic degradation rate, g $COD_{removed}$ L^{-1} day^{-1}

X_r is mixed liquor volatile suspended solids concentration inside reactor (VSS), mg L^{-1}

SRT is solid retention time, day

HRT is hydraulic retention time, day

C_{inf} is total influent COD concentration, g L^{-1}

C_{eff} is permeate COD concentration, g L^{-1}

C_s is COD concentration from supernatant of MLSS within reactor after 13,000 rpm centrifugation for 30 min, g L^{-1}

Y_{obs} is observed biomass yield, gVSS g^{-1} $COD_{removed}$

Based on the relatively stable operating conditions with average COD removal efficiencies in the range of 95 - 99 % (Table 6-2) and average methane conversion factors of 86 - 98 % (Table 6-5) as well as the relatively long operating period of 20 - 34 days from run 8, 9 and 10 compared to other runs, the obtained results from run 8, 9 and 10 were used to calculate Y_{obs}. Note that these values do not take into account any attached microbial growth on the surface of particles in the MBAnMBR.

Average Y_{obs} values calculated from Equation 6-3 are presented in Table 6-6. These were 0.058 and 0.059 g VSS g^{-1} $COD_{removed}$ for run 8, 0.59 and 0.72 g VSS g^{-1} $COD_{removed}$ for run 9 and 0.057 and 0.059 g VSS g^{-1} $COD_{removed}$ for run 10 for the GSAnMBR and MBAnMBR, respectively. From Table 6-6, it can be seen that standard deviation values of each average calculated Y_{obs} from each run for both reactors is quite large, indicating that they had not been operated under real steady state conditions. However, average Y_{obs} from these three operational runs showed similar values in the range of 0.057 - 0.059 g VSS g^{-1} $COD_{removed}$ for the GSAnMBR and 0.059 - 0.072 g VSS g^{-1} $COD_{removed}$ for the MBAnMBR. Average Y_{obs} from three runs evaluated corresponding to each operational period are calculated as 0.058 g VSS g^{-1} $COD_{removed}$ for the GSAnMBR and 0.063 g VSS g^{-1} $COD_{removed}$ for the MBAnMBR, respectively.

The Y_{obs} of 0.058 and 0.063 g VSS g^{-1} $COD_{removed}$ for both reactors were similar to the typical value range of Y_g for methanogens (Rittmann and McCarty, 2001) and other high-rate anaerobic systems reported in the literature. For instance, Borja and Banks (1994) investigated ice-cream wastewater treatment (average influent COD of 5.2 g L^{-1}) in continuous UASB reactors at eight different HRTs (5.0 - 0.4 days) in order to verify the use of a Monod kinetics model, and reported a sludge yield coefficient of 0.16 g VSS g^{-1} $COD_{removed}$ and sludge decay rate coefficient of 0.028 day^{-1}. Anderson, Kasapgil and Ince (1996) use a side-stream cross flow ultrafiltration AnMBR coupled with a 120 L completely-mixed suspended growth anaerobic reactor for brewery

wastewater (real wastewater and glucose-basis substrate with influent concentration of 80 - 90 g COD L^{-1}) at an OLR of 20 g COD L^{-1} day^{-1} under various SRT (58 - 480 days) and MLSS concentrations (10 - 51 g L^{-1}), and found an overall sludge growth yield and decay rate of 0.0378 g VSS g^{-1} COD and 0.00370 day^{-1} evaluated by Monod kinetic model. A low average dispersed biomass yield of 0.014 ± 0.007 g VSS g^{-1} $COD_{removed}$ was reported by Aslam *et al.* (2017b) who operated a single-stage anaerobic fluidized bed ceramic membrane bioreactor filled with 50 % (v/v) GAC to treat synthetic wastewater (acetate + propionate -basis) at 25 °C. The very low sludge production may be because most of active microorganisms were maintained on GAC particles and were not removed with bulk VSS wastage. An average soluble COD of 23 mg L^{-1} could be achieved by this system under OLR of 2 - 6.8 g COD m^{-3} day^{-1}.

Y_{obs} for AnMBRs in this study are far lower than Y_g values reported for conventional AeMBR treating various types of wastewater, which are in the range of 0.28 - 0.80 g VSS g^{-1} COD (Huang, Gui and Qian, 2001; Al-Malack, 2006; Arévalo *et al.*, 2014). This confirms one of the considerable advantages for AnMBR implementation, that sludge production rates are low and the cost for excess sludge disposal can be significantly reduced.

Considering the Y_{obs} of 0.058 and 0.063 g VSS g^{-1} $COD_{removed}$ for the GSAnMBR and MBAnMBR, using a rule of thumb, and regardless of the true Y_g and endogenous decay, daily biomass productions for each incoming OLR can be calculated. For example, with the net flux of 3.6 LMH, influent concentration of 3,700 mg COD L^{-1} with R_t assumed to be 97 % for both reactors, OLR was evaluated to be 4.7 g $COD_{removed}$ L^{-1} day^{-1} in run 2 and 3, with liquid working volume of 6.6 L for both reactors. This corresponds to a biomass production of 1.80 and 1.95 g $VSS_{produced}$ day^{-1} for the GSAnMBR and MBAnMBR respectively. Assuming that the average MLVSS concentrations in both reactors are 10,000 mg L^{-1}, thus the excess sludge purges that equal the biomass production rate can be calculated as 0.180 and 0.195 L day^{-1} for the GSAnMBR and MBAnMBR. According to these excess sludge extraction rates, the critical SRTs that could prevent wash-out of active microorganisms and organic overload are calculated as not less than 36.7 and 33.8 days for the GSAnMBR and MBAnMBR, respectively.

This potentially explains the occurrences of system failure in run 3 (also run 2), in which reactors were operated with very short SRTs of 42 and 23 days in run 2 and run 3 for the GSAnMBR and of 32 and 20 days in run 2 and run 3 for the MBAnMBR. It is clearly from the results that the active biomass washout has a strong negative influence on COD removal performance, methane production and sludge permeability.

Overall, as mentioned previously, attainable flux, OLR, F/M ratio, MLSS concentration and SRT are strongly interconnected. To achieve high efficiency for organic removal and biogas production

under high OLR operation, single-stage high-rate AnMBR have to maintain a reasonably low F/M which then requires high MLSS and relatively long SRT. However, high MLSS result in flux decline and rapid fouling, particularly when the system is designed for a high particulate organic fraction in the incoming influent. For long-term operation, therefore, in order to control MLSS concentrations inside the reactor, a certain amount of sludge withdrawal other than regular daily excess sludge wastage had to be applied occasionally, such as the end of run 4, 6, 8 and 9 (Figure 6-12). Changing the MLSS concentration by varying the SRT has been known to change the mixed suspension characteristic (Le-Clech, Jefferson and Judd, 2003). This operational strategy led to unsteady state conditions resulting in changes in MLSS properties both before and after sludge withdrawal which could therefore exacerbate the fouling propensity (Le-Clech, Chen and Fane, 2006). Le-Clech, Chen and Fane (2006) also noted that variations in MLSS rheology before sludge withdrawal are influenced by very high MLSS concentration, whilst the changes after sludge wastage were caused by the instantaneous stress experienced by microorganisms. The results have shown that the use of PEG scouring particles could enhance permeate production considerably and had no adverse effect on biological aspect. However, mixed suspension rheology related to operational strategies and MLSS concentration is still of prime importance for filtration performance.

Certain AnMBR studies suggested that optimised operating conditions with relatively low MLSS could allow fluxed to be improved. For example, Pretel *et al.* (2014) used pilot AnMBR to treat sulphate-rich urban wastewater with SRTs from 30 - 70 days, and reported that at a mixed liquor total solids (MLTS) concentration of 32,500 mg L^{-1}, a flux of 10 LMH could achieved whilst at lower MLTS of 13,000 mg L^{-1} flux could be improved up to 20 LMH. However, low to moderate sludge productions in the range of 0.16 - 0.55 g TSS g^{-1} $COD_{removed}$ was found which may affect the further operating cost for sludge disposal.

Pacheco-Ruiz, Heaven and Banks (2017) operated flat-plate AnMBRs for 245 days on a low-to-intermediate strength substrate with high suspended solids. The SRTs in one reactor was progressively reduced which allowed very accurate measurement of sustainable membrane flux rates and growth yields at different SRTs. The results showed membrane flux and MLSS filterability was highest at short SRT, although specific methane production (SMP) was lower since a proportion of COD removal was accounted for by higher biomass yield. There was no advantage in operating at an SRT < 25 days. When considering the most suitable SRT there is thus a trade-off between membrane performance, SMP and waste sludge yield.

Another interesting simple approach which might be helpful to control low MLSS in membrane tank is the use of a primary sedimentation tank. Pretel *et al.* (2015) proposed the approach of using a primary settling tank and further anaerobic digestion coupled with an anaerobic reactor

and membrane tank to minimise MLSS in the membrane tank for urban wastewater treatment. Based on simulation results, the reported that MLSS in the membrane tank could be reduced from 10,000 -18,000 mg L^{-1} to 5,000 -10,000 mg L^{-1} resulting in flux enhancement from 16 - 19 LMH to 24 - 29 LMH with the application of additional primary settling tank and anaerobic digestion units.

As a result, optimisation of MLSS conditions accompanied by a physical cleaning process with scouring particles might be a potential alternative approach to achieve more effect AnMBR implementation, and should be studied further in future investigations.

6.2.6 Sludge particle size distribution

The original inoculum (day 0) for both reactors and digestate from the GSAnMBR and MBAnMBR on day 308 when the systems had been terminated were for determination of the particle size distribution (PSD) by laser diffraction particle analyser. The sludge particle size distribution is presented in Figure 6-13.

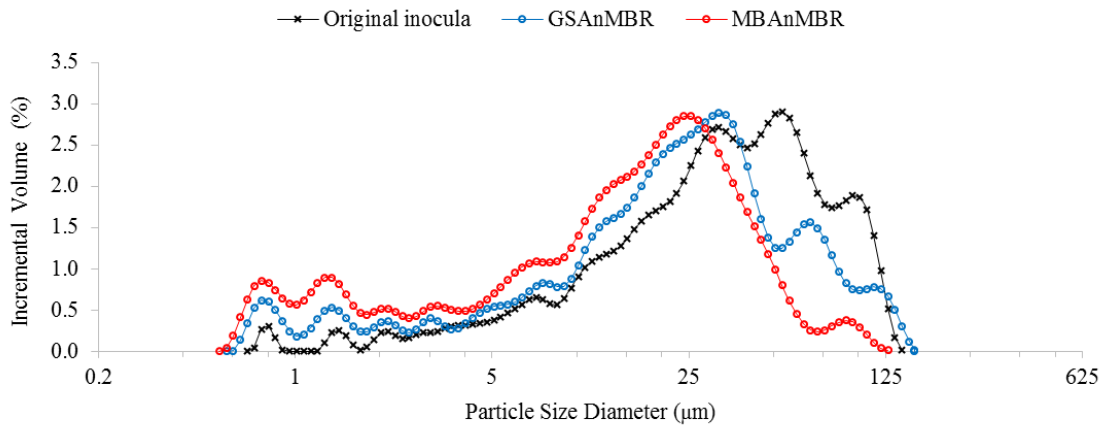

Figure 6-13 Particle size distribution

Mean sizes of 40.7, 29.6 and 19.6 µm and median sizes of 33.5, 22.3 and 16.0 µm were found for original inocula, GSAnMBR and MBAnMBR, respectively.

The mean and median size in the PSD for the GSAnMBR in the current study was in a similar range to that of other studies which operated AnMBRs with gas sparging for fouling control. For example, Gao *et al.* (2011a) reported mean particle sizes of 28 - 36 µm for a submerged AnMBR treating pulp and paper mill wastewater (37 °C) and Huang, Ong and Ng (2013) found median floc sizes in the range of 21 - 28 µm in a flat-sheet AnMBR treating real domestic wastewater at different SRTs.

In the current study, the PSD of MLSS and new produced biomass after long-term operation for the GSAnMBR were slightly shifted towards finer fractions, when compared with the original inoculum. Certain studies have stated that aeration or gas sparging could cause floc breakage and fine particles as well as EPS release (Ivanovic and Leiknes, 2008; Wu and He, 2012), both of which are considered to be major contributors for gel/cake layer formation (Jeison and van Lier, 2007a; Meng *et al.*, 2007b; Gao *et al.*, 2011b). Nonetheless, this analysis demonstrated that no significant sludge floc breakage was found at a sparging rate of 5 L min^{-1} with the gaslift-loop configuration setting in this study.

The correlation between a larger portion of fine anaerobic flocs (< 15 μm) with a high filtration resistance had been studied by Lin *et al.* (2009). Meng *et al.* (2007b) also demonstrated that biomass flocs with smaller sizes than 50 μm were prone to deposit on the membrane surface and eventually impair the membrane permeability.

The distribution of fine particles in the fraction below 1 μm in the GSAnMBR can be seen in Figure 6-13. Since the nominal pore size of the Kubota membrane used in this study is 0.4 μm, it is postulated that the particle aggregates larger than the pore size should be detached from the membrane by shear stress and backtransport velocity induced by gas bubbles and liquid cross-flow when operating below critical flux. However, when the fine particles appear with other complex bridging mixtures (e.g., SMP and EPS) and gel/cake layer formation occurred (mostly reversible fouling) after long-term operation, these foulants were no longer effectively removed from the membrane surface by the two-phase gas-liquid flow alone.

When considering the MBAnMBR, a slight shift in the PSD towards smaller size and higher presence of fine particle fractions was observed. This result is in agreement with AeMBR studies using aeration coupled with suspended granules (Yang *et al.*, 2009; Jamal Khan *et al.*, 2011; Jin, Ong and Ng, 2013). It is believed that the presence of a higher small fine particle fraction and mean size reduction was mainly caused by floc disintegration due to the imposed shear stress generated by particle movement. The breakage of flocs in the mixed suspension may have a negative effect on membrane filterability due to the released SMP and small fine colloids which tend to contribute to membrane pore blockage and constriction. Particularly, in the case of the MBAnMBR lower gel/cake formation on the membrane surface, which acts as secondary dynamic membrane layer, is expected; therefore, membrane pore blockage or pore narrower could cause severe irreversible fouling.

The results from section 6.2.2 demonstrated, however, that most of the time in long-term filtration the MBAnMBR could produce greater fluxes than the GSAnMBR with lower TMP and higher membrane permeability under similar operational conditions. This means that the external

reversible fouling occurring in the GSAnMBR represents the major contribution to the fouling when compared to internal irreversible fouling due to small particles blocking the pores in the MBAnMBR case.

6.2.7 Filtration resistance

The systems were terminated on day 308, and fouling characteristics within the reactors after long-term operation are presented in Figure 6-14.

Thereafter, fouled membrane panels were taken to carry out clean water (tap water) flux experiments to evaluate filtration resistances.

The membrane fouling resistances (R) were quantitatively calculated using the resistance-in-series model given in Equation 5-1 and Equation 5-2.


(a) (b)

Figure 6-14 Fouling characteristics within the reactors after system termination (a) GSAnMBR and (b) MBAnMBR

The resistance determination was as follow: (1) R_T was evaluated by measuring the permeate flux of tap water using the fouled membrane; (2) after gel/cake layer of fouled membrane has been physically removed by soft-sponged wiping, the filterability tests were performed. The difference between (1) and (2) was taken as R_c. (3) after stage (2) membrane panels were taken for chemical

cleaning by two hours soaking in 0.2 % citric acid, 0.5 % NaOCl and 1 % oxalic acid, subsequently (Judd and Judd, 2006). In this stage, clean water filtration abilities were taken as to be R_m and (4) subtracting (3) from (2), R_p was obtained. Whereas, R_T is equal to R_m for the virgin membrane case.

Clean water flux productions and filtration resistances after systems termination for the GSAnMBR and MBAnMBR are shown in Figure 6-15 and Figure 6-16, respectively.

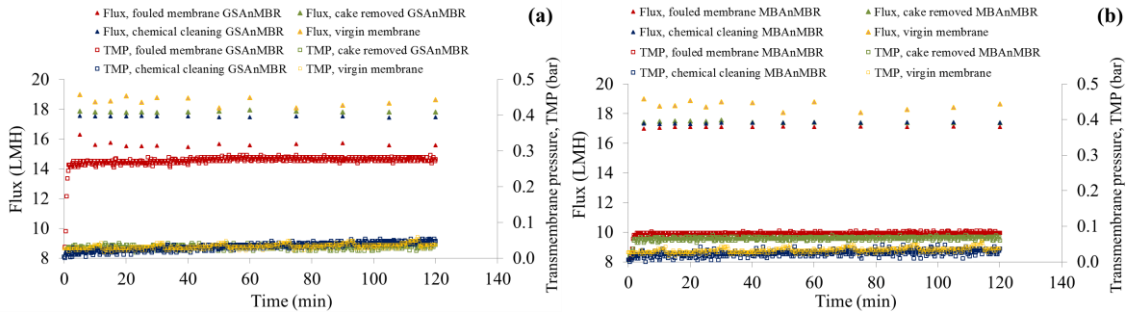

Figure 6-15 Flux and TMP variations for resistance-in-series model (a) GSAnMBR and (b) MBAnMBR

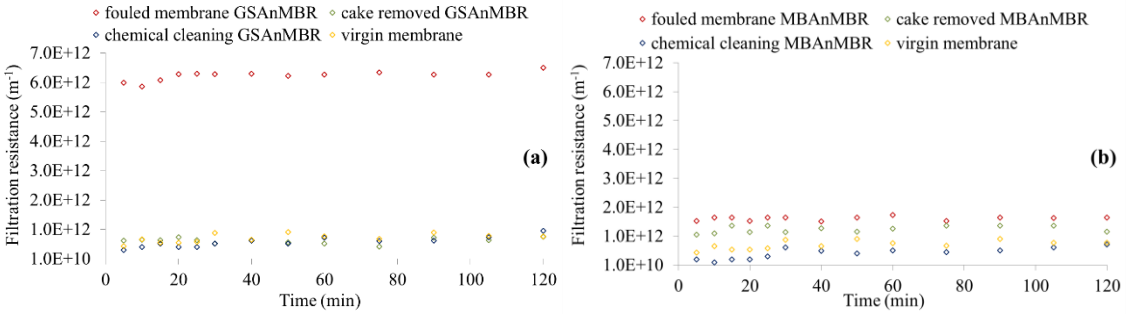

Figure 6-16 Filtration resistances (a) GSAnMBR and (b) MBAnMBR

Pictures of fouled, soft-sponged cake removed and chemically cleaned membrane for both reactors are shown in Figure 6-17 and Figure 6-18.

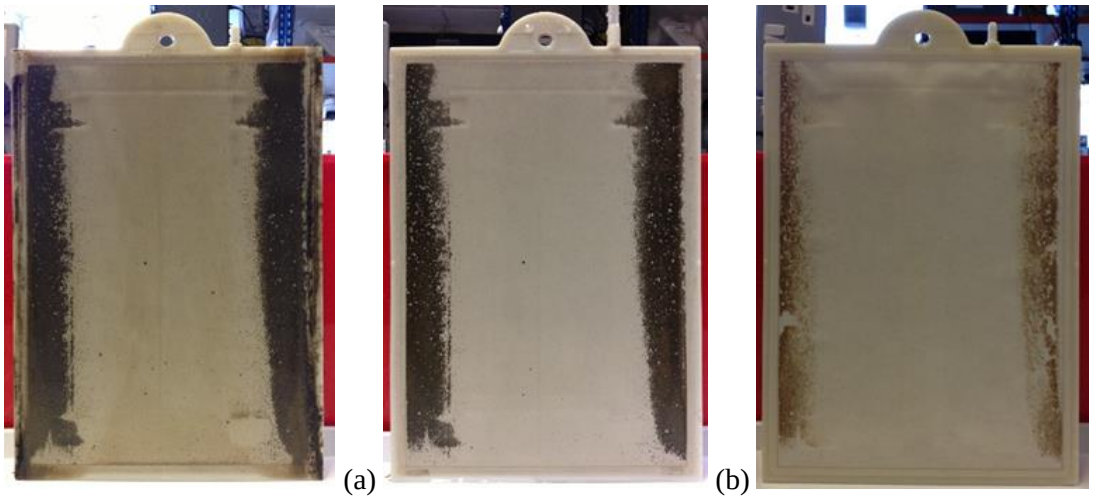

Figure 6-17 Fouled membrane characteristics for GSAnMBR (a) fouled membrane, (b) after soft-sponged cake remove and (c) after chemical cleaning

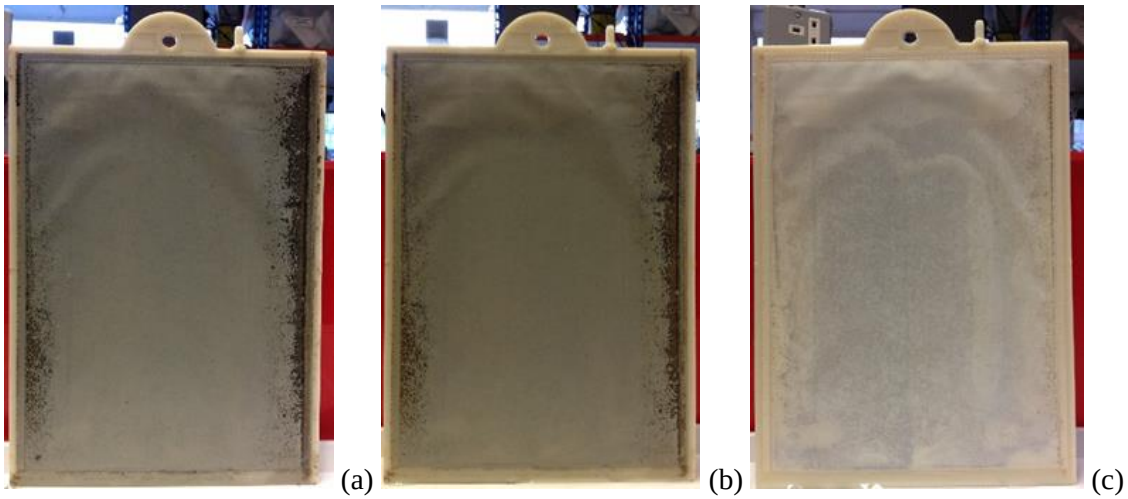

Figure 6-18 Fouled membrane characteristics for MBAnMBR (a) fouled membrane, (b) after soft-sponged cake remove and (c) after chemical cleaning

Figure 6-14 (a) and Figure 6-17 (a) show the GSAnMBR after receiving one chemical cleaning and after the system had been operated continuously for 183 days. Unlike the experiments in section 6.1, no thick cake layer was observed on the membrane surface. Only a brownish thin gel layer was found in the middle zone of the membrane surface and a thin blackish cake layer covered the outer side edges of the membrane panel where the two-phase upward flow velocities are relatively low (upward flow velocity profiles can be seen in section 4.2). This indicated that a sparging intensity of 5 L min^{-1} with an operating net flux of 2.8 - 3.0 LMH is sufficient to prevent thick cake from forming on the membrane surface during long-term operation. For the MBAnMBR, from Figure 6-14 (b) and Figure 6-18 (a), the gel/cake layer formation appeared less intense when compared to the GSAnMBR, which demonstrated that external reversible fouling could be alleviated effectively by scouring particles under the same given sparging intensity.

It should be noted from Figure 6-17 and Figure 6-18 that a certain fouling layer (the blackish areas) could not be removed from the membrane surface by soft-sponge wiping or even chemical cleaning, indicating that this fouling fraction is potentially formed by inorganic or recalcitrant organic foulants. Hence, membrane chemical cleaning by cleaning-in-place (CIP) or cleaning-in-air (the drained membrane tank or cleaning-off-place, CIA) may need to be conducted occasionally during long-term operation.

Filtration resistances at 120th min and resistance distributions were illustrated in Table 6-7.

Table 6-7 Fouling resistance distribution for GSAnMBR, MBAnMBR and virgin membrane

Resistance distribution	GSAnMBR		MBAnMBR		virgin membrane	
	x10^{11} m^{-1}	(% of R_T)	x10^{11} m^{-1}	(% of R_T)	x10^{11} m^{-1}	(% of R_T)
R_c	57.60	(88.34)	4.80	(29.09)	-	-
R_p	0.11	(0.17)	4.40	(26.67)	-	-
R_m	7.47	(11.46)	7.30	(44.24)	7.79	(100)
R_T	65.20	(100.00)	16.50	(100.00)	7.79	(100)

It can be clearly seen from Table 6-7 that cake resistance represents the largest proportion of 88.34 % of the total membrane resistance for the GSAnMBR. The results are in agreement with several studies which reported that external or gel/cake layer forming is always the major contributor to the total fouling in MBRs operations (Jeison and van Lier, 2007b; Lin *et al.*, 2009; Hu *et al.*, 2012; Liu *et al.*, 2012; Mahmoud and Liao, 2017). Total fouling resistance could be reduced significantly by about 4-fold or between 65.20 x 10^{11} and 16.50 x 10^{11} m^{-1} for the GSAnMBR and MBAnMBR, respectively, under the same sparging intensity for long-term operation of more than 300 days, with no chemical cleaning in the latter case. This is because the external reversible fouling could be effectively mitigated by physical cleaning obtained from non-adsorbent scouring media, while neither liquid turbulence nor gas bubbles could reach the membrane surface, which is protected by the laminar boundary layer (Aslam *et al.*, 2017a).

As expected, when the secondary dynamic membrane layer is diminished by abrasive agents, the internal irreversible fouling becomes dominant. The R_p of 4.40 x1 0^{11} m^{-1} which is 26.67 % of R_T in the MBAnMBR is much higher than the 0.11 x 10^{11} m^{-1} (0.17 % of R_T) in the GSAnMBR. Using the regular chemical cleaning process with cleaning protocol reported in Judd and Judd (2006), both reversible and irreversible fouling could be recovered, with recovery factors of 104.3 and 106.7 % compared to the virgin membrane for the GSAnMBR and MBAnMBR, respectively. This may also imply that the use of PEG granules (10 % v/v) as scouring media under a sparging

intensity of 5 L min^{-1} did not show significant evidence of membrane surface damage or adverse effects on the filtration function after long-term operation.

Overall, the results demonstrated that, although small substances and fine colloidal materials play important roles in irreversible fouling resistance, mainly by causing pore blockage, cake elimination on the membrane surface by suspended scouring granules means that the total resistance remains lower than in the absence of scouring agents.

6.2.8 SEM analysis

One of the potential negative aspects of the application of non-adsorbent granules as scouring media coupled with gas sparging is the loss of membrane integrity. Therefore, after the cleaning process, small pieces of membrane surface from both reactors were gently removed from the membrane panels using a sharp scalpel. Prior to examining the membrane surface morphologies using SEM, membrane samples were dried in a critical point apparatus. Membrane surface sampling positions and SEM images for the GSAnMBR and MBAnMBR are presented in Figure 6-19 and Figure 6-20.

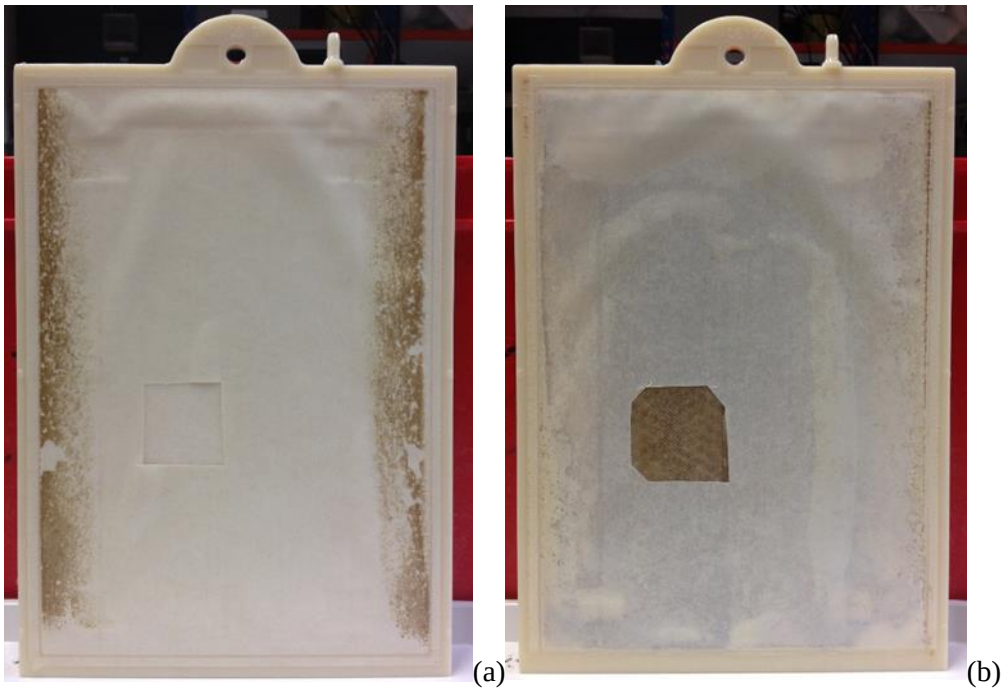

(a) (b)

Figure 6-19 Positions of membrane surface sampling (a) GSAnMBR and (b) MBAnMBR

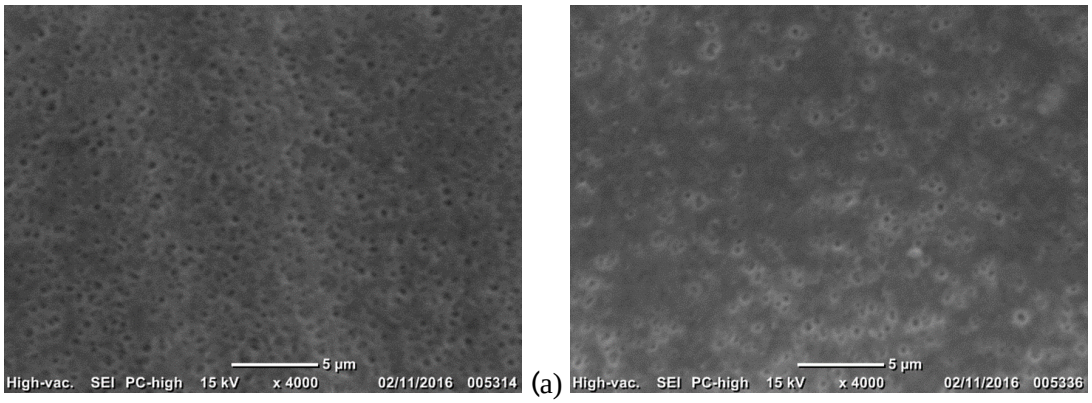

Figure 6-20 SEM images of membrane surface at the end of experiment after chemical cleaning process (a) GSAnMBR and (b) MBAnMBR

From the SEM images in Figure 6-20, it can be seen that the MBAnMBR tend to show more membrane pore blockage and other irreversible fouling formation than occurred in the GSAnMBR, for the aforementioned reasons. When considering the total filtration resistance (R_T) and recovery factor from the previous section, however, after long-term operation and with one chemical cleaning, the filterability of the MBAnMBR can be recovered comparable to the GSAnMBR and virgin membrane.

In addition, any deterioration of membrane lifespan caused by media abrasion is a cause for concern. For example, Siembida *et al.* (2010) reported successful operation of AeMBR accompanied by mechanical cleaning using polypropylene granules for > 600 days without chemical cleaning. Flux could be enhanced by up to 20 % while the effluent quality remained superior. The AeMBR with granulate showed a significant drop in rejection rates to 40 %, however, and brush marks on the membrane surface were observed from SEM images. Similar results were reported by Kurita, Kimura and Watanabe (2015) who operated a PVDF flat-sheet AeMBR with 4 mm cylindrical PEG granules making up 5 % of the reactor volume (the same scouring particle material as used in this study) to retard fouling under aeration rates of 4 and 9 m^3 $hour^{-1}$. From their SEM results, no membrane damage was observed at 4 m^3 $hour^{-1}$ aeration; however, severe damage marks on membrane surface were detected at the aeration rate of 9 m^3 $hour^{-1}$ after around 40 days of operation.

In the current study, although the recovery factor of 106 % for the MBAnMBR was slightly higher than 104.3 % in the GSAnMBR (as shown in section 6.2.7), the results from SEM images showed no significant evidence of membrane damaged at the membrane sampling points (Figure 6-20 (b) and Figure 6-19 (b)). This indicates that the soft-hydrogel texture of PEG granules applied with 5 L min^{-1} (0.3 m^3 $hour^{-1}$) sparging intensity in a gaslift-loop configuration after 308 days of operation for the MBAnMBR did not affected the chlorinated polyethylene membrane integrity in this study.

Another noticeable finding in this stage is that attached microbial growth and biofilm can potentially be formed on the permeate side of the membrane. From Figure 6-21, when comparing the GSAnMBR and MBAnMBR, although the MBAnMBR had received chemical cleaning after systems termination, a brownish stain could be seen on the permeate side.

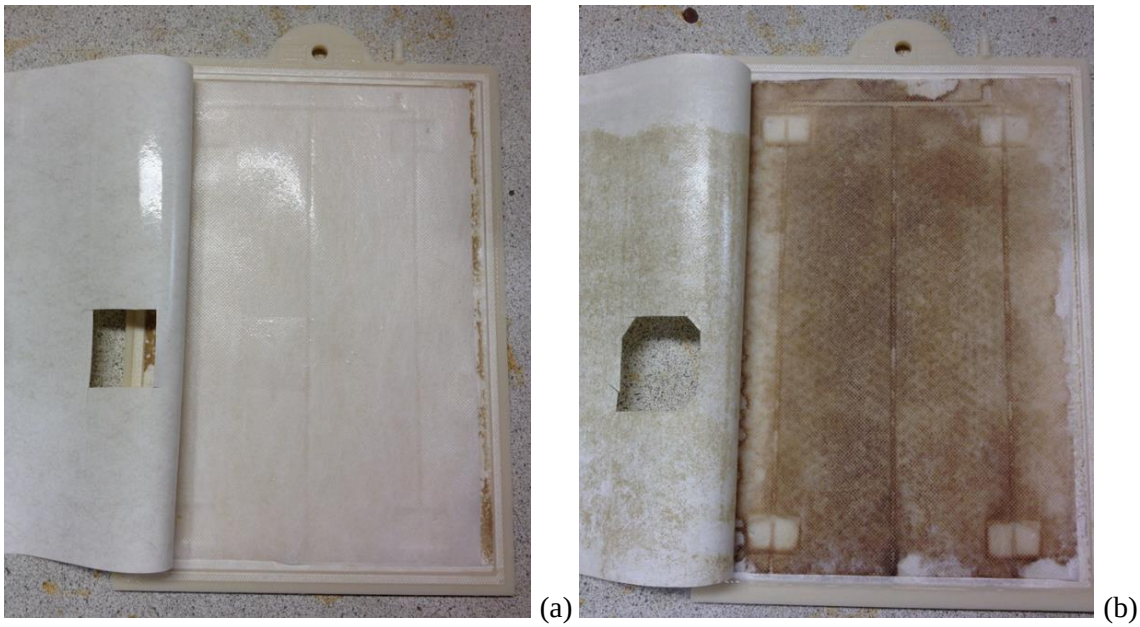

(a) (b)

Figure 6-21 Fouling characteristics on the permeate side of membrane after systems termination (a) GSAnMBR and (b) MBAnMBR

The same problem was reported by van den Brink *et al.* (2013) who operated AeMBR with mechanical cleaning using a spatula to scrap the membrane surface. They showed that after long-term continuous filtration with low flux for more than 1 year, the harsh physical cleaning could effectively remove the fouling layer from the filtration side of the membrane surface. The permeate side, however, was intensively covered by a biofilm layer with bacteria, protozoa and EPS.

Therefore, the trace of stain seen in this study could imply that a gel layer or biofilm can be developed on the permeate side of the membrane surface and on the membrane support layer inside the membrane panel, because the secondary dynamic membrane layer on the filtration side was eliminated due to particle scouring after long-term operation. Hence, fouling caused by this biofilm build-up on the side where neither gas bubbles nor scouring media can reach may be a concern, particularly for long-term filtration without regular chemical cleaning. As a result, membrane chemical cleaning, particularly the chemical cleaning-in-place method should be applied occasionally during long-term operation of an MBAnMBR in order to minimise the problems of membrane pore blockage and biofilm formation on the permeate side of the membrane.

6.3 Conclusions

A study was undertaken of AnMBR treating low to medium strength dairy wastewater by conventional two-phase gas-liquid flow (GSAnMBR) and GSAnMBR coupled with non-adsorbent particles operated as three-phase moving bed AnMBR (MBAnMBR). The results indicated that using non-adsorbent media as scouring agents or flux enhancers, for which regeneration and replenishment are not required, is a useful approach for fouling mitigation in AnMBR systems. Continuous long-term operation of more than 300 days for both GSAnMBR and MBAnMBR was achieved, with the following key findings and conclusions.

A biogas sparging intensity of 2.5 L min^{-1} (U_g of 0.014 m s^{-1}) and initial net flux setting of 5.5 LMH (instantaneous flux 6.9 LMH) conducted with initial MLSS of 8,000 mg L^{-1} could not sustain this attainable net flux for long-term operation, although results obtained from simulated conditions with a model mixed suspension in Chapter 5 used as a guideline for system design and operations. A jump in TMP caused by formation of thick external cake layer resulting in a severe loss of active filtration area occurred after only 18 - 22 days of operation for both the GSAnMBR and the MBAnMBR, indicating that fouling formation in a real live anaerobic system is far more intense than that occurring in simulated conditions and in AeMBR systems, particularly during unsteady state periods of systems acclimatisation.

With a biogas sparging intensity of 5 L min^{-1} (U_g of 0.028 m s^{-1}) and the initial net flux setting of 3.7 LMH (instantaneous flux 4.6 LMH) at an initial MLSS of 5,000 mg L^{-1} in the acclimatisation period, total COD removal (R_t) efficiencies of > 95 % could be achieved after 28 days of operation and this attainable net flux value could be maintained for more than 3 months at an OLR of ~ 4.5 g $COD_{removed}$ L^{-1} day^{-1}, indicating a rapid microbial adaptation in the start-up period for both reactors.

When regular daily excess sludge wastage was not applied (SRT > 1,200 days), MLSS in both reactors increased to 12,000 - 14,000 mg L^{-1} resulting in a rapid increase in TMP, suggesting that the optimal MLSS concentration is below this range. As a result, regular daily sludge wastage and occasional sludge withdrawal to control the MLSS concentration inside the reactors was conducted in certain stages of the experiments. By this operational strategy, the system inevitably experienced unsteady state conditions which affect both organic removal efficiency and membrane filtration performance. Unsteady state can cause mixed suspension rheology changes due to high MLSS concentrations before sludge withdrawal and higher foulant fractions such as VFAs, EPS and SMP released from microorganisms under stress induced by sudden variations of operating conditions after sludge extraction. Therefore, considering the results obtained in this chapter, further studies are recommended to focus on optimisation of operating conditions related

to AnMBR operation at low MLSS coupled with physical scouring particle cleaning in order to improve flux production and capacities of organic treatment and produced biogas potential.

During stable operating periods from the viewpoint of organic removal efficiency, attainable net flux and methane production rates, average R_t values in the range of ~ 95 - 99 % could be achieved by the GSAnMBR and MBAnMBR, respectively, of which 84 - 87 % and 80 - 86 % were due to the anaerobic inoculum in the bioreactor (R_s) in each case. This means that most of the incoming organic matter was treated by active dispersed microbial growth and the rest of the dissolved organic constituents were rejected by the membrane to a certain extent. Even in the case of the MBAnMBR where only a small dynamic membrane layer is expected, high R_s and R_t were still found.

Under the same incoming organic concentration of ~ 3,800 mg COD L^{-1}, higher OLRs of 4.9 - 5.6 g $COD_{removed}$ L^{-1} day^{-1} (F/M ratios of 0.44 - 0.50 g $COD_{removed}$ gVSS day^{-1}) were achieved for the MBAnMBR compared to OLRs of 3.9 - 4.5 g $COD_{removed}$ L^{-1} day^{-1} (F/M ratios of 0.39 - 0.43 g $COD_{removed}$ gVSS day^{-1}) for the GSAnMBR, with comparable treated effluent concentrations in the range of 48 -76 mg COD L^{-1}. The higher OLRs for the MBAnMBR were mainly due to its higher attainable net flux production with higher permeability when compared to the GSAnMBR under similar operational conditions.

In this study, the recommended attainable net fluxes to maintain stable flux in long-term operation without rapid TMP jump were 2.8 and 3.7 LMH for the GSAnMBR and MBAnMBR, respectively, indicating that under the same given energy input for gas sparging, net flux could be enhanced by at least 24.3 % (even up to 35 %) with the assistance of scouring particles to give higher membrane permeability without membrane backflushing or chemical cleaning. Consequently, higher VMPs of 1.68 - 1.94 m^3_{biogas} $m^{-3}_{reactor}$ day^{-1} were achieved for the MBAnMBR compared to 1.24 - 1.40 m^3_{biogas} $m^{-3}_{reactor}$ day^{-1} for the GSAnMBR, with similar biogas methane contents of 77 - 79 % in both systems. SMPs ranged from 0.30 - 0.34 m^3 CH_4 kg^{-1} $COD_{removed}$ corresponding to 85.8 - 97.8 % of theoretical methane potential from consumed organic matter for both reactors, implying that the synthetic dairy wastewater recipe used in this study is viable for anaerobic digestion. Under stable operating conditions, the AnMBRs were sufficiently robust to cope with the applied OLR and no significant intermediate products accumulated in the systems.

Throughout the 308 days of the experimental period, the VSS/TSS ratio was in the range of 86 - 98 % indicating that significant fractions of inert solids accumulated in systems with applied SRTs of 20 - 240 days and > 1,200 days. Under relatively stable continuous operating conditions with SRTs from 55 - 120 days, both reactors showed similar average observed biomass yields (Y_{obs})

in the range of 0.058 - 0.063 g $VSS_{produced}$ g^{-1} $COD_{removed}$, indicating the low excess sludge for disposal which is one of the benefits of AnMBR systems.

At the end of the experimental period, the PSD for the MBAnMBR had shifted towards small fine particle fractions when compared to the GSAnMBR. This is believed to be due to biomass disintegration caused by the shear stress exerted by movement of scouring particles. These fine particles are prone to deposit on/in the membrane. The results showed, however, that the MBAnMBR could generally produce higher attainable net flux with higher permeability than the GSAnMBR under similar operating conditions during the experimental period, illustrating that these fine particle fractions are not the major contributor to the total filtration resistance.

Results from resistance-in-series experiments showed that cake resistance (R_c) represents the major contributor to the total fouling resistance (R_T) for both reactors. The R_c of 4.8 x 10^{11} m^{-1} in MBAnMBR was far lower than that of 57.6 x 10^{11} m^{-1} in the GSAnMBR. This is because external reversible fouling could be mitigated effectively by the application of physical scouring media. The lack of a secondary dynamic membrane layer caused higher pore blockage resistance (R_p) of 4.4 x 10^{11} m^{-1} for the MBAnMBR compared to 0.11 x 10^{11} m^{-1} in the GSAnMBR. The R_T of to 16.5 x 10^{11} m^{-1} in the MBAnMBR was ~ 4-fold lower than the value of 65.2 x 10^{11} m^{-1} in the GSAnMBR due to the presence of the scouring particles.

Results from SEM analysis showed no significant evidence of damage on the sampled membrane surfaces. After 308 days of operation followed by chemical cleaning, the membrane recovery factors for the GSAnMBR and MBAnMBR were 104.3 and 106.7 % respectively compared to the virgin membrane. Taken with the SEM results this could indicate that using PEG granules (10 % v/v) as scouring agents under 5 L min^{-1} intensity did not adversely affect the chlorinated polyethylene membrane integrity and filtration function. However, one notable potential problem that occurred with the use of scouring particles is fouling build-up on the permeate side of membrane surface. As the secondary dynamic membrane layer was eliminated, foulants caused by biofilm layer formation and attached microbial growth could develop on the permeate side, suggesting that occasional chemical cleaning may still be required.

Chapter 7: **Conclusions and recommendations for future work**

The extent of which this work has fulfilled the initial objectives outlined in section 1.3 and the conclusions which can be drawn from this study are presented in this chapter. In addition, areas of research that could be explored in more detail in future are suggested.

7.1 Conclusions

The aim of this thesis was to study and optimise the use of gas-liquid two-phase and gas-liquid-non-adsorbent particle three-phase flow in submerged flat-sheet AnMBR for dairy wastewater treatment. The first stage of this study was focused on optimisation of hydrodynamic parameters mainly related to bubbling characteristics, crossflow velocity and tank geometry for gas-sparged two-phase flow using tap water as a medium. Thereafter, the application of non-adsorbent particles (LDPE carriers) coupled with gas-sparged two-phase flow for fouling mitigation purposes under simulated anaerobic conditions using a model mixed suspension was investigated. Finally, the obtained results from the first two stages were used to design and construct lab-scale submerged flat-sheet AnMBRs for synthetic dairy wastewater treatment. Long-term performance over more than 300 days of operation for both a two-phase GSAnMBR and a three-phase MBAnMBR were examined. Based on these frameworks, the key conclusions drawn can be described as follows.

7.1.1 Optimisation of hydrodynamic parameters for the gas-sparged two-phase flow

Gas-sparged two-phase flow is the most common practical method for fouling mitigation and mixing purposes and at the same time represents the largest fraction of energy consumed for operation of flat-sheet AnMBR. Therefore, hydrodynamic aspects related to energy input for gas sparging should be optimised. Considering the tank configuration, gaslift-loop flow gave more favourable hydrodynamic conditions than a gas-mixed without annular-loop flow regime under the same given energy for gas bubbling. Results from Chapter 4 and 5 illustrated that without the annular-loop flow regime, an internal liquid circulation loop and lateral motion of the bubble swarm on the membrane surface were observed and then stagnant flow zones were created which reduced the total backtransport velocity. Due to the lack of a continuous annular-loop flow pattern, the achievement of complete mixing conditions is also limited. For the gaslift-loop configuration, regarding continuous annular flow recirculation inside the tank, the results showed that increasing A_d/A_r from 1.78 to 3.71 could enhance liquid crossflow velocity in the riser zone.

Although results from section 4.2.1 revealed that increasing A_d/A_r ratios in this range did not significantly improve average circulation flow velocity, it was recommended that A_d/A_r should be designed to be larger than 1.78. In order to prevent too high flow friction loss and to promote continuous deflection flow velocity at the bottom zone of the reactor, it was also suggested that the design value for the A_d/A_b ratio should be close to 1. Considering the parameters D_{V50} which relates representative bubble diameters to accumulated volume and D_{32} relating volume to projected area as well as the ratio of bubble-membrane contact area/bubble-membrane covered area for the created bubbles swarm, it was found that nozzle sizes of ∅ 3 and 4 mm generated higher bubble fractions which have bubble sizes larger than the membrane gap compared to nozzle sizes of ∅ 1 and 2 mm under the same given sparging intensity. This indicated that generated bubbles from ∅ 3 and 4 mm nozzles tend to contribute higher shear stress compared to smaller bubble sizes generated from ∅ 1 and 2 mm nozzles due to the pseudo-2D confined cap bubble flow regime between the membrane channel. On the other hand, smaller nozzle sizes of ∅ 1 and 2 mm contributed higher liquid crossflow velocity compared to ∅ 3 and 4 mm nozzles as bubbles are generated more evenly along the perforated sparger ducts and then uniformly distributed over the entire membrane surface. It is difficult to draw a firm conclusion whether shear stress or backtransport velocity plays a larger role for fouling mitigation since these two factors complement each other and occur in the same time. Increased sparging intensity can deduce to the improvement of the obtained shear stress and crossflow velocity but increases the energy demand. Moreover, the beneficial effects of hydrodynamic parameters are expected to plateau when sparging intensity is further increased beyond certain values. Hence, design of sparging system to balance contributed shear stress, crossflow velocity and bubble uniformity (i.e. shear stress and crossflow velocity) under a specific sparging intensity is of prime importance to achieve effective energy input for fouling control. It is also likely that there are optimal nozzle design for each given sparging intensity. For example, results from section 4.3 showed that a ∅ 3 mm nozzle gave better fouling mitigation tendency compared to ∅ of 1, 2 and 4 mm under a 5 L min^{-1} sparging rate, whilst in section 5.1 a modified sparger with unequal nozzle sizes of ∅ 1.5 and 3 mm gave better fouling control than ∅ 3 mm at 2.5 L min^{-1} sparging rate. This indicated that the choice of nozzle size and sparger arrangement must be given serious consideration in sparging system design and these factors should not be selected arbitrarily. The results suggested that practical sparging system design should start with determination of optimal sparging intensity. In this study, which did not take account of the variety of mixed suspension rheology in real AnMBR applications, results from section 4.2 identified a threshold sparging intensity at U_g of 0.033 m s^{-1} (resulting in U_{lr} of ~ 0.35 - 0.45 m s^{-1}), and this sparging intensity could be applicable for other real flat-sheet systems that utilise a membrane gap width similar to the one applied in this study. Results from section 5.7 also illustrated that energy demand for the gas

blower, SGD_m and SGD_p are affected directly by the liquid depth in reactor, as the static pressure head caused by liquid depth influences the pressure drop over the perforated sparger tube. Therefore, practical nozzle size and sparging design should be carried out after the optimal U_g and liquid depth had been determined. For example, an inclined perforated sparger tube or varied nozzle sizes could be applied to compensate for pressure drop and friction resistance inside sparger duct in order to achieve an optimal balance between contributed shear stress and cross velocity via uniform bubble distribution. The optimisation of perforated sparger tube design is recommended for further detailed investigations in future studies.

7.1.2 The use of non-adsorbent particles operated as three-phase moving bed flow for AnMBR operation

Experiments were carried out using LDPE particles as scouring particles coupled with gas sparging under simulated AnMBR conditions. Results from Chapter 5 showed that the practical selection of scouring particles and filling ratios are crucial aspects for systems application. The LDPE particles revealed certain drawbacks for three-phase mechanical cleaning process. The SG of 0.86 - 0.96 for LDPE beads made it difficult to circulate them inside the gaslift-loop reactor; buoyant LPDE beads could slow down continuous flow leading to a requirement for a higher liquid downward flow velocity in the downcomer zone. Since the LDPE carriers are smaller than the membrane channel width, a higher particle filling ratio may be needed in order to enhance the probability and frequency of LDPE particles collisions with the membrane surface. Results from section 5.3 showed that to improve the critical flux from 6 LMH for the case without scouring particles, up to 7.5 and 9.0 LMH, higher LDPE filling ratios of 11.1 and 22.2 % v/v were needed. 11.1 % v/v LDPE operated with the gas-mixed without annular-loop flow configuration showed good fouling mitigation from short-term experiments. 31.1 % v/v LDPE addition showed serious problems of particles entrapment, potentially caused by the small shape and size of LDPE beads and the too high packing density accompanied by a stagnant flow zone created by the gas-mixed regime without annular-loop flow. As a result, in configurations with the same or similar membrane gap, LDPE granules with packing rations of 11.1 % v/v are appropriate and higher values are not recommended.

For the long-term live system operations, conventional GSAnMBR and MBAnMBR (10 % v/v PEG granules) treating synthetic dairy wastewater were carried out. Based on 308 days of operation from Chapter 6, the results indicated that the use of non-adsorbent particles had no adverse effects on biological aspects or organic removal efficiency in comparison with operation as a conventional GSAnMBR. During stable operating conditions, high comparative total organic removal efficiencies (R_t) in the range of 95 - 99 % could be achieved, of which 80 - 87 % by biological means (R_s) for both GSAnMBR and MBAnMBR systems. This result indicated that

most of the incoming organic matter was treated by active dispersed microbial growth and the rest of the dissolved organic constituents were rejected by the membrane to certain extent. Even in the case of the MBAnMBR which is expected to have little or no dynamic membrane layer, high R_s and R_t could still be achieved. Under similar operating condition for both systems, the attainable flux for MBAnMBR could be improved by 24 - 35 % whilst comparative high organic treatment efficiency and methane product rate could still be achieved, illustrating that with the assistance of scouring particles, the flux capacity of AnMBR system and thus its organic loading and methane production could be significantly enhanced under the same given energy input for biogas sparging.

The potential negative effects caused by applying scouring particles were evaluated. The results from particle size distribution analysis showed that the fraction of fine particles increased indicating biomass floc disintegration due to the scouring particles. However, these fractions did not greatly affect organic treatment efficiency or total filtration resistance. Results from SEM analysis did not show significant evidence of chlorinated polyethylene polymeric membrane damage caused by the use of PEG scouring particles under 5 L min^{-1} sparging intensity after long-term operation. However, it was noted from the SEM images that the MBAnMBR appeared to have more foulants compacted on/in the membrane surface than the case without scouring particles. Although results demonstrated that reversible gel/cake resistance and total filtration resistance had been mitigated effectively by the scouring agent, internal irreversible pore blockage became dominant. There were signs of fouling on the permeate side of membrane surface where neither gas bubbles or scouring particles can reached, and as a result it is suggested that membrane chemical cleaning should occasionally be conducted during continuous long-term operation.

7.1.3 Operating parameters for GSAnMBR and MBAnMBR

For AnMBR operation, parameters such as attainable flux, HRT, OLR, SRT, F/M ratio and MLSS concentration are strongly interconnected and it is thus difficult to identify optimal value for each parameter independently. Based on the fouling behaviour seen in this study, recommended operating MLSS concentrations are below 12,000 - 14,000 mg L^{-1}. As a result, it is recommended that sludge is wasted to maintain the MLSS concentration in bioreactors below this range. To avoid the creation of unsteady state conditions which may have adverse effects on reactor performance and mixed suspension rheology, it is recommend that this procedure is carried out on a regular basis.

Under the same incoming organic concentration of ~ 3,800 mg COD L^{-1}, the MBAnMBR achieved higher OLRs of 4.9 - 5.6 g $COD_{removed}$ L^{-1} day^{-1} (F/M ratios of 0.44 - 0.50 g $COD_{removed}$ gVSS day^{-1}) compared to OLRs of 3.9 - 4.5 g $COD_{removed}$ L^{-1} day^{-1} (F/M ratios of 0.39 - 0.43 g

$COD_{removed}$ gVSS day^{-1}) for the GSAnMBR, with comparable treated effluents in the range of 48 -76 mg COD L^{-1}. This was mainly due to the higher attainable net flux in the MBAnMBR compared to the GSAnMBR under similar operational conditions. Under relatively stable continuous operating conditions with SRTs ranging from 55 - 120 days, similar average observed biomass yield (Y_{obs}) in the range of 0.058 - 0.063 g $VSS_{produced}$ g^{-1} $COD_{removed}$ were found for both reactors. These operational parameters can be applied as a guidance for submerged flat-sheet AnMBR treating dairy wastewater.

7.2 Recommendations for future work

Based on the outcomes of this research, the following recommendations for future study are proposed.

7.2.1 Optimisation of sparger design for the two- and three-phase flow for AnMBR systems

The results from this study have shown that bubble size (which affects contributed shear stress), liquid crossflow velocity and the homogeneity of bubble distribution along the sparger tube and across the membrane surface play an important role for two-phase flow membrane cleaning. In addition, sparging rate, nozzle size and pressure drop over the sparger significantly affect the produced bubble size and size distribution. In order to balance between shear stress, backtransport velocity and the uniformity of bubble distribution, sophisticated gas sparger design is required. It is recommended that practical sparger design starts with the determination of liquid depth in the tank which should be comparable to real scale AnMBR systems. Threshold U_g should also be identified. Thereafter, optimal sparger tube arrangement and nozzle size design to compensate pressure drop and friction resistance along the sparger tube can further be studied in detail.

For the three-phase flow, there are very limited studies about optimization of the sparging system. Unlike from two-phase flow, scouring media can collide directly with the membrane whereas neither gas bubbles nor liquid turbulence could reach the membrane surface which is protected by a laminar boundary layer (Aslam *et al.*, 2017a). Based on this, small nozzle sizes may have advantages due to their favorable bubbles distribution characteristics. However, other hydrodynamic parameters such as particle packing density (number of media), mass, flow velocity, collision frequency, should be further investigated for optimisation of three-phase flow.

7.2.2 Optimisation of MBAnMBR operation combined with low MLSS concentrations

Results from this study demonstrated that scouring particles could mitigate fouling effectively. However, mixed suspension rheology related to operational strategies and MLSS concentrations

is still of prime importance for filtration performance. Operating single-stage high-rate MBAnMBR, high MLSS concentration to cope with high incoming OLR and to maintain low F/M ratio stimulates low membrane permeability. Hence, future works on operation of MBAnMBR as filtration unit coupled with other high-rate reactors to diminish the membrane exposure to high MLSS concentration are suggested. For example, for dispersed microbial growth system, Pretel *et al.* (2015) proposed the approach to use a primary settling tank and further anaerobic digestion coupled with an anaerobic reactor and membrane tank to minimise MLSS in the membrane tank. Another approach is to apply MBAnMBR as the add-on unit for other existing anaerobic reactors such as UASB, AFB and ABR to increase organic treatment efficiencies. Practical methods to control MLSS concentration and optimal SRT should further be examined. Although the designs that limit membrane-biomass contact are not guaranteed to reduce fouling, with the assistance of scouring particles, producible net flux should be enhanced.

7.2.3 Applying chemical cleaning in place for MBAnMBR

Results from this study have shown that after long-term operation of MBAnMBR, membrane pore blockage filtration resistance was found increase significantly, although total filtration resistance was still low. This may have been due to the development of biofilm and attached microbial growth at the permeate side of membrane due to the lack of a dynamic membrane layer. Therefore, membrane chemical cleaning, particularly, an in-situ cleaning in place method should be conducted occasionally and the protocol of chemical cleaning should be evaluated.

Bibliography

Akram, A. and Stuckey, D.C. (2008) 'Flux and performance improvement in a submerged anaerobic membrane bioreactor (SAMBR) using powdered activated carbon (PAC)', *Process Biochemistry*, 43(1), pp. 93-102.

Al-Malack, M.H. (2006) 'Determination of biokinetic coefficients of an immersed membrane bioreactor', *Journal of Membrane Science*, 271(1–2), pp. 47-58.

Alresheedi, M.T. and Basu, O.D. (2014) 'Support media impacts on humic acid, cellulose, and kaolin clay in reducing fouling in a submerged hollow fiber membrane system', *Journal of Membrane Science*, 450, pp. 282-290.

An, Y. *et al.* (2009a) 'Characterization of membrane foulants in an anaerobic non-woven fabric membrane bioreactor for municipal wastewater treatment', *Chemical Engineering Journal*, 155(3), pp. 709-715.

An, Y. *et al.* (2009b) 'Municipal Wastewater Treatment Using a UASB Coupled with Cross-Flow Membrane Filtration', *Journal of Environmental Engineering*, 135(2), pp. 86-91.

Anderson, G.K., Kasapgil, B. and Ince, O. (1996) 'Microbial Kinetics of a Membrane Anaerobic Reactor System', *Environmental Technology*, 17(5), pp. 449-464.

Aquino, S.F. *et al.* (2006) 'Characterization of dissolved compounds in submerged anaerobic membrane bioreactors (SAMBRs)', *Journal of Chemical Technology & Biotechnology*, 81(12), pp. 1894-1904.

Arévalo, J. *et al.* (2014) 'Effect of temperature on membrane bioreactor performance working with high hydraulic and sludge retention time', *Biochemical Engineering Journal*, 88, pp. 42-49.

Arros-Alileche, S. *et al.* (2008) 'The membrane role in an anaerobic membrane bioreactor for purification of dairy wastewaters: A numerical simulation', *Bioresource Technology*, 99(17), pp. 8237-8244.

Aslam, M. *et al.* (2017a) 'Membrane bioreactors for wastewater treatment: A review of mechanical cleaning by scouring agents to control membrane fouling', *Chemical Engineering Journal*, 307, pp. 897-913.

Aslam, M. *et al.* (2014) 'The effect of fluidized media characteristics on membrane fouling and energy consumption in anaerobic fluidized membrane bioreactors', *Separation and Purification Technology*, 132, pp. 10-15.

Aslam, M. *et al.* (2017b) 'Low energy single-staged anaerobic fluidized bed ceramic membrane bioreactor (AFCMBR) for wastewater treatment', *Bioresource Technology*, 240, pp. 33-41.

Aun Ng, C., Sun, D. and Fane, A.G. (2006) 'Operation of Membrane Bioreactor with Powdered Activated Carbon Addition', *Separation Science and Technology*, 41(7), pp. 1447-1466.

Bacchin, P., Aimar, P. and Field, R.W. (2006) 'Critical and sustainable fluxes: Theory, experiments and applications', *Journal of Membrane Science*, 281(1), pp. 42-69.

Baek, S., Pagilla, K. and Kim, H.-J. (2010) 'Lab-scale study of an anaerobic membrane bioreactor (AnMBR) for dilute municipal wastewater treatment', *Biotechnology and Bioprocess Engineering*, 15(4), pp. 704-708.

Bello, R.A., Robinson, C.W. and Moo-Young, M. (1985) 'Gas holdup and overall volumetric oxygen transfer coefficient in airlift contactors', *Biotechnology and Bioengineering*, 27(3), pp. 369-381.

Bérubé, P.R. *et al.* (2006) 'Quantifying the shear at the surface of submerged hollow fiber membranes', *Journal of Membrane Science*, 279(1), pp. 495-505.

Bibliography

Berube, P.R., Hall, E.R. and Sutton, P.M. (2006) 'Parameters governing permeate flux in an anaerobic membrane bioreactor treating low-strength municipal wastewaters: a literature review', *Water Environ Res*, 78(8), pp. 887-96.

Bialek, K. *et al.* (2011) 'Quantitative and qualitative analyses of methanogenic community development in high-rate anaerobic bioreactors', *Water Research*, 45(3), pp. 1298-1308.

Bohm, L. *et al.* (2012) 'The importance of fluid dynamics for MBR fouling mitigation', *Bioresour Technol*, 122, pp. 50-61.

Borja, R. and Banks, C.J. (1994) 'Kinetics of an upflow anaerobic sludge blanket reactor treating ice-cream wastewater', *Environmental Technology*, 15(3), pp. 219-232.

Borja, R. and Banks, C.J. (1995) 'Response of an anaerobic fluidized bed reactor treating ice-cream wastewater to organic, hydraulic, temperature and pH shocks', *Journal of Biotechnology*, 39(3), pp. 251-259.

Braak, E. *et al.* (2011) 'Aeration and hydrodynamics in submerged membrane bioreactors', *Journal of Membrane Science*, 379(1–2), pp. 1-18.

Brockmann, M. and Seyfried, C.F. (1997) 'Sludge activity under the conditions of crossflow microfiltration', *Water Science and Technology*, 35(10), pp. 173-181.

Buntner, D., Sánchez, A. and Garrido, J.M. (2013) 'Feasibility of combined UASB and MBR system in dairy wastewater treatment at ambient temperatures', *Chemical Engineering Journal*, 230(0), pp. 475-481.

Carvalho, F., Prazeres, A.R. and Rivas, J. (2013) 'Cheese whey wastewater: Characterization and treatment', *Science of The Total Environment*, 445–446, pp. 385-396.

Casu, S. *et al.* (2012) 'Wastewater treatment in a submerged anaerobic membrane bioreactor', *J Environ Sci Health A Tox Hazard Subst Environ Eng*, 47(2), pp. 204-9.

Cerón-Vivas, A., Morgan-Sagastume, J.M. and Noyola, A. (2012) 'Intermittent filtration and gas bubbling for fouling reduction in anaerobic membrane bioreactors', *Journal of Membrane Science*, 423–424(0), pp. 136-142.

Chaiprapat, S. *et al.* (2016) 'Influences of liquid, solid, and gas media circulation in anaerobic membrane bioreactor (AnMBR) as a post treatment alternative of aerobic system in seafood industry', *Journal of Membrane Science*, 509, pp. 116-124.

Chang, I.-S. and Judd, S.J. (2002) 'Air sparging of a submerged MBR for municipal wastewater treatment', *Process Biochemistry*, 37(8), pp. 915-920.

Chang, M.-C. *et al.* (2006) 'Performance and filtration characteristics of non-woven membranes used in a submerged membrane bioreactor for synthetic wastewater treatment', *Desalination*, 191(1–3), pp. 8-15.

Chang, S. and Fane, A.G. (2001) 'The effect of fibre diameter on filtration and flux distribution — relevance to submerged hollow fibre modules', *Journal of Membrane Science*, 184(2), pp. 221-231.

Charfi, A., Aslam, M. and Kim, J. (2018) 'Modelling approach to better control biofouling in fluidized bed membrane bioreactor for wastewater treatment', *Chemosphere*, 191, pp. 136-144.

Chatzipaschali, A.A. and Stamatis, A.G. (2012) 'Biotechnological Utilization with a Focus on Anaerobic Treatment of Cheese Whey: Current Status and Prospects', *Energies*, 5(9), p. 3492.

Chen, C. *et al.* (2016) 'Challenges in biogas production from anaerobic membrane bioreactors', *Renewable Energy*, 98, pp. 120-134.

Chen, F., Bi, X. and Ng, H.Y. (2016) 'Effects of bio-carriers on membrane fouling mitigation in moving bed membrane bioreactor', *Journal of Membrane Science*, 499, pp. 134-142.

Chen, V. *et al.* (1997) 'Particle deposition during membrane filtration of colloids: transition between concentration polarization and cake formation', *Journal of Membrane Science*, 125(1), pp. 109-122.

Chisti, M.Y., Halard, B. and Moo-Young, M. (1988) 'Liquid circulation in airlift reactors', *Chemical Engineering Science*, 43(3), pp. 451-457.

Cho, B.D. and Fane, A.G. (2002) 'Fouling transients in nominally sub-critical flux operation of a membrane bioreactor', *Journal of Membrane Science*, 209(2), pp. 391-403.

Chu, L.-B., Yang, F.-L. and Zhang, X.-W. (2005) 'Anaerobic treatment of domestic wastewater in a membrane-coupled expended granular sludge bed (EGSB) reactor under moderate to low temperature', *Process Biochemistry*, 40(3–4), pp. 1063-1070.

Cicek, N. *et al.* (2001) 'Effect of solids retention time on the performance and biological characteristics of a membrane bioreactor', *Water Science and Technology*, 43(11), pp. 43-50.

Clift, R., Grace, J.R. and Weber, M.E. (2005) *Bubbles, Drops, and Particles*. Dover Publications.

Colleran, E., Finnegan, S. and Lens, P. (1995) 'Anaerobic treatment of sulphate-containing waste streams', *Antonie van Leeuwenhoek*, 67(1), pp. 29-46.

Collins, G. *et al.* (2006) 'New Low-Temperature Applications of Anaerobic Wastewater Treatment', *Journal of Environmental Science and Health, Part A*, 41(5), pp. 881-895.

Connaughton, S., Collins, G. and O'Flaherty, V. (2006) 'Psychrophilic and mesophilic anaerobic digestion of brewery effluent: A comparative study', *Water Research*, 40(13), pp. 2503-2510.

Cui, Z.F., Chang, S. and Fane, A.G. (2003) 'The use of gas bubbling to enhance membrane processes', *Journal of Membrane Science*, 221(1–2), pp. 1-35.

Defrance, L. and Jaffrin, M.Y. (1999) 'Comparison between filtrations at fixed transmembrane pressure and fixed permeate flux: application to a membrane bioreactor used for wastewater treatment', *Journal of Membrane Science*, 152(2), pp. 203-210.

Demirel, B. and Scherer, P. (2008) 'The roles of acetotrophic and hydrogenotrophic methanogens during anaerobic conversion of biomass to methane: a review', *Reviews in Environmental Science and Bio/Technology*, 7(2), pp. 173-190.

Demirel, B., Yenigun, O. and Onay, T.T. (2005) 'Anaerobic treatment of dairy wastewaters: a review', *Process Biochemistry*, 40(8), pp. 2583-2595.

Deng, L. *et al.* (2016a) 'Biofouling and control approaches in membrane bioreactors', *Bioresource Technology*, 221, pp. 656-665.

Deng, L. *et al.* (2016b) 'New functional biocarriers for enhancing the performance of a hybrid moving bed biofilm reactor–membrane bioreactor system', *Bioresource Technology*, 208, pp. 87-93.

Dereli, R.K. *et al.* (2012) 'Potentials of anaerobic membrane bioreactors to overcome treatment limitations induced by industrial wastewaters', *Bioresource Technology*, 122(0), pp. 160-170.

Dhaked, R.K., Singh, P. and Singh, L. (2010) 'Biomethanation under psychrophilic conditions', *Waste Management*, 30(12), pp. 2490-2496.

Doyle, J.D. and Parsons, S.A. (2002) 'Struvite formation, control and recovery', *Water Research*, 36(16), pp. 3925-3940.

Drews, A. (2010) 'Membrane fouling in membrane bioreactors—Characterisation, contradictions, cause and cures', *Journal of Membrane Science*, 363(1–2), pp. 1-28.

Ducom, G., Puech, F.-P. and Cabassud, C. (2003) 'Gas/Liquid Two-phase Flow in a Flat Sheet Filtration Module: Measurement of Local Wall Shear Stresses', *The Canadian Journal of Chemical Engineering*, 81(3-4), pp. 771-775.

Ducom, G., Puech, F.P. and Cabassud, C. (2002) 'Air sparging with flat sheet nanofiltration: a link between wall shear stresses and flux enhancement', *Desalination*, 145(1–3), pp. 97-102.

Ersahin, M.E. *et al.* (2014) 'Applicability of dynamic membrane technology in anaerobic membrane bioreactors', *Water Research*, 48(0), pp. 420-429.

Ersu, C.B. and Ong, S.K. (2008) 'TREATMENT OF WASTEWATER CONTAINING PHENOL USING A TUBULAR CERAMIC MEMBRANE BIOREACTOR', *Environmental Technology*, 29(2), pp. 225-234.

Essemiani, K. *et al.* (2001) 'Spherical cap bubbles in a flat sheet nanofiltration module: experiments and numerical simulation', *Chemical Engineering Science*, 56(21–22), pp. 6321-6327.

Fan, B. and Huang, X. (2002) 'Characteristics of a Self-Forming Dynamic Membrane Coupled with a Bioreactor for Municipal Wastewater Treatment', *Environmental Science & Technology*, 36(23), pp. 5245-5251.

Fane, A.G. *et al.* (2005) 'Low pressure membrane processes ~ doing more with less energy', *Desalination*, 185(1–3), pp. 159-165.

Fenu, A. *et al.* (2010) 'Energy audit of a full scale MBR system', *Desalination*, 262(1–3), pp. 121-128.

Field, R.W. *et al.* (1995) 'Critical flux concept for microfiltration fouling', *Journal of Membrane Science*, 100(3), pp. 259-272.

Fouladitajar, A. *et al.* (2014) 'Gas sparging to enhance permeate flux and reduce fouling resistances in cross flow microfiltration', *Journal of Industrial and Engineering Chemistry*, 20(2), pp. 624-632.

Fox, R.A. and Stuckey, D.C. (2015) 'The effect of sparging rate on transmembrane pressure and critical flux in an AnMBR', *Journal of Environmental Management*, 151(0), pp. 280-285.

Galib, M. *et al.* (2016) 'Energy-positive food wastewater treatment using an anaerobic membrane bioreactor (AnMBR)', *Journal of Environmental Management*, 182, pp. 477-485.

Gander, M., Jefferson, B. and Judd, S. (2000) 'Aerobic MBRs for domestic wastewater treatment: a review with cost considerations', *Separation and Purification Technology*, 18(2), pp. 119-130.

Gao, D.-W. *et al.* (2014) 'Treatment of domestic wastewater by an integrated anaerobic fluidized-bed membrane bioreactor under moderate to low temperature conditions', *Bioresource Technology*, 159, pp. 193-198.

Gao, W.J. *et al.* (2011a) 'Effects of temperature and temperature shock on the performance and microbial community structure of a submerged anaerobic membrane bioreactor', *Bioresource Technology*, 102(19), pp. 8733-8740.

Gao, W.J. *et al.* (2011b) 'Structure of cake layer in a submerged anaerobic membrane bioreactor', *Journal of Membrane Science*, 374(1–2), pp. 110-120.

Gao, W.J.J. *et al.* (2010) 'Influence of elevated pH shocks on the performance of a submerged anaerobic membrane bioreactor', *Process Biochemistry*, 45(8), pp. 1279-1287.

Gerardi, M.H. (2003) *The microbiology of anaerobic digesters*. Available at: http://search.ebscohost.com/login.aspx?direct=true&scope=site&db=nlebk&db=nlabk&AN=91876.

Ghosh, R. (2002) 'Study of membrane fouling by BSA using pulsed injection technique', *Journal of Membrane Science*, 195(1), pp. 115-123.

Ghyoot, W.R. and Verstraete, W.H. (1997) 'Coupling Membrane Filtration to Anaerobic Primary Sludge Digestion', *Environmental Technology*, 18(6), pp. 569-580.

Gil, J.A. *et al.* (2010) 'Monitoring and analysis of the energy cost of an MBR', *Desalination*, 250(3), pp. 997-1001.

Giménez, J.B. *et al.* (2012) 'Methane recovery efficiency in a submerged anaerobic membrane bioreactor (SAnMBR) treating sulphate-rich urban wastewater: Evaluation of methane losses with the effluent', *Bioresource Technology*, 118(0), pp. 67-72.

Giménez, J.B. *et al.* (2011) 'Experimental study of the anaerobic urban wastewater treatment in a submerged hollow-fibre membrane bioreactor at pilot scale', *Bioresource Technology*, 102(19), pp. 8799-8806.

Grotenhuis, J.T.C. (1992) *Structure and stability of methanogenic granular sludge*. Proefschrift Wageningen. Grotenhuis. Available at: http://edepot.wur.nl/203137.

Grundestam, J. and Hellstrom, D. (2007) 'Wastewater treatment with anaerobic membrane bioreactor and reverse osmosis', *Water Sci Technol*, 56(5), pp. 211-7.

Guglielmi, G. *et al.* (2007) 'Sub-critical fouling in a membrane bioreactor for municipal wastewater treatment: experimental investigation and mathematical modelling', *Water Res*, 41(17), pp. 3903-14.

Gutiérrez, J.L.R., Encina, P.A.G. and Fdz-Polanco, F. (1991) 'Anaerobic treatment of cheese-production wastewater using a UASB reactor', *Bioresource Technology*, 37(3), pp. 271-276.

Habib, R. *et al.* (2017) 'Influence of relaxation modes on membrane fouling in submerged membrane bioreactor for domestic wastewater treatment', *Chemosphere*, 181, pp. 19-25.

Haridas, A. *et al.* (2005) 'The Buoyant Filter Bioreactor: a high-rate anaerobic reactor for complex wastewater—process dynamics with dairy effluent', *Water Research*, 39(6), pp. 993-1004.

Hawkes, F.R., Donnelly, T. and Anderson, G.K. (1995) 'Comparative performance of anaerobic digesters operating on ice-cream wastewater', *Water Research*, 29(2), pp. 525-533.

Herrera-Robledo, M., Morgan-Sagastume, J.M. and Noyola, A. (2009) 'Biofouling and pollutant removal during long-term operation of an anaerobic membrane bioreactor treating municipal wastewater', *Biofouling*, 26(1), pp. 23-30.

Ho, C.-C. and Zydney, A.L. (2002) 'Transmembrane pressure profiles during constant flux microfiltration of bovine serum albumin', *Journal of Membrane Science*, 209(2), pp. 363-377.

Ho, J. and Sung, S. (2010) 'Methanogenic activities in anaerobic membrane bioreactors (AnMBR) treating synthetic municipal wastewater', *Bioresource Technology*, 101(7), pp. 2191-2196.

Ho, J.H., Khanal, S.K. and Sung, S. (2007) 'Anaerobic membrane bioreactor for treatment of synthetic municipal wastewater at ambient temperature', *Water Sci Technol*, 55(7), pp. 79-86.

Hong, S.P. *et al.* (2002) 'Fouling control in activated sludge submerged hollow fiber membrane bioreactors', *Desalination*, 143(3), pp. 219-228.

Hu, A. and Stuckey, D. (2006) 'Treatment of Dilute Wastewaters Using a Novel Submerged Anaerobic Membrane Bioreactor', *Journal of Environmental Engineering*, 132(2), pp. 190-198.

Hu, A. and Stuckey, D. (2007) 'Activated Carbon Addition to a Submerged Anaerobic Membrane Bioreactor: Effect on Performance, Transmembrane Pressure, and Flux', *Journal of Environmental Engineering*, 133(1), pp. 73-80.

Hu, J. *et al.* (2012) 'Effect of carriers on sludge characteristics and mitigation of membrane fouling in attached-growth membrane bioreactor', *Bioresource Technology*, 122, pp. 35-41.

Huang, X., Gui, P. and Qian, Y. (2001) 'Effect of sludge retention time on microbial behaviour in a submerged membrane bioreactor', *Process Biochemistry*, 36(10), pp. 1001-1006.

Huang, X., Wei, C.-H. and Yu, K.-C. (2008) 'Mechanism of membrane fouling control by suspended carriers in a submerged membrane bioreactor', *Journal of Membrane Science*, 309(1), pp. 7-16.

Huang, Z., Ong, S.L. and Ng, H.Y. (2011) 'Submerged anaerobic membrane bioreactor for low-strength wastewater treatment: Effect of HRT and SRT on treatment performance and membrane fouling', *Water Research*, 45(2), pp. 705-713.

Huang, Z., Ong, S.L. and Ng, H.Y. (2013) 'Performance of submerged anaerobic membrane bioreactor at different SRTs for domestic wastewater treatment', *Journal of Biotechnology*, 164(1), pp. 82-90.

Hwang, K.-J. and Hsu, C.-E. (2009) 'Effect of gas–liquid flow pattern on air-sparged cross-flow microfiltration of yeast suspension', *Chemical Engineering Journal*, 151(1–3), pp. 160-167.

Ivanovic, I. and Leiknes, T. (2008) 'Impact of aeration rates on particle colloidal fraction in the biofilm membrane bioreactor (BF-MBR)', *Desalination*, 231(1), pp. 182-190.

Iversen, V. *et al.* (2009) 'Impacts of membrane flux enhancers on activated sludge respiration and nutrient removal in MBRs', *Water Research*, 43(3), pp. 822-830.

Jamal Khan, S. *et al.* (2011) 'Performance of suspended and attached growth MBR systems in treating high strength synthetic wastewater', *Bioresource Technology*, 102(9), pp. 5331-5336.

Jamal Khan, S., Visvanathan, C. and Jegatheesan, V. (2012) 'Effect of powdered activated carbon (PAC) and cationic polymer on biofouling mitigation in hybrid MBRs', *Bioresource Technology*, 113, pp. 165-168.

Jeison, D. *et al.* (2009) 'Effects of the acidogenic biomass on the performance of an anaerobic membrane bioreactor for wastewater treatment', *Bioresource Technology*, 100(6), pp. 1951-1956.

Jeison, D., van Betuw, W. and van Lier, J.B. (2008) 'Feasibility of Anaerobic Membrane Bioreactors for the Treatment of Wastewaters with Particulate Organic Matter', *Separation Science and Technology*, 43(13), pp. 3417-3431.

Jeison, D. and van Lier, J.B. (2006) 'Cake layer formation in anaerobic submerged membrane bioreactors (AnSMBR) for wastewater treatment', *Journal of Membrane Science*, 284(1–2), pp. 227-236.

Jeison, D. and van Lier, J.B. (2007a) 'Cake formation and consolidation: Main factors governing the applicable flux in anaerobic submerged membrane bioreactors (AnSMBR) treating acidified wastewaters', *Separation and Purification Technology*, 56(1), pp. 71-78.

Jeison, D. and van Lier, J.B. (2007b) 'Thermophilic treatment of acidified and partially acidified wastewater using an anaerobic submerged MBR: Factors affecting long-term operational flux', *Water Research*, 41(17), pp. 3868-3879.

Jensen, P.D. *et al.* (2015) 'Anaerobic membrane bioreactors enable high rate treatment of slaughterhouse wastewater', *Biochemical Engineering Journal*, 97, pp. 132-141.

Jeong, E. *et al.* (2010) 'Effects of the hydraulic retention time on the fouling characteristics of an anaerobic membrane bioreactor for treating acidifi ed wastewater', *Desalination and Water Treatment*, 18(1-3), pp. 251-256.

Jiang, T. *et al.* (2008) 'Modelling the production and degradation of soluble microbial products (SMP) in membrane bioreactors (MBR)', *Water Research*, 42(20), pp. 4955-4964.

Jin, L., Ong, S.L. and Ng, H.Y. (2013) 'Fouling control mechanism by suspended biofilm carriers addition in submerged ceramic membrane bioreactors', *Journal of Membrane Science*, 427(0), pp. 250-258.

Johir, M.A.H. *et al.* (2011) 'Influence of supporting media in suspension on membrane fouling reduction in submerged membrane bioreactor (SMBR)', *Journal of Membrane Science*, 374(1), pp. 121-128.

Judd, S. (2008) 'The status of membrane bioreactor technology', *Trends in Biotechnology*, 26(2), pp. 109-116.

Judd, S. and Judd, C. (2006) *The MBR book : principles and applications of membrane bioreactors in water and wastewater treatment*. Oxford: Elsevier.

Judd, S.J. (2016) 'The status of industrial and municipal effluent treatment with membrane bioreactor technology', *Chemical Engineering Journal*, 305, pp. 37-45.

Judd, S.J.C.K. (2011) *The MBR book principles and applications of membrane bioreactors for water and wastewater treatment*. Available at: http://app.knovel.com/web/toc.v/cid:kpMBRBPAM3.

Kang, I.-J., Yoon, S.-H. and Lee, C.-H. (2002) 'Comparison of the filtration characteristics of organic and inorganic membranes in a membrane-coupled anaerobic bioreactor', *Water Research*, 36(7), pp. 1803-1813.

Karadag, D. *et al.* (2015) 'A review on anaerobic biofilm reactors for the treatment of dairy industry wastewater', *Process Biochemistry*, 50(2), pp. 262-271.

Kataoka, N. *et al.* (1992) 'Examination of bacterial characteristics of anaerobic membrane bioreactors in three pilot-scale plants for treating low-strength wastewater by application of the colony-forming-curve analysis method', *Appl Environ Microbiol*, 58(9), pp. 2751-7.

Kato, M.T., Field, J.A. and Lettinga, G. (1997) 'The anaerobic treatment of low strength wastewaters in UASB and EGSB reactors', *Water Science and Technology*, 36(6–7), pp. 375-382.

Kettunen, R.H. and Rintala, J.A. (1997) 'The effect of low temperature (5–29 °C) and adaptation on the methanogenic activity of biomass', *Applied Microbiology and Biotechnology*, 48(4), pp. 570-576.

Khalili-Garakani, A. *et al.* (2011) 'Analyze and control fouling in an airlift membrane bioreactor: CFD simulation and experimental studies', *Process Biochemistry*, 46(5), pp. 1138-1145.

Kim, J. *et al.* (2010) 'Anaerobic Fluidized Bed Membrane Bioreactor for Wastewater Treatment', *Environmental Science & Technology*, 45(2), pp. 576-581.

Kira, F. *et al.* (2012) 'Study on Flows inside and outside an Air Diffuser for Membrane Bioreactor', *Journal of Fluid Science and Technology*, 7(1), pp. 78-88.

Kocadagistan, E. and Topcu, N. (2007) 'Treatment investigation of the Erzurum City municipal wastewaters with anaerobic membrane bioreactors', *Desalination*, 216(1–3), pp. 367-376.

Kornboonraksa, T. and Lee, S.H. (2009) 'Factors affecting the performance of membrane bioreactor for piggery wastewater treatment', *Bioresour Technol*, 100(12), pp. 2926-32.

Krause, S. *et al.* (2010) 'Enhanced membrane bioreactor process without chemical cleaning', *Water Science and Technology*, 61(10), p. 2575.

Kurita, T., Kimura, K. and Watanabe, Y. (2014) 'The influence of granular materials on the operation and membrane fouling characteristics of submerged MBRs', *Journal of Membrane Science*, 469, pp. 292-299.

Kurita, T., Kimura, K. and Watanabe, Y. (2015) 'Energy saving in the operation of submerged MBRs by the insertion of baffles and the introduction of granular materials', *Separation and Purification Technology*, 141, pp. 207-213.

Kurita, T., Mogi, T. and Kimura, K. (2016) 'Influence of different biofilm carriers on the operation and membrane fouling of submerged membrane bioreactors', *Separation and Purification Technology*, 169, pp. 43-49.

Kwon, D.Y. *et al.* (2000) 'Experimental determination of critical flux in cross-flow microfiltration', *Separation and Purification Technology*, 19(3), pp. 169-181.

Laera, G. *et al.* (2005) 'Zero net growth in a membrane bioreactor with complete sludge retention', *Water Res*, 39(20), pp. 5241-9.

Lay, W.C.L., Liu, Y. and Fane, A.G. (2010) 'Impacts of salinity on the performance of high retention membrane bioreactors for water reclamation: A review', *Water Research*, 44(1), pp. 21-40.

Le-Clech, P. *et al.* (2003) 'Fluid hydrodynamics in submerged and sidestream membrane bioreactors', *Water Sci Technol*, 48(3), pp. 113-9.

Le-Clech, P., Chen, V. and Fane, T.A.G. (2006) 'Fouling in membrane bioreactors used in wastewater treatment', *Journal of Membrane Science*, 284(1–2), pp. 17-53.

Le-Clech, P., Jefferson, B. and Judd, S.J. (2003) 'Impact of aeration, solids concentration and membrane characteristics on the hydraulic performance of a membrane bioreactor', *Journal of Membrane Science*, 218(1), pp. 117-129.

Le Clech, P. *et al.* (2003) 'Critical flux determination by the flux-step method in a submerged membrane bioreactor', *Journal of Membrane Science*, 227(1–2), pp. 81-93.

Lee, E. *et al.* (2016) 'Effects of FeCl3 addition on the operation of a staged anaerobic fluidized membrane bioreactor (SAF-MBR)', *Water Sci Technol*, 74(1), pp. 130-7.

Lee, J., Ahn, W.-Y. and Lee, C.-H. (2001) 'Comparison of the filtration characteristics between attached and suspended growth microorganisms in submerged membrane bioreactor', *Water Research*, 35(10), pp. 2435-2445.

Lee, S. and Kim, M.-H. (2013) 'Fouling characteristics in pure oxygen MBR process according to MLSS concentrations and COD loadings', *Journal of Membrane Science*, 428, pp. 323-330.

Lee, S. *et al.* (2009) 'Removal of 17β-estradiol by powdered activated carbon—Microfiltraion hybrid process: The effect of PAC deposition on membrane surface', *Journal of Membrane Science*, 326(1), pp. 84-91.

Lee, W.-N., Kang, I.-J. and Lee, C.-H. (2006) 'Factors affecting filtration characteristics in membrane-coupled moving bed biofilm reactor', *Water Research*, 40(9), pp. 1827-1835.

Leiknes, T. *et al.* (2006) 'Assessment of membrane reactor design in the performance of a hybrid biofilm membrane bioreactor (BF-MBR)', *Desalination*, 199(1–3), pp. 328-330.

Lettinga, G. (1995) 'Anaerobic digestion and wastewater treatment systems', *Antonie van Leeuwenhoek*, 67(1), pp. 3-28.

Lettinga, G. *et al.* (1999) 'High-rate anaerobic treatment of wastewater at low temperatures', *Appl Environ Microbiol*, 65(4), pp. 1696-702.

Lettinga, G., Rebac, S. and Zeeman, G. (2001) 'Challenge of psychrophilic anaerobic wastewater treatment', *Trends in Biotechnology*, 19(9), pp. 363-370.

Lew, B. *et al.* (2009) 'Anaerobic membrane bioreactor (AnMBR) for domestic wastewater treatment', *Desalination*, 243(1–3), pp. 251-257.

Li, J. *et al.* (2012) 'Microbial community and biomass characteristics associated severe membrane fouling during start-up of a hybrid anoxic–oxic membrane bioreactor', *Bioresource Technology*, 103(1), pp. 43-47.

Liao, B.-Q., Kraemer, J.T. and Bagley, D.M. (2006) 'Anaerobic Membrane Bioreactors: Applications and Research Directions', *Critical Reviews in Environmental Science and Technology*, 36(6), pp. 489-530.

Lin, H. *et al.* (2011a) 'Feasibility evaluation of submerged anaerobic membrane bioreactor for municipal secondary wastewater treatment', *Desalination*, 280(1–3), pp. 120-126.

Lin, H. *et al.* (2011b) 'Membrane Bioreactors for Industrial Wastewater Treatment: A Critical Review', *Critical Reviews in Environmental Science and Technology*, 42(7), pp. 677-740.

Lin, H. *et al.* (2011c) 'New insights into membrane fouling in a submerged anaerobic membrane bioreactor based on characterization of cake sludge and bulk sludge', *Bioresource Technology*, 102(3), pp. 2373-2379.

Lin, H. *et al.* (2013) 'A review on anaerobic membrane bioreactors: Applications, membrane fouling and future perspectives', *Desalination*, 314(0), pp. 169-188.

Lin, H. *et al.* (2011d) 'Enhanced performance of a submerged membrane bioreactor with powdered activated carbon addition for municipal secondary effluent treatment', *Journal of Hazardous Materials*, 192(3), pp. 1509-1514.

Lin, H.J. *et al.* (2009) 'Sludge properties and their effects on membrane fouling in submerged anaerobic membrane bioreactors (SAnMBRs)', *Water Res*, 43(15), pp. 3827-37.

Lin, H.J. *et al.* (2010) 'Factors affecting sludge cake formation in a submerged anaerobic membrane bioreactor', *Journal of Membrane Science*, 361(1–2), pp. 126-134.

Liu, R. *et al.* (2000) 'Study on hydraulic characteristics in a submerged membrane bioreactor process', *Process Biochemistry*, 36(3), pp. 249-254.

Liu, X. *et al.* (2016) 'Numerical simulations of impact of membrane module design variables on aeration patterns in membrane bioreactors', *Journal of Membrane Science*, 520, pp. 201-213.

Liu, Y. *et al.* (2012) 'The ratio of food-to-microorganism (F/M) on membrane fouling of anaerobic membrane bioreactors treating low-strength wastewater', *Desalination*, 297(0), pp. 97-103.

Lobos, J. *et al.* (2005) 'Effects of starvation conditions on biomass behaviour for minimization of sludge production in membrane bioreactors', *Water Science and Technology*, 51(6-7), p. 35.

Lobos, J. *et al.* (2008) 'Sequencing versus continuous membrane bioreactors: Effect of substrate to biomass ratio (F/M) on process performance', *Journal of Membrane Science*, 317(1), pp. 71-77.

Luna, H.J. *et al.* (2014) 'EPS and SMP dynamics at different heights of a submerged anaerobic membrane bioreactor (SAMBR)', *Process Biochemistry*, 49(12), pp. 2241-2248.

Mahmoud, I. and Liao, B. (2017) 'Effects of sludge concentration and biogas sparging rate on critical flux in a submerged anaerobic membrane bioreactor', *Journal of Water Process Engineering*, 20, pp. 51-60.

Maqbool, T., Khan, S.J. and Lee, C.-H. (2014) 'Effects of filtration modes on membrane fouling behavior and treatment in submerged membrane bioreactor', *Bioresource Technology*, 172, pp. 391-395.

Martin Garcia, I. *et al.* (2013) 'Impact on reactor configuration on the performance of anaerobic MBRs: Treatment of settled sewage in temperate climates', *Water Research*, 47(14), pp. 4853-4860.

Martin, I. *et al.* (2011) 'Modelling the energy demands of aerobic and anaerobic membrane bioreactors for wastewater treatment', *Environmental Technology*, 32(9), pp. 921-932.

Martinez-Sosa, D., Helmreich, B. and Horn, H. (2012) 'Anaerobic submerged membrane bioreactor (AnSMBR) treating low-strength wastewater under psychrophilic temperature conditions', *Process Biochemistry*, 47(5), pp. 792-798.

Martinez-Sosa, D. *et al.* (2011) 'Anaerobic submerged membrane bioreactor (AnSMBR) for municipal wastewater treatment under mesophilic and psychrophilic temperature conditions', *Bioresour Technol*, 102(22), pp. 10377-85.

Matsushige, K. *et al.* (1990) 'The effects of temperature on anaerobic filter treatment for low-strength organic wastewater', *Environmental Technology*, 11(10), pp. 899-910.

McCarty, P.L., Bae, J. and Kim, J. (2011) 'Domestic Wastewater Treatment as a Net Energy Producer–Can This be Achieved?', *Environmental Science & Technology*, 45(17), pp. 7100-7106.

McHugh, S., Collins, G. and O'Flaherty, V. (2006) 'Long-term, high-rate anaerobic biological treatment of whey wastewaters at psychrophilic temperatures', *Bioresource Technology*, 97(14), pp. 1669-1678.

McKeown, R.M. *et al.* (2012) 'Low-temperature anaerobic digestion for wastewater treatment', *Current Opinion in Biotechnology*, 23(3), pp. 444-451.

McKeown, R.M. *et al.* (2009a) 'Psychrophilic methanogenic community development during long-term cultivation of anaerobic granular biofilms', *ISME J*, 3(11), pp. 1231-42.

McKeown, R.M. *et al.* (2009b) 'Long-term (1243 days), low-temperature (4–15 °C), anaerobic biotreatment of acidified wastewaters: Bioprocess performance and physiological characteristics', *Water Research*, 43(6), pp. 1611-1620.

Melin, T. *et al.* (2006) 'Membrane bioreactor technology for wastewater treatment and reuse', *Desalination*, 187(1), pp. 271-282.

Meng, F. *et al.* (2009) 'Recent advances in membrane bioreactors (MBRs): Membrane fouling and membrane material', *Water Research*, 43(6), pp. 1489-1512.

Meng, F. *et al.* (2007a) 'New insights into membrane fouling in submerged membrane bioreactor based on rheology and hydrodynamics concepts', *Journal of Membrane Science*, 302(1), pp. 87-94.

Meng, F. and Yang, F. (2007) 'Fouling mechanisms of deflocculated sludge, normal sludge, and bulking sludge in membrane bioreactor', *Journal of Membrane Science*, 305(1), pp. 48-56.

Meng, F. *et al.* (2008) 'A comprehensive study on membrane fouling in submerged membrane bioreactors operated under different aeration intensities', *Separation and Purification Technology*, 59(1), pp. 91-100.

Meng, F. *et al.* (2007b) 'Characterization of Cake Layer in Submerged Membrane Bioreactor', *Environmental Science & Technology*, 41(11), pp. 4065-4070.

Mercier, M., Fonade, C. and Lafforgue-Delorme, C. (1997) 'How slug flow can enhance the ultrafiltration flux in mineral tubular membranes', *Journal of Membrane Science*, 128(1), pp. 103-113.

Metcalf & Eddy, I. (2003) *Wastewater engineering : treatment and reuse*. Fourth edition / revised by George Tchobanoglous, Franklin L. Burton, H. David Stensel. Boston : McGraw-Hill, [2003] ©2003.

Metzger, U. *et al.* (2007) 'Characterisation of polymeric fouling in membrane bioreactors and the effect of different filtration modes', *Journal of Membrane Science*, 301(1–2), pp. 180-189.

Miller, D.J. *et al.* (2014) 'Comparison of membrane fouling at constant flux and constant transmembrane pressure conditions', *Journal of Membrane Science*, 454(0), pp. 505-515.

Miyahara, T., Tsuchiya, K. and Fan, L.S. (1988) 'Wake properties of a single gas bubble in three-dimensional liquid-solid fluidized bed', *International Journal of Multiphase Flow*, 14(6), pp. 749-763.

Moghaddam, M.R. *et al.* (2006) 'Filter clogging in coarse pore filtration activated sludge process under high MLSS concentration', *Water Sci Technol*, 54(10), pp. 55-66.

Munz, G. *et al.* (2007) 'Powdered activated carbon and membrane bioreactors (MBRPAC) for tannery wastewater treatment: long term effect on biological and filtration process performances', *Desalination*, 207(1), pp. 349-360.

Ndinisa, N.V., Fane, A.G. and Wiley, D.E. (2006) 'Fouling Control in a Submerged Flat Sheet Membrane System: Part I – Bubbling and Hydrodynamic Effects', *Separation Science and Technology*, 41(7), pp. 1383-1409.

Ndinisa, N.V. *et al.* (2006) 'Fouling Control in a Submerged Flat Sheet Membrane System: Part II—Two-Phase Flow Characterization and CFD Simulations', *Separation Science and Technology*, 41(7), pp. 1411-1445.

Ng, C.A. *et al.* (2013) 'Optimization of membrane bioreactors by the addition of powdered activated carbon', *Bioresource Technology*, 138, pp. 38-47.

Ngo, H.-H., Guo, W. and Xing, W. (2008) 'Evaluation of a novel sponge-submerged membrane bioreactor (SSMBR) for sustainable water reclamation', *Bioresource Technology*, 99(7), pp. 2429-2435.

Nguyen Cong Duc, E. *et al.* (2008) 'Local hydrodynamic investigation of the aeration in a submerged hollow fibre membranes cassette', *Journal of Membrane Science*, 321(2), pp. 264-271.

Nozhevnikova, A.N. *et al.* (2001a) 'Production and oxidation of methane at low temperature by the microbial population of municipal sludge checks situated in north-east Europe', *Water Sci Technol*, 44(4), pp. 89-95.

Nozhevnikova, A.N. *et al.* (2001b) 'Temperature characteristics of methanogenic archaea and acetogenic bacteria isolated from cold environments', *Water Sci Technol*, 44(8), pp. 41-8.

O'Flaherty, V. *et al.* (1998) 'LONG-TERM COMPETITION BETWEEN SULPHATE-REDUCING AND METHANE-PRODUCING BACTERIA DURING FULL-SCALE ANAEROBIC TREATMENT OF CITRIC ACID PRODUCTION WASTEWATER', *Water Research*, 32(3), pp. 815-825.

O'Reilly, C. and Colleran, E. (2005a) 'Microbial sulphate reduction during anaerobic digestion: EGSB process performance and potential for nitrite suppression of SRB activity', *Water Sci Technol*, 52(1-2), pp. 371-6.

O'Reilly, C. and Colleran, E. (2005b) 'Microbial sulphate reduction during anaerobic digestion: EGSB process performance and potential for nitrite suppression of SRB activity', *Water science and technology : a journal of the International Association on Water Pollution Research*, 52(1-2), pp. 371-376.

O'Flaherty, V., Collins, G. and Mahony, T. (2006) 'The Microbiology and Biochemistry of Anaerobic Bioreactors with Relevance to Domestic Sewage Treatment', *Reviews in Environmental Science and Bio/Technology*, 5(1), pp. 39-55.

Ognier, S., Wisniewski, C. and Grasmick, A. (2004) 'Membrane bioreactor fouling in sub-critical filtration conditions: a local critical flux concept', *Journal of Membrane Science*, 229(1), pp. 171-177.

Omil, F. *et al.* (2003) 'Anaerobic filter reactor performance for the treatment of complex dairy wastewater at industrial scale', *Water Research*, 37(17), pp. 4099-4108.

Ozgun, H. *et al.* (2013) 'A review of anaerobic membrane bioreactors for municipal wastewater treatment: Integration options, limitations and expectations', *Separation and Purification Technology*, 118(0), pp. 89-104.

Pacheco-Ruiz, S., Heaven, S. and Banks, C.J. (2017) 'Effect of mean cell residence time on transmembrane flux, mixed-liquor characteristics and overall performance of a submerged anaerobic membrane bioreactor', *Environ Technol*, 38(10), pp. 1263-1274.

Padmasiri, S.I. *et al.* (2007) 'Methanogenic population dynamics and performance of an anaerobic membrane bioreactor (AnMBR) treating swine manure under high shear conditions', *Water Res*, 41(1), pp. 134-44.

Park, H., Choo, K.-H. and Lee, C.-H. (1999) 'Flux Enhancement with Powdered Activated Carbon Addition in the Membrane Anaerobic Bioreactor', *Separation Science and Technology*, 34(14), pp. 2781-2792.

Perle, M., Kimchie, S. and Shelef, G. (1995) 'Some biochemical aspects of the anaerobic degradation of dairy wastewater', *Water Research*, 29(6), pp. 1549-1554.

Petruy, R. and Lettinga, G. (1997) 'Digestion of a milk-fat emulsion', *Bioresource Technology*, 61(2), pp. 141-149.

Phattaranawik, J. *et al.* (2007) 'Membrane bioreactor with bubble-size transformer: Design and fouling control', *AIChE Journal*, 53(1), pp. 243-248.

Pollice, A. *et al.* (2005) 'Sub-critical flux fouling in membrane bioreactors — a review of recent literature', *Desalination*, 174(3), pp. 221-230.

Prazeres, A.R., Carvalho, F. and Rivas, J. (2012) 'Cheese whey management: A review', *Journal of Environmental Management*, 110, pp. 48-68.

Pretel, R. *et al.* (2015) 'Designing an AnMBR-based WWTP for energy recovery from urban wastewater: The role of primary settling and anaerobic digestion', *Separation and Purification Technology*, 156, pp. 132-139.

Pretel, R. *et al.* (2014) 'The operating cost of an anaerobic membrane bioreactor (AnMBR) treating sulphate-rich urban wastewater', *Separation and Purification Technology*, 126, pp. 30-38.

Prieske, H. *et al.* (2010) 'Optimised hydrodynamics for membrane bioreactors with immersed flat sheet membrane modules', *Desalination and Water Treatment*, 18(1-3), pp. 270-276.

Prieske, H., Drews, A. and Kraume, M. (2008) 'Prediction of the circulation velocity in a membrane bioreactor', *Desalination*, 231(1–3), pp. 219-226.

Remy, M. *et al.* (2010) 'Why low powdered activated carbon addition reduces membrane fouling in MBRs', *Water Research*, 44(3), pp. 861-867.

Rittmann, B.E. and McCarty, P.L. (2001) *Environmental biotechnology : principles and applications*.

Rodgers, M., Zhan, X.-M. and Dolan, B. (2004) 'Mixing Characteristics and Whey Wastewater Treatment of a Novel Moving Anaerobic Biofilm Reactor', *Journal of Environmental Science and Health, Part A*, 39(8), pp. 2183-2193.

Rosenberger, S., Helmus, F.P. and Drews, A. (2016) 'Addition of Particles for Fouling Minimization in Membrane Bioreactors – Permeability Performance, Fluid Dynamics, and Rheology', *Chemie Ingenieur Technik*, 88(1-2), pp. 29-38.

Rosenberger, S. *et al.* (2011) 'Principles of an enhanced MBR-process with mechanical cleaning', *Water Science and Technology*, 64(10), p. 1951.

Saddoud, A. *et al.* (2006) 'A Comparative Study on the Anaerobic Membrane Bioreactor Performance During the Treatment of Domestic Wastewaters of Various Origins', *Environmental Technology*, 27(9), pp. 991-999.

Saddoud, A., Hassaïri, I. and Sayadi, S. (2007) 'Anaerobic membrane reactor with phase separation for the treatment of cheese whey', *Bioresource Technology*, 98(11), pp. 2102-2108.

Saddoud, A. and Sayadi, S. (2007) 'Application of acidogenic fixed-bed reactor prior to anaerobic membrane bioreactor for sustainable slaughterhouse wastewater treatment', *Journal of Hazardous Materials*, 149(3), pp. 700-706.

Safley Jr, L.M. and Westerman, P.W. (1994) 'Low-temperature digestion of dairy and swine manure', *Bioresource Technology*, 47(2), pp. 165-171.

Salazar-Peláez, M.L., Morgan-Sagastume, J.M. and Noyola, A. (2011) 'Influence of hydraulic retention time on fouling in a UASB coupled with an external ultrafiltration membrane treating synthetic municipal wastewater', *Desalination*, 277(1–3), pp. 164-170.

Santos, A., Ma, W. and Judd, S.J. (2011) 'Membrane bioreactors: Two decades of research and implementation', *Desalination*, 273(1), pp. 148-154.

Sato, R., Hayashi, K. and Tomiyama, A. (2015) 'Effects of liquid viscosity on flows inside and outside a bubble diffuser pipe', *Experimental Thermal and Fluid Science*, 66, pp. 197-205.

Shelton, D.R. and Tiedje, J.M. (1984) 'General method for determining anaerobic biodegradation potential', *Applied and Environmental Microbiology*, 47(4), pp. 850-857.

Shen, L.-g. *et al.* (2015) 'Membrane fouling in a submerged membrane bioreactor: Impacts of floc size', *Chemical Engineering Journal*, 269, pp. 328-334.

Shim, J.K., Yoo, I.-K. and Lee, Y.M. (2002) 'Design and operation considerations for wastewater treatment using a flat submerged membrane bioreactor', *Process Biochemistry*, 38(2), pp. 279-285.

Shin, C. and Bae, J. (2018) 'Current status of the pilot-scale anaerobic membrane bioreactor treatments of domestic wastewaters: A critical review', *Bioresource Technology*, 247, pp. 1038-1046.

Shin, C. *et al.* (2016) 'Integrity of hollow-fiber membranes in a pilot-scale anaerobic fluidized membrane bioreactor (AFMBR) after two-years of operation', *Separation and Purification Technology*, 162, pp. 101-105.

Shin, C. *et al.* (2014) 'Pilot-scale temperate-climate treatment of domestic wastewater with a staged anaerobic fluidized membrane bioreactor (SAF-MBR)', *Bioresource Technology*, 159, pp. 95-103.

Siembida, B. *et al.* (2010) 'Effect of mechanical cleaning with granular material on the permeability of submerged membranes in the MBR process', *Water Research*, 44(14), pp. 4037-4046.

Singhania, R.R. *et al.* (2012) 'Immersed membrane bioreactors: An overview with special emphasis on anaerobic bioprocesses', *Bioresource Technology*, 122(0), pp. 171-180.

Skouteris, G. *et al.* (2012) 'Anaerobic membrane bioreactors for wastewater treatment: A review', *Chemical Engineering Journal*, 198–199(0), pp. 138-148.

Skouteris, G. *et al.* (2015) 'The effect of activated carbon addition on membrane bioreactor processes for wastewater treatment and reclamation – A critical review', *Bioresource Technology*, 185, pp. 399-410.

Smith, A.L., Skerlos, S.J. and Raskin, L. (2013) 'Psychrophilic anaerobic membrane bioreactor treatment of domestic wastewater', *Water Research*, 47(4), pp. 1655-1665.

Smith, A.L. *et al.* (2012) 'Perspectives on anaerobic membrane bioreactor treatment of domestic wastewater: A critical review', *Bioresource Technology*, 122(0), pp. 149-159.

Sofia, A., Ng, W.J. and Ong, S.L. (2004) 'Engineering design approaches for minimum fouling in submerged MBR', *Desalination*, 160(1), pp. 67-74.

Sombatsompop, K., Visvanathan, C. and Ben Aim, R. (2006) 'Evaluation of biofouling phenomenon in suspended and attached growth membrane bioreactor systems', *Desalination*, 201(1–3), pp. 138-149.

Spagni, A. *et al.* (2010) 'Filterability in a submerged anaerobic membrane bioreactor', *Desalination*, 250(2), pp. 787-792.

Stuckey, D.C. (2012) 'Recent developments in anaerobic membrane reactors', *Bioresource Technology*, 122(0), pp. 137-148.

Tiranuntakul, M., Schneider, P.A. and Jegatheesan, V. (2011) 'Assessments of critical flux in a pilot-scale membrane bioreactor', *Bioresource Technology*, 102(9), pp. 5370-5374.

Trzcinski, A.P. and Stuckey, D.C. (2009) 'Continuous treatment of the organic fraction of municipal solid waste in an anaerobic two-stage membrane process with liquid recycle', *Water Research*, 43(9), pp. 2449-2462.

Trzcinski, A.P. and Stuckey, D.C. (2010) 'Treatment of municipal solid waste leachate using a submerged anaerobic membrane bioreactor at mesophilic and psychrophilic temperatures: Analysis of recalcitrants in the permeate using GC-MS', *Water Research*, 44(3), pp. 671-680.

Ueda, T. and Hata, K. (1999) 'Domestic wastewater treatment by a submerged membrane bioreactor with gravitational filtration', *Water Research*, 33(12), pp. 2888-2892.

Ueno, Y. *et al.* (2007) 'Production of hydrogen and methane from organic solid wastes by phase-separation of anaerobic process', *Bioresour Technol*, 98(9), pp. 1861-5.

van den Brink, P. *et al.* (2013) 'Potential of mechanical cleaning of membranes from a membrane bioreactor', *Journal of Membrane Science*, 429, pp. 259-267.

van der Marel, P. *et al.* (2009) 'An improved flux-step method to determine the critical flux and the critical flux for irreversibility in a membrane bioreactor', *Journal of Membrane Science*, 332(1–2), pp. 24-29.

van Lier, J.B. *et al.* (2001) 'New perspectives in anaerobic digestion', *Water Sci Technol*, 43(1), pp. 1-18.

Verrecht, B. *et al.* (2008) 'An aeration energy model for an immersed membrane bioreactor', *Water Research*, 42(19), pp. 4761-4770.

Vidal, G. *et al.* (2000) 'Influence of the content in fats and proteins on the anaerobic biodegradability of dairy wastewaters', *Bioresource Technology*, 74(3), pp. 231-239.

Visvanathan, C. and Abeynayaka, A. (2012) 'Developments and future potentials of anaerobic membrane bioreactors (AnMBRs)', *Membrane Water Treatment*, 3(1), pp. 1-23.

Vyrides, I. and Stuckey, D.C. (2009) 'Saline sewage treatment using a submerged anaerobic membrane reactor (SAMBR): Effects of activated carbon addition and biogas-sparging time', *Water Research*, 43(4), pp. 933-942.

Walker, M., Banks, C.J. and Heaven, S. (2009a) 'Development of a coarse membrane bioreactor for two-stage anaerobic digestion of biodegradable municipal solid waste', *Water Sci Technol*, 59(4), pp. 729-35.

Walker, M., Banks, C.J. and Heaven, S. (2009b) 'Two-stage anaerobic digestion of biodegradable municipal solid waste using a rotating drum mesh filter bioreactor and anaerobic filter', *Bioresource Technology*, 100(18), pp. 4121-4126.

Walker, M. *et al.* (2009) 'Potential errors in the quantitative evaluation of biogas production in anaerobic digestion processes', *Bioresource Technology*, 100(24), pp. 6339-6346.

Wang, S. *et al.* (2009) 'Performance and kinetic evaluation of anaerobic moving bed biofilm reactor for treating milk permeate from dairy industry', *Bioresource Technology*, 100(23), pp. 5641-5647.

Wang, W. *et al.* (2006) 'Excess sludge reduction performance of an aerobic SBR process equipped with a submerged mesh filter unit', *Process Biochemistry*, 41(4), pp. 745-751.

Wang, X.-M. and Li, X.-Y. (2008) 'Accumulation of biopolymer clusters in a submerged membrane bioreactor and its effect on membrane fouling', *Water Research*, 42(4–5), pp. 855-862.

Wang, Y. *et al.* (2010) 'Direct Microscopic Observation of Forward Osmosis Membrane Fouling', *Environmental Science & Technology*, 44(18), pp. 7102-7109.

Wang, Z. *et al.* (2014) 'Membrane cleaning in membrane bioreactors: A review', *Journal of Membrane Science*, 468, pp. 276-307.

Wei, C.-H. *et al.* (2014) 'Sustainable organic loading rate and energy recovery potential of mesophilic anaerobic membrane bioreactor for municipal wastewater treatment', *Bioresource Technology*, 166, pp. 326-334.

Wei, C.H. *et al.* (2006) 'Effect of a suspended carrier on membrane fouling in a submerged membrane bioreactor', *Water Sci Technol*, 53(6), pp. 211-20.

Wei, P. *et al.* (2013) 'CFD modeling of hydrodynamic characteristics of slug bubble flow in a flat sheet membrane bioreactor', *Journal of Membrane Science*, 445(0), pp. 15-24.

Wen, C., Huang, X. and Qian, Y. (1999) 'Domestic wastewater treatment using an anaerobic bioreactor coupled with membrane filtration', *Process Biochemistry*, 35(3–4), pp. 335-340.

Wibisono, Y. *et al.* (2014) 'Two-phase flow in membrane processes: A technology with a future', *Journal of Membrane Science*, 453(0), pp. 566-602.

Wijekoon, K.C., Visvanathan, C. and Abeynayaka, A. (2011) 'Effect of organic loading rate on VFA production, organic matter removal and microbial activity of a two-stage thermophilic anaerobic membrane bioreactor', *Bioresource Technology*, 102(9), pp. 5353-5360.

Wilmarth, T. and Ishii, M. (1994) 'Two-phase flow regimes in narrow rectangular vertical and horizontal channels', *International Journal of Heat and Mass Transfer*, 37(12), pp. 1749-1758.

Wu, B. *et al.* (2009) 'Effect of adsorption/coagulation on membrane fouling in microfiltration process post-treating anaerobic digestion effluent', *Desalination*, 242(1–3), pp. 183-192.

Wu, D., Howell, J.A. and Field, R.W. (1999) 'Critical flux measurement for model colloids', *Journal of Membrane Science*, 152(1), pp. 89-98.

Wu, J. and He, C. (2012) 'Effect of cyclic aeration on fouling in submerged membrane bioreactor for wastewater treatment', *Water Research*, 46(11), pp. 3507-3515.

Wu, J. *et al.* (2008a) 'Effects of relaxation and backwashing conditions on fouling in membrane bioreactor', *Journal of Membrane Science*, 324(1), pp. 26-32.

Wu, Z. *et al.* (2008b) 'Effects of various factors on critical flux in submerged membrane bioreactors for municipal wastewater treatment', *Separation and Purification Technology*, 62(1), pp. 56-63.

Xie, K. *et al.* (2010) 'Performance and fouling characteristics of a submerged anaerobic membrane bioreactor for kraft evaporator condensate treatment', *Environmental Technology*, 31(5), pp. 511-521.

Xu, J. (1999) 'Experimental study on gas–liquid two-phase flow regimes in rectangular channels with mini gaps', *International Journal of Heat and Fluid Flow*, 20(4), pp. 422-428.

Yamanoi, I. and Kageyama, K. (2010) 'Evaluation of bubble flow properties between flat sheet membranes in membrane bioreactor', *Journal of Membrane Science*, 360(1–2), pp. 102-108.

Yang, F. *et al.* (2012) 'Performance of different configurations of hybrid growth membrane bioreactor (HG-MBR) for treatment of mixed wastewater', *Desalination*, 284, pp. 261-268.

Yang, J., Spanjers, H. and van Lier, J.B. (2012) 'Non-feasibility of magnetic adsorbents for fouling control in anaerobic membrane bioreactors', *Desalination*, 292, pp. 124-128.

Yang, Q.-Y. *et al.* (2009) 'Filtration characteristics of activated sludge in hybrid membrane bioreactor with porous suspended carriers (HMBR)', *Desalination*, 249(2), pp. 507-514.

Yang, Q., Chen, J. and Zhang, F. (2006) 'Membrane fouling control in a submerged membrane bioreactor with porous, flexible suspended carriers', *Desalination*, 189(1–3), pp. 292-302.

Ye, M. *et al.* (2006) 'Study on the suitable thickness of a PAC-precoated dynamic membrane coupled with a bioreactor for municipal wastewater treatment', *Desalination*, 194(1–3), pp. 108-120.

Ying, Z. and Ping, G. (2006) 'Effect of powdered activated carbon dosage on retarding membrane fouling in MBR', *Separation and Purification Technology*, 52(1), pp. 154-160.

Zhang, K., Cui, Z. and Field, R.W. (2009) 'Effect of bubble size and frequency on mass transfer in flat sheet MBR', *Journal of Membrane Science*, 332(1–2), pp. 30-37.

Zhang, K. *et al.* (2011a) 'Effect of the bubbling regimes on the performance and energy cost of flat sheet MBRs', *Desalination*, 283(0), pp. 221-226.

Zhang, Q., Tan, G.H. and Stuckey, D.C. (2017) 'Optimal biogas sparging strategy, and the correlation between sludge and fouling layer properties in a submerged anaerobic membrane bioreactor (SAnMBR)', *Chemical Engineering Journal*, 319, pp. 248-257.

Zhang, X. *et al.* (2010) 'Formation of dynamic membrane in an anaerobic membrane bioreactor for municipal wastewater treatment', *Chemical Engineering Journal*, 165(1), pp. 175-183.

Zhang, X. *et al.* (2011b) 'Membrane fouling in an anaerobic dynamic membrane bioreactor (AnDMBR) for municipal wastewater treatment: Characteristics of membrane foulants and bulk sludge', *Process Biochemistry*, 46(8), pp. 1538-1544.

Zsirai, T. *et al.* (2012) 'Efficacy of relaxation, backflushing, chemical cleaning and clogging removal for an immersed hollow fibre membrane bioreactor', *Water research*, 46(14), pp. 4499-4507.